Deposit & Copying of Dissertation Declaration

UNIVERSITY OF CAMBRIDGE

Board of Graduate Studies

Please note that you will also need to bind a copy of this Declaration into your final, hardbound copy of thesis - this has to be the very first page of the hardbound thesis.

1 Surname (Family Name)	Forenames(s)	Title
Hunter	Emma Joanne	Ms

2 Title of Dissertation as approved by the Degree Committee
The Roles of the Collagen Binding Integrins in the Regulation of Endothelial Cell Function

In accordance with the University Regulations in *Statutes and Ordinances* for the PhD, MSc and MLitt Degrees, I agree to deposit one print copy of my dissertation entitled above and one print copy of the summary with the Secretary of the Board of Graduate Studies who shall deposit the dissertation and summary in the University Library under the following terms and conditions:

1. Dissertation Author Declaration

I am the author of this dissertation and hereby give the University the right to make my dissertation available in print form as described in 2. below.

My dissertation is my original work and a product of my own research endeavours and includes nothing which is the outcome of work done in collaboration with others except as declared in the Preface and specified in the text. I hereby assert my moral right to be identified as the author of the dissertation.

The deposit and dissemination of my dissertation by the University does not constitute a breach of any other agreement, publishing or otherwise, including any confidentiality or publication restriction provisions in sponsorship or collaboration agreements governing my research or work at the University or elsewhere.

2. Access to Dissertation

I understand that one print copy of my dissertation will be deposited in the University Library for archival and preservation purposes, and that, unless upon my application restricted access to my dissertation for a specified period of time has been granted by the Board of Graduate Studies prior to this deposit, the dissertation will be made available by the University Library for consultation by readers in accordance with University Library Regulations and copies of my dissertation may be provided to readers in accordance with applicable legislation.

3 Signature	Date
	06.03.2020

Corresponding Regulation

Before being admitted to a degree, a student shall deposit with the Secretary of the Board one copy of his or her hard-bound dissertation and one copy of the summary (bearing student's name and thesis title), both the dissertation and the summary in a form approved by the Board. The Secretary shall deposit the copy of the dissertation together with the copy of the summary in the University Library where, subject to restricted access to the dissertation for a specified period of time having been granted by the Board of Graduate Studies, they shall be made available for consultation by readers in accordance with University Library Regulations and copies of the dissertation provided to readers in accordance with applicable legislation.

The Roles of the Collagen Binding Integrins in the Regulation of Endothelial Cell Function

Emma Joanne Hunter

Darwin College

Department of Biochemistry

University of Cambridge

This dissertation is submitted for the degree of Doctor of Philosophy

September 2019

Declaration

This dissertation is the result of my own work and includes nothing which is the outcome of work done in collaboration except as declared in the Preface and specified in the text.

It is not substantially the same as any that I have submitted, or, is being concurrently submitted for a degree or diploma or other qualification at the University of Cambridge or any other University or similar institution except as declared in the Preface and specified in the text. I further state that no substantial part of my dissertation has already been submitted, or, is being concurrently submitted for any such degree, diploma or other qualification at the University of Cambridge or any other University or similar institution except as declared in the Preface and specified in the text.

This thesis does not exceed the prescribed 60,000 word limit.

Acknowledgements

With particular thanks to Richard Farndale for agreeing to be my supervisor and Samir Hamaia for helping me with everything throughout the four years. Thanks also to JD Malcor, Sally Hunter and Nick Pugh for proofreading and advice. I'm very grateful to the British Heart Foundation for funding my PhD, and the Biochemistry Department for further funding and support.

A huge thanks to everyone in Richard Farndale's Group for all the help I have received over the years, including scientific advice, emotional support and cake – JD Malcor, Dan Bax, Natalia Davidenko, Isuru Induruwa, Peter Kim, Rachel Frame, Emily Capes, Abhishek Jalan, Arek Bonna, Stephanie Jung and Masaaki Moroi.

Abstract

The aim of this project was to first investigate the binding preferences of collagen binding integrins (α1β1, α2β1, α10β1 and α11β1), and to then assess their role in the regulation of endothelial cell (EC) behaviour using human umbilical vein endothelial cells (HUVECs). First, quantitative real-time polymerase chain reaction (qPCR) was performed to quantify the expression levels of the four integrins. Functional roles of these integrins were then investigated using commercially available inhibitors (TC-I-15, Obtustatin and 6F1) to modulate integrin function, and small interfering RNA (siRNA) to reduce expression levels.

qPCR demonstrates that α2 is the most abundant receptor subunit transcript in HUVECs followed by α10 and α1; α11 was barely detectable. After integrin inhibition or knockdown, functional assays measuring changes in proliferation, apoptosis, adhesion, migration and angiogenesis were carried out.

Synthetic triple helical collagenous peptides (THPs), based on the canonical GFOGER amino acid sequence, were used to probe the binding preferences of the integrins. Initially recombinant integrin αI-domains were studied, before utilising C2C12 cell lines stably expressing the full-length integrin receptors. The four integrins showed very similar, overlapping, binding profiles, with α1β1 and α10β1 binding strongly to GLOGEN motifs and moderately to GFOGER, and α2β1 and α11β1 binding strongly to GFOGER and moderately to GLOGEN.

The specificities of the inhibitors TC-I-15, Obtustatin, and 6F1, for different integrins were characterised using static adhesion assays and real-time xCELLigence adhesion assays. TC-I-15 showed cross-reactivity between α1β1 and α2β1 and inhibited both receptors, Obtustatin was specific to α1β1 only and 6F1 was specific to α2β1. No cellular toxicity was observed for any of these inhibitors. siRNA was optimised to efficiently and selectively target each receptor and 90% knockdowns of α1β1, α2β1 and α10β1 mRNA were achieved in HUVECs.

Functional assays were carried out downstream of integrin inhibition or siRNA treatment. HUVEC proliferation, measured by cell number quantification and 5-ethynyl-2'-deoxyuridine (EdU) incorporation analysis, was unaffected by inhibition or siRNA knockdown of any integrin receptor. Knockdown or inhibition of α2β1 severely hindered HUVEC

attachment and spreading to collagen and THPs, measured by static and real-time adhesion assays. Cell migration, in time-lapse microscopy random movement assays, was also impaired after either knockdown or inhibition of α2β1. In addition, inhibition of α2β1 using TC-I-15 and 6F1 impeded angiogenesis in tube formation assays on a Geltrex substrate. However, siRNA knockdown of α2β1 had no effect on tube formation. This observation highlights the differences in signalling events between inhibiting a receptor that is present and simply lacking the receptor altogether. No compensatory upregulation of other α-subunits was observed.

In conclusion, the inhibition or knockdown of integrin α2β1 has a significant effect on the behaviour of HUVECs. In contrast, inhibition or knockdown of α1β1 and α10β1 does not significantly affect HUVEC cellular response. Additionally, the results presented here suggest that inhibitors and antibodies targeting collagen-binding integrins must be rigorously tested for cross-reactivity before use. Finally, these findings show that TC-I-15 could have an interesting therapeutic value in blocking angiogenesis and the migration of endothelial cells.

List of Publications and Academic Presentations

Presentations

18.07.2018-19.07.2018 – Poster presentation at the Endothelial Cell Phenotypes in Health and Disease, Gordon Research Conference, Lucca, Italy. Hunter EJ, Hamaia SW, Farndale RW "Inhibitors for the Collagen Binding Integrins Disrupt Tube Formation in HUVECs"

Published Papers

Jalan AA, Sammon D, Hartgerink JD, Brear P, Stott K, Hamaia SW, Hunter EJ, Walker DR, Leitinger B, Farndale RW. Chain alignment of collagen I deciphered using computationally designed heterotrimers. Nat Chem Biol 2020. Doi: 10.1038/s41589-019-0435-y PMID: 31907373

Malcor JD, Juskaite V, Gavriilidou D, Hunter EJ, Davidenko N, Hamaia S, Sinha S, Cameron RE, Best SM, Leitinger B, Farndale RW. Coupling of a specific photoreactive triple-helical peptide to crosslinked collagen films restores binding and activation of DDR2 and VWF. Biomaterials. 2018 Nov;182:21-34. doi: 10.1016/j.biomaterials.2018.07.050. Epub 2018 Jul 31. PMID: 30099278; PMCID: PMC6131271.

Hamaia SW, Luff D, Hunter EJ, Malcor JD, Bihan D, Gullberg D, Farndale RW. Unique charge-dependent constraint on collagen recognition by integrin α10β1. Matrix Biol. 2017 May;59:80-94. doi: 10.1016/j.matbio.2016.08.010. Epub 2016 Aug 25. PMID: 27569273; PMCID: PMC5380659.

Contents

List of Abbreviations

Acronym	Full name	Acronym	Full name
AAV	Adeno-associated viruses	ITGA1	Integrin alpha1
AcOH	Acetic acid	ITGA10	Integrin alpha10
ADAM	A Disintegrin and Metalloprotease	ITGA11	Integrin alpha11
ADMIDAS	Domain adjacent to MIDAS	ITGA2	Integrin alpha2
ADP	Adenosine diphosphate	JAMs	Junctional adhesion molecule
AJ	Adherens junctions	JNK	MAPK c-Jun NH2-terminal kinase
Ang	Angiopoietin	KD	Knockdown
ANOVA	Analysis of variance	KO	knockout
APOBEC1	Apolipoprotein B mRNA editing enzyme, catalytic polypeptide 1	LAIR-1	Leukocyte-associated immunoglobulin-like receptor 1
ATP	Adenosine triphosphate	LB	Luria broth
AV Buffer	Annexin V binding buffer	LDEV	Lactose dehydrogenase elevating virus
BBB	Blood brain barrier	LDH	Lactate dehydrogenase
Bcl-2	B-cell lymphoma 2 protein	LPS	Lipopolysaccharide from E.coli
BE	Immortalised bronchial epithelial cells	MAPK	Mitogen activated kinase
bFGF	Basic fibroblast growth factor	MCAM	Melanoma Cell Adhesion Molecule
Bmp4	Bone morphogenic protein 4	MIDAS	Metal ion dependant adhesion site
BrdU	Bromodeoxyuridine	miRNAs	Micro RNAs
BSA	Bovine Serum Albumin	MMP	Metalloproteinase
CAECs	Coronary artery endothelial cells	mRNA	Messenger RNA
CAM	Chick Chorioallantoic Membrane	NADPH	Nicotinamide adenine dinucleotide phosphate
Cas	CRISPR associated nuclease	NaOH	Sodium chloride
Cdc42	Cell Division Control Protein 42	NFEC	Neonatal foreskin ECs (NFECs)
CDK	Cyclin-dependent kinases	NHEJ	Non-homologous end joining
CDKI	Cyclin-dependent kinase inhibitor	NIR	Helix NIR far red dead-cell stain
cDNA	Reverse transcribed DNA	NO	Nitric oxide
CEC	Circulating endothelial cells	Nrp	Neuropilin
CEPCs	Circulating endothelial progenitor cells	OSCAR	Osteoclast-associated receptor
cGMP	Cyclic guanosine monophosphate	PBS	Phosphate Buffered saline
CHO	Chinese Hamster Ovary	PCR	Polymerase chain reaction
cpf1	CRISPR from Prevotella and Francisella 1	PDGF	Platelet derived growth factor
CRISPR	Clustered Regularly Interspaced Short Palindromic Repeats	PECAM-1	Platelet endothelial cell adhesion moelcule-1
crRNA	CRISPR RNA	PI	Propidium Iodide
CT	Cycle threshold	PI3K	Phosphatidylinositol kinase
D4	DharmaFECT 4	PIP2/3	Phosphatidylinositol

DARC	Duffy antigen receptor for chemokines	PKA	Protein kinase A
DDR1/2	Discoidin domain receptor 1 or 2	PKC	Protein kinase C
DL4	Delta-like-4	PLGF	Placental growth factor
DMEM	Dulbecco's modified eagle media	PMA	Phorbol 12-myristate 13-acetate
DNA	Deoxyribonucleic acid	PNK	T4 Polynucleotide Kinase
EBM	Endothelial basal media 2	PS	Phosphatidylserine
EC	Endothelial cell	PTEN	Phosphatase and Tensin homolog protein
ECM	Extracellular matrix	PVDF	Polyvinylidene difluoride
EDTA	Ethylenediaminetetraacetic acid	qPCR	Quantitative real time polymerase chain reaction
EdU	5-ethynyl-2-deoxyuridine	RBCs	Red blood cells
EGF	Epithelial growth factor	RFP	Ref fluorescent protein
EGM	Endothelial growth media 2	RISC	RNA induced silencing complex
ELISA	Enzyme linked immunosorbent assay	RNA	Ribonucleic acid
eNOS	Endothelial nitric oxide synthase	ROS	Reactive oxygen species
ERK	Extracellular signal–regulated kinases	RT	Room temperature
FAK	Focal adhesion kinase	SDS-PAGE	Sodium dodecyl sulphate Polyacrylamide gel electrophoresis
FBS	Foetal bovine serum	siRNA	Short interfering Ribonucleic acid
fI	Factor I	SP	Short Peptides
fII	Factor II	SPARC	Secreted protein acidic and rich in cysteine
fIX	Factor IX	spCAS9	Streptococcus pyogenes Cas9
fIXa	Activated Factor IX	Src	Proto-oncogene tyrosine-protein kinase
fVII	Factor VII	SVECs	Saphenous vein endothelial cells
fVIIa	Activated Factor VII	tacrRNA	Trans-activating crRNA
fX	Factor X	TBS	TRIS buffered saline
fXa	Activated Factor X	TF	Tissue factor
fXVI	Factor CVI	TFPI	Tissue factor pathway inhibitor
GAPDH	Glyceraldehyde 3-phosphate dehydrogenase	TGFα	Transforming growth factor alpha
GAPs	GTPase activating proteins	TGFβ	Transforming growth factor beta
GEFs	GTPase exchange factors	THD	Triple helical domain
GFP	Green fluorescent protein	THP	Triple helical peptide
GJ	Gap junction	TIMP	TIMP metallopeptidase inhibitor
GP1b	Platelet glycoprotein 1b	TJ	Tight junction
GPVI	Platelet glycoprotein VI	TMB	3,3′,5,5′-Tetramethylbenzidine
GST	Glutathione S-transferase	TNFα	Tumour necrosis factor α
GTP	Guanosine triphosphate	VCAM	Vascular cell adhesion molecule
HCAECS	Human coronary artery endothelial cells	VE-Cad	Vascular endothelial cadherin

HDMVECs	Human dermal microvascular endothelial cells	VEGF	Vascular endothelial growth factor
HEK293	Human embryonic kidney cell line	VEGFR	Vascular endothelial growth factor receptor
HEVECs	High endothelial venule ECs	VP64	4 Copies of Herpes virus VP16
HIF	Hypoxia Inducible transcription factor	VSMC	Vascular smooth muscle cell
HIF-PHs	Hypoxia-inducible factor prolyl hydroxylases	VSV-G	Vesicular stomatitis virus G
HPRT1	Hypoxanthine Phosphoribosyltransferase 1	VVOs	Vesiculo-vacuolar organelle
HRP	Horseradish peroxidase	VWD	Von Willebrand disease
HUVECs	Human umbilical vein endothelial cells	VWF	Von Willebrand factor
ICAM	Intercellular Adhesion Molecule 1	WB	Western blot
IGF	Insulin-like growth factor 1	WPBs	Weibel Palade bodies
IGF-IR	Insulin-like growth factor 1 receptor	YWHAZ	Tyrosine 3-monooxygenase/tryptophan 5-monooxygenase activation protein zeta
IHH	Indian hedgehog	ZO-1	Zonula occludens-1
IL-1α	Interleukin-1α	ZONAB	ZO-1–associated nucleic acid binding proteins
IPTG	Isopropyl-β-D-thiogalactoside		

List of Tables

List of Figures

Introduction

Contents

1.1 Chapter Summary

This chapter aims to give a detailed background understanding and literature review of endothelial cell (EC) behaviour and function with an emphasis on the interactions between ECs and their extracellular matrix (ECM) and how this relates to the regulation of EC behaviour. The integrin family of adhesion receptors is described in detail with respect to ECs and the regulation of EC behaviour.

1.2 Endothelial Cells

The vascular endothelium consists of a thin monolayer of ECs that line all blood vessels in the body, from arteries to veins to capillaries (Figure 1.1) and is paramount in regulating blood flow and maintaining tissue homeostasis[12]. The endothelium provides a physical barrier between the solutes in the blood and the surrounding tissues and has been implicated in the regulation of fluid filtration, haemostasis, neutrophil trafficking, hormone trafficking, thrombosis and platelet activation. EC dysfunction has been implicated in stroke, heart disease, vascular diseases, diabetes, chronic kidney failure, cancer, atherosclerosis and infectious diseases[12-14]. ECs interact with macrophages, platelets, monocytes, clotting factors and signalling molecules; these interactions are often dynamic and complex. Signal transduction

between the Extracellular Matrix (ECM) and EC monolayer is an important regulator of EC behaviour in each of these functions[15]. ECs are reactive, multifunctional and highly sensitive to physiological conditions. While generally quiescent, ECs can also exist in inflammatory, thrombotic or angiogenic phenotypes[9, 16, 17].

1.3 Endothelial Cell Development

The endothelium is critical to the transport of metabolites and the removal of waste products from tissues, therefore the vascular circulatory system is the first organ to develop in vertebrate embryos by a process termed vasculogenesis[18]. Much of what is known about vasculogenesis comes from murine, zebrafish and avian embryonic studies due to the difficulty in obtaining ethical approval for studying human embryos. In early mouse embryonic development, bone morphogenic protein (Bmp)4 promotes the formation of the mesoderm. Endothelial cell precursors are then formed by the differentiation of mesoderm into clusters of hemangioblasts, induced by basic fibroblast growth factor (bFGF) and activin A[19-23]. Peripheral hemangioblasts differentiate into angioblasts which in turn aggregate, coalesce and form endothelial cell tubes with a lumen[18] while central hemangioblasts differentiate into hematopoietic stem cells and smooth muscle cells[21]. Shear stress, the physical friction created by the flow of blood across the EC surface, is thought to play a role in EC differentiation[21]. In mouse embryoid-body derived cells, shear stress induces platelet endothelial cell adhesion molecule (PECAM-1, also called CD31) expression *in vitro*, a key component of intercellular junctions in ECs[24]. In mouse embryos shear stress is necessary for the vascular remodelling of the yolk sac[25]. In human and murine embryos Bmp4 and Indian hedgehog (IHH) are thought to promote endothelial differentiation[26-28]. While in zebrafish, prostaglandin-E2 is thought to promote endothelial maturation[29]. Mutations in pathways required for vascular development, for example, Notch[30], vascular endothelial growth factor (VEGF)[31-33] and Angiopoietin (Ang)/Tie signalling[34], often result in vascular defects that ultimately result in embryonic lethality in mice, highlighting the importance of correct vascular development. Integrins play major roles in embryonic development and cell differentiation. As a result knockout (KO) of the β1 integrin subunit results in embryonic death[35].

1.3 Endothelial Structure and Function

ECs can be characterised by the expression of several markers. These include PECAM-1, Von Willebrand factor (VWF), vascular endothelial-cadherin (VE-Cad), melanoma cell adhesion molecule (MCAM, also known as CD146) and vascular endothelial growth factor receptor-2 (VEGFR2) (reviewed in[36]). PECAM-1 is a mechanotransducer glycoprotein expressed on the surface of ECs, monocytes and platelets. In ECs it regulates vascular permeability and transduces mechanical signals inside the cell[37]. VE-Cad is another mechanotransducer that also regulates cell-cell adhesion in ECs to modulate monolayer permeability[38]. VWF is expressed and stored in secretory vesicles called Weibel-Palade Bodies

Figure 1.1: Diagram of Vessel Structure.

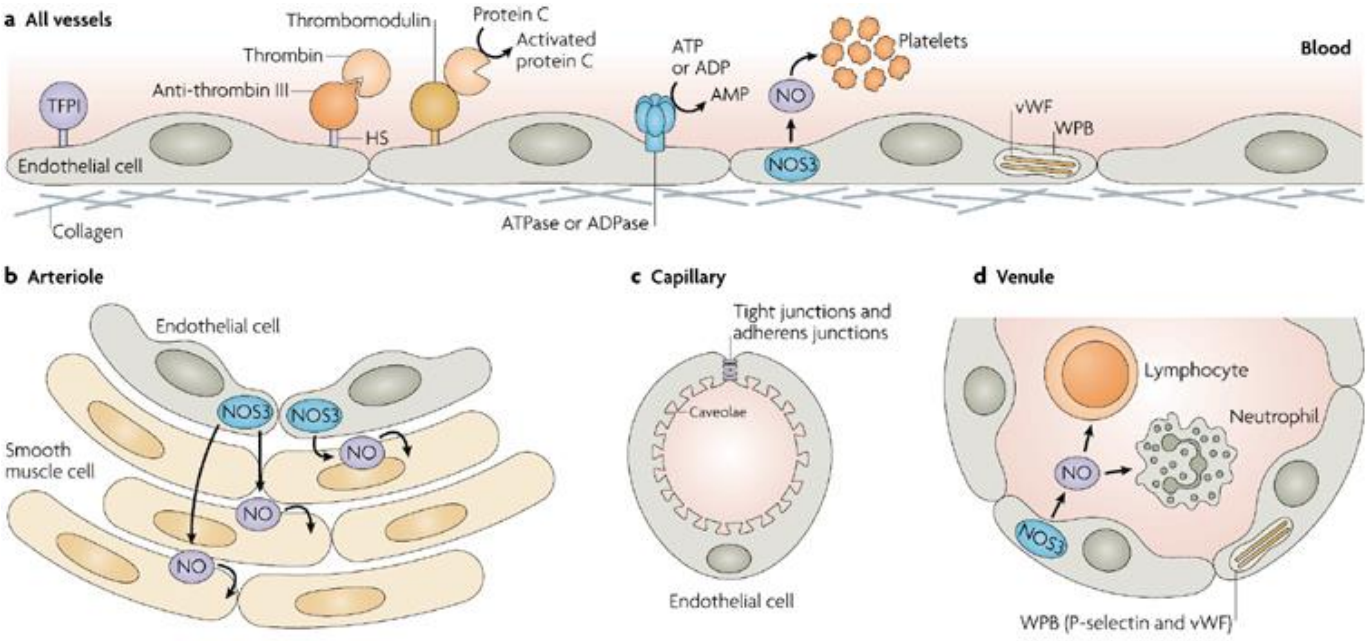

Adapted from '*Evolving functions of endothelial cells in inflammation'* by Pober et al, 2007[9]. In this diagram, a) gives an overview of EC function and vessel structure common to all blood vessels. Various signalling molecules relevant to the maintenance of vascular tone are shown. For example TFP1 is an inhibitor of platelet activation and thrombus formation. NO is nitric oxide, which is synthesised by NOS3 and secreted by endothelial cells to relax smooth muscle cells. VWF is shown stored in endothelial cells in WPBs. Anti-thrombin is shown bound to thrombin to inhibit thrombin activation of platelets. b) shows the vessel structure in arterioles where ECs release NO to relax smooth muscle cells, c) shows capillaries which are the smallest vessels containing just ECs and pericytes and d) shows venules where lymphocytes and neutrophils are most active.

(WPBs) inside ECs. These show up clearly as granular spots in the cytoplasm of ECs in fluorescence microscopy when staining for VWF. WPBs can also contain P-Selectin, interleukin (IL)-8, angiopeoietin-2 (Ang2), endothelin-1, tissue-type plasminogen activator and CD63, suggesting an important role in the regulation of inflammatory pathways[39-45]; they allow the rapid release of signalling molecules and cytokines in response to changes in the EC microenvironment.

Endothelial cells are flat, polarised, and will align depending on the direction of blood flow. They can also remodel their alignment in response to altered flow direction induced by surgical realignment of cells[46]. One important function of ECs is to form a semi-permeable monolayer that regulates the controlled transport of metabolites and waste products between the blood and the surrounding tissues, contributing to the control of tissue homeostasis[47]. ECs control the paracellular transport of metabolites, notably via the opening and closing of cell-cell junctions, of which there are three main types; tight junctions (TJs), gap junctions (GJs) and adherens junctions (AJs)[48]. Some endothelial cells also utilize specialised vesicle transport systems called vesiculo-vacuolar organelles (VVOs)[49], transendothelial channels or caveolae (Figure 1.1 C). TJs, AJs and GJs are similar in that they are formed of clusters of transmembrane proteins associated with a cytoplasmic plaque comprised of scaffolding proteins, signalling molecules and cytoskeleton components[50]. These junctions link the cytoskeleton and the cell membrane and can transduce signals to and from the cell.

TJs consist of tetraspan transmembrane proteins, such as occludins, tricellulin and claudins, and single span transmembrane proteins such as junctional adhesion molecules (JAMs) -A, -B -C and -D[48]. There are 24 claudins, expressed in a tissue specific manner. Their extracellular loop structure creates charge-selective channels that determine the ion selectivity of the paracellular barrier[51, 52]. JAMs regulate the leukocyte adhesion and transmigration across the endothelium and contribute to the formation of cell polarity[53, 54]. In addition to regulating paracellular permeability, TJs also supress proliferation via the interaction between ZO-1 and ZONAB and the suppression of Raf-1 signalling by occludin[55, 56]. Endothelial AJs contain VE-Cad anchored to the cytoskeleton by β-catenin and plakoglobin[48, 57], alongside other actin-binding proteins like vinculin and α-actinin[58]. AJs can be destabilised by the Proto-oncogene tyrosine-protein kinase (Src)-facilitated phosphorylation and subsequent ubiquitin-mediated internalisation of VE-Cad[59, 60], whereas Ang-1 or basic

fibroblast growth factor (bFGF) can inhibit VE-Cad internalisation and help maintain vascular integrity[61, 62].

Healthy, resting endothelium secretes basal levels of nitric oxide (NO) continuously[16, 63]. This NO synthesis and subsequent release from the endothelium is increased in response to a variety of molecules, such as, acetylcholine, histamine, thrombin, serotonin, ADP, bradykinin or norepinephrine as well as in response to shear stress[16, 64, 65]. ECs generate NO from L-arginine and NADPH using the enzyme Endothelial NO Synthase (eNOS) which exists in two isoforms: a constitutively active, calcium-dependent isoform and a cytokine-inducible Ca^{2+}-independent isoform[63, 66]. NO relaxes vascular tone and maintains vascular homeostasis in a variety of ways. For example, NO relaxes vascular smooth muscle by activating guanylate cyclase, resulting in increased cGMP, which in turn decreases smooth muscle Ca^{2+} levels to promote vasodilation[64, 67]. NO released into the lumen inhibits platelet activation to maintain a quiescent state of anti-coagulation[68, 69]. NO also inhibits the adhesion of leukocytes to the vessel wall by modulating the expression or function CD11/CD18 on the surface of leukocytes[70]. ECs also secrete prostacyclin which inhibits platelet adhesion to the vessel wall[71]. In this relaxed state, ECs facilitate the transport of metabolic molecules across the endothelium, regulate vascular tone and contribute to lipid homeostasis, summarised in Figure 1.1 b and 1.1 d.

Conversely, Tumor Necrosis Factor-α (TNFα), Lipopolysaccharides (LPS), Histamine, C-Reactive Protein (CRP), IL-1/-6/-8 and Thrombin all elicit an inflammatory or pro-coagulant response from the endothelium where release of p-selectin, VWF and other signalling molecules from WPBs results in platelet activation, adhesion and ultimately, thrombosis[12]. Because this pro-inflammatory phenotype can be induced by vascular injury, leukocyte adhesion is also increased to promote immune function at sites of injury; vascular cell adhesion molecule (VCAM) and intercellular adhesion molecule (ICAM) are both leukocyte receptors expressed on activated ECs[72]. VWF is a glycoprotein involved in blood clotting; a deficiency in VWF causes Von Willebrand Disease (VWD) characterised by delayed clot formation and prolonged bleeding[73]. VWF contains collagen binding domains, platelet binding domains and multimerization domains[73]. VWF polymerises, head-to-head and tail-to-tail, into long tubular structures in WPBs where it is stored until endothelial activation or vessel wall injury. Once secreted and under flow, VWF unfolds and the multimers act as a rope that catches and tethers

circulating platelets to collagen that is exposed at sites of vascular injury[73, 74]. Platelets are anuclear cellular fragments derived from megakaryocytes that aggregate when activated and contribute to blood clot formation in the coagulation cascade described below[74]. Platelets are activated by their binding to VWF through their platelet glycoprotein 1b (GP1b)-V-IX complex, and the binding of platelet α2β1 and glycoprotein VI (GPVI) to collagen. Platelet interaction with all three proteins leads to platelet aggregation and thrombus formation[74]. Thromboxane and ADP released from damaged ECs also activates platelets[75]. VWF may also contribute to the regulation of angiogenesis. siRNA knockdown (KD) of VWF resulted in increased angiogenesis in HUVECs, alongside increased angiopoietn-2 and increased VEGF dependent proliferation and migration. The same study found increased vascularisation in VWF deficient mice[76].

The coagulation cascade involves a large number of proteins and enzymes called clotting factors (f), some of which are named using roman numerals here, for example, factor VIIa becomes fVIIa (where the a denotes the activated form). Fibrinogen is also called fI, prothrombin is fII and VWF is fXVI. Many of the clotting factors exist as inactive precursors that are activated by proteolytic processing and, when activated, exhibit proteolytic function themselves[77]. One pathway of the coagulation cascade starts with an inactive integral membrane protein called tissue factor (TF) or fIII which associates with fVIIa in blood plasma to form an active serine protease enzyme. This enzyme in turn activates coagulation by converting fIX to fIXa and fX to fXa[77]. These associate with fVIIIa and fVa respectively, leading to the release of thrombin, which processes fibrinogen to fibrin and directly activates platelets[77]. Fibrin freely associates to form fibrin clots, which will aggregate platelets and contribute to the clot formation[77]. Activated platelets undergo morphological changes, which increase their surface area, and release α- and Dense granules[74]. The α-granules contain P-selectin, fibrinogen, fibronectin, fV, fVIII, PDGF and TGFα. Dense granules contain ATP, ADP, calcium, serotonin, histamine and epinephrine[78]. TF is found in the membrane of many cells, including cells that surround larger blood vessels and keratinocytes in the skin, to form a protective haemostatic layer around blood vessels[79]. The coagulation cascade is only started when many conditions are met. fVII must first be proteolytically converted to fVIIa, TF in the membrane of non-endothelial cells must then be in contact with blood plasma to pick up fVIIa, phospholipids are required for the binding of fIX and fX and damaged cell membranes are more

likely to contain the active TF:fVIIa complex (reviewed in[77]). Conversely, tissue factor pathway inhibitor (TFPI) is expressed in resting ECs as two isoforms, TFPIα and TFPIβ. TFPIα is secreted and TFPIβ is expressed on the cell surface[80]. TFPI potently inhibits fVIIa[81] and fXa[82] and so impedes two early stages of coagulation to regulate hemostasis[83].

Endothelial homeostasis between these pro- and anti-coagulation states is vital to maintaining a healthy vasculature; de-regulation of these cell behaviours in EC dysfunction contributes to hypertension and atherosclerosis, pathological thrombosis, stroke and infarction[14]. One example of EC dysfunction is characterised by unregulated, chronic endothelial activation accompanied by a loss of anti-thrombotic signalling, whereby ECs switch to a pro-inflammatory or pro-coagulation state unnecessarily[17]. This chronic inflammation, like that found in rheumatoid arthritis, can contribute to atherosclerosis. This is a disease of blood vessels which is characterised by a build-up of oxidised low-density lipoprotein (oxLDL), ECM proteins, oxLDL activated macrophages and ECM-secreting vascular smooth muscle cells (VSMCs) in the vessel wall, called an atherosclerotic plaque[84]. The plaque is full of pro-thrombotic molecules and can facilitate the aggregation of platelets, creating microthrombi. The plaque can rupture, releasing ECM proteins and microthrombi into the blood stream which can lead to vessel blockages and stroke[84]. EC dysfunction contributes to atherosclerosis by upregulating the expression of platelet and leukocyte adhesion molecules on the EC surface[17, 85]. Additionally, the decrease in NO seen in EC dysfunction results in increased VSMC proliferation[86], increased vasoconstriction and increased platelet and leukocyte adhesion to vessel walls, further contributing to atherosclerotic plaque build-up in blood vessels and reducing blood flow[87]. Inflammatory mediators can also increase EC expression of TF[77], which increases the likelihood of the coagulation cascade being triggered and erroneous blood clot formation in pathological thrombosis. Sustained chronic inflammation can result in apoptosis or detachment of ECs into the blood stream in endothelial dysfunction; high levels of TNFα can stimulate apoptosis via decreased p53 and increased p73[88]. These detached Circulating ECs (CECs) or EC microparticles released from apoptotic ECs, are elevated in peripheral blood from patients with myocardial infarction[89, 90]. CEC quantification can then be used in the assessment of EC dysfunction[91-93] or vascular injury[94]. When ECs are activated in inflammatory conditions, the surface expression and subsequent release of VCAM1, ICAM1 and E-selectin is increased, providing another way to determine EC dysfunction[95-97].

EC damage can be repaired to an extent by circulating endothelial progenitor cells (CEPCs) which have a higher proliferative potential and are derived from bone marrow; CEPCs migrate to sites of injury where damaged ECs have detached and proliferate to repair the endothelium[98, 99]. CEPCs are distinct from CECs and express immature markers CD34 and CD133 whereas CECs and mature ECs express markers of endothelial maturity MCAM and are negative for CD133[99-102]. Elevated CECs or CEPCs in peripheral blood have been found in a wide range of cancers including lymphoma, melanoma and glioma, in breast, colonic gastric, oesophageal, ovarian, testicular and prostate among others[103-107]. These circulating ECs have angiogenic potential and could vascularise tumours, helping them to grow.

Reactive oxygen species (ROS) are highly reactive free radicals such as the superoxide anion (O_2-·), hydroxyl radical (HO·), nitric oxide radical (NO·) or hydrogen peroxide (H_2O_2). Low levels of ROS are generated normally during respiration and metabolism and they are essential signalling molecules[108]. However, increased ROS are produced alongside inflammation and injury. When the oxidative potential of ROS outstrips the endogenous anti-oxidant defence systems, these molecules become destructive and this is termed oxidative stress. Increased ROS concentrations will cause cell injury and eventually cell death[109]. In the endothelium high levels of ROS can increase vascular permeability[110, 111] and promote leukocyte adhesion[112, 113] contributing to endothelial dysfunction. Increased ROS has been shown to decrease eNOS expression in bovine ECs[114], which could lead to a decrease in vasodilatory NO secretion and a tip towards an inflammatory phenotype. The ROS O_2-· converts NO to peroxynitrite (ONOO-·), another powerful oxidant. This decreases the bioavailability of NO, resulting in a decrease of NO signalling which would normally relax vascular tone and promote an anti-inflammatory state[115]. Additionally, in response to ROS, a number of proinflammatory genes are upregulated, further contributing to a pro-inflammatory and atherogenic phenotype[116]. The activation of pro-inflammatory pathways also results in increased ROS production which locks the ECs into a cycle of oxidative stress, damage and inflammation resulting in EC dysfunction and cardiovascular disease progression. ROS also oxidatively modify other molecules, such as lipoproteins and phospholipids, which when oxidised, contribute to atherogenesis[117]. Finally, ROS can result in eNOS damage, if the eNOS enzyme becomes dysfunctional it can uncouple oxygen reduction from NO synthesis which will result in further ROS production[116]. In conclusion, oxidative stress caused by increased ROS promotes an inflammatory phenotype

that contributes to atherogenesis, EC dysfunction and ultimately cardiovascular disease. Other risk factors that contribute to endothelial dysfunction include smoking, ageing, diabetes, hypertension, hypercholesteremia, obesity and chronic infection (reviewed in[118]).

1.5 Endothelial Heterogeneity

Endothelial cells are highly specialised and will differ in structure and expression profile depending on their source and function. For example arterial ECs will experience higher shear stress than venule ECs, large vessel ECs are surrounded by muscle whereas capillaries consist of ECs and often pericytes, which help maintain haemostasis and tissue homeostasis[119]. ECs convert shear stress into biochemical signals via mechanotransducers such as VEGFR2, PECAM-1 and VE-Cad[37, 120]. The resulting biochemical signals activate transcription factors that maintain cell phenotype. One study[121] found that 285 genes were more abundant in

Figure 1.2: Diagram of Capillary Structure.

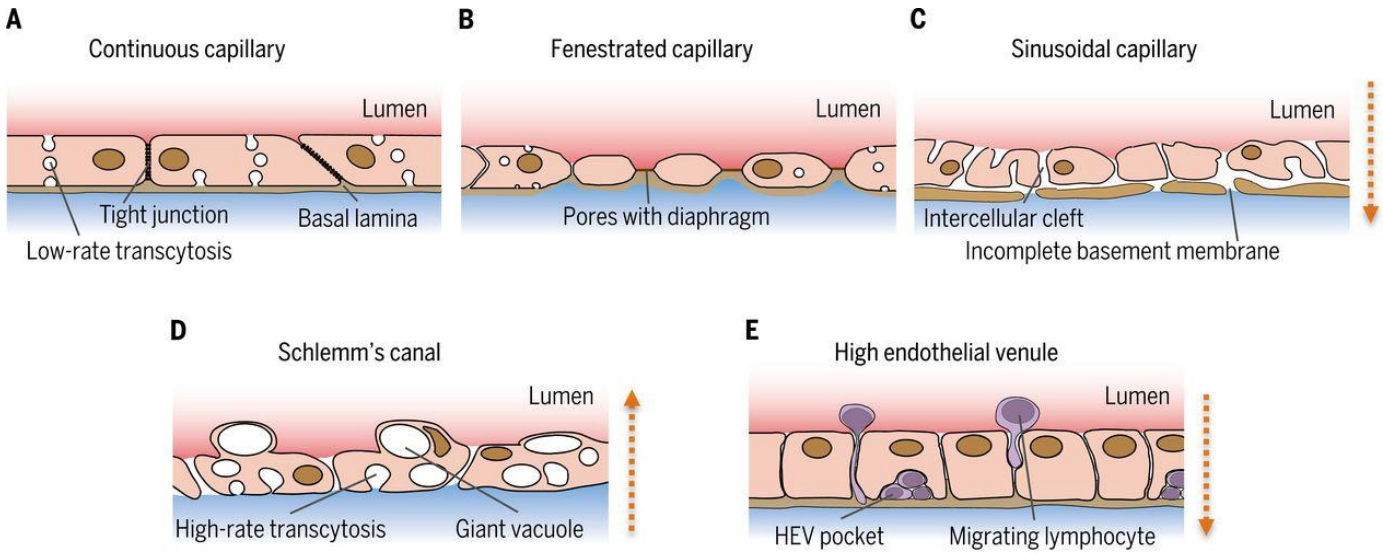

Adapted from '*Organotypic vasculature: From descriptive heterogeneity to functional pathophysiology*'[1]. Diagram showing EC heterogeneity in capillaries with respect to capillary function and vascular permeability. A) shows continuous capillary structure surrounded by the basal lamina where vascular permeability is reduced in the presence of TJs. B) shows fenestrated capillaries with gaps between the ECs to allow increased vascular permeability. C) shows sinusoidal capillaries found in liver where the basal lamina is incomplete allowing for diffusion of molecules. D) shows the structure of the endothelium in the Schlemm's canal where large vacuoles are present to allow for the transport of aqueous humor in the eye and E) shows vessel structure in HEVs, which are involved in lymphocyte migration.

saphenous vein ECs (SVECs) than coronary artery ECs (CAECs), and that many of these genes were associated with atherosclerosis related pathways. 111 genes were upregulated in CAECs, relating to inhibitors of proliferation and lipid metabolism. The same study found that stimulation with low-density lipoprotein (LDL) induced greater changes in gene expression in CAECs than SVECs, again highlighting differences in functional response between different ECs. Additionally, CD36, a glycoprotein involved in the transport of fatty acids into cells, is expressed on HDMECs but not HUVECs[122].

Capillaries can be described as continuous, fenestrated and sinusoidal (Figure 1.2). Continuous capillaries are found ubiquitously including in the brain; they form a barrier that allows free diffusion of water, very small molecules and lipid soluble molecules with tightly controlled active transcytosis of larger molecules such as glucose (Figure 1.2A). Fenestrated capillaries, like those in the intestine, endocrine glands and kidneys, are more permeable and are filled with small pores (fenestrations) that allow free transport of larger molecules (Figure 1.2B). Sinusoidal capillaries that have large gaps between cells and in the associated basal lamina which allow the free transport of larger molecules are found in the bone marrow, spleen and liver (Figure 1.2C). ECs in the anterior eye chamber acquire a Schelmm's canal (Figure 1.2D) that allows fast transport of aqueous humour from the eye. Also, high endothelial venules (Figure 1.2E) found in lymphoid tissues[123] contain specialised cuboid ECs that facilitate lymphocyte migration (reviewed in[1]).

Caveolae are flask-shaped invaginations in the membrane of many cell types, especially abundant in ECs, that are rich in cholesterol, glycosphingolipids and caveolins. Caveolae are important in cholesterol transport, endocytosis, potocytosis and cell signalling[124]. They are thought to be involved in the transportation of molecules across the EC monolayer. It is possible that caveolae fuse to form channels through some ECs. Muscle ECs contain many caveolae to facilitate the differentiation and transport of molecules to the muscle tissue whereas blood brain barrier (BBB) ECs contain very few caveolae as they need to tightly restrict the flow of solutes to the brain[125]. Caveolae are also far more prevalent in capillary ECs than in artery or vein endothelial cells[126]. It is thought that caveolae can fuse to form VVOs, which can form channels through ECs. VVOs are more prevalent in venule ECs[127]. Matrix metalloproteinases (MMPs) are a family of zinc-dependent endopeptidases and their expression also differs between ECs, HUVECs express higher levels of MMP1, 2 and the MMP

inhibitor, TIMP1, than neonatal foreskin ECs (NFECs) but after phorbol 12-myristate 13-acetate (PMA) stimulation, NFECs express much higher TIMP1 and MMP9 than HUVECs[128]. Tumour microvessels are generally more angiogenic and more permeable than normal blood vessels. This increased permeability is partly due to the increased presence of VVOs[129, 130]. ECs from the same tissue also show heterogeneity largely because they are adapted to constantly respond to temporal changes in the microenvironment, making them susceptible to variation. Therefore, it is vital to use the correct ECs to study different endothelial traits, for example HUVECs would be unsuitable for studying the BBB and large vessel artery ECs would be inappropriate for the study of glomeruli renal EC function. However, there are general traits shared by ECs, such as inflammatory response and angiogenic potential, and HUVECs can be used to study these. HUVECs are a useful tool for studying ECs due to their well-defined characteristics, availability affordability, human origin and robust endothelial phenotype. In addition, HUVECs can be obtained as pools from several donors, limiting batch-to-batch variability. HUVECs were chosen as model endothelial cells throughout this project[131, 132].

It is thought that some of the specialisation and differentiation in ECs is lost once they are isolated and cultured *in vitro*. In one study of rat lung ECs, 41% of plasma membrane proteins expressed *in vivo* are not detectable *in vitro*[133]. Another study found that characteristics specific to high endothelial venule ECs (HEVECs) isolated from tonsils were lost just two days after culturing *in vitro*, specifically, the venule-specific Duffy antigen receptor for chemokines (DARC), HEVEC-specific fucosyltransferase Fuc-TVII and type XV collagen[134]. Shear stress and haemodynamic forces contribute to the regulation of EC function and maintenance of EC phenotype; ECs will behave differently under still or flow conditions. Furthermore, ECs are generally quiescent, non-proliferative cells. The process of EC isolation and subsequent culture of cells can introduce changes in phenotype. Additionally, expansion of cells over multiple passages requires a transformation to a more proliferative phenotype. This could lead to some loss of differentiation and specialisation of ECs. Finally, culturing ECs alone does not take into account the impact of other cell types such as VSMCs, pericytes, red blood cells and immune cells that will all alter the microenvironment of the ECs and initiate changes in EC behaviour. All these points highlight important differences between *in vitro* and *in vivo* systems that must be considered when interpreting and extrapolating data. Despite their limitations, *in vitro* experiments are still a valuable tool when studying isolated pathways

and simplified biochemical interactions and are a great starting point. In contrast, *in vivo* assays are generally much longer, more complicated and more expensive but also allow for the study of complex systems in a more physiologically relevant system. This project focusses on *in vitro* studies of HUVECs as a starting point to investigating the effects of integrin modulation on HUVEC cell behaviour.

1.6 Integrins

Integrins are a family of 24 transmembrane cell adhesion receptors that form α/β heterodimers from 18-α subunits and 8 β-subunits (Figure 1.3). Their primary function is to facilitate adhesion of cells to each other and the ECM. They have an extracellular 'head' N-terminal domain and a cytoplasmic 'tail' C-terminal domain, and mediate signal transduction between the ECM and the cytoplasm by linking outside signals to the cytoskeleton; they form bi-directional signalling hubs capable of integrating signals from multiple pathways[7, 135, 136]. Integrins interact and form clusters with co-receptors and other integrins to amplify signals[137]. Integrin expression is cell type-dependent, and most integrins bind a selection of ECM or cell-surface ligands. They play essential roles in embryonic development, cell migration, proliferation and angiogenesis, and have been implicated in tumorigenesis and inflammation[138]. Figure 1.4 shows the general structure of integrin receptor heterodimers. Both α and β subunits have large extracellular domains with multiple subdomains. The α subunit has a β-propeller structure at the 'head' end, followed by 'thigh' and 'calf' domains, a transmembrane domain and finally a small cytoplasmic domain. The β subunit has a β-I-domain, a PSI (plexin/semaphoring/integrin) domain, a hybrid domain, four epithelial growth factor (EGF) domains and a cystatin-like domain followed by a transmembrane domain and a small cytoplasmic tail.

Nine of the integrin α subunits contain an αI-domain (Figure 1.4), an approximately 200 amino acid insertion in the β propeller structure, that shares homology with VWF A domains. This αI-domain is a Rossman fold with five β sheets surrounded by seven α-helices. It contains a metal-ion-dependent adhesion site (MIDAS) that requires co-ordination of Mg^{2+} for the binding of the αI-domains to their ligand[7, 136]. Conformational changes take place in the αI-domain when Mg^{2+} is present, allowing the αI-domain to bind to the relevant ligand. In the case of α2β1 a C-helix is also present around the MIDAS, creating a groove that can bind to a glutamate residue in collagen[8, 139]. The αI-domains show a lot of homology between integrins,

but the rest of the subunit is variable[7]. It is thought that cells express an excess of β-subunits and the expression of α-subunits determines surface receptor expression[140]. For the integrins that have an αI-domain, the α-subunit determines ligand specificity. The β-subunit is connected to the cytoskeleton and also contains an I-domain, termed a βI-domain, that contains a MIDAS, and a site that is adjacent to the MIDAS called the ADMIDAS[7].

Integrins exist in active or inactive conformations. For example the platelet integrin αIIbβ3 exists in high density on the surface of platelets but in an inactive conformation[141], otherwise αIIbβ3 would bind circulating fibrinogen and could lead to unnecessary platelet activation, aggregation and thrombosis. Instead, αIIbβ3 is activated from within the platelet, allowing subsequent binding to VWF, fibrinogen and fibronectin[142]. A similar mechanism works with leukocytes; in resting leukocytes, the β2 subunits are inactive, only becoming activated under inflammatory conditions where they adhere to ICAM on the surface of ECs[143].

Figure 1.3. Diagram of The Integrin family.

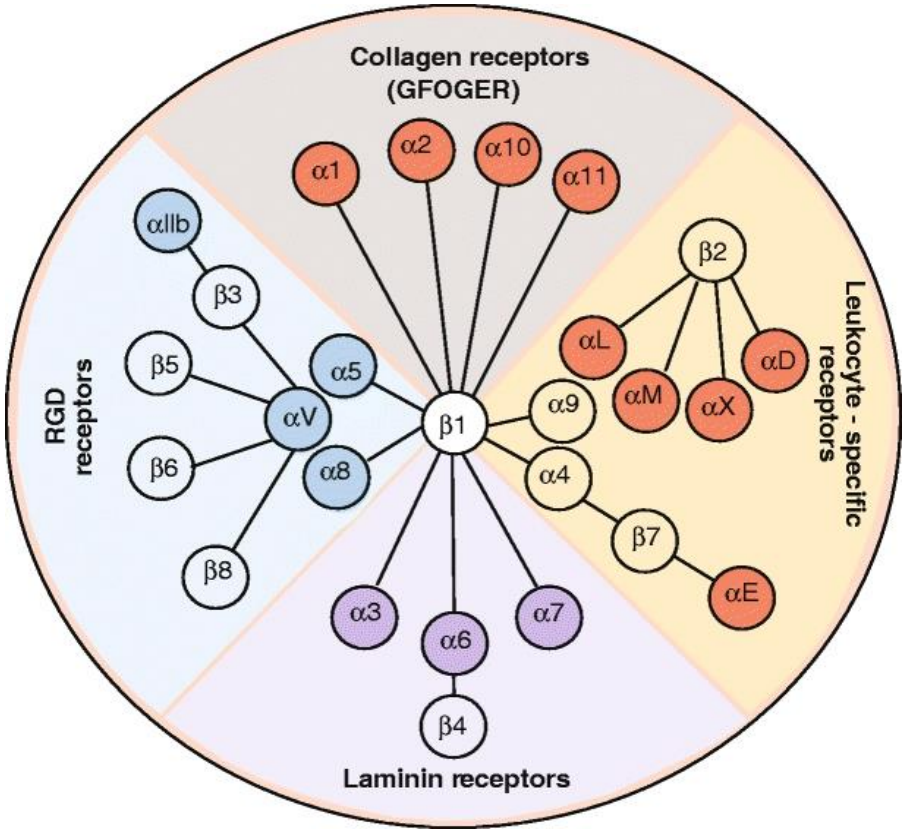

Adapted from '*Integrins', Barczyk 2010* [7]. This diagram shows the entire mammalian integrin family and describes the heterodimers that are made from each class of monomers. The integrins are organised here by the ligands that they adhere to, or the cells they are specific to.

There are four known collagen-binding integrins, α1β1, α2β1, α10β1 and α11β1. All are thought to be expressed in ECs[7, 136], α1β1 and α2β1 also bind weakly to laminin[144, 145]. The range of pathways involving integrins highlights their importance in tissue function and homeostasis across a variety of organs, Table 1.1 summarises KO studies of each integrin and their effects on embryonic development. Some integrin KOs result in severe, embryonic lethal phenotypes (β1, α4, α5, β8, α3, α6, α8, αv, β4), some result in viable embryos with impaired leukocyte function (αL, αM, αE, β2, β7), or defects in inflammation (β6), haemostasis (αIIb, β3, α2), angiogenesis (α1, β3) or bone remodelling (β3) (reviewed in[120]). Whole organism ablation of β1 integrin in mice leads to embryonic fatal phenotype before E5.5[146] and EC specific

Figure 1.4. Diagram of Integrin Structure.

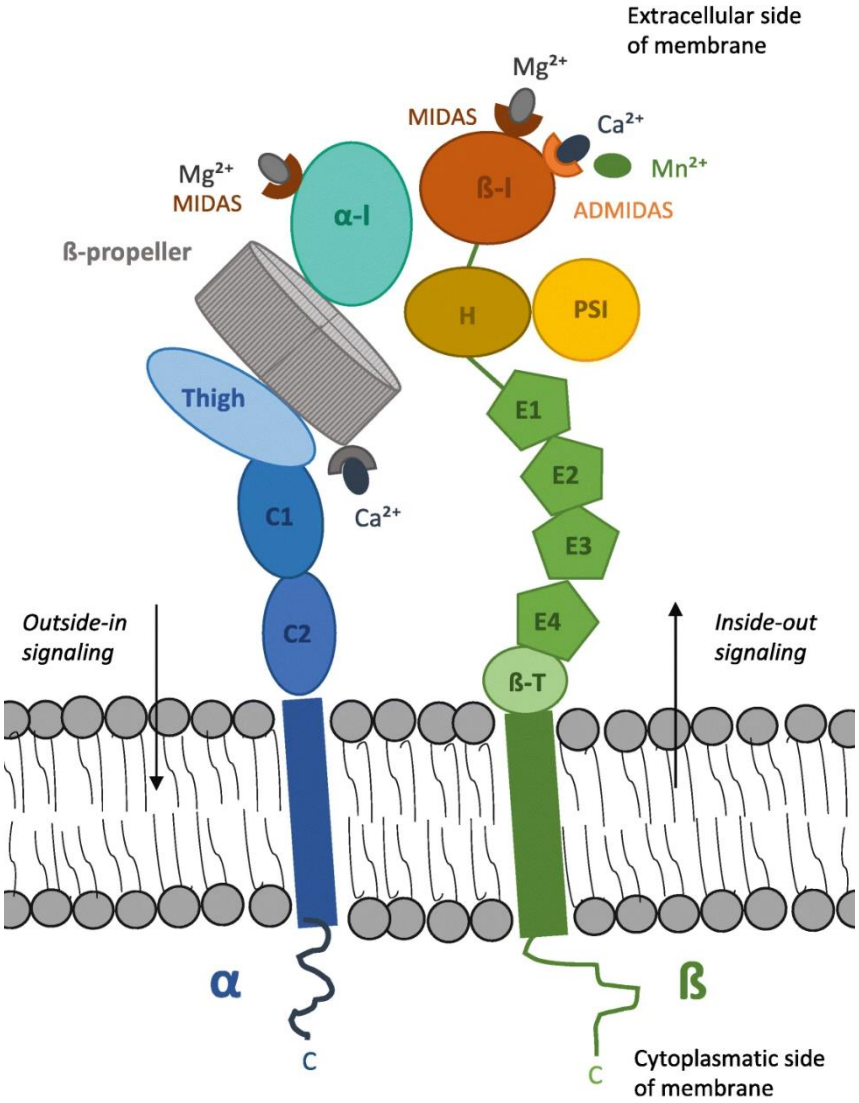

This figure shows the structure of integrin heterodimers adapted from *'The functional role of integrins during intra- and extravasation within the metastatic cascade'*[3]. The α-subunit is shown in blue with the β-propeller domain in grey. C1 and C2 denote the calf domains, metal ion binding sites are shown and labelled with the ion they bind to. The β-subunit is shown in green, orange, brown and yellow with the MIDAS and ADMIDAS shown in dark brown and pink respectively. E1-4 denotes the EGF domains and H labels the hybrid domain and β-T names the β-tail/transmembrane domain.

ablation of β1 integrin in mice results in severe vascular defects that are lethal around day e9-11.5[35, 147]. Isolated β1-null ECs showed impaired adhesion to laminin and collagen and impaired cell survival[35]. Ablation of α1 or α2 subunits has a much less severe effect, with α1 null mice producing viable offspring with minor defects in collagen synthesis and angiogenesis[148, 149]. α2-null mice show delayed platelet aggregation. However, mice deficient in both α2β1 and α11β1 show dwarfism as a result of diminished insulin growth factor (IGF) levels[150]. Integrin mediated signalling is essential for cell survival and many cell responses to growth factors are dependent on cell adhesion to a substrate via integrins. As a consequence, many cell types must be adhered to the matrix through integrins to survive[151, 152].

Table 1.1 – Effects of Integrin Knockouts in Mice

Subunit	Viability	Phenotype
α1	V, F	No obvious developmental defects, reduced tumour vascularization, minor defects in collagen synthesis and angiogenesis
α2	V, F	Few obvious developmental defects, delayed platelet aggregation and reduced binding to monomeric collagen, reduced mammary gland branching
α3	P	Kidney tubule defects, reduced branching morphogenesis in lungs, mild skin blistering, lamination defects in neocortex
α4	E11/14	Defects in placenta (chorioallantoic fusion defect) and heart (epicardium, coronary vessels). Chimeras show defects in haematopoiesis
α5	E10-11	Defects in mesoderm (posterior somites) and vascular development, neural crest apoptosis. Chimeras show muscular dystrophy
α6	P	Severe skin blistering, other epithelial tissues also defective. Lamination defects in cortex and retina.
α7	V, F	Muscular dystrophy, defective myotendinous junctions
α8	P	Small or absent kidneys, inner ear hair cell defects
α9	V	Die within 10 days of birth, chylothorax due to lymphatic duct defect
α10	V, F	Growth retardation of the long bones, abnormal chondrocyte growth and shape[153]
α11	V, F	Reduced granulation tissue formation and impaired wound contraction. Dwarfism and impaired incisors [154, 155]
αv	E10/P	Two classes: embryonic lethality due to placental defects, perinatal lethality with cerebral vascular defects probably due to neuroepithelial defects, cleft palate. Most blood vessels develop normally
αIIb	V, F	Haemorrhage, no platelet aggregation

αL	V, F	Impaired leukocyte recruitment
αM	V, F	Defective phagocytosis and apoptosis of neutrophils, mast cell development defects, adipose accumulation.
αX		Not yet reported
αD		Not yet reported
αE	V, F	Greatly reduced numbers of intraepithelial lymphocytes.
β1	E6.5	Peri-implantation lethality, ICM deteriorates, embryos fail to gastrulate. Extensive analyses of chimeras.
β2	V, F	Leucocytosis, impaired inflammatory responses, skin infections, T cell proliferation defects
β3	V, F	Haemorrhage, no platelet aggregation, osteosclerosis, hypervascularisation of tumours
β4	P	Severe skin blistering, other epithelial tissues also defective
β5	V, F	No immediately obvious developmental defects
β6	V, F	Inflammation in skin and airways, impaired lung fibrosis—all probably due to failure to activate TGFβ
β7	V	Deficits in gut-associated lymphocytes—no Peyer's patches, reduced intraepithelial lymphocytes.
β8	E10/P	Two classes: embryonic lethality due to placental defects, perinatal lethality with cerebral vascular defects probably due to neuroepithelial defects. Most blood vessels develop normally.

Table 1 adapted from *Integrins: Bidirectional, Allosteric Signaling Machines*[142]

Abbreviations – V = Viable, F = Fertile, E = Embryonic lethal, P = Perinatal lethal

Integrins α1β1 and α2β1 are the most defined in ECs and are important in regulating angiogenesis and proliferation. Addition of VEGF upregulates α1β1 and α2β1 expression, along with cell proliferation, spreading on collagen and angiogenesis[156]. While inhibitors for α1β1 and α2β1 impede angiogenesis[157-159]. The VEGF dependent interaction of collagen I with α1β1 and α2β1 induces the activation of the mitogen activated protein kinase (MAPK) pathway, which suppresses apoptosis and promotes cell survival[160, 161]. The α1β1 integrin binding to collagen also negatively regulates collagen synthesis; in α1-null mice the normal negative feedback loop does not exist and so excess dermal collagen is continually synthesised and then broken down again[162]. Because α1β1 and α2β1 have been implicated in the regulation of proliferation and angiogenesis it is not surprising that they are both implicated in cancer progression. The α1β1 integrin is upregulated in colorectal cancer[163] and knockdown of the

α1 subunit (noted ITGA1) in tumour xenografts results in reduced tumour progression in HT29 and T84 cells alongside increased tumour cell necrosis[164]. Additionally, inhibition of α1β1 integrin results in decreased tumour angiogenesis[165]. Both α1β1 and α2β1 enhance cancer cell migration and metastasis, for example, by upregulating MMP synthesis via MAPK signalling[166]. The α2β1 integrin also promotes prostate cancer metastasis to the skeleton, resulting in a poor prognosis for patients[167].

However, little is known about the expression and functions of α10β1 and α11β1 in ECs despite α10 being the second most abundant integrin transcript in early passage ECs (Haematlas database and Dr Peter Kim, unpublished work). Primarily, α10β1 is expressed in chondrocytes[7, 136] and α11β1 is expressed in fibroblasts, mesenchymal cells, skeletal muscle and osteoblasts[155, 168]. α10β1 has recently been shown to be upregulated in glioblastoma tissues derived from human patients. siRNA knockdown of α10β1 in glioblastoma cells resulted in decreased migration and increased cell death, implementing α10β1 in the regulation of cancer metastasis[169]. In addition, α10β1 is also upregulated in malignant melanoma cells compared to primary melanocytes and knockdown of α10β1 resulted in reduced migration of melanoma cells[170]. Integrin α10β1 has also been found to drive tumorigenesis and metastasis in sarcoma resulting in much poorer prognosis for patients[171].

Integrin α11β1 is a receptor for osteolectin which is involved in the differentiation of osteogenic progenitors to mature osteoblasts[172]. KO of the α11 subunit (noted ITGA11) in skeletal progenitor cells in mice results in impaired osteogenesis and accelerated bone loss in adulthood[172]. Also, α11β1, upregulated by TGFβ, plays a role in cardiac myofibroblast differentiation and KO of ITGA11 drastically changes the phenotype of hepatic stellate myofibroblast cells [173-176]. Inhibition of the hedgehog pathway decreased ITGA11 expression in hepatic stellate cells, in a mouse liver fibrosis model and in human liver slices ex vivo, leading to decreased fibrosis[176]. Integrins α11β1 and α2β1 were found to regulate the cell survival of mesenchymal stem cells; short hairpin (sh)RNA knockdown of either of these integrins resulted in mitochondrial leakage and Bcl-2 protein upregulation[177]. Given the varied roles of these integrins in other cells, it can be hypothesised that integrins are present in and have important functional roles in ECs.

Integrins bind collagen via their αI-domain to 'GxOGEx' (using the one-letter amino acid code, where O is hydroxyproline, a post-translational modification of proline, and x is any

natural amino acid) motifs located on the collagen sequence, in a divalent metal ion dependent manner[7, 136, 137, 139]. Cryptic binding sites for different integrins could also be revealed in the tertiary and quaternary structure of different collagen fibres and mesh networks, and these could be important in regulating integrin signalling. For example, one study found that ECs cultured on regularly aligned, nano-patterned collagen fibres supported EC populations with decreased monocyte adhesion (anti-inflammatory) and increased cell viability compared with cells cultured on randomly aligned matrixes[178].

1.7 Extracellular Matrix and Collagen

The ECM is a dynamic, acellular compartment present throughout mammalian tissues and is specialised for each tissue function. Fibrillar and non-fibrillar collagens are major constituents of the blood vessel ECM, which also includes fibrinogens, laminins, heparin sulphate, entactin and proteoglycans[179]. The ECM forms a structural surface for organised cell attachment that relays signals to and from the endothelium to allow ECs to react to different physiological stimuli[12]. The ECM plays an important role in regulating EC behaviour and ECs themselves modify the composition of the ECM[180]. ECs maintain and remodel their local niche by secreting ECM components including MMPs which degrade collagen, and α1β1 and α2β1 have been implicated in the regulation of both collagen and MMP synthesis[162, 181, 182]. Fragments created upon collagen cleavage can act as differential signalling molecules on a range of pathways[10]. For instance, a C-terminal fragment of the non-collagenous domain of collagen XVIII, termed endostatin, inhibits VEGF-induced EC migration[183]. Arresten, a proteolytic fragment of collagen IV, binds to integrin α1β1, resulting in the inhibition of MAPK induced cell proliferation and anti-apoptotic Bcl expression, enhancing apoptosis in ECs[184, 185]. Growth factors and other signalling molecules are also sequestered in the ECM and are released upon collagen degradation. Therefore, it is relevant to study the interactions between ECs and their surrounding matrix.

Collagen is the most abundant protein in the human body and is the main constituent of the ECM. It gives tensile strength to skin, bone, cartilage and blood vessel walls. Collagens are characterised by their triple-helical domains (THDs) (Figure 1.5), formed from 3 polypeptide α-chains containing repeating (G-X-Y) sequences where G is Glycine, X is often proline and Y is often hydroxyproline[6, 10]. The formation of the triple helix conformation is driven by a network of hydrogen bonds perpendicular to the helix axis[186], resulting in a one

Figure 1.5. Structural Representations of the Triple Helical Domains of Collagen.

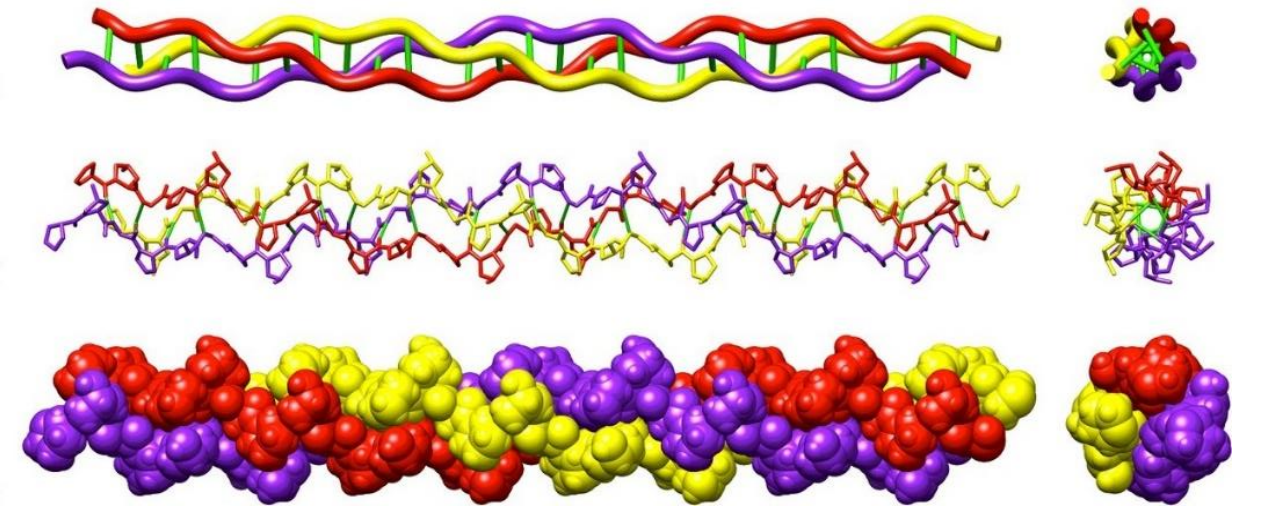

Adapted from '*Collagen Structure: new tricks from a very old dog'* Bella 2016[6]. The middle diagram shows how the side chains of each peptide residue are arranged, while the other two show the general shape of the helix

amino acid stagger between α-chains. This unique triple helix conformation is essential for the collagen assembly in fibrils which is required for the structural role of collagen within the extracellular matrix. The triple helix conformation is also necessary for the recognition of collagen-binding cell-surface receptors and cell-secreted proteins and is crucial to its biological function. Members of the collagen family form a diverse family of 28 proteins. Figure 1.6 summarises the different α-chains of the collagen family and how they are structured to give an idea of the diversity of the collagen family. Collagens are organised into tertiary structures and form networks in the ECM; collagens II and III are fibrillar homotrimeric proteins, whereas collagens I, IV and XI are heterotrimeric[10, 187]. The α-chains of collagens I, II, III, V, VIII and X are almost entirely triple helical, whereas a helical structure makes up only 10% of collagen XII[10] and collagen VI α-chains contain mostly VWF A-domains that participate in protein-protein interactions. Collagen IV is a major protein constituent of the endothelial ECM, alongside laminin, and has been shown to influence EC behaviour and proliferation[180]. Other collagens found in the basal lamina include: collagen I, III, IV, V, VI, VIII[84]. The structure of collagen IV is interesting in that the long THD is peppered with non-helical regions, allowing for

Figure 1.6: Representations of the Collagen Family α-Chains

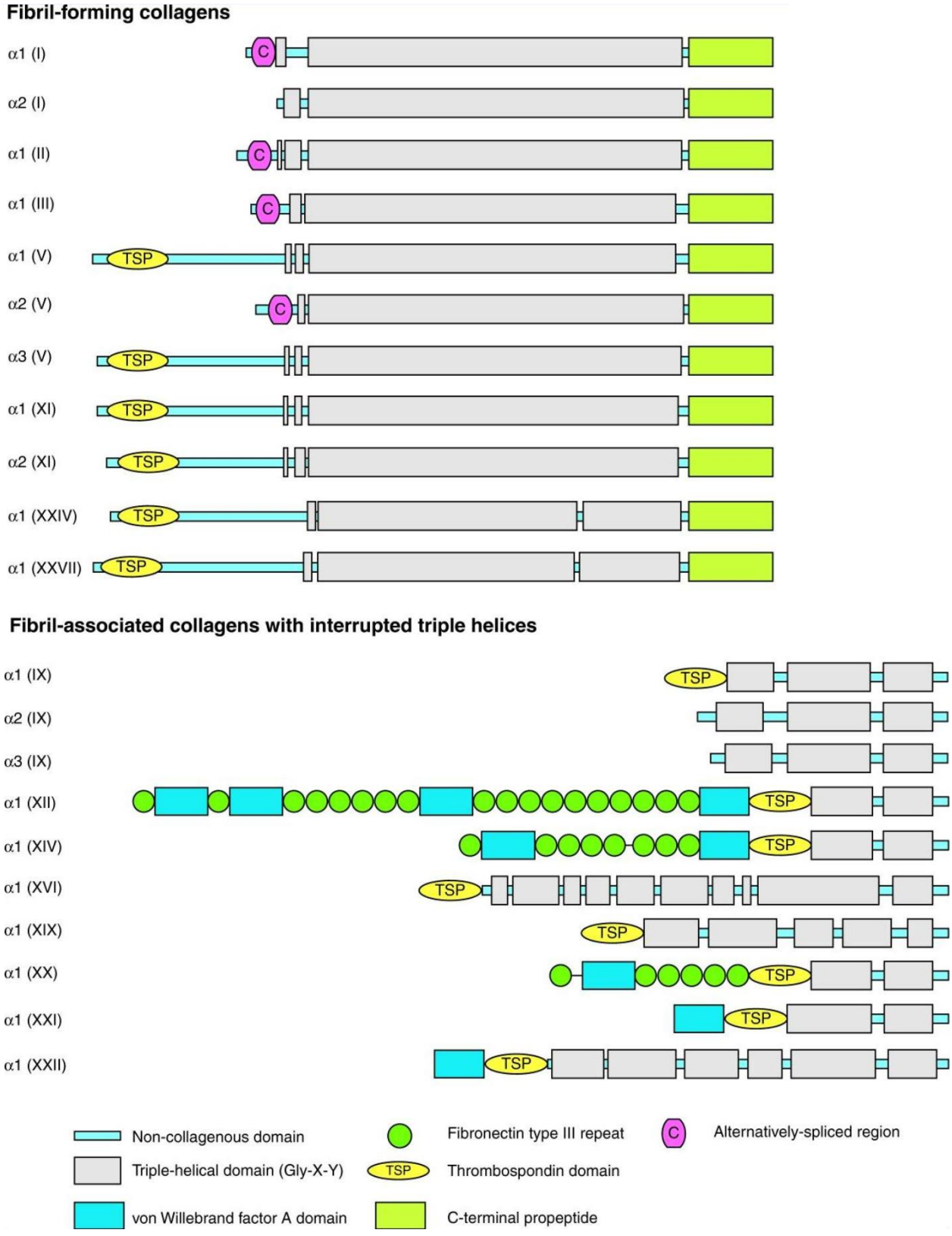

Adapted from '*The Collagen Family*', Ricard-Blum 2011[10]. This diagram shows the different domains and different structures of all the members of the collagen family in depth. The fibril forming collagens are mostly triple helical whereas the fibril associated collagens are more varied containing plenty of non-collagenous interruptions in the THP domains.

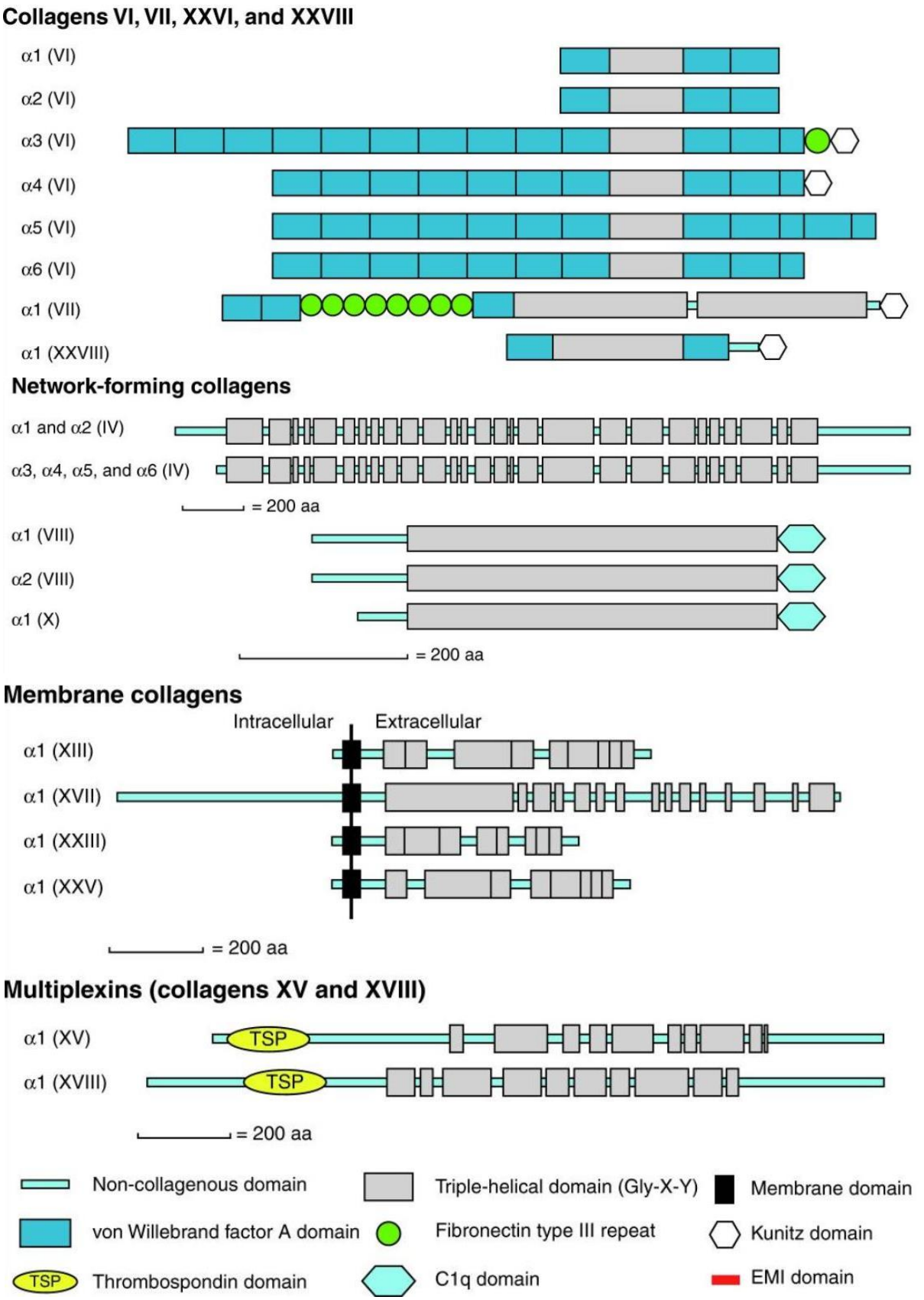

Figure 1.6 continued: Adapted from '*The Collagen Family*', Ricard-Blum 2011[10]. This diagram illustrates the variety in the collagen family. The α-chains of collagens XI, XII, XXVI and XXVIII contain mostly VWF A-domains whereas the network forming collagen IV is almost entirely THD interrupted with lots of short non-collagenous domains and the membrane collagens contain a unique membrane domain.

flexible sections that can crosslink other matrix proteins. Collagens XIII, XVII, XXIII and XXV are transmembrane collagens[188, 189] which could play a role in signal transduction from the ECM. Collagen XVII has a long cytoplasmic non-collagenous domain whereas XIII, XXIII and XXV have much shorter intracellular domain. Induction of collagen XIII expression in ECs can mediate transmigration of monocytes along the EC monolayer in renal fibrosis[190].

Collagens form fibrils and networks with other collagens, and the supramolecular structure depends on collagen composition. For example, collagens II, III, XI and IX will associate to form fibrillar structures whereas collagen IV will form networks, collagen VI will form beaded filaments and collagens VIII and X form hexagonal structures[10]. Fibril-associated collagens will then associate with collagen fibrils, adding additional functional domains for protein-protein interactions. Collagens are degraded by MMPs in many physiological processes related to cell migration, development and tissue repair. However, these functions can be highjacked in pathological processes such as tumour metastasis[166, 191]. In this project, soluble collagen I was mainly used as it is found ubiquitously in the ECM, is commercially available at a reasonable cost and is made almost entirely of THD structure. Collagen I also contains several known integrin binding sites and so proved valuable for studying integrins in ECs. Collagen IV was tested alongside collagen I in preliminary experiments but since no advantage was seen using the much more expensive collagen IV, it was decided that collagen I would suffice for the majority of studies here. Geltrex™ (LDEV-free reduced growth factor basement membrane matrix), the Thermo equivalent of Matrigel, was used for all assays analysing tube formation. Geltrex™, like Matrigel, is a basement membrane matrix extracted from murine Engelbreth-Holm-Swarm tumours, containing mostly collagen IV, laminin, entactin and heparin sulphate proteoglycans along with some growth factors and cytokines in low levels[192, 193].

1.8 The Regulation of Migration in Endothelial Cells

Cell migration is a tightly controlled process involved in development, wound healing, immune response and angiogenesis[194] but can also be pathological when deregulated, for example when cancer cells become highly motile and metastasise[194] and in chronic inflammatory diseases, vascular diseases, multiple sclerosis, osteoporosis and mental retardation[194]. ECs are generally non-migratory in stable blood vessels but can be stimulated to migrate during wound healing or angiogenesis. For directional migration to occur the ECs must polarise in response to a chemoattractant such as VEGF so that a leading and trailing

edge are established[161, 195]. The leading edge sends out membrane protrusions called filopodia that adhere to the ECM ahead of the cell. The filopodia are driven by cytoskeletal actin polymerisation[194, 196, 197]. The adhesion of filopodia to the ECM will stabilise the protrusions and link the cytoskeleton to the ECM. This creates traction between the ECM and the cell cytoskeleton, pulling the cell forward. The trailing edge must then detach from the ECM to allow the whole cell to migrate[194]. Each stage of cell migration must be carefully regulated from cell polarisation to filopodia protrusions to cell attachment and de-adhesion. Integrins are adhesion receptors and so play an important role in each of these stages[197]. Strong adhesions in the filopodia will enhance cell migration whereas strong adhesions in the trailing edge will slow down migration and so it's imperative that localised regulation of processes takes place. Both α1β1 and α2β1 have been implicated in VEGF mediated EC migration[160] and α10β1 has been implicated in the regulation of glioblastoma migration and so could also play a novel role in EC migration here[169].

1.9 The Regulation of Angiogenesis in Endothelial Cells

Angiogenesis, the process of forming new blood vessels from pre-existing vasculature, is tightly regulated and complex. The ECM provides both a physical scaffold and a signalling platform for ECs. In a concerted response to pro-angiogenic signals, the ECs must remodel the ECM, breaking cell-cell and cell-matrix adhesions, change their morphology, invade surrounding tissue, migrate to a new position and then re-form cell-cell and cell-matrix contacts[18, 179, 198]. Many signalling molecules and pathways are involved, for example VEGF and bFGF are known to enhance angiogenesis by stimulating ECs to secrete MMPs[166, 199]. Resulting degradation of the ECM also releases ECM-bound cytokines and growth factors, like VEGF, which further stimulates cell proliferation and angiogenesis. Once ECs have sprouted and started to form a new branch of blood vessel, other cells like pericytes must be recruited to stabilise the mature blood vessel[179, 180, 200]. Hypoxia, a main driver of angiogenesis, will induce VEGF expression in many tissues, including the endothelium, to stimulate angiogenesis in tissues that are not receiving enough oxygen. Hypoxia is detected by transcription factors called hypoxia-inducible factors (HIFs). In the presence of oxygen HIFs are hydroxylated, then ubiquitinylated and targeted for degradation by HIF-prolyl hydroxylases (HIF-PHs). In hypoxia, the HIF-PHs cannot hydroxylate HIFs and they are not subsequently ubiquitinylated resulting in a build-up of HIFs and the subsequent transcription of HIF-targeted genes like VEGF[201, 202].

Pathogenic deregulation of angiogenesis is associated with wound healing defects, rheumatoid arthritis, diabetic microvascular disease, macular degeneration, ischemia and inflammation[179]. Angiogenesis is upregulated in many cancers and is essential in supplying tumour blood supply. ECs isolated from tumours have been found to express higher levels of collagens I and III than ECs from surrounding healthy tissue[203]. The role of collagen-binding integrins in regulating angiogenesis has been partly investigated. For instance, a range of studies have shown that VEGF mediates integrin α1β1 and α2β1 up-regulation in migrating ECs, and inhibition of these integrins blocks angiogenesis without effect on existing vasculature[157]. As a corollary, inhibiting synthesis of collagen I and IV, the primary ligands for α1β1 and α2β1, inhibits capillary formation[198]. Specific inhibition of α1β1 by Obtustatin inhibits angiogenesis in a CAM assay and Lewis lung carcinoma syngeneic model[204]. In conclusion it is been demonstrated that VEGF upregulates angiogenesis in a α1β1- and α2β1-dependent manner; these integrins are established as regulators of angiogenesis. However, the roles of α10β1, relatively abundant in HUVECs, and α11β1 in angiogenesis have not yet been explored.

1.10 Other Endothelial Collagen Receptors

ECs may also express some other collagen binding proteins, for example platelet-glycoprotein VI (GPVI), discoidin domain receptor (DDR)1, DDR2, secreted protein acidic and rich in cysteine (SPARC), osteoclast-associated immunoglobulin-like receptor (OSCAR), leukocyte-associated immunoglobulin-like receptor 1 (LAIR-1) and G-protein-coupled receptor 56 (GPR56).

SPARC is a macromolecule secreted in the ECM that modulates cell-matrix interactions, SPARC binds collagen but has no adhesive properties for cells. SPARC is anti-proliferative and de-adhesive *in vitro*[205, 206], it binds to and inhibits platelet derived growth factor (PDGF) and VEGF[206] and it mediates the disassembly of focal adhesions in ECs leading to cell rounding[207]. There are conflicting studies for the role of SPARC in cancer progression. On the one hand, SPARC seems to be generally anti-tumorigenic as solid tumours implanted in SPARC-null mice grow much larger than in control mice with no change in angiogenic growth factor expression[208]. The same study also found alterations in collagen synthesis resulting in smaller, less mature collagen fibres suggesting a role for SPARC in modulating the ECM[208]. Additionally, SPARC also regulates the secretion of the ECM proteins fibronectin and laminin[209]. In glioma

and neuroblastoma SPARC expression impairs tumour growth and angiogenesis[205]. However, SPARC has also been shown to promote metastasis and invasion of cancer cells in melanoma, glioma, and carcinomas in breast and pancreas (reviewed in[205]). SPARC is expressed in microvascular ECs in response to VEGF[210, 211] and it is thought to regulate EC shape and barrier function by increasing vascular permeability[211, 212]. SPARC contributes to the regulation of the BBB permeability[210]. SPARC is also upregulated during blood vessel development and after vascular injury, suggesting a role in angiogenesis and wound healing[213].

DDR1 and DDR2 are collagen-binding, transmembrane, receptor tyrosine kinases RTKs that adhere to, and are activated by, several types of collagen[214]. They contain a collagen-binding discoidin-domain alongside transmembrane, and tyrosine kinase domains[215]. DDR1 and DDR2 are proposed to bind to a GVMGFO motif found in collagen I, II and III. Interestingly, this is the same sequence proposed to bind to VWF and SPARC[216]. DDR1 is expressed in epithelial cells and immune cells such as T-cells whereas DDR2 is expressed in mesenchymal cells, fibroblasts, chondrocytes and neutrophils[215]. DDR1 and DDR2 are both expressed in de-differentiated epithelial cancers and fibrosarcoma cells[215]. DDRs shed their ectodomains after collagen binding via a disintegrin and metalloproteinase (ADAM10) mediated proteolysis, that terminates DDR signalling[217]. DDRs are involved in the regulation of cell migration, which is unsurprising given their role in cell adhesion. DDR1 expression increases migration in squamous cell carcinoma cells, T-cells, THP-1 human monocytic cells and glioma cells, possibly due to the DDR-mediated upregulation of MMP expression (reviewed in[215]). DDR2 has been shown to regulate fibroblast migration through Matrigel[218] and VSMC migration in hypoxic conditions[219]. Both DDRs interact with integrins resulting in increased integrin activation and increased integrin-mediated cell adhesion in human embryonic kidney (HEK293) cells[220]. It has been proposed that DDRs are microenvironment sensors that detect damaged collagen fibres because the binding sites for DDRs are obscured in larger, highly ordered fibrils but exposed in newly formed or damaged fibrils[215]. DDRs have not been studied in ECs but are shown to interact with α2β1 and α1β1, to upregulate integrin-mediated cell adhesion. Studying DDRs in ECs is therefore also relevant to this project.

OSCAR is a collagen binding receptor found in osteoclasts, monocytes, granulocytes, macrophages, and monocyte-derived dendritic cells[221, 222]. OSCAR regulates osteoclast differentiation and dendritic cell migration and survival and has been implicated in the

regulation of the osteoimmune system[221]. OSCAR promotes immune cell activation, maturation and survival and promotes proinflammatory signalling. Ligation of OSCAR triggers intracellular Ca^{2+} release and secretion of interleukin (IL)-8 which is a cytokine associated with chemotaxis, cell adhesion and angiogenesis[221, 223]. OSCAR has been detected, but not well characterised, in ECs[221]. OSCAR has been found in the membrane fraction of ECs and is thought to promote EC survival in HUVECs[224]. Expression of OSCAR is upregulated by ox-LDL in HCAECs[224].

LAIR-1 is a transmembrane glycoprotein collagen receptor that inhibits immune cells, presumably to downregulate unnecessary immune response[225]. LAIR-1 is expressed on almost all immune cells including T-cells, B-cells, monocytes, monocyte derived dendritic cells, eosinophils, basophils and mast cells[226]. LAIR-1 is also found on CD34+ haematopoietic progenitor cells, peripheral blood cells and thymus lymphocytes[226]. Crosslinking of LAIR-1 on natural killer immune cells using antibodies inhibits their function in lysing targeted cells and LAIR-1 can also inhibit T-cell mediated cytotoxicity[227]. LAIR-1 KO mice developed normally and appeared healthy in a pathogen-free environment but show a higher frequency of activated T-cells.[225]

Finally, GPVI is a platelet collagen receptor that regulates platelet aggregation[228]. GPVI adheres to GPO repeats in the collagen triple helix and forms dimers that cluster together on the platelet surface to amplify platelet activation[228]. GPVI binding to collagen is a prerequisite for platelet integrin α2β1 activation and subsequent thrombus formation[229]. Previous unpublished work by Dr Peter Kim in Professor Farndale's group found that ECs adhered to GPO repeats and it was hypothesised that ECs express GPVI. However, no further studies were carried out to clarify this observation.

1.11 Aims of the project

As described in this introduction, ECs and their surrounding ECM are ubiquitous throughout all organs of the body. ECs help regulate vascular tone, tissue homeostasis and inflammatory response and as a result they have important roles in many diseases[230]. EC dysfunction and the switch from a quiescent to pro-inflammatory and pro-coagulant state contributes to a range of cardiovascular diseases, including atherosclerosis and stroke[12]. EC dysfunction and associated cardiovascular disease can be caused by smoking, poor diet, obesity, age and inactivity and is a leading cause of mortality in the UK[12, 68, 91, 230]. The

endothelium is surrounded by a biologically active matrix of scaffolding and signalling proteins that help regulate EC behaviour and the continuous signalling between ECs and their ECM could yield novel therapeutics for EC dysfunction and associated cardiovascular disease. The work presented here aims to study ECs and their surrounding ECM to further understand the causes and progression of cardiovascular disease with intent to treat cardiovascular diseases more efficiently. Additionally, angiogenesis is paramount to tumour progression and again, the study of ECs and their ECM in the context of angiogenesis is essential to finding new therapeutic targets for the inhibition of tumour angiogenesis to help treat cancers.

This project aims to study the expression and function of the four collagen-binding integrins in HUVECs. It builds upon work undertaken by a previous PhD student in the Farndale group, Dr Peter Kim. HUVECs were chosen as model ECs as they are well characterised, human in origin and easily available. HUVECs are suitable for this project as this work does not aim to investigate a particular endothelial phenotype specific to a subset of endothelial cells. Rather the project aims to looks at EC behaviour generally. HUVECs show an endothelial phenotype *in vitro* but cannot be passaged in excess of 5 times as they may lose their endothelial phenotype[134].

First, commercially available HUVECs will be validated and characterised by their expression of EC markers such as VEGFR2, VE-Cad, MCAM, PECAM-1 and VWF using flow cytometry. Next, qPCR will be used to check for the presence and relative expression levels of these integrins in activated and non-activated states, alongside VWF, SPARC and DDR1 and 2.

Synthetic collagen II and III and XIII peptide Toolkits, synthesised in the Farndale group, contain overlapping sequences that map the triple helical domains (THDs) of these three collagens. Collagen THDs are made of three chains, each composed of Gx^1x^2 repeats where x^1 is often Proline and x^2 is often a 4R-hydroxyproline (a post-translational modification of the proline side chain, noted O in the one-letter amino acid code)[231]. The formation of the triple helix is driven by a network of hydrogen bonds perpendicular to the helix axis[186], resulting in a one amino acid stagger between peptide strands. This unique conformation is essential for the collagen assembly in fibrils which is required for the structural role of collagen within the extracellular matrix. The triple helix conformation is also necessary for the recognition of collagen-binding cell-surface receptors and cell-secreted proteins and is crucial to its biological function. These toolkit triple helical peptides (THPs) are designed to mimic the native structure

of collagen and have been used to pinpoint the binding site of VWF A3 in Collagen III [139, 232-235], and by inference, the partially conserved site in Collagens I and II. In solution, these peptide strands spontaneously bundle together to form a triple helix. In addition, GPC triplets were added in the N-terminal and C-terminal end of peptide strands to enable THP linkage to tissue culture plates. In addition to toolkit peptides, shorter THPs (SPs) have been synthesised containing 5 GPP repeats at each end and a central short integrin-targeting host sequence designed from variations of GFOGER or GLOGEN found in different collagens. A list of these peptides can be found in Chapter 4.2 and the host sequences found in different collagens is summarised in Chapter 4, table 4.1.

The THPs containing integrin binding motifs loosely based on GFOGER, named SPs, will also be used to study the adhesion of the four integrins to collagen. First recombinant integrin I-domains will be tested before moving on to study the full length heterodimeric receptor using C2C12 cell lines that have been stably transfected to express one of the four collagen binding integrins[236]. Static adhesion assays and real-time adhesion studies using the xCELLigence electrical impedance system will be used to investigate differences in binding specificity. Ultimately these differences will be exploited using peptides to ligate specific integrin receptors, if possible. Adhesion experiments will then be repeated in HUVECs to compare the binding profile of HUVECs to C2C12s with respect to integrin expression.

Inhibitors, siRNA and CRISPR will be explored as methods to modulate integrin signalling and the downstream effects of receptor inhibition or knockdown on HUVEC function will be assessed. Changes in proliferation, apoptosis, angiogenic capability and migration will be quantified in each condition. To study proliferation cell number quantification assays and EdU incorporation microscopy assays will be used downstream of integrin KO or inhibition. To quantify apoptosis, fluorescent Annexin V will be used in microscopy and flow cytometry assays. Additionally, a lactate dehydrogenase (LDH) detection cytotoxicity kit will be used to quantify necrosis. Time lapse migration assays will be used downstream of inhibition and siRNA to determine the effects on cell movement in random walk conditions. Lastly, tube formation assays using Geltrex will be used to quantify the effects of integrin KD or inhibition on tube formation.

Throughout this dissertation the nomenclature “α1β1” refers to the full-length integrin heterodimer whereas “ITGA1” refers to the α-subunit.

Chapter 2 – Materials and Methods

Contents

2.1 Chapter Summary

This chapter aims to introduce all the reagents, materials and protocols used to carry out all the experiments described in this project.

2.2 List of Materials and Reagents

Table 2.1: List of all materials and reagents used

Name	Company/Source	Catalogue Number
µ-Slide 4 Well Ph+	Ibidi	80446
Angiogenesis µ-slides	Ibidi	81506
Annexin V-PE	Biolegend	640947
BSA	GE Healthcare	-
C2C12 cells	Samir Hamaia	-
Cell Proliferation Kit III (EdU-488; FC)	Promocell	PK-CA724-488FC
Chemotaxis µ-slides Collagen coated	Ibidi	80322
Chemotaxis µ-slides Ibidi-treat	Ibidi	80326
CLICK PLUS EDU 488 FLOW KIT	Thermo	C10633
Collagen I PureCol® EZ Gel	Advanced BioMatrix	5074-35ML
Collagen IV	Sigma	C5533
cOmplete™ Mini Protease Inhibitor	Sigma	11836153001
Cryo-SFM for cryopreservation	Promocell	C-29910
Cytotoxicity Detection Kit (LDH)	Roche	11644793001
DharmaFECT 1	Dharmacon	T-2001-01
DharmaFECT 2	Dharmacon	T-2002-01
DharmaFECT 3	Dharmacon	T-2003-02
DharmaFECT 4	Dharmacon	T-2004-01
DMEM	Thermo	41966-029
Endothelial Basal Medium 2 (EBM2)	Promocell	C-22211
Endothelial Growth Medium 2 (EGM2)	Promocell	C-22111
FBS	Thermo	C-22211
Fibronectin	Sigma	FC010-1MG
G418	Thermo	11811031
Geltrex™ (Matrigel)	Thermo	A1413202
Helix NIR	Biolegend	425301
Hoechst 33342	Thermo	H1399
Human E-Selectin DuoSet ELISA	R&D systems	DY724
Human ICAM-1/CD54 DuoSet ELISA	R&D systems	DY720-05
Human VCAM-1/CD106 DuoSet ELISA	R&D systems	DY809
HUVECs, cryopreserved	Promocell	C-12208 Lot Numbers and genders: 416Z042 m/m/f/f newborn 426Z006 m/m/f/m newborn 426Z007 f/f/m/f newborn 420Z015.2 f/m/f/m newborn
Interleukin (IL)-1α	Miltenyi Biotech	130-093-894

Keratinocyte-SFM (1X)	Thermo	17005042
Laminin	Sigma	L6274-.5MG
Lipofectamine LTX	Thermo	15338100
Lipofectamine RNAiMAX	Thermo	13778075
Lipopolysaccharides from E.coli	Sigma	L4391-1MG
M3 Protein Fragment	Samir Hamaia	N/A
Nunc Tissue Culture Flasks 75cm2	Thermo	156499
Obtustatin	R&D systems	4664/100U
Odyssey Blocking buffer PBS	Licor	927-40000
OptiMEM	Thermo	31985070
PCR Mycoplasma Test Kit I/C	Promocell	PK-CA91-1024
Penicillin-Streptomycin Solution	Sigma	P4333-100ML
Phorbol12-myristate13-acetate (PMA)	Abcam	ab120297
Pierce™ TMB Substrate Kit	Thermo	34021
Plasmid Plus Maxi Kit	Qiagen	12963
pMDG.2 (Gift from Dr Frank McCaughan)	Addgene	12259
Polybrene	Sigma	TR-1003-G
PromoFectin	Promocell	PK-CT-2000-HUV
Propidium Iodide	Sigma	P4170-25MG
psPAX2 (Gift from Dr Frank McCaughan)	Addgene	12260
Puromycin	Sigma	P8833-25MG
px458 (Gift from Dr Frank McCaughan)	Addgene	48138
Rezasurin	Promocell	PK-CA707-10054
Rhodamine Phalloidin	Thermo	R415
Rneasy Plus RNA extraction kit	Qiagen	74134
siGLO Green Transfection Indicator	Dharmacon	D-001630-01-05
Silencer Select Negative Control #2	Thermo	4390846
Silencer Select ITGA1	Thermo	4390825 - s7534, s7532
Silencer Select ITGA10	Thermo	4392421 - s16180, s16181
Silencer Select ITGA11	Thermo	4390825/242,4392421/240
Silencer Select ITGA2	Thermo	4399666/s541358, s541359
Silencer Select GAPDH	Thermo	4390850
Silencer Select Negative Control #1	Thermo	4390844
TaqMan DDR1 Assay	Thermo	4331182, Hs01058430_m1
TaqMan DDR2 Assay	Thermo	4351372, Hs01025956_m1
TaqMan GAPDH Assay	Thermo	4331182, Hs99999905_m1
TaqMan ANGPT2	Thermo	Hs01048042_m1
TaqMan TIE1	Thermo	Hs00892698_m1
TaqMan Gene Expression Master Mix	Thermo	4369016
TaqMan HPRT1 Assay	Thermo	4448490, Hs02800695_m1

TaqMan ITGA1 Assay	Thermo	4331182, Hs00235006_m1
TaqMan ITGA10 Assay	Thermo	4351372, Hs01006921_m1
TaqMan ITGA11 Assay	Thermo	4331182, Hs01012939_m1
TaqMan ITGA2 Assay	Thermo	4331182, Hs00158127_m1
TaqMan Reverse Transcription Kit	Thermo	N8080234
TaqMan SPARC Assay	Thermo	4331182, Hs00234160_m1
TaqMan vWF assay	Thermo	4331182 - Hs01109453_m1
TC-I-15	R&D systems	4527/10
Tumour Necrosis Factor (TNF)α	Thermo	PHC3015
TransfeX™ Transfection Reagent	ATCC®	ACS-4005
tRFP CRISPR Lentiviral Plasmid	Addgene	57819
TryplE	Thermo	12604021
Trypsin-EDTA	Sigma	T4174-100ML
VEGF-165, human	Promocell	C-64420
Vitronectin	Sigma	5051-0.1MG

2.3 List of Antibodies

A list of antibodies used in this project is detailed in table 2.2.

Target and conjugate	Application	Company	Product Number
GST HRP conjugated	ELISA	Sigma	GERPN1236
CD144 (VE-Cadherin), human, FITC	FC	Miltenyi Biotech	130-100-713
CD146, human, Alexa Fluor® 488	FC	Biolegend	342007
CD309/VEGFR2, human, Alexa Fluor® 488	FC	Biolegend	359913
CD31-FITC, human (clone: AC128)	FC	Miltenyi Biotech	130-098-171
CD45, human, APC	FC	Biolegend	368511
CD49a, ITGA1, Alexa Fluor 488	FC	Thermo	PA5-46887
GAPDH	WB	Abcam	ab9484
IRDye® 680LT Goat anti-Rat IgG Secondary Antibody	WB	Licor	926-68029
ITG1/CD49a (639508)	WB	R&D systems	MAB5676-SP
ITGA2 - 6F1	Inh/WB	Professor Barry Coller of the Rockefeller University, New York.	
ITGA2/CD49b	WB	R&D systems	MAB12331
Mouse IgG H&L Alexa Fluor® 488 isotype control	FC	Abcam	ab150113
α-Tubulin Loading control	WB	Abcam	ab4074
WB = Western blot, FC = Flow cytometry, Inh = inhibitory, ELISA = enzyme linked immunosorbent assay			

2.4 Cell culture

Pooled HUVECs were cultured in endothelial growth media 2 (EGM2) unless stated otherwise. C2C12s, HT1080s, HEK293T were grown in DMEM/10% FBS and 1% penicillin/streptomycin. Immortalised Bronchial Epithelial (BE) cells were a gift from Dr Frank McCaughan, University of Cambridge, and were grown in Keratinocyte-SFM (1X). All cells were maintained at 37°C, 5% CO_2. All cells were stored in liquid nitrogen or at -80°C and defrosted in a 37°C water bath before being placed directly into media pre-warmed to 37°C. HUVECs were seeded at 500,000 per 75cm^2 flask and passaged at 70% confluence using TryplE to detach the cells at room temperature. 10% FBS in PBS was added to counteract the TryplE. All other cells were passaged using Trypsin/EDTA at 37°C for 5 minutes and DMEM with 10% FBS to quench the trypsin.

All experiments using cells were carried out under sterile conditions. Cells were counted using a haemocytometer. Thermo, Nunc tissue culture plates and flasks were used for all cells. HUVECs were used at passage three, four or five. Low passage cells were cryopreserved in Promocell Cryo SFM cell freezing media and stored at -80°C for later use.

2.5 Media and Buffers

Table 2.3 – List of Buffers and Media used

Buffer/Media	Recipe
TBS	50nM TRIS, 150mM NaCl, pH 7.4, 1L H_2O
Lysis buffer for ELISAs	1 % TRITON X100 in TBS
Blocking buffer PBS	3 % BSA in PBS
Blocking buffer TBS	3 % BSA in TBS
TBS-T	TBS + 0.05% Tween-20
PBS-T	PBS + 0.05% Tween-20
AV Buffer	10mM HEPES, 140mM NaCl, 2.5mM CaCl
Laemmli Buffer	4% SDS, 20% Glycerol, 125mM TRIS, 10% β-mercaptoethanol, 0.02% Bromophenol blue

2.6 Protein Expression – VWF A domains and αI-domains

The αI-domains of all four integrins and VWF A1 and A3 domains were cloned by Dr S. Hamaia (Department of Biochemistry, University of Cambridge) and expressed as glutathione S-transferase (GST)-tagged constructs. SHuffle® cells were transformed and grown on

100µg/ml Ampicillin plates. Resulting colonies were grown in LBE media containing 100µg/ml Ampicillin. Once the bacterial suspension reached 0.5 optical density (OD), the temperature was lowered to 30°C and expression was induced with the addition of 0.5M IPTG. After overnight incubation, the protein was extracted using Triton™ X100, sonication, centrifugation and glutathione-agarose beads in a purification column. Several different preparations were used for these experiments. Each condition was performed in triplicate and at least three independent repeats of the experiment were carried out.

2.7 Immunofluorescence Imaging of EC Markers

HUVECs were cultured on tissue culture plastic in EGM2 at varying densities. After 24 hours, cells were washed with PBS fixed with 4%PFA in H_2O. Fixed cells were blocked with 3% BSA in PBS for 1 hour at room temperature (RT) before adding primary antibodies in 1% BSA in PBS overnight at 4°C. Wells were washed with 1%BSA in PBS 3 times before adding secondary antibodies and Hoechst in 1% BSA in PBS for one hour at RT protected from light. Wells were washed three times with PBS and left in PBS for imaging on the Leica DM6000 microscope. Images were analysed using ImageJ 1.51 (National Institute of Health). The presence of EC markers were tested in each batch of pooled HUVECs used.

2.8 DuoSet ELISAs after HUVEC Activation

Nunc tissue culture plates were coated with collagen I EZ-Gel at 10µg/ml. HUVECs were cultured on collagen I coated surfaces overnight in EGM2. The following day 20ng/ml TNFα, 10ng/ml IL-1α or 1µg/ml LPS was added to the cells and left overnight for 16 hours. The following day, the media was aspirated, spun at 1000 xG and stored at -80°C. The cells were lysed on ice in PBS containing 1% Triton X-100 and 1 cOmplete Mini Protease inhibitor cocktail tablet per 10ml Lysis buffer. Cells were scraped in lysis buffer and the lysates were incubated on ice for 30 minutes before centrifuging at 13000 X G for 20 minutes. Supernatants were stored at -80°C and pellets were discarded.

All reagents, antibodies and standards from the DuoSet ELISA kits were made following manufacturers recommendations. Immulon 2HB plates were coated with either VCAM, ICAM or E-selectin capture antibodies overnight in PBS at the manufacturers recommended concentration. The next morning plates were washed three times with 200µl PBS and blocked with 1% BSA in PBS for one hour. VCAM, ICAM or E-Selectin standard curves, HUVEC cell lysates (diluted 1:10 with 1% BSA) or media from HUVEC cultures were added to the blocked wells for

1 hour. After three washes with 200µl PBS-T, VCAM, ICAM or E-Selectin capture antibodies (biotin conjugated) were added, in 1% BSA in PBS for one hour. After three washes with PBS-T streptavidin-HRP was added for 20 minutes protected from light. After 4 washes with PBS-T, the Roche TMB substrate kit was added (1:1 ratio, 100µl/well) and the colour was allowed to develop until the blue was clearly visible. The reaction was quenched with 2M H_2SO_4 and the plate was read in a SpectraMax plate reader at 450nm.

Each condition was performed in triplicate and at least three independent experiments were carried out, each with a different batch of pooled HUVECs.

2.9 Lentiviral CRISPR/Cas-9

Plasmids, protocols and technical advice were kindly provided by Dr Frank McCaughan, Department of Biochemistry, Cambridge. The packaging plasmids used were psPAX-2 (Figure 2.1) and pMDG.2 (Figure 2.2) while guide RNA's were cloned into Addgene 57819 plasmid (Figure 2.3). Guide RNA sequences were obtained using the CRISPR design program at: http://crispr.mit.edu/ and integrin DNA sequence information on the Ensembl gene browser.

Guide RNA primers (3 sets for each target) were ordered from Sigma and annealed (boiled at 95°C for 3min before cooling down at 0.1°C/s to 22°C in a thermocycler) to create small inserts with Bbsm1 compatible sticky ends. Addgene 57819 plasmid was digested with Bbsm1 and the guide RNA sequences were inserted using T4 ligase. DH5α cells were transformed and grown on ampicillin plates, colonies were collected and grown in 2XTY media, Qiagen miniprep kits were used to extract the plasmids and these were sent for sequencing using the U6 promoter. Plasmids with the correct guide sequences (sgRNA plasmids) were amplified in bacterial systems and extracted using Qiagen endo-free plasmid maxi kits.

Packaging plasmids and lentiviral CRISPR guide RNA plasmids were transfected into HEK293T cells. HEK293T cells were seeded at 4 million per 10cm dish in DMEM + 10% FBS with no antibiotics and the following day these HEK293T cells were transfected with 1.5µg pMD2.G : 4.5µg psPAX2 : 6µg sgRNA plasmid using lipofectamine™ diluted in OptiMEM® media. After 24 hours DMEM was replaced with DMEM +20% FBS to remove transfection reagents. After another 48 hours the supernatant containing viral particles was harvested, filtered through a 45µM filter and aliquoted into 200µl viral samples and stored at -80°C.

BE or HUVECs were grown in complete media until 70% confluent in a 6-well plate. Media was changed to basal EBM or DMEM + 8µg/ml polybrene. 50µl of the viral particle

solution was added to the cells and incubated for 6 hours. The media was replaced with complete media and cells were incubated for 24 hours. Cells were checked each day for red fluorescence on a Leica DM6000 microscope, and eventually a MoFlo Astrios cell sorter was used to separate red cells from the rest, which were analysed for expression of the target protein.

2.10 Knockdown using siRNA

Reverse siRNA transfection protocols were used. Two Silencer Select siRNAs for each target were pooled as described the materials table, except where siGLO was used to optimise transfection reagent concentration. The pooled siRNA was used as below (Table 2.4):

Table 2.4 – siRNA concentrations used

Condition	Target siRNA	Negative control siRNA	Final [siRNA]
ITGA1	50nM	100nM	150nM
ITGA2	50nM	100nM	150nM
ITGA10	50nM	100nM	150nM
All	50nM + 50nM + 50nM	-	150nM
Negative control	-	150nM	150nM

The siRNA was diluted with OptiMEM in the tissue culture vessel, 250µl per well for a 6-well plate. DharmaFECT4 (D4) was mixed with OptiMEM in a sterile tube at 1:50 ratio and incubated for 5 minutes, 250µl per well for a 6-well plate. The diluted D4 was then added to the diluted siRNA in the wells and incubated for 20 minutes. Cells were then added in 2ml of EGM2 without Heparin per well at 60,000/ml, and incubated for 8 hours at 37°C, 5% CO_2. After 8 hours the media was replaced with pre-warmed complete EGM2. The cells were passaged after 24-48 hours. All experiments were carried out after 48-72 hours siRNA.

2.11 RNA Extraction, cDNA synthesis and qPCR

For quantitative real-time polymerase chain reaction (qPCR), the Qiagen RNeasy Plus Mini Kit was used to extract total RNA from cells, in a Qiacube automated machine with 30µl elution volume, as per manufacturer's instructions. β-mercaptoethanol was added to the RLT lysis buffer at 10µl/ml and genomic DNA removal columns were used. A corresponding cDNA library was created using the TaqMan reverse transcription reagents as follows (Table 2.5):

Table 2.5 – Reverse Transcription Volumes

Reagent	Volume	Final Concentration
H_2O	Variable – make up to 50µl	-
10x Reverse transcription buffer	5µl	1X
$MgCl_2$	3.5µl	1.75mM
dNTP mix (2.5mM each)	10µl	0.5mM each
RNase Inhibitor	2.5µl	1.0U/µl
Random Hexamers	2.5µl	2.5µM
Multiscribe reverse transcriptase	2.5µl	2.5U/µl
RNA, in H2O	Variable	<1µg
Total	50µl	-

The Reverse transcription reaction was placed in a thermocycler using the recommended protocol (10min at 25°C, 30min at 37°C, 5min at 95°C, 10min at 4°C). RNA was either used straight away for qPCR or stored at -20°C until use. The qPCR reaction was set up as below and the reaction was run on an Applied Biosystems 7300 Real-Time PCR System as per manufacturer's instructions. TaqMan predesigned primer and probe sets were used, the sequences for these are not available but the product information is listed in the table of reagents (Table 2.6).

Table 2.6 – qPCR Volumes

Reagent	Volume for 1 reaction
H_2O	Variable – make up to 20µl
Taqman Gene Expression Master Mix	10µl
20x Target assay	1µl
20x HPRT1 control assay	1µl
cDNA	1-5µl
Total	20µl

To quantify changes in mRNA expression, the HPRT1 CT value was subtracted from each experimental CT value (in triplicate), giving a ΔCT number. These ΔCTs were averaged and the fold change was calculated by the equation $2^{-\Delta CT}$. Where siRNA was used, the ΔCT value for the control condition was subtracted from the ΔCT value for the siRNA KD condition and the resulting ΔΔCT value was used to calculate percentage expression using $2^{-\Delta\Delta CT}$. Three technical

repeats were carried out with each batch of cDNA and at least three separate knockdown experiments were performed using different batches of pooled HUVECs.

2.12 Western Blots

Cells were grown in 12-well plates, seeded at 50,000-100,000 per well in EGM2. After 24 hours cells were lysed directly with 150µl of Laemmli buffer and scraped into screw top Eppendorf tubes. Lysates were vortexed and then boiled for 5 minutes and stored at -20°C or used straight away. Lysates were loaded in NuPage gels and run using the NuPage Gel Electrophoresis system at 200V for 45 minutes. Gels were washed and blotted onto Immobilon-FL PVDF membranes using the BioRad TransBlot® Turbo™ Semi-Dry transfer system in blotting buffer using the "High MW" protocol for 11 minutes. Membranes were then washed in PBS and blocked using the Odyssey PBS blocking buffer for one hour. Primary antibodies were added in Odyssey blocking buffer at 4°C overnight. After 3x 10min washes in PBS-T, the Licor secondary antibodies were added at 1:10,000 in Odyssey blocking buffer protected from light for 1 hour. After 3x 10min washes with PBS-T and 2x 10minute washes with PBS the membranes were visualised using a Licor Odyssey CLx Western Blot imaging system and associated software. Western blots were carried out using lysates from three separate siRNA knockdown experiments using different batches of pooled HUVECs.

2.13 Cellular Static Adhesion Assays

Immulon 2HB 96-well plates were coated with 100µl per well of peptides at 10µg/ml in 0.01M acetic acid or with proteins/antibodies at concentrations stated) overnight at 4°C. After 3x 200µl/well washes with PBS, plates were blocked with 200µl/well filtered 3% BSA in PBS at room temperature for one hour. Plates were washed again, and 100µl per well of cells were added at 10, 15 or 20k cells per well at RT for one hour. Unbound cells were washed away with 3x washes of 200µl per well of PBS. Remaining cells were lysed with 50µl per well of 2% TRITON X-100 in double-distilled water for one hour at room temperature. Cells were detected using 50µl per well of the Roche cytotoxicity LDH kit. The catalyst and substrate solutions of the kit were mixed at a ratio of 1:45 and 50µl was added to the wells to detect LDH in the cell lysate. Absorbance was read at 490nm on a SpectraMax 190 microplate reader. Each condition was performed in triplicate and each experiment was repeated at least three times using different batches of pooled HUVECs.

2.14 Protein Static Adhesion Assays

Immulon 2HB 96-well plates were coated with 100µl per well of peptides at 10µg/ml in 0.01M acetic acid or with proteins/antibodies at concentrations stated overnight at 4°C. After 3x 200µl per well washes with washing buffer (1mg/ml BSA in TBS), plates were blocked with 200µl per well of filtered 3% BSA in TBS for one hour. αI-domains and other proteins were added at 10µg/ml washing buffer for one hour. After 3x washes with washing buffer, detection antibodies (HRP conjugated anti-GST or anti-His followed by anti-mouse HRP conjugate) were added for one hour. Plates were washed 4x with 200µl per well of washing buffer and bound protein was quantified using the Pierce™ TMB Substrate Kit. The colorimetric reaction was stopped with an equal volume of 1M H2SO4 and absorbance was read at 450nm on a SpectraMax 190 microplate reader. Each condition was performed in triplicate and each experiment was repeated at least three times using several batches of proteins unless stated otherwise.

2.15 Migration Random Walk Assays

Ibidi µ-slide 4-well Ph+ chamber slides were coated with 100µl per well of peptides at 10µg/ml in 0.01M acetic acid or with proteins/antibodies at concentrations stated in PBS overnight at 4°C, before blocking with 3% BSA in PBS for one hour at room temperature. After 3 washes with PBS, 700µl per well of cells were added at 14,000 cells/ml and left for 4 hours to attach. After 4 hours, phase images were taken every 5 minutes for 9 hours using an automated Leica DM6000 microscope in a humidified incubated chamber, 37°C, 5% CO2. The TrackMate plugin in ImageJ was used to quantify migration as average distance moved by one cell. Cells visible for over 80 frames were counted, cells that died or left the field of view were not analysed. 10 fields of view, all from a single well, were analysed for each condition and three independent experimental repeats were carried out using different batches of pooled HUVECs.

2.16 Real-Time Adhesion Assays Using xCELLigence

A real-time xCELLigence RTCA SP electrical impedance system was used to measure cell adhesion and spreading in real time. xCELLigence plates were coated with peptides or proteins as described above for one hour at room temperature or overnight at 4°C and blocked with 3% BSA in PBS for one hour. Wells were washed with PBS and equilibrated with 50µl of serum-free

media (DMEM or EBM) at 37°C. A baseline reading was taken before adding 15,000 or 20,000 cells per well in 50µl of EGM for HUVECs and serum-free DMEM for all other cell types. Electrical impedance readings were taken automatically every 5 minutes for 4 hours at 37°C, 5% CO_2. Each condition was performed in triplicate and three independent experiments were carried out.

2.17 Tube Formation Assays

10µl of Geltrex was added to each well of an Ibidi angiogenesis µ-slide and incubated at 37°C for 1 hour. HUVECs were detached, counted and added at 4000 per well (in 50µl) in EGM2 with or without inhibitors, or 48 hours post-siRNA. Slides for tube formation assays were incubated at 37°C for 24 hours. Phase images were taken at 6- and 24-hour time points. The *Angiogenesis Analyzer* plugin by Giles Carpentier, (Faculte des Sciences et Technologie, Universite Paris Est Creteil Val-de-Marne, France) was used to analyse and quantify images. (Gilles Carpentier, Contribution: Angiogenesis Analyzer. ImageJ News, 5 October 2012). Each condition was performed in triplicate and at least three independent experiments were carried out using different batches of pooled HUVECs.

2.18 EdU Proliferation Microscopy Assay

The Click-iT EdU proliferation assay Alexa Fluor 488 kit from Thermo Fisher Scientific was used to quantify proliferation. Cells were cultured on collagen coated surfaces in a 24-well plate at 20,000 per well. After addition of siRNA or inhibitors, cells were incubated for 24 hours in EGM2. EdU was then added at 20µM for 2 hours, cells were fixed with 4% PFA in H_2O, washed 3x with PBS and permeabilised with 0.1% Triton X100 in PBS for 5 minutes. After 3 washes the Click-iT reaction cocktail was added for 30 minutes, as per the manufacturer's instructions. Cells were finally stained using Hoechst and images for 10 randomly selected fields of view in each well were taken, each field of view typically contained around 200 cells. An ImageJ macro was created to count EdU positive (green nucleus) vs all cells (blue nucleus) and the percentage of green cells was calculated. The ImageJ macro involved the following ImageJ functions in order:

- "Subtract background" to remove any anomalies introduced from the surface coating
- "Colour threshold" to set a intensity threshold for the presence of a nucleus
- "Convert to mask" to make the image binary based on the colour thresholding

- "Fill holes" to ensure that one nucleus is not mistaken for several
- "Watershed" to separate two adjacent nuclei so that both are counted
- "Analyse particles" to count the number of particles (nuclei) in each image. This function also measures the size, area and position of each particle but for counting nuclei only the number of particles is needed.

Each condition was performed in triplicate and at least three independent experiments were carried out using different batches of pooled HUVECs.

2.19 Cell Spreading Assay – Microscopy

Cells were cultured on collagen I coated surfaces in a 24-well plate at 20,000 per well. After addition of siRNA or inhibitors, cells were incubated for 1 hour in EGM2 at 37°C. Cells were then fixed with 4% PFA in H_2O, washed 3x with PBS and permeabilised with 0.1% Triton X100 in PBS for 5 minutes. After 3 washes with PBS, rhodamine phalloidin and Hoechst were added for one hour in PBS with 1% BSA. After three washes cells were imaged in PBS using the Leica microscope described above, with 10 fields of view per well. An ImageJ macro was created, as before, to count the number of cells per field of view and the area covered by cells, per field of view. The area per cell was calculated from these measurements. The ImageJ macro was the same as described in 2.18 except the colour threshold parameters differed slightly to ensure an accurate measurement of cell area. Each condition was performed in triplicate and three independent experiments were carried out using different batches of pooled HUVECs.

2.20 Annexin V Apoptosis Assay – Microscopy

Wells of a 24-well plate were coated with collagen or peptides as described above. Cells were seeded in EGM2 at 20,000 cells/well and left for 4 hours to attach. The media was then changed to EBM + 0.2% FBS + 20ng/ml TNFα. After 6, 24 or 48 hours, cells were washed with AV Buffer and incubated in AV buffer plus Annexin V PE and Hoechst for 15 minutes. After 3 washes with AV buffer, cells were visualised using a Leica DM6000 microscope in AV buffer. 5 randomly selected fields of view for each well were acquired. ImageJ was used to quantify the average amount of PE fluorescence per cell. The fluorescence intensity was measured using the ImageJ function and this was divided by the number of nuclei, counted

using the macro above. Each condition was performed in triplicate and at least three independent experiments were carried out using different batches of pooled HUVECs.

2.21 Annexin V Apoptosis Assay – Flow Cytometry

Wells of a 12-well plate were coated with collagen or peptides as before. Cells were seeded in EGM2 at 50,000 cells/well and left for 4 hours to attach. The media was then changed to EBM + 0.2% FBS + 20ng/ml TNFα. After 6, 24 or 48 hours, cells were detached using TryplE as above and washed with AV Buffer, then resuspended 100µl of AV Buffer +2.5µl Annexin V-PE and Helix NIR dye for 15 minutes. The cells were then diluted with 500µl of AV Buffer and immediately run on an Accuri C6 flow cytometer. Unstained and FMO controls were used to gate Annexin V/Helix NIR positive vs negative cells and percentages were calculated. One well was analysed per condition and at least three independent experiments were carried out using different batches of pooled HUVECs.

2.22 Cytotoxicity Assay – LDH

Cells were grown in 12 or 24-well plates, coated as before with collagen or peptides. After 24 hours of treatment (siRNA, serum starving, TNFα or treatment as stated), media was collected and stored at 4°C until detection. Stored media was aliquoted into a 96-well plate (100µl per well) in triplicate. The Roche cytotoxicity kit was used to quantify LDH released by necrotic cells in the media: the catalyst and substrate solutions were mixed at a ratio of 1:45 and 50µl was added to the wells. Once the red colour had developed, absorbance was read using a SpectraMax 190 microplate reader at 490nm. A standard curve was created by lysing a known number of cells with 2% Triton X100 for comparison. Each condition was performed in triplicate and at least three independent experiments were carried out using different batches of pooled HUVECs.

2.23 – Diagrams of Plasmids Used in Lentiviral CRISPR

Figure 2.1. Diagram of psPAX2.

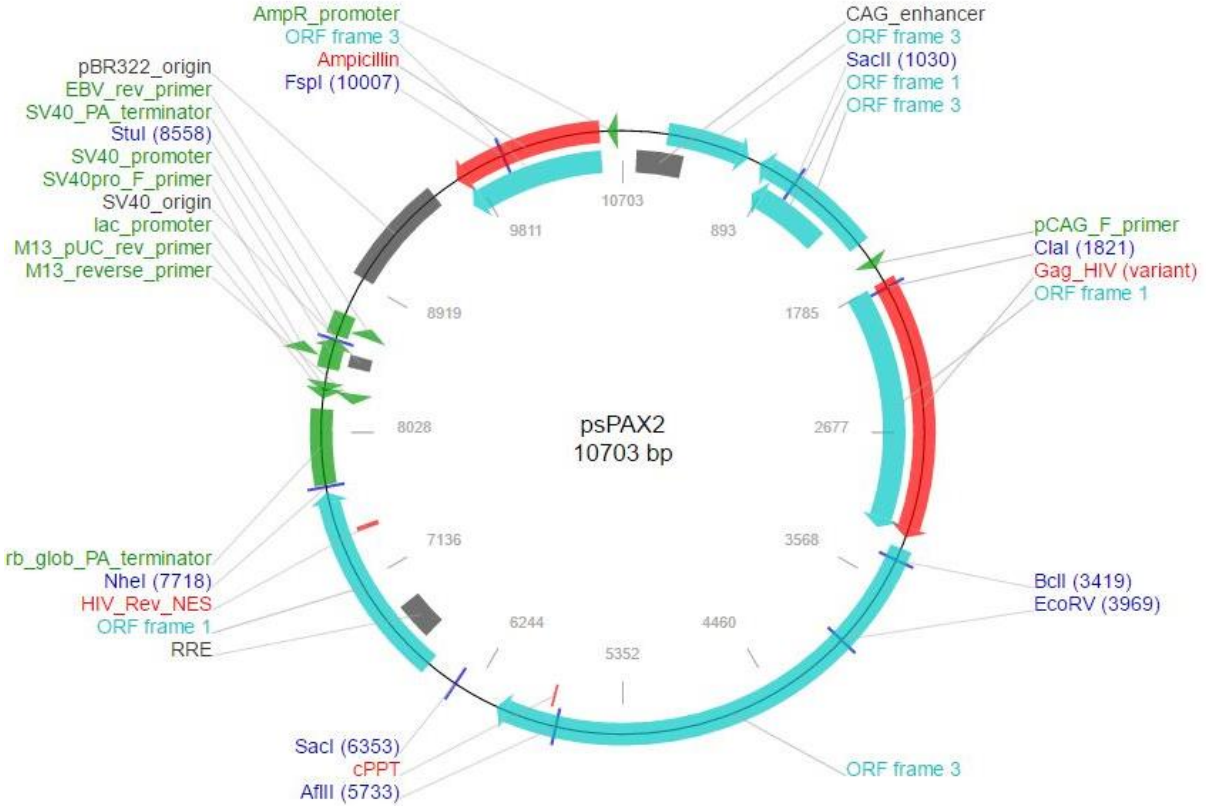

An illustration of the psPAX2 packaging plasmid used to create lentiviral particles for the integrin knockouts. Figure taken from the Addgene website: https://www.addgene.org/12260/

Figure 2.2. Diagram of pMD2.G.

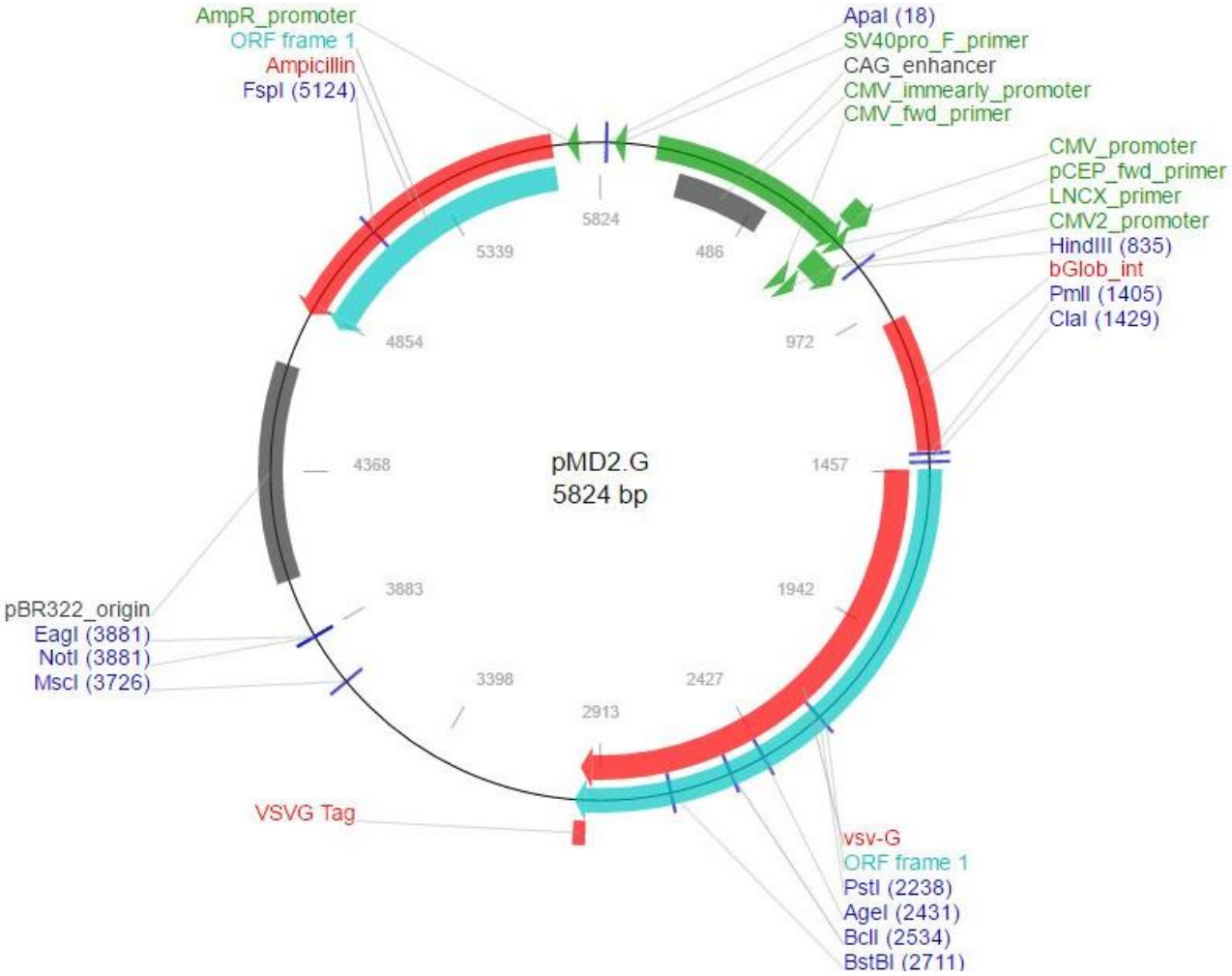

An illustration of the pMD2.G packaging plasmid used to create lentiviral particles for the integrin knockouts. Figure taken from the Addgene website: https://www.addgene.org/12259/

Figure 2.3. Diagram of 57819.

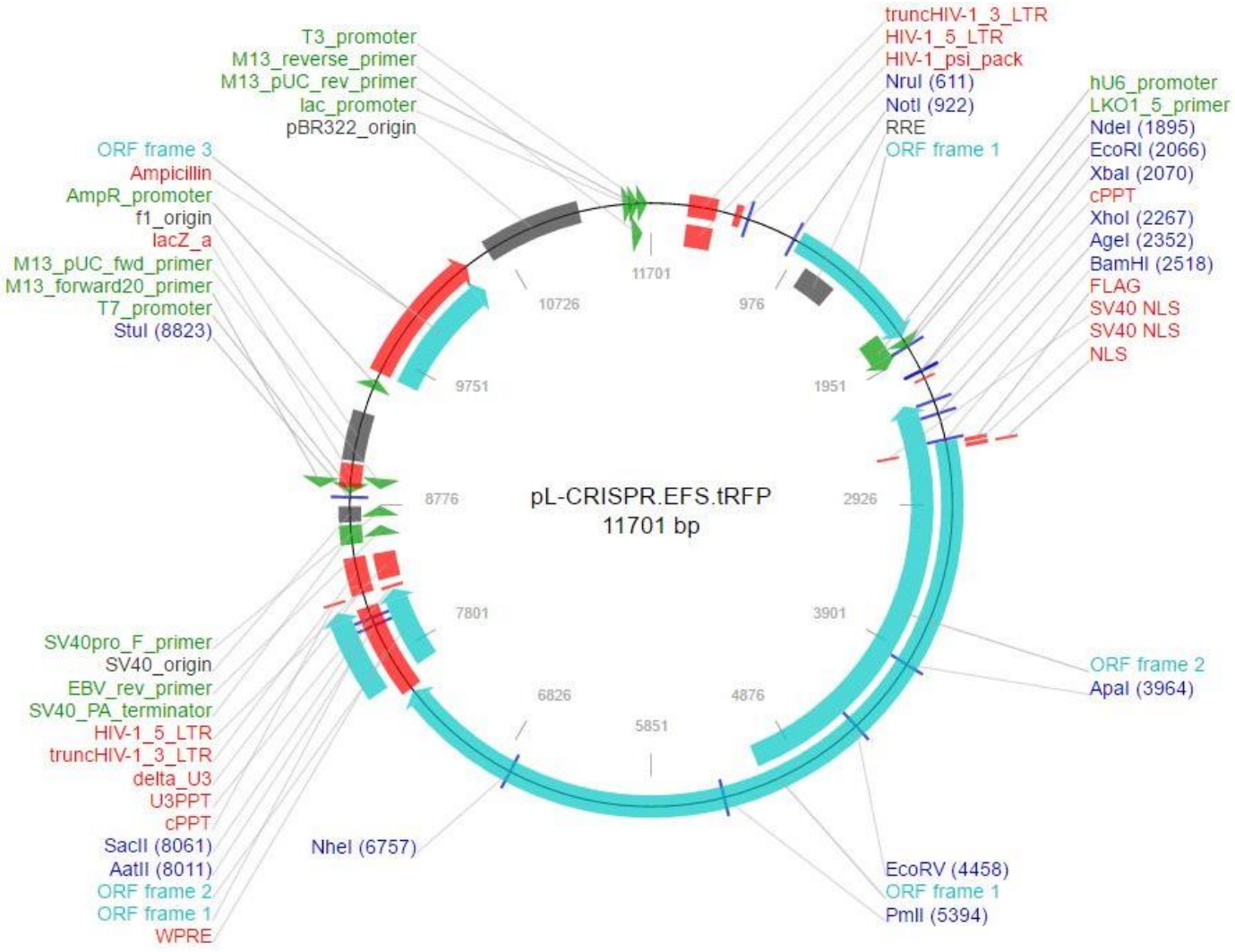

An illustration of the CRISPR plasmid used to create lentiviral particles for the integrin knockouts. Figure taken from the Addgene website: https://www.addgene.org/57819/

2.24 Toolkit Peptides

Toolkit peptides and derivatives were synthesised in-house (by Dr JD Malcor and Dr Arkadiusz Bonna, Department of Biochemistry, University of Cambridge) as triple helical homotrimers. Peptide strands were assembled using solid phase peptide chemistry on an automated microwave-assisted synthesiser to enable rapid, cost-effective and efficient synthesis. Peptides were then cleaved from the resin beads, purified by preparative reverse-phase high performance liquid chromatography, freeze dried and characterized by mass spectrometry. Peptides were dissolved at 5 mg/ml in 0.01 M acetic acid, heated to 70°C for 5

min and let to cool down overnight to enable triple helix folding. Peptides were diluted from this stock solution to 10 µg/ml in 0.01M acetic acid for the coating of empty tissue culture wells prior to experiments. The sequences of the toolkit peptides are listed below (using the one letter amino acid code, where O is hydroxyproline.

Toolkit II Sequences:

1	GPC$(GPP)_5$- GPMGPMGPRGPOGPAGAOGPQGFQGNO-$(GPP)_5$GPC
2	GPC$(GPP)_5$- GPQGFQGNOGEOGEOGVSGPMGPRGPO-$(GPP)_5$GPC
3	GPC$(GPP)_5$- GPMGPRGPOGPOGKOGDDGEAGKOGKA-$(GPP)_5$GPC
4	GPC$(GPP)_5$- GEAGKOGKAGERGPOGPQGARGFOGTO-$(GPP)_5$GPC
5	GPC$(GPP)_5$- GARGFOGTOGLOGVKGHRGYOGLDGAK-$(GPP)_5$GPC
6	GPC$(GPP)_5$- GYOGLDGAKGEAGAOGVKGESGSOGEN-$(GPP)_5$GPC
7	GPC$(GPP)_5$- GESGSOGENGSOGPMGPRGLOGERGRT-$(GPP)_5$GPC
8	GPC$(GPP)_5$- GLOGERGRTGPAGAAGARGNDGQOGPA-$(GPP)_5$GPC
9	GPC$(GPP)_5$- GNDGQOGPAGPOGPVGPAGGOGFOGAO-$(GPP)_5$GPC
10	GPC$(GPP)_5$- GGOGFOGAOGAKGEAGPTGARGPEGAQ-$(GPP)_5$GPC
11	GPC$(GPP)_5$- GARGPEGAQGPRGEOGTOGSOGPAGAS-$(GPP)_5$GPC
12	GPC$(GPP)_5$- GSOGPAGASGNOGTDGIOGAKGSAGAO-$(GPP)_5$GPC
13	GPC$(GPP)_5$- GAKGSAGAOGIAGAOGFOGPRGPOGPQ-$(GPP)_5$GPC
14	GPC$(GPP)_5$- GPRGPOGPQGATGPLGPKGQTGEOGIA-$(GPP)_5$GPC
15	GPC$(GPP)_5$- GQTGEOGIAGFKGEQGPKGEOGPAGPQ-$(GPP)_5$GPC
16	GPC$(GPP)_5$- GEOGPAGPQGAOGPAGEEGKRGARGEO-$(GPP)_5$GPC
17	GPC$(GPP)_5$- GKRGARGEOGGVGPIGPOGERGAOGNR-$(GPP)_5$GPC
18	GPC$(GPP)_5$- GERGAOGNRGFOGQDGLAGPKGAOGER-$(GPP)_5$GPC
19	GPC$(GPP)_5$- GPKGAOGERGPSGLAGPKGANGDOGRO-$(GPP)_5$GPC
20	GPC$(GPP)_5$- GANGDOGROGEOGLOGARGLTGROGDA-$(GPP)_5$GPC
21	GPC$(GPP)_5$- GLTGROGDAGPQGKVGPSGAOGEDGRO-$(GPP)_5$GPC
22	GPC$(GPP)_5$- GAOGEDGROGPOGPQGARGQOGVMGFO-$(GPP)_5$GPC
23	GPC$(GPP)_5$- GQOGVMGFOGPKGANGEOGKAGEKGLO-$(GPP)_5$GPC
24	GPC$(GPP)_5$- GKAGEKGLOGAOGLRGLOGKDGETGAA-$(GPP)_5$GPC
25	GPC$(GPP)_5$- GKDGETGAAGPOGPAGPAGERGEQGAO-$(GPP)_5$GPC
26	GPC$(GPP)_5$- GERGEQGAOGPSGFQGLOGPOGPOGEG-$(GPP)_5$GPC
27	GPC$(GPP)_5$- GPOGPOGEGGKOGDQGVOGEAGAOGLV-$(GPP)_5$GPC
28	GPC$(GPP)_5$- GEAGAOGLVGPRGERGFOGERGSOGAQ-$(GPP)_5$GPC
29	GPC$(GPP)_5$- GERGSOGAQGLQGPRGLOGTOGTDGPK-$(GPP)_5$GPC
30	GPC$(GPP)_5$- GTOGTDGPKGASGPAGPOGAQGPOGLQ-$(GPP)_5$GPC
31	GPC$(GPP)_5$- GAQGPOGLQGMOGERGAAGIAGPKGDR-$(GPP)_5$GPC
32	GPC$(GPP)_5$- GIAGPKGDRGDVGEKGPEGAOGKDGGR-$(GPP)_5$GPC
33	GPC$(GPP)_5$- GAOGKDGGRGLTGPIGPOGPAGANGEK-$(GPP)_5$GPC
34	GPC$(GPP)_5$- GPAGANGEKGEVGPOGPAGSAGARGAO-$(GPP)_5$GPC
35	GPC$(GPP)_5$- GSAGARGAOGERGETGPOGPAGFAGPO-$(GPP)_5$GPC
36	GPC$(GPP)_5$- GPAGFAGPOGADGQOGAKGEQGEAGQK-$(GPP)_5$GPC
37	GPC$(GPP)_5$- GEQGEAGQKGDAGAOGPQGPSGAOGPQ-$(GPP)_5$GPC
38	GPC$(GPP)_5$- GPSGAOGPQGPTGVTGPKGARGAQGPO-$(GPP)_5$GPC
39	GPC$(GPP)_5$- GARGAQGPOGATGFOGAAGRVGPOGSN-$(GPP)_5$GPC
40	GPC$(GPP)_5$- GRVGPOGSNGNOGPOGPOGPSGKDGPK-$(GPP)_5$GPC
41	GPC$(GPP)_5$- GPSGKDGPKGARGDSGPOGRAGEOGLQ-$(GPP)_5$GPC
42	GPC$(GPP)_5$- GRAGEOGLQGPAGPOGEKGEOGDDGPS-$(GPP)_5$GPC

43 GPC$(GPP)_5$- GEOGDDGPSGAEGPOGPQGLAGQRGIV-$(GPP)_5$GPC
44 GPC$(GPP)_5$- GLAGQRGIVGLOGQRGERGFOGLOGPS-$(GPP)_5$GPC
45 GPC$(GPP)_5$- GFOGLOGPSGEOGKQGAOGASGDRGPO-$(GPP)_5$GPC
46 GPC$(GPP)_5$- GASGDRGPOGPVGPOGLTGPAGEOGRE-$(GPP)_5$GPC
47 GPC$(GPP)_5$- GPAGEOGREGSOGADGPOGRDGAAGVK-$(GPP)_5$GPC
48 GPC$(GPP)_5$- GRDGAAGVKGDRGETGAVGAOGAOGPO-$(GPP)_5$GPC
49 GPC$(GPP)_5$- GAOGAOGPOGSOGPAGPTGKQGDRGEA-$(GPP)_5$GPC
50 GPC$(GPP)_5$- GKQGDRGEAGAQGPMGPSGPAGARGIQ-$(GPP)_5$GPC
51 GPC$(GPP)_5$- GPAGARGIQGPQGPRGDKGEAGEOGER-$(GPP)_5$GPC
52 GPC$(GPP)_5$- GEAGEOGERGLKGHRGFTGLQGLOGPO-$(GPP)_5$GPC
53 GPC$(GPP)_5$- GLQGLOGPOGPSGDQGASGPAGPSGPR-$(GPP)_5$GPC
54 GPC$(GPP)_5$- GPAGPSGPRGPOGPVGPSGKDGANGIO-$(GPP)_5$GPC
55 GPC$(GPP)_5$- GKDGANGIOGPIGPOGPRGRSGETGPA-$(GPP)_5$GPC
56 GPC$(GPP)_5$- GPRGRSGETGPAGPOGNOGPOGPOGPO-$(GPP)_5$GPC

Toolkit III Sequences:

1 GPC$(GPP)_5$- GLAGYOGPAGPOGPOGPOGTSGHOGSO-$(GPP)_5$GPC
2 GPC$(GPP)_5$- GTSGHOGSOGSOGYQGPOGEOGQAGPS-$(GPP)_5$GPC
3 GPC$(GPP)_5$- GEOGQAGPSGPOGPOGAIGPSGPAGKD-$(GPP)_5$GPC
4 GPC$(GPP)_5$- GPSGPAGKDGESGROGROGERGLOGPO-$(GPP)_5$GPC
5 GPC$(GPP)_5$- GERGLOGPOGIKGPAGIOGFOGMKGHR-$(GPP)_5$GPC
6 GPC$(GPP)_5$- GFOGMKGHRGFDGRNGEKGETGAOGLK-$(GPP)_5$GPC
7 GPC$(GPP)_5$- GETGAOGLKGENGLOGENGAOGPMGPR-$(GPP)_5$GPC
8 GPC$(GPP)_5$- GAOGPMGPRGAOGERGROGLOGAAGAR-$(GPP)_5$GPC
9 GPC$(GPP)_5$- GLOGAAGARGNDGARGSDGQOGPOGPO-$(GPP)_5$GPC
10 GPC$(GPP)_5$- GQOGPOGPOGTAGFOGSOGAKGEVGPA-$(GPP)_5$GPC
11 GPC$(GPP)_5$- GAKGEVGPAGSOGSNGAOGQRGEOGPQ-$(GPP)_5$GPC
12 GPC$(GPP)_5$- GQRGEOGPQGHAGAQGPOGPOGINGSO-$(GPP)_5$GPC
13 GPC$(GPP)_5$- GPOGINGSOGGKGEMGPAGIOGAOGLM-$(GPP)_5$GPC
14 GPC$(GPP)_5$- GIOGAOGLMGARGPOGPAGANGAOGLR-$(GPP)_5$GPC
15 GPC$(GPP)_5$- GANGAOGLRGGAGEOGKNGAKGEOGPR-$(GPP)_5$GPC
16 GPC$(GPP)_5$- GAKGEOGPRGERGEAGIOGVOGAKGED-$(GPP)_5$GPC
17 GPC$(GPP)_5$- GVOGAKGEDGKDGSOGEOGANGLOGAA-$(GPP)_5$GPC
18 GPC$(GPP)_5$- GANGLOGAAGERGAOGFRGPAGPNGIO-$(GPP)_5$GPC
19 GPC$(GPP)_5$- GPAGPNGIOGEKGPAGERGAOGPAGPR-$(GPP)_5$GPC
20 GPC$(GPP)_5$- GAOGPAGPRGAAGEOGRDGVOGGOGMR-$(GPP)_5$GPC
21 GPC$(GPP)_5$- GVOGGOGMRGMOGSOGGOGSDGKOGPO-$(GPP)_5$GPC
22 GPC$(GPP)_5$- GSDGKOGPOGSQGESGROGPOGPSGPR-$(GPP)_5$GPC
23 GPC$(GPP)_5$- GPOGPSGPRGQOGVMGFOGPKGNDGAO-$(GPP)_5$GPC
24 GPC$(GPP)_5$- GPKGNDGAOGKNGERGGOGGOGPQGPO-$(GPP)_5$GPC
25 GPC$(GPP)_5$- GGOGPQGPOGKNGETGPQGPOGPTGPG-$(GPP)_5$GPC
26 GPC$(GPP)_5$- GPOGPTGPGGDKGDTGPOGPQGLQGLO-$(GPP)_5$GPC
27 GPC$(GPP)_5$- GPQGLQGLOGTGGPOGENGKOGEOGPK-$(GPP)_5$GPC
28 GPC$(GPP)_5$- GKOGEOGPKGDAGAOGAOGGKGDAGAO-$(GPP)_5$GPC
29 GPC$(GPP)_5$- GGKGDAGAOGERGPOGLAGAOGLRGGA-$(GPP)_5$GPC
30 GPC$(GPP)_5$- GAOGLRGGAGPOGPEGGKGAAGPOGPO-$(GPP)_5$GPC
31 GPC$(GPP)_5$- GAAGPOGPOGAAGTOGLQGMOGERGGL-$(GPP)_5$GPC
32 GPC$(GPP)_5$- GMOGERGGLGSOGPKGDKGEOGGOGAD-$(GPP)_5$GPC
33 GPC$(GPP)_5$- GEOGGOGADGVOGKDGPRGPTGPIGPO-$(GPP)_5$GPC

34 GPC$(GPP)_5$- GPTGPIGPOGPAGQOGDKGEGGAOGLO-$(GPP)_5$GPC
35 GPC$(GPP)_5$- GEGGAOGLOGIAGPRGSOGERGETGPO-$(GPP)_5$GPC
36 GPC$(GPP)_5$- GERGETGPOGPAGFOGAOGQNGEOGGK-$(GPP)_5$GPC
37 GPC$(GPP)_5$- GQNGEOGGKGERGAOGEKGEGGPOGVA-$(GPP)_5$GPC
38 GPC$(GPP)_5$- GEGGPOGVAGPOGGSGPAGPOGPQGVK-$(GPP)_5$GPC
39 GPC$(GPP)_5$- GPOGPQGVKGERGSOGGOGAAGFOGAR-$(GPP)_5$GPC
40 GPC$(GPP)_5$- GAAGFOGARGLOGPOGSNGNOGPOGPS-$(GPP)_5$GPC
41 GPC$(GPP)_5$- GNOGPOGPSGSOGKDGPOGPAGNTGAO-$(GPP)_5$GPC
42 GPC$(GPP)_5$- GPAGNTGAOGSOGVSGPKGDAGQOGEK-$(GPP)_5$GPC
43 GPC$(GPP)_5$- GDAGQOGEKGSOGAQGPOGAOGPLGIA-$(GPP)_5$GPC
44 GPC$(GPP)_5$- GAOGPLGIAGITGARGLAGPOGMOGPR-$(GPP)_5$GPC
45 GPC$(GPP)_5$- GPOGMOGPRGSOGPQGVKGESGKOGAN-$(GPP)_5$GPC
46 GPC$(GPP)_5$- GESGKOGANGLSGERGPOGPQGLOGLA-$(GPP)_5$GPC
47 GPC$(GPP)_5$- GPQGLOGLAGTAGEOGRDGNOGSDGLO-$(GPP)_5$GPC
48 GPC$(GPP)_5$- GNOGSDGLOGRDGSOGGKGDRGENGSO-$(GPP)_5$GPC
49 GPC$(GPP)_5$- GDRGENGSOGAOGAOGHOGPOGPVGPA-$(GPP)_5$GPC
50 GPC$(GPP)_5$- GPOGPVGPAGKSGDRGESGPAGPAGAO-$(GPP)_5$GPC
51 GPC$(GPP)_5$- GPAGPAGAOGPAGSRGAOGPQGPRGDK-$(GPP)_5$GPC
52 GPC$(GPP)_5$- GPQGPRGDKGETGERGAAGIKGHRGFO-$(GPP)_5$GPC
53 GPC$(GPP)_5$- GIKGHRGFOGNOGAOGSOGPAGQQGAI-$(GPP)_5$GPC
54 GPC$(GPP)_5$- GPAGQQGAIGSOGPAGPRGPVGPSGPO-$(GPP)_5$GPC
55 GPC$(GPP)_5$- GPVGPSGPOGKDGTSGHOGPIGPOGPR-$(GPP)_5$GPC
56 GPC$(GPP)_5$- GPIGPOGPRGNRGERGSEGSOGHOGQO-$(GPP)_5$GPC
57 GPC$(GPP)_5$- GERGSEGSOGHOGQOGPOGPOGAOGPC-$(GPP)_5$GPC

Short Peptide Sequences:

GPC$(GPP)_5$- GNRGER-$(GPP)_5$GPC
GPC$(GPP)_5$- GHDGEK-$(GPP)_5$GPC
GPC$(GPP)_5$- GHDGDK-$(GPP)_5$GPC
GPC$(GPP)_5$- GFQGEK-$(GPP)_5$GPC
GPC$(GPP)_5$- GSQGEK-$(GPP)_5$GPC
GPC$(GPP)_5$- GPKGER-$(GPP)_5$GPC
GPC$(GPP)_5$- GNOGER-$(GPP)_5$GPC
GPC$(GPP)_5$- GFOGEK-$(GPP)_5$GPC
GPC$(GPP)_5$- GFSGER-$(GPP)_5$GPC
GPC$(GPP)_5$- GRSGET-$(GPP)_5$GPC
GPC$(GPP)_5$- GKOGER-$(GPP)_5$GPC
GPC$(GPP)_5$- GSOGEK-$(GPP)_5$GPC
GPC$(GPP)_5$- GQKGEI-$(GPP)_5$GPC
GPC$(GPP)_5$- GVOGER-$(GPP)_5$GPC
GPC$(GPP)_5$- GLOGEK-$(GPP)_5$GPC
GPC$(GPP)_5$- GLOGEN-$(GPP)_5$GPC
GPC$(GPP)_5$- GLOGER-$(GPP)_5$GPC
GPC$(GPP)_5$- GROGER-$(GPP)_5$GPC
GPC$(GPP)_5$- GVOGEA-$(GPP)_5$GPC
GPC$(GPP)_5$- GMOGER-$(GPP)_5$GPC
GPC$(GPP)_5$- GAOGER-$(GPP)_5$GPC
GPC$(GPP)_5$- GLOGEA-$(GPP)_5$GPC
GPC$(GPP)_5$- GLKGEN-$(GPP)_5$GPC
GPC$(GPP)_5$- GLSGER-$(GPP)_5$GPC

$GPC(GPP)_5$- GFOGDR-$(GPP)_5GPC$
$GPC(GPP)_5$- GASGER-$(GPP)_5GPC$
$GPC(GPP)_5$- GQRGER-$(GPP)_5GPC$
$GPC(GPP)_5$- GLKGER-$(GPP)_5GPC$
$GPC(GPP)_5$- GFOGER-$(GPP)_5GPC$

2.25 Statistical Analysis

PRISM GraphPad 8.2.1 was used for all statistical tests. Where siRNA is used, the mean value for each condition is compared to the mean value for the control condition using ordinary one-way ANOVA and Dunnett's multiple comparisons test unless otherwise stated. Dunnett's multiple comparisons test was used here because each siRNA condition was compared to the negative control siRNA condition and Dunnett's test was the most appropriate test for this comparison. Dunnett's test was also recommended by the PRISM GraphPad software for this application. Where inhibitors or activators are used, ordinary one-way ANOVA analysis is used with Sidak's multiple comparisons test and the mean for each condition is compared with the mean for the appropriate control condition. TC-I-15 is compared with the TC-I-15 vehicle control (NaOH) and everything else is compared to the control, both using Sidak's multiple comparison test or T-tests where stated. Sidak's test was used here because it is a relatively stringent test and each condition was compared to the relevant control condition rather than an overall control for the experiment. The test results are included in the text and P values that indicate statistical significance are highlighted in bold. If a Student's T-test is used, it is stated and described in the text. The Student's T-test is used to compare pairs of data sets only, with no multiple comparisons. Two-way ANOVA and Tukey's multiple comparisons tests are used for some of the static adhesion assays and some qPCR expression data and this is stated in the text. Tukey's multiple comparisons test is used to compare each condition to all other conditions in the experiment, rather than comparing each condition to a control condition.

Chapter 3 – Integrin Adhesion Studies

Contents

3.1 – Chapter Summary

This chapter focusses on using THPs synthesised in the Farndale Group to probe integrin binding preferences with the aim of determining specific peptides ligands targeting specific integrins. In the first instance, binding of integrin αI-domains to THPs containing proposed integrin-binding motifs was assessed. To verify the data produced in this work, further experiments were performed using C2C12 cells that were stably transfected to express full-length integrin receptors. The mRNA expression profiles of the four collagen-binding integrins was determined in HUVECs alongside other collagen receptors and the EC marker VWF. HUVECs were validated for expression of endothelial markers such as VWF, PECAM-1, VEGFR2, and MCAM. Finally, the integrin THP binding profiles determined using C2C12 cells was compared with the adhesion profiles of HUVECs on the same THPs. In this chapter, and indeed the rest of the thesis, α2β1 refers to the full-length integrin heterodimer whereas ITGA2 refers to the α-subunit alone.

3.2 – Introduction

Integrins are primarily a group of adhesion receptors that anchor cells to the ECM, or to other cells, before activating a wide range of downstream signalling pathways. These

depend on the cell type and presence of other integrin-associated proteins. For example platelet αIIBβ3 adhesion to fibrinogen leads to platelet aggregation[141] and α2β1 adhesion to collagen in leukocytes promotes T-cell survival through a MAPK/ERK pathway[237]. The ligands vary between the 24 integrins and the main ligands are summarised below[238] in Table 3.1. However, there are many other protein-protein interactions not listed here:

Table 3.1 – Different Integrin Ligands

Ligand	Found in	Integrins
RGD motif	Fibronectin, vitronectin, laminin, fibrinogen, VWF	αVβ1, αVβ3, αVβ5, αVβ6, αVβ8, α5β1, α8β1, αIIbβ3
LDV motif	Fibronectin, VCAM1, CD45	α4β1, α4β7, α9β1, αLβ2 αMβ2 αXβ2 αDβ2, αEβ7
GFOGER motif	Collagens	α1β1, α2β1, α10β1, α11β1
Laminin	Laminin	α3β1, α6β1, α7β1, α6β4

Figure 3.1: Diagram of the Structure of the MIDAS From ITGA2 αI-domain

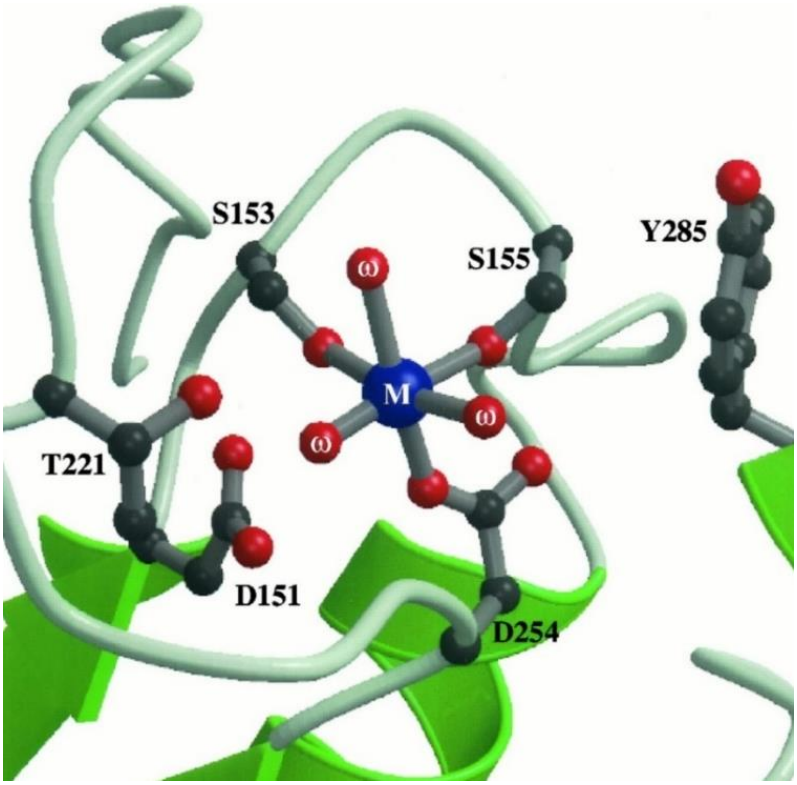

adapted from: *'Crystal Structure of the I Domain from Integrin α2β1'* by Jonas Emsley et al. J. Biol. Chem. 1997[8]

The coordinated Mg^{2+} ion (M) with associated water molecules (ω). Loops in grey, helices in green. Side chains of the MIDAS are shown, alongside the side chain from the C-Helix, which regulates ITGA2 αI-domain adhesion.

Each integrin will recognise a different motif, or set of motifs, and the differences in binding affinities could play a role in regulating cell function by targeting a specific integrin to trigger subsequent signalling pathways. An enrichment of α1β1 specific motifs in the ECM could upregulate α1β1 adhesion and could lead to increased α1β1-dependent downstream signalling events. Crystal structures have been obtained for the α1β1 and α2β1 αI-domains[8, 239]. They are proposed to bind collagen in a similar way as the MIDAS is strictly conserved. However, there could be subtle differences that infer selective binding preferences in different collagens. For the ITGA2 αI-domain, the MIDAS is made up from D151, S153, S155, T221, D254 from the Rossman fold structure and Y285 from the C-helix[8] (Figure 3.1) creating a groove. An E residue from the collagen motif would coordinate the Mg^{2+} ion in the MIDAS to facilitate binding in the groove created by the C-helix (Figure 3.2). The C-helix groove is thought to be 25Å x 20Å in dimension, containing the prominent Y285. In this model from *Emsley et al*[8] (Figure 3.1 and 3.2), substituting the E residue in collagen for a shorter D residue would annul binding due to steric clashes. Other residues predicted to be involved in binding are D219,

Figure 3.2: Diagram of the I-domain of α2β1 Binding to Collagen.

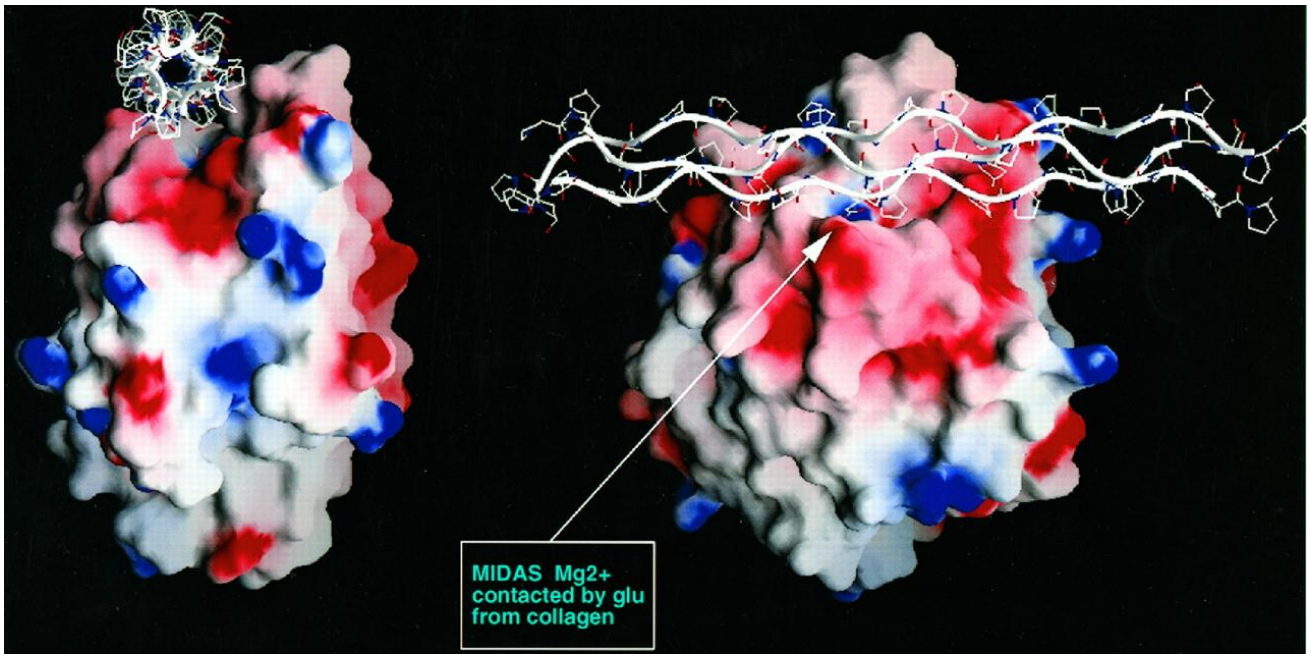

Adapted from '*Crystal Structure of the I Domain from Integrin α2β1*' Emsley et al 1997[8] showing the electron density map of integrin α2β1 αI-domain binding to a THP. A glutamate residue fits into the groove created by the MIDAS and the C-helix. Blue = positive charge, red = negative charge and white = neutral. Collagen is shown as a backbone triple helix.

L220, E256, H258, Y285, N289, L291, N295, K298. The MIDAS, C-helix and groove are conserved between the ITGA1 and ITGA2 αI-domains[239], however the C-helix differs in that the Y285 is replaced with a S, and L286 becomes Y in ITGA1. An activating mutation in ITGA1 (E317A) causes the C-helix to unwind, changing the position of Y285 and moving the helix into an open conformation which upregulates activity[240].

Previous work in the Prof Farndale group established that GFOGER and GLOGEN are strong ligands for all four collagen binding integrins, with GFOGER targeting preferentially α2β1 and α11β1 while GLOGEN targets preferentially α1β1 and α10β1[235, 241] and so this was taken as a starting point for exploring other motifs. Collagen protein sequences were probed for any potential integrin binding sites that resembled the GFOGER or GLOGEN motifs already established. THPs, described in Chapter 2.23, containing these motifs were synthesised. THPs are homotrimeric peptide sequences that readily form triple helices due to their GPC$(GPP)_5$ repeats at both the N and C terminus surrounding the central integrin-motif sequence[232, 234]. These THPs mimic the natural triple helical structure of the triple helical domains (THDs) of collagen but they are short and contain functional sequences. Table 3.2 summarises the motifs that synthesised and tested, referred to from now on as Short Peptides (SPs). To probe the different binding preferences of the 4 collagen-binding integrins, α1β1, α2β1, α10β1, α11β1, static adhesion assays were employed using these collagen mimetic SPs. Two motifs, GHDGDK and GFSGER, from the SPs are not present in any human collagen THDs but were included to test the effect of changing E to D in GHDGEK, and a change from A to F in GASGER.

GPP10, a THP composed only of 10 GPP triplets and GPC triplets on both the N- and C-terminal, was synthesised to serve as a negative control. This was used to check that any activity is due to the inserted GFOGER-like motif rather than the general triple helical structure imposed by GPP triplets, or the GPP repeats themselves. While GPP10 is an inert negative control, it is important to note that the helical structure is likely to be tighter in the repeated GPP repeats seen in GPP10 than in native collagen. This change in conformation could affect integrin binding as well. Integrins with a MIDAS require metal ions to function[8] (Figure 3.1), so for each experiment either Mg^{2+} was added to facilitate binding or a metal ion chelator, ethylenediaminetetraacetic acid (EDTA), was added to sequester metal ions. If binding was observed in the presence of EDTA it can be assumed to be non-specific, as the MIDAS in the αI-domain will not be able to function without Mg^{2+}.

	Collagen Type																					
Peptide	I	II	III	IV	V	VI	VII	VIII	IX	X	XI	XIII	XV	XIX	XX	XXI	XXII	XXIII	XXIV	XXV	XXVII	XXVIII
GAOGER		A1^{x2}	A1^{x2}	A2		A1 A3	A1^{x2}		A3													
GASGER	A1																	A1				
GFOGDR					A1																	
GFOGEK				A6		A3				A1												
GFOGER	A1	A1		A1 A3 A4^{x2} A5			A1				A1 A2											
GFQGEK				A6																		
GFSGER																						
GHDGDK																						
GHDGEK												A1										
GKOGER	A2									A1												
GLKGEN			A1																			
GLKGER				A1 A2 A4 A6			A1			A1									A1			
GLOGEK				A1^{x3} A2 A5 A6	A1 A2 A3	A1			A2		A2											
GLOGEN			A1													A1	A1					
GLOGER	A1 A2^{x2}	A1					A1^{x2}															
GLOGEA				A4							A1										A1	
GLSGER			A1																			
GMOGER	A1	A1	A1		A2				A3													
GNOGER					A1												A1		A1			
GNRGER			A1									A1										
GPKGER				A6	A1		A1				A1	A1	A1	A1^{x2}	A1		A1			A1		
GQKGEI								A1				A1				A1						
GQRGER	A1	A1			A2																	
GRORGER	A1 A2		A1				A1			A1												
GRSGET		A1																				
GSOGEK				A1	A3							A1^{x2}										
GSQGEK																						
GVOGER								A2														A1
GVOGEA		A1																				

Table 3.2. List of integrin-binding peptide motifs in THPs. showing the distribution of collagen motifs in the COL (triple helical) domains of different human collagens. A1 = THD alpha 1 chain. A1^{x2} means the motif is found twice in that domain. GHDGDK and GFSGER are not found anywhere in the COL domains of human collagens. GHDGDK was created to test the effects of E to D mutation in GHDGEK whereas GFSGER is a mutation of the GASGER found in collagen I.

Simplified systems using recombinant αI-domains were used as a starting point to study the interactions between integrins and collagens. The αI-domains contain the binding sites for collagen[8]. These αI-domains were cloned by Dr Samir Hamaia and expressed in bacterial systems as GST-tagged constructs. These were used in static adhesion assays alongside the SPs described above. In order to study integrins in a simplified cellular set-up, C2C12 that are stably transfected to express one of the four collagen-binding integrins were used in adhesion studies to assess the behaviour of the full-length heterodimer integrin in the hope of finding peptides that are specific for each of the four integrins. C2C12 cells were stably transfected by Dr Samir Hamaia to express one of the four α-subunits, which then associates with the mouse β1 subunit inside the cell to form the full-length functional receptor. C2C12 cells are an immortalised mouse myoblast cell line that were chosen because they do not naturally express any collagen-binding integrins and so any positive binding observed in the transfected cells that is absent in the non-transfected (C2C12 control) cells can be assumed to be a result of the transfected human α-subunit, as described in[242].

3.3 Binding of Recombinant αI-domains to Short Peptides

First, GST-tagged αI-domains were expressed in bacteria, extracted and purified using anti-GST affinity columns. The αI-domains for ITGA1 and ITGA2 were straightforward to express and both were functional showing high affinity specific binding when tested with collagen and GFOGER. However, ITGA10 and ITGA11 proved much more difficult to express and while GST-tagged proteins were recovered in abundance, they were not functional. This may be due to differences in folding between the αI-domains. It is possible a regulatory protein that aids αI-domain folding in ITGA10 and ITGA11 is missing or that the conditions required for successful protein folding and function are simply not met. The β1-subunit could also be necessary for proper function or folding of these integrins and the αI-domain alone may not be enough to bind in these conditions. Immulon 2HB plates were coated with peptides overnight in 0.01M AcOH and blocked with BSA before integrin αI-domains were added and left to adhere. After stringent wash steps, an anti-GST HRP conjugated antibody was used to detect remaining bound αI-domain using a TMB substrate colourimetric assay. Integrin αI-domain binding is shown in Figure 3.3 as a function of absorbance. Binding took place in a cation-dependent manner, with no binding in the presence of EDTA. This suggests that there were no non-specific adhesion and that the detected absorbance was due to binding through

integrins. This was confirmed by the absence of binding on BSA-coated wells. The absence of adhesion on GPP10 further implied that no non-specific binding to the triple helix structure of peptides occurred. Table 3.3 and 3.4 show a summary of the statistical analysis of the Mg^{2+} values for each peptide using Dunnett's multiple comparison test comparing each value to that of GPP10, P values are adjusted for multiple comparisons.

Figure 3.3: Integrin αI-Domain Adhesion to Short Peptides

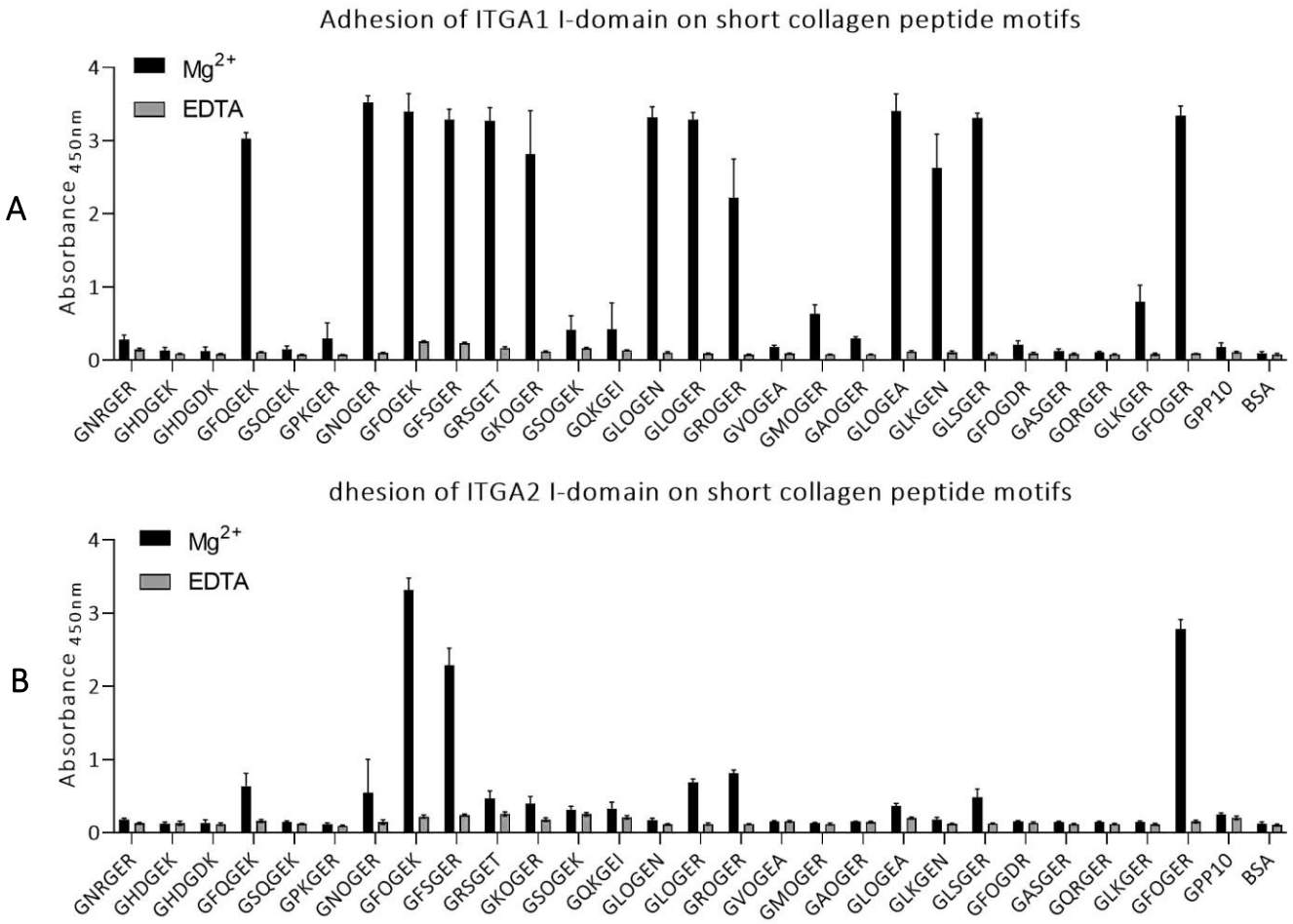

Graph showing the binding of recombinant ITGA1 and ITGA2 αI-domains to SPs as a function of as absorbance at 450nm, at a 1hr time point. Black bars represent the presence of Mg^{2+} and grey bars represent the presence of EDTA, as thus show non-specific binding. The mean absorbance from three separate repeats is plotted with the error bars indicating SD

Table 3.3 – Statistical analysis for ITGA1 αI-domain

Peptide	Mean	SD	P	Peptide	Mean	SD	P
GAOGER	0.3023	0.019	0.9323	GLOGER	3.284	0.102	**<0.0001**
GASGER	0.1274	0.027	0.9991	GLSGER	3.314	0.063	**<0.0001**
GFOGDR	0.2105	0.053	0.9996	GMOGER	0.6356	0.121	**<0.0001**
GFOGEK	3.395	0.246	**<0.0001**	GNOGER	3.519	0.092	**<0.0001**
GFOGER	3.341	0.133	**<0.0001**	GNRGER	0.2798	0.066	0.9864
GFQGEK	3.025	0.084	**<0.0001**	GPKGER	0.2932	0.218	0.9677
GFSGER	3.288	0.143	**<0.0001**	GQKGEI	0.4217	0.361	0.1175
GHDGDK	0.1287	0.053	0.9991	GQRGER	0.1067	0.015	0.9986
GHDGEK	0.1325	0.042	0.9992	GROGER	2.218	0.533	**<0.0001**
GKOGER	2.818	0.591	**<0.0001**	GRSGET	3.274	0.177	**<0.0001**
GLKGEN	2.629	0.459	**<0.0001**	GSOGEK	0.4139	0.195	0.1447
GLKGER	0.8004	0.226	**<0.0001**	GSQGEK	0.1482	0.047	0.9995
GLOGEA	3.403	0.235	**<0.0001**	GVOGEA	0.1798	0.023	>0.9999
GLOGEN	3.319	0.145	**<0.0001**	BSA	0.09458	0.055	0.9937
Analysis of mean absorbance values compared to the GPP10 control mean. P values were obtained using Dunnett's Multiple comparison test, adjusted for multiple comparisons							

Table 3.4 – Statistics analysis for ITGA2 αI-domain

Peptide	Mean	SD	P	Peptide	Mean	SD	P
GAOGER	0.1505	0.009	0.3926	GLOGER	0.6888	0.047	**<0.0001**
GASGER	0.1469	0.013	0.3445	GLSGER	0.4835	0.113	**<0.0001**
GFOGDR	0.1585	0.006	0.5142	GMOGER	0.1352	0.007	0.2127
GFOGEK	3.312	0.166	**<0.0001**	GNOGER	0.5523	0.450	**<0.0001**
GFOGER	2.779	0.135	**<0.0001**	GNRGER	0.1744	0.025	0.7792
GFQGEK	0.6320	0.180	**<0.0001**	GPKGER	0.1178	0.016	0.0921
GFSGER	2.291	0.229	**<0.0001**	GQKGEI	0.3258	0.091	0.8073
GHDGDK	0.1354	0.041	0.2149	GQRGER	0.1477	0.010	0.3543
GHDGEK	0.1245	0.020	0.1292	GROGER	0.8139	0.042	**<0.0001**
GKOGER	0.3974	0.096	**0.0442**	GRSGET	0.4683	0.104	0.0002
GLKGEN	0.1734	0.038	0.7624	GSOGEK	0.3108	0.051	0.9657
GLKGER	0.1493	0.012	0.3755	GSQGEK	0.1471	0.016	0.3462
GLOGEA	0.3689	0.032	0.1942	GVOGEA	0.1576	0.007	0.5005
GLOGEN	0.1729	0.026	0.7556	BSA	0.1261	0.022	0.1402
Analysis of mean absorbance values compared to the GPP10 control mean. P values were obtained using Dunnett's Multiple comparison test, adjusted for multiple comparisons							

The binding profiles of the two integrins were markedly different. ITGA1 αI-domain showed strong binding to most peptides tested whereas the ITGA2 counterpart was much less active, binding to only 3 motifs. Whilst previous work indicates that α1β1 preferentially binds GLOGEN over GFOGER, here strong binding to both ligands was observed. The αI-domain binds motifs from several collagen sequences with a high specificity; out of the collagen IV motifs. ITGA1 bound to GFQGEK, GFOGEK, GLOGEA and GFOGER and moderate binding affinity to

GROGER was observed. Numerous peptides which were specific for ITGA1 did not bind ITGA2. The differential affinities of the integrins for peptide sequences indicates that peptides could be used as a tool to probe ITGA1 function in ECs. Whilst no clear conclusive consensus sequence for ITGA1 αI-domain was determined, analysis of the ITGA1 binding motifs raises some important points which are summarised below with bullet points for simplicity:

- GLKGE**N** supported moderate binding whilst GLKGE**R** does not. did not. However, the GER motif supported binding in many other peptides. This suggests that the overall change in shape or charge conferred by a mutation from N to R in the presence of GLK impedes binding.
- G**N**OGER but not G**M**OGER supported binding. No other peptides have methionine in the 2nd position in the consensus sequence, but other THPs that have hydrophobic side chains (GLOGEN, GLOGER) and larger side chains (GFOGER) showed strong binding.
- GLOGE**R** and GLOGE**N** showed similar binding profiles , suggesting that an R (positively charged) to N (polar neutral) mutation does not impede binding at this position.
- G**F**QGEK supported binding whilst G**S**QGEK did not, suggesting a F (hydrophobic) to S (polar neutral) in the 2nd position blocks binding.
- G**L**OGEA supported high binding but G**V**OGEA did not. Both L and V have hydrophobic aliphatic side chains, but V is one carbon shorter.
- GFOGE**R** and GFOGE**K** both supported high binding. Both R and K have basic side chains, but many peptides with N in the 6th position also show high binding, so this is not a requirement.
- GL**O**GEN and GL**K**GEN both show high binding suggesting the 3rd position can be basic or polar neutral. There are no tight restrictions on the 3rd position.
- Changing the 5th position from **E** to **D** abolishes binding in GFOG**E**R as predicted by Emsley et al[8] for ITGA2 αI-domain.

The binding profile of the αI-domain of ITGA1 suggests that there are no restrictions on the 2nd, 3rd and 6th positions of the recognition motif and that it may be the overall shape and confirmation of the helix rather than the specific residues that confers specificity. The groove in the I-domain contains a mixture of positive, negative and neutral side chains, thus the variability of the recognition sequence may stem from this[8].

The binding profile of ITGA2 αI-domain was much less active, binding only GFOGER (collagen type I, II, IV, VII, XI), GFOGEK (collagen type IV, VI, X) and GFSGER. This suggests that $GFx^{3}GEx^{6}$, where x^{3} is neutral, x^{6} is basic and the 5^{th} position is a glutamate, is necessary for binding. The absence of binding to other SPs could be due to missing regulatory elements in the β-subunit. Alternatively, the αI-domain could be in a less active confirmation when expressed as an αI-domain recombinant protein alone, without the rest of the β-propeller from the α-subunit or the rest of the α-subunit itself. There are no peptides specific for the ITGA2 αI-domain.

3.4 Binding of integrin expressing C2C12 cells to Short Peptides

Adhesion of recombinant proteins of αI-domains is a good starting point for studying integrins, but this approach is limited as only one domain of the receptor is present and there are no functional αI-domains for ITGA10 and ITGA11. The β1 subunit and the rest of the α-subunit could play a role in the regulation of integrin function, as the β-subunit has its own I-domain, so it is important to validate any findings using full length receptors. Also, protein adhesion assays here only study the simple interactions between the αI-domain and the peptide whereas in a physiological setting there are several other receptors and signalling molecules that would associate and interact with integrins on the cell surface. It is therefore necessary to validate the αI-domain assays in whole cells.

Static adhesion assays using SPs, as above, were carried out under sterile conditions. After blocking, C2C12 cells expressing collagen binding integrins were added at 20,000/well in serum-free DMEM and left at RT for one hour to adhere to coated peptides. After three gentle washes the remaining cells were lysed in 50µl of 2% Triton x100. The Roche cytotoxicity LDH kit was used to quantify the number of cells still attached to the peptides after washing as a function of LDH activity in a colorimetric assay. Results are shown in Figure 3.4.

The binding profiles of the four integrins were very similar. The α2β1 receptor showed the more active profile, indicated by binding to a large number of peptides, whereas the α1β1 (and α10β1, α11β1) showed a less active binding profile compared to experiments using αI-domain recombinant proteins. This is possibly due to the absence of the regulatory function of the β1 subunit and the rest of the α-subunit in the recombinant proteins. Binding of the αI-domain to GNOGER, GKOGER, GLOGER, GORGER and GMOGER was lost in the full length α1β1

receptor whereas the full length α2β1 adhered to more THPs than the ITGA2 αI-domain. The β1-subunit could potentially interact with each α-subunit differently. For example, the β1-subunit could stabilise a less active confirmation of the ITGA1 αI-domain but could encourage a more active confirmation of the ITGA2 αI-domain. Further studies are needed to confirm this hypothesis. It is possible that other co-receptors are present in C2C12 cells that subtly influence the activity of the integrin heterodimers, explaining the differences seen between isolated αI-domains and full-length receptors. The data presented from the C2C12 cell adhesion assays is more physiologically relevant as it takes place in a cellular setting with full-length receptors rather than isolated αI-domains.

Table 3.5 – List of peptide specificity

Peptides that bind all integrins		Peptides specific for α2β1	
Motif	Collagen Type	Motif	Collagen Type
GFOGEK	IV, VI and X	GAOGER	II, III, IV, VI, VII, IX
GFOGER	I, II, IV, VII and XI	GKOGER	I and X
GFSGER	not found in human collagens	GMOGER	I, II, III, V, IX
GLOGEK	IV, V, VI, IX and XI	GNOGER	V, XXII and XXIV
GLOGEN	III XXI and XXII	GNRGER	III and XIII
GLOGER	I II and VII	GSOGEK	IV, V, XIII

Other peptide specificities		
Motif	Collagen Type	Integrin specificity
GFQGEK	IV	α1β1 and α2β1 only
GLKGER	IV VII and X	α2β1 and α10β1 only
GLOGEA	IV XI and XXVII	Not α11β1
GLKGEN	III	Not α11β1
GLSGER	III	Not α11β1
GRSGET	II	α1β1, α2β1 only
GROGER	I, III, VII, X	Not α10β1

Figure 3.4 Adhesion of Integrin Expressing C2C12 to Short Peptides

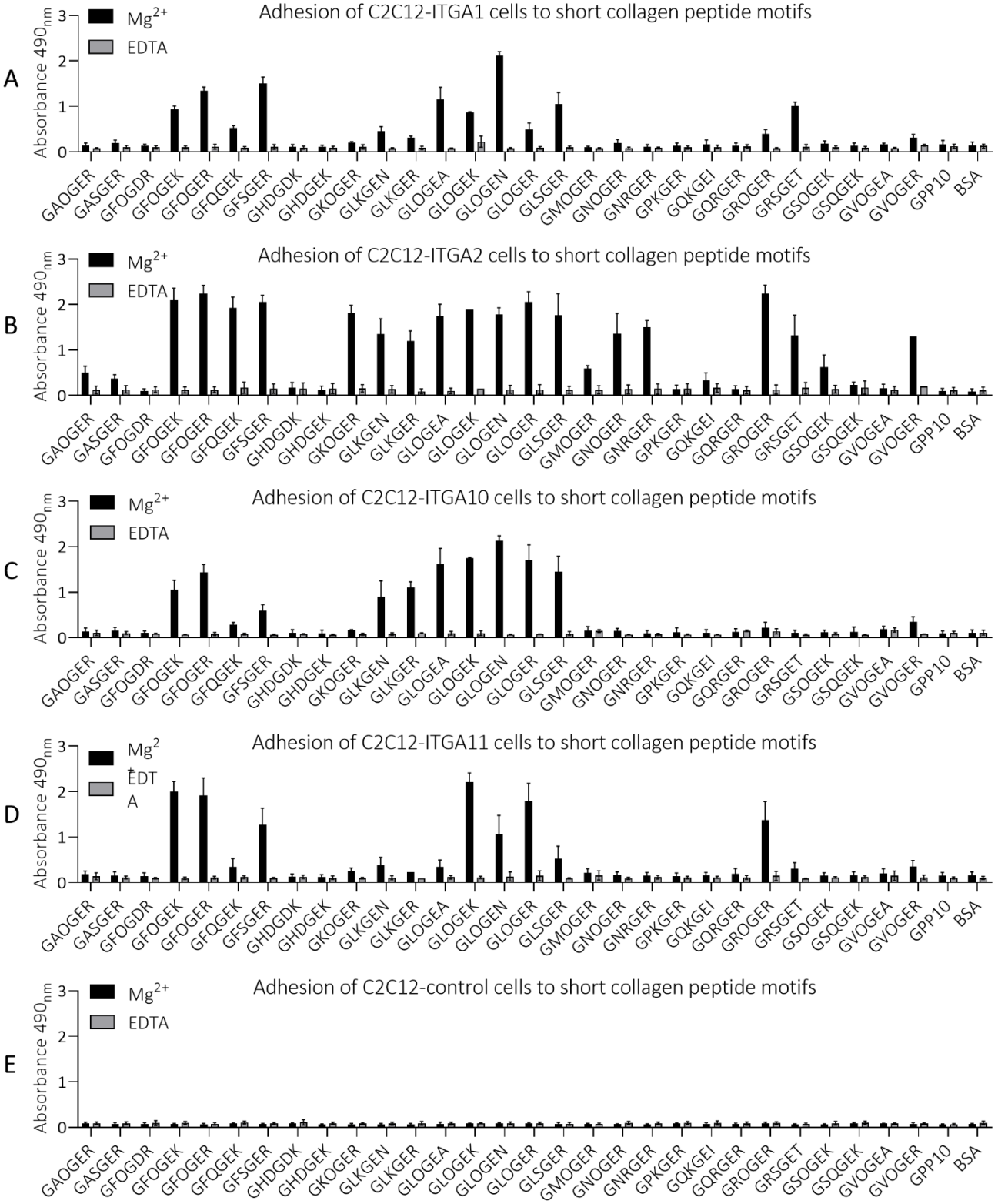

Adhesion is shown as absorbance at 490nm after cell lysis and quantification with the LDH colorimetric cytotoxicity assay. The black bars indicate Mg^{2+} dependent adhesion while the grey bars indicate addition of the metal ion chelator EDTA. SPs are shown in alphabetical order, GPP10 is a negative control peptide. BSA represents empty wells coated with BSA without THPs.

The C2C12 control cells showed no binding both with Mg^{2+} and EDTA. Therefore, the binding seen with the transfected C2C12 cells is assumed to be due to the transfected human α-subunit. None of the cell lines showed binding in the EDTA condition (grey bars) meaning that all adhesion was metal ion dependent, suggesting again that any binding seen in the presence of Mg^{2+} is due to the transfected integrins. Table 3.5 summarises the peptides that have specific integrin binding patterns. Unfortunately, only α2β1 shows binding to specific peptides. As a consequence, binding to α2β1 will mask adhesion of other integrins when more than one type of integrin is present. Tables 3.6 to 3.9 summarise the statistical analyses.

This comprehensive study of collagenous integrin binding motifs types suggests that there are multiple, varied binding sites for all four collagen-binding integrins across the entire human collagen family. However, it also shows that peptides alone cannot be used to ligate single integrins in ECs as there is considerable overlap of binding motifs across the four receptors. In addition, the more active binding profile of α2β1 masks the attachment to other integrins and prevents us from determining the specific effect of each integrin on cellular response using THPs. Generally, the consensus binding motif among all four integrins is $Gx^2x^3GEx^6$, where x^2 is F or L, x^3 is O or S and x^6 is K, N or R, in agreement with our previous publication[243]; an R at x^2 will rule out binding of α10β1 due to a clash between positively charged R215 in the αI-domain and the R at x^2. These results also suggest that A or K at x^3 attenuate binding of α11β1.

Table 3.6: Statistical analysis of C2C12-ITGA1 adhesion to THPs.

Peptide	Mean absorbance	SD	n	P	Peptide	Mean absorbance	SD	n	P
GAOGER	0.141	0.054	4	0.9993	GLOGER	0.493	0.143	4	**<0.0001**
GASGER	0.194	0.064	4	0.9994	GLSGER	1.049	0.257	4	**<0.0001**
GFOGDR	0.128	0.045	4	0.9989	GMOGER	0.098	0.027	4	0.9482
GFOGEK	0.937	0.067	4	**<0.0001**	GNOGER	0.192	0.083	4	0.9994
GFOGER	1.342	0.085	4	**<0.0001**	GNRGER	0.118	0.044	4	0.9943
GFQGEK	0.522	0.058	4	**<0.0001**	GPKGER	0.132	0.064	4	0.9990
GFSGER	1.502	0.143	4	**<0.0001**	GQKGEI	0.168	0.099	4	>0.9999
GHDGDK	0.114	0.049	4	0.9935	GQRGER	0.137	0.059	4	0.9992
GHDGEK	0.110	0.037	4	0.9926	GROGER	0.402	0.087	4	**0.0005**
GKOGER	0.204	0.023	4	0.9991	GRSGET	1.016	0.080	4	**<0.0001**
GLKGEN	0.461	0.097	4	**<0.0001**	GSOGEK	0.183	0.061	4	0.9997
GLKGER	0.321	0.029	2	0.2742	GSQGEK	0.131	0.066	4	0.9990
GLOGEA	1.149	0.272	4	**<0.0001**	GVOGEA	0.166	0.026	4	>0.9999
GLOGEK	0.871	0.013	2	**<0.0001**	BSA	0.317	0.069	2	0.3106
GLOGEN	2.116	0.090	4	**<0.0001**	GPP10	0.169	0.083	4	

Mean absorbances are compared to the mean absorbance of GPP10 using two-way ANOVA and Dunnett's multiple comparisons test.

Table 3.7: Statistical analysis C2C12-ITGA2 adhesion to THPs

Peptide	Mean absorbance	SD	n	P	Peptide	Mean absorbance	SD	n	P
GAOGER	0.504	0.144	4	**0.0147**	GLOGER	2.054	0.229	4	**<0.0001**
GASGER	0.373	0.085	4	0.2764	GLSGER	1.767	0.474	4	**<0.0001**
GFOGDR	0.102	0.050	4	>0.9999	GMOGER	0.592	0.065	4	**0.0010**
GFOGEK	2.097	0.260	4	**<0.0001**	GNOGER	1.362	0.443	4	**<0.0001**
GFOGER	2.238	0.182	4	**<0.0001**	GNRGER	1.498	0.147	4	**<0.0001**
GFQGEK	1.922	0.240	4	**<0.0001**	GPKGER	0.144	0.084	4	0.9995
GFSGER	2.059	0.148	3	**<0.0001**	GQKGEI	0.337	0.159	3	0.5962
GHDGDK	0.174	0.111	4	0.9991	GQRGER	0.143	0.070	4	0.9995
GHDGEK	0.121	0.090	4	0.9998	GROGER	2.237	0.191	4	**<0.0001**
GKOGER	1.812	0.173	3	**<0.0001**	GRSGET	1.326	0.445	3	**<0.0001**
GLKGEN	1.354	0.334	4	**<0.0001**	GSOGEK	0.621	0.272	3	**0.0014**
GLKGER	1.202	0.222	3	**<0.0001**	GSQGEK	0.226	0.071	4	0.9929
GLOGEA	1.756	0.248	4	**<0.0001**	GVOGEA	0.163	0.085	4	0.9993
GLOGEK	1.882	0.000	1	**<0.0001**	BSA	1.297	0.000	1	**<0.0001**
GLOGEN	1.782	0.148	4	**<0.0001**	GPP10	0.099	0.056	4	

Mean absorbances are compared to the mean absorbance of GPP10 using two-way ANOVA and Dunnett's multiple comparisons test.

Table 3.8 Statistical analysis C2C12-ITGA10 adhesion to THPs

Peptide	Mean absorbance	SD	n	P	Peptide	Mean absorbance	SD	n	P
GAOGER	0.139	0.073	4	0.9993	GLOGER	1.704	0.335	4	**<0.0001**
GASGER	0.153	0.075	4	0.9990	GLSGER	1.453	0.338	4	**<0.0001**
GFOGDR	0.109	0.039	4	0.9999	GMOGER	0.158	0.090	4	0.9989
GFOGEK	1.056	0.209	4	**<0.0001**	GNOGER	0.145	0.060	4	0.9992
GFOGER	1.437	0.176	4	**<0.0001**	GNRGER	0.096	0.063	4	>0.9999
GFQGEK	0.289	0.046	4	0.2219	GPKGER	0.118	0.099	4	0.9997
GFSGER	0.593	0.134	4	**<0.0001**	GQKGEI	0.107	0.071	4	0.9999
GHDGDK	0.102	0.074	4	>0.9999	GQRGER	0.125	0.073	4	0.9996
GHDGEK	0.098	0.070	4	>0.9999	GROGER	0.214	0.129	4	0.8926
GKOGER	0.162	0.016	4	0.9988	GRSGET	0.113	0.050	4	0.9998
GLKGEN	0.910	0.338	4	**<0.0001**	GSOGEK	0.119	0.043	4	0.9997
GLKGER	1.102	0.129	2	**<0.0001**	GSQGEK	0.126	0.110	4	0.9996
GLOGEA	1.618	0.348	4	**<0.0001**	GVOGEA	0.186	0.066	4	0.9925
GLOGEK	1.758	0.008	2	**<0.0001**	BSA	0.353	0.108	2	0.1339
GLOGEN	2.135	0.106	4	**<0.0001**	GPP10	0.100	0.051	4	

Mean absorbances are compared to the mean absorbance of GPP10 using two-way ANOVA and Dunnett's multiple comparisons test.

Table 3.9: Statistical analysis C2C12-ITGA11 adhesion to THPs

Peptide	Mean absorbance	SD	n	P	Peptide	Mean absorbance	SD	n	P

GAOGER	0.186	0.072	4	0.9996	GLOGER	1.805	0.381	4	**<0.0001**
GASGER	0.160	0.078	4	>0.9999	GLSGER	0.529	0.275	4	**0.0067**
GFOGDR	0.144	0.076	4	>0.9999	GMOGER	0.214	0.093	4	0.9991
GFOGEK	2.002	0.226	4	**<0.0001**	GNOGER	0.181	0.054	4	0.9996
GFOGER	1.917	0.386	4	**<0.0001**	GNRGER	0.150	0.078	4	>0.9999
GFQGEK	0.346	0.184	4	0.5635	GPKGER	0.146	0.069	4	>0.9999
GFSGER	1.276	0.363	4	**<0.0001**	GQKGEI	0.164	0.064	4	0.9999
GHDGDK	0.137	0.056	4	0.9998	GQRGER	0.193	0.119	4	0.9995
GHDGEK	0.129	0.049	4	0.9997	GROGER	1.376	0.408	4	**<0.0001**
GKOGER	0.257	0.068	4	0.9933	GRSGET	0.305	0.137	4	0.8675
GLKGEN	0.389	0.169	4	0.2771	GSOGEK	0.161	0.063	4	0.9999
GLKGER	0.231	0.000	1	0.9993	GSQGEK	0.164	0.076	4	0.9999
GLOGEA	0.349	0.149	4	0.5447	GVOGEA	0.203	0.103	4	0.9993
GLOGEK	2.212	0.202	3	**<0.0001**	BSA	0.360	0.124	3	0.5752
GLOGEN	1.064	0.418	4	**<0.0001**	GPP10	0.151583	0.076204	4	

Mean absorbances are compared to the absorbance of GPP10 using two-way ANOVA and Dunnett's multiple comparisons test.

3.5 Collagen Receptor Expression in HUVECs

As this project focuses on studying the collagen binding integrins and their role in HUVECs, the expression levels of each receptor were first characterised. qPCR was used to detect the mRNA expression levels of each integrin in HUVECs. The mRNA expression of the EC

Figure 3.5. Comparison of Endogenous Controls For Use in qPCR.

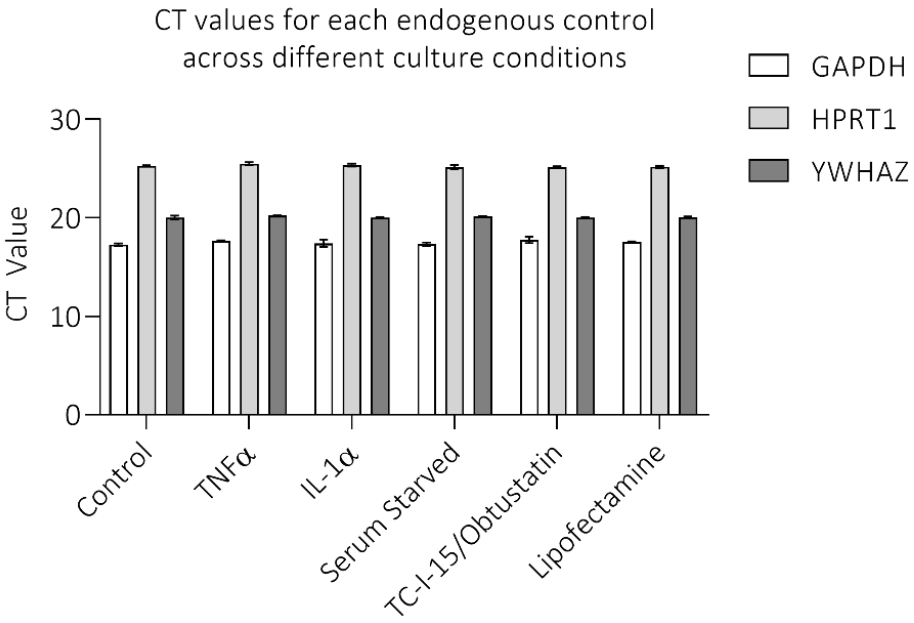

Graph showing the CT values for each endogenous control after activation with various cytokines. 20ng/ml TNFα, 10ng/ml IL-1α, 0.2% FBS, 200µM TC-I-15, 20µM Obtustatin or 1µl of lipofectamine was added to cell cultures in 12 well plates and incubated at 37°C overnight. The expression levels of each control were remarkably stable across these conditions

marker VWF was also evaluated, together with the three other collagen-binding proteins that share the common binding motif with VWF, DDR1, DDR2 and SPARC, for comparison. TaqMan primers and probes were used to detect integrin transcripts. To control for differences in cDNA concentration in each assay, a TaqMan primer/probe set was used to detect an endogenous housekeeping transcript for normalisation. The mRNA transcripts for HPRT1, GAPDH and YWHAZ were all tested for their suitability as an endogenous control transcript in HUVECS. HUVECs were cultured for 24 hours in EGM2 with the addition of cytokines, integrin inhibitors, or serum starvation. qPCR was used to detect the transcript levels of each endogenous control over these conditions. Figure 3.5 shows the comparison of the cycle threshold (CT) values of each endogenous control tested. The values were remarkably consistent across three repeats. siRNA targeting GAPDH was used in experiments described in chapter 5 to optimise siRNA KD, which was characterised using qPCR. Therefore, GAPDH cannot be used as an endogenous control for the quantification of GAPDH KD. Both YWHAZ and HPRT1 would be suitable but YWHAZ is expressed at higher levels, so HPRT1 was chosen for all subsequent studies.

Figure 3.6: Comparison of Collagen Receptor Expression in HUVECs.

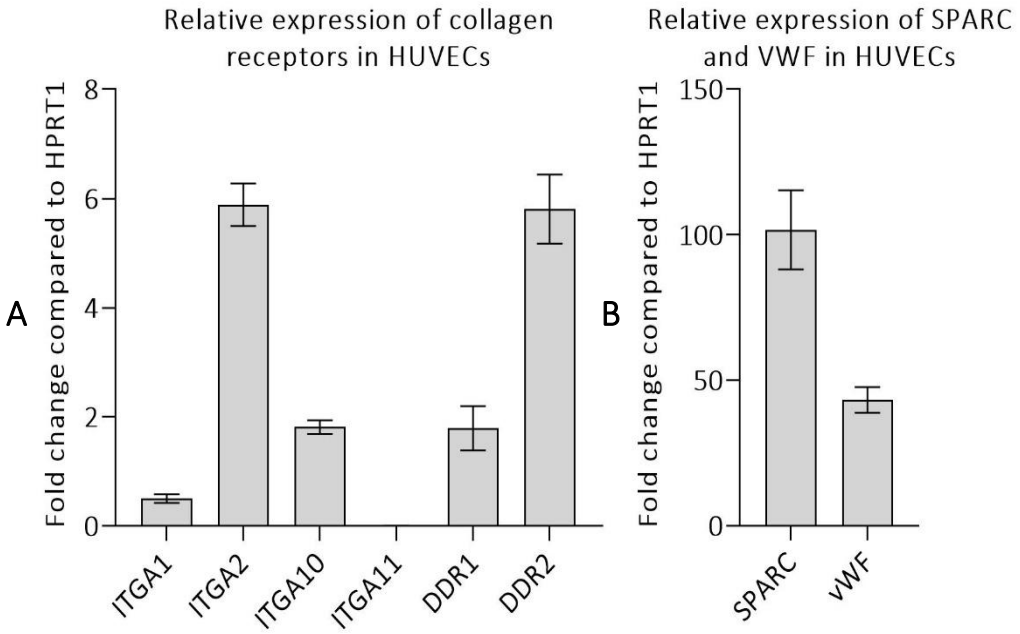

Graphs showing the relative expression levels of several collagen receptor mRNA transcripts shown as fold change relative to HPRT1. Note the difference in scale between A) and B), with SPARC at 100 and VWF at around 50. Table 3.8 (below) summarises the one-way ANOVA, Tukey's multiple comparisons statistical analysis. VWF and SPARC were compared separately using an unpaired T-test.

To characterise the integrin expression patterns in HUVECs using qPCR, HUVECs were cultured in tissue culture plates in EGM2 media before total mRNA extraction using Qiagen RNeasy Plus RNA extraction kits. Total RNA was reverse transcribed into cDNA using TaqMan reverse transcription reagents with random hexamers. Predesigned TaqMan gene expression assays were used to quantify the expression of different collagen receptors at the mRNA level. All experiments were repeated using cDNA libraries derived from at least 3 pools of HUVECs and qPCR was carried out in triplicate. The ΔΔCT method was used to normalise CT values to the endogenous control and expression data is shown in Figure 3.6 as fold change relative to HPRT1. ITGA1, ITGA2, ITGA10 and ITGA11 refer to the detection of the mRNA transcript of the integrin α1, α2, α10 and α11 subunits respectively. Figure 3.6 shows the expression data as the mean with error bars showing SD. Table 3.10 summarises the statistical analysis of this data using one-way ANOVA and Tukey's multiple comparison's test for all receptors except VWF and SPARC which were compared using a students' T-Test. The means of the fold-changes relative to HPRT1 are shown with SD, n and P values for the multiple comparisons.

Table 3.10 – Statistical analysis of receptor expression

	Mean fold change	SD	n	P = vs ITGA1	P = vs ITGA2	P = vs ITGA10	P = vs ITGA11	P = vs DDR1	P = vs DDR2
ITGA1	0.5048	0.265	11		**<0.0001**	**0.0042**	0.8782	0.1373	**<0.0001**
ITGA2	5.886	1.288	11	**<0.0001**		<0.0001	**<0.0001**	**<0.0001**	>0.9999
ITGA10	1.815	0.411	11	**0.0042**	**<0.0001**		**0.0038**	>0.9999	**<0.0001**
ITGA11	0.0054	0.004	11	0.8782	**<0.0001**	**0.0038**		**0.0491**	**<0.0001**
DDR1	1.794	0.704	3	0.1373	**<0.0001**	>0.9999	0.0491		**<0.0001**
DDR2	5.806	1.095	3	**<0.0001**	>0.9999	**<0.0001**	**<0.0001**	**<0.0001**	
Mean fold change values for each condition are compared to the mean fold change values for all other conditions using one-way ANOVA and Tukey's multiple comparison test. A students T-test was used to compare VWF and SPARC									

VWF	43.31	7.592	3	SPARC vs VWF *P=**0.0149**
SPARC	101.7	23.49	3	

VWF is an endothelial marker that shows relatively high (50x fold change compared to HPRT1) expression levels. This contributes to validating the endothelial phenotype of the cells. Of the four collagen-binding integrins, ITGA2 was found to be the most abundant integrin (5.886 x fold change compared to HPRT1, ****P<0.0001 compared to all the other integrins Figure 3.6), followed by ITGA10 (1.815 x fold change compared to HPRT1) and then ITGA1 (0.5048 x fold change compared to HPRT1), whereas ITGA11 was barely detectable (0.0054 x

fold change compared to HPRT1). There was no significant difference between ITGA1 and ITGA11 expression. This agrees with unpublished work by Dr Peter Kim (personal communication) Expression of ITGA2 has been characterised in a variety of ECs including HUVECs whereas ITGA1 is well defined in microvascular ECs[157, 158]. Both are upregulated by VEGF[160], which is included in the EGM2 media at low levels (0.5ng/ml). It is possible that addition of more VEGF will upregulate the ITGA1 subunit. The ITGA10 subunit has not been characterised in ECs but is present at the mRNA level according to these experiments. Therefore, one of the main objectives of this project was to characterise the expression and role of α10β1 integrin in HUVECs.

Collagen receptors DDR1 (1.794-fold increase compared to HPRT1) and DDR-2 (5.806-fold increase compared to HPRT1) were both detected in HUVECs. DDR-2 is seen at similar levels to ITGA2 and DDR-1 is found at similar levels to ITGA10. These receptors have not been well characterised in ECs but some studies suggest DDR2 is upregulated in activated ECs[244]. It is therefore possible that higher levels would be seen after addition of TNFα, LPS or ILs. One study found that DDR2 is also expressed in high levels in ECs in human tumours, and the loss of DDR2 supresses tumour metastasis[245]. The same study also found that induced overexpression of DDR2 in HUVECs has been found to increase proliferation, migration and angiogenesis. DDR1 has been detected, but not characterised, in brain microvascular cells[246]. DDR1 interacts with the integrin β1 subunit and DDR1 overexpression in human fibroblasts and 3T3 cells, results in increased activated β1, increased β1 adhesion to collagen and increased β1 glycosylation which affects integrin function[247, 248] This suggests a regulating role for DDR1 in β1 function[249]. The same study found that α2β1 expression almost doubled in DDR1 overexpression and decreased after DDR1 KO[249]. Interestingly, SPARC is expressed in relatively high levels (101.7 x fold change compared to HPRT1) and twice as abundant as the EC marker VWF (43.31 x fold change compared to HPRT1, *P=0.0149). SPARC is thought to regulate EC barrier function by inducing cell-shape changes resulting in increased barrier permeability in pulmonary artery, bovine microvascular and bovine aortic ECs[210, 212]. Elevated SPARC expression in tumours results in a VCAM dependent increase of vascular permeability and contributes to cancer cell metastasis[250]. SPARC is a de-adhesive protein that promotes cell de-attachment[205, 206] whereas integrins promote strong cell adhesion to collagen. Hence, while it

is outside the scope of this project, it would be interesting to further characterise SPARC functions in HUVECs, given its high levels of mRNA expression.

In conclusion, the mRNA for the ITGA2 subunit was detected in much higher amounts than the other three integrins, with ITGA10 being the second most abundant transcript, followed by ITGA1, while ITGA11 was undetectable. There is a pool of β1 subunit in the cell that pair up with the α-subunits to form the heterodimer[140]. The protein expression of these integrins is therefore determined by the expression of the α-subunits.

3.6 Characterisation of pooled HUVECs

Before carrying out any further integrin studies in HUVECs, experiments were performed to characterise their endothelial phenotype. There are several markers for EC phenotype, VWF being the most commonly used marker as many commercially available antibodies have been thoroughly validated for use in ECs and VWF is easily visualised in WBPs as rod-shaped granules in the cytoplasm[132]. VE-Cad is an EC marker expressed on the cell surface as an adhesion molecule, it controls cell-cell junction adhesion and blood vessel formation, and contributes to the regulation of proliferation and apoptosis[38]. CD45 is a marker for hematopoietic lineage, it is expressed in EC progenitor cells and should be largely absent in mature ECs. CD45 is also express in leukocytes and lymphocytes. CD31 is a common marker for EC phenotype that is highly expressed on the surface of ECs. It is also expressed on platelets, monocytes, neutrophils and is important in leukocyte migration. MCAM is another membrane EC marker, binding to laminin. Finally, VEGFR2, a receptor for VEGF that mediates angiogenesis, is expressed mainly in ECs but can also be detected in a number of other cells including endometrial epithelium, hematopoietic stem cells, liver sinusoidal ECs, Sertoli cells and Leydig cells, platelets and megakaryocytes, sensory and autonomic neurons, Schwann cells, Muller glial cells, retinal progenitors, and osteoblasts (EC markers are reviewed in[36]). HUVECs will be tested for the presence of these markers by immunofluorescence and flow cytometry. VWF has been detected at the mRNA level in Figure 3.6.

Pooled HUVECs were purchased from Promocell. They are marketed as positive for VWF and CD31. EC markers VWF and CD31 were detected by immunofluorescence in HUVECs cultured to passage 5 in EGM2 media. Cells were fixed in 4% PFA before staining in 1% BSA in

PBS and image acquisition by microscopy. A representative field of view for PECAM-1 is shown in Figure 3.7 with Hoechst nuclear staining. VWF staining in sparse and confluent cells is shown in Figure 3.8 alongside rhodamine phalloidin actin staining and Hoechst nuclear staining.

Figure 3.7: Expression of Endothelial Markers in HUVECs.

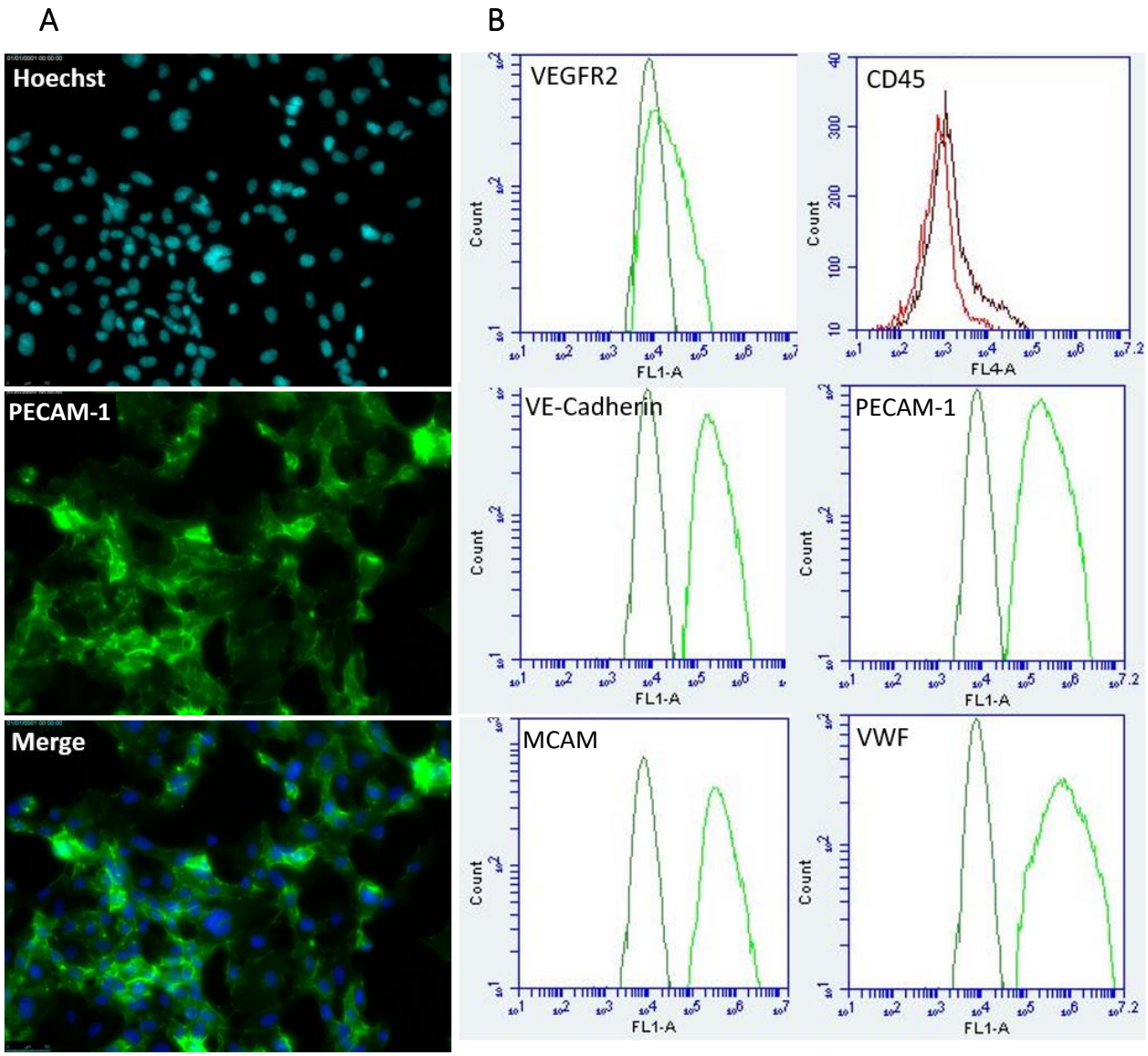

A: immunofluorescence staining for CD31 (green) and Hoechst (blue). B: flow cytometry staining for various HUVEC cell markers. For flow cytometry assays, the darker green/red shows isotype control stained cells whereas the lighter colour shows the marker stained cells. Experiments were repeated with unstained cells and the curves were comparable to isotype controls, not shown here for simplicity.

Figure 3.8: VWF staining in HUVECs.

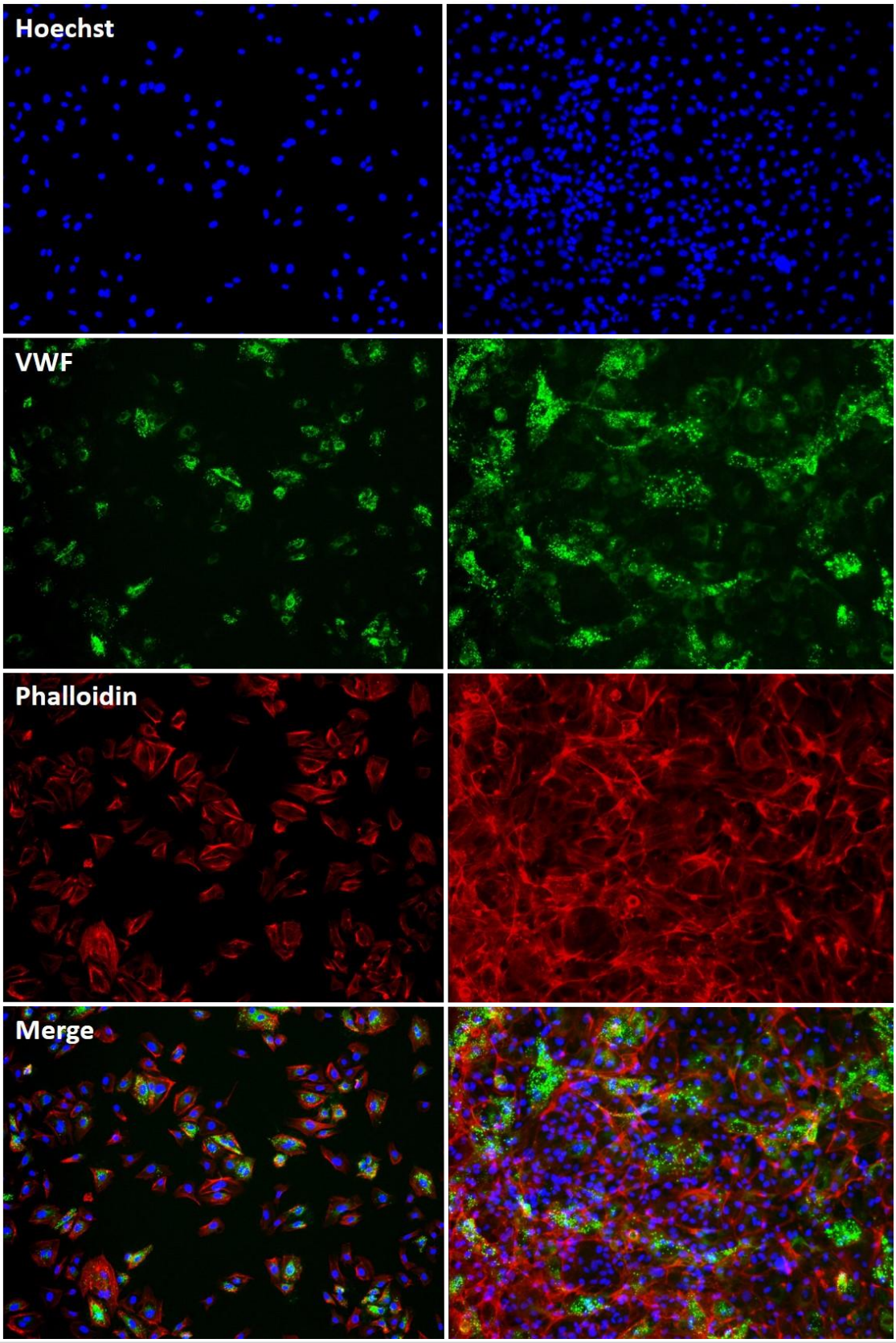

Immunofluorescence images showing Hoechst (blue), VWF (green) and actin (red), on 4% PFA fixed HUVECs at passage 5. Sparsely populated (left) and densely populated (right) cells are shown. WBPs are clearly visible as VWF+ rod shaped granules in the cytoplasm. VWF staining is variable, possibly due to heterogeneity in the HUVEC population, cells are pooled from 4 donors

All cells exhibited positive staining for the EC marker PECAM-1 in both immunofluorescence and flow cytometry, suggesting an EC phenotype (Figure 3.7). Positive staining for PECAM-1, VE-Cad, VWF, and MCAM was also observed using flow cytometry (Figure 3.7), suggesting that these cells were indeed endothelial. However, flow cytometry staining for VEGFR2 was heterogenous, with some cells showing strong staining, whilst others did not. As VEGFR2 is not solely expressed in ECs, and ECs will express other VEGFRs (e.g. VEGFR1) this could be explained by differences in expression levels, or cross reactivity of the antibody with different proteins. Evidence for an endothelial origin for these cells is provided by the strong expression of the other EC markers. CD45 is expressed on haematopoietic progenitor cells, as well as lymphocytes and leukocytes, and is used to differentiate mature ECs from immature EC progenitor cells. ECs did not express CD45, suggesting that ECs are mature and differentiated[36].

The VWF staining in Figure 3.8 is heterogenous with some cells showing clear, bright VWF positive WPBs as green rod-shaped granules in the cytoplasm, whereas other cells show less bright VWF staining. This could be due to differences in sensitivity between the two methods: the flow cytometer might be a more sensitive instrument and so could pick up lower levels of VWF that may not be captured by immunofluorescence. These ECs are pooled from 4 donors and this heterogeneity may be reflected here in different intensities of fluorescence.

3.7 Activation of HUVECs with Inflammatory Agents

HUVECs exist in resting or activated, proinflammatory states and respond to inflammatory signals in their microenvironment[96]. To test whether HUVECs were physiologically functional, HUVECs were treated with TNFα, IL-1α and lipopolysaccharides (LPS) and then tested for inflammatory response. HUVECs will upregulate surface expression of VCAM, ICAM and E-Selectin when they are activated and will release soluble portions of these receptors into the blood stream *in vivo* or cell culture media *in vitro*. Duoset ELISA kits (R&D) were used to detect soluble VCAM, ICAM and E-Selectin released into the media and in cell lysates after overnight incubation with inflammatory cytokines.

HUVECs were seeded on collagen I coated surfaces and TNFα, IL-1α and LPS were then added overnight (16h) in EGM2. The media from the wells was then collected, centrifuged at 1000 xG for 5 mintues to remove cell debris and stored at -80°C. Cells were lysed with ice-cold

Figure 3.9: Detection of VCAM, ICAM and E-selectin in activated HUVECs.

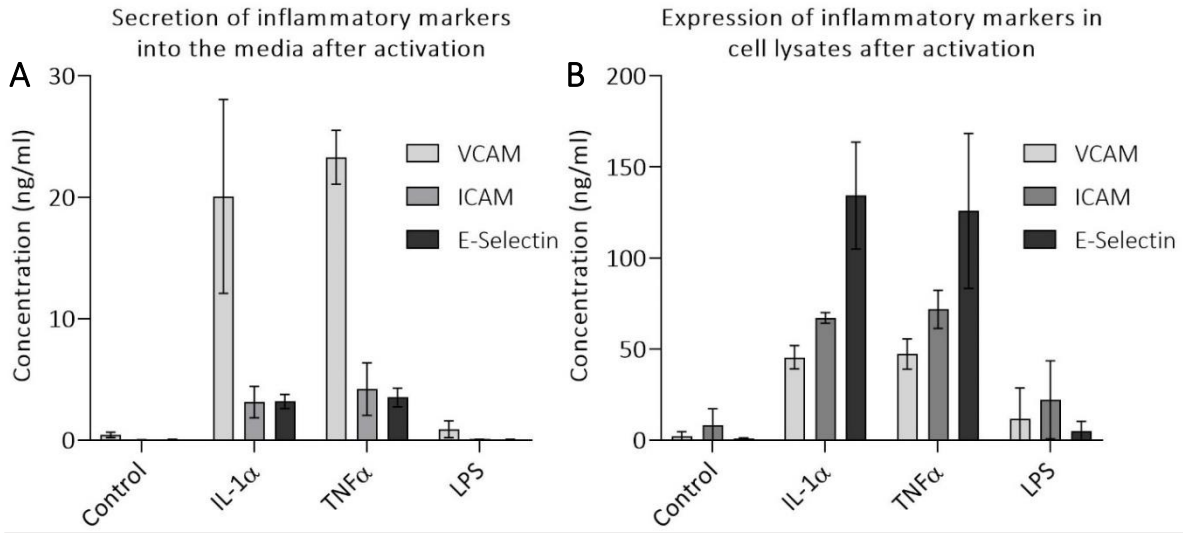

Detection of VCAM, ICAM and E-selectin released in the media (A) or upregulated in cell lysates (B) after overnight activation with 20ng/ml TNFα, 10ng/ml IL-1α or 1µg/ml LPS. TNFα and IL-1α both stimulate expression and release of inflammatory markers. DuoSet ELISAs were used, concentrations of VCAM, ICAM and E-Selectin were calculated from standard curves.

lysis buffer containing TritonX100 and cOmplete mini protease inhibitors and left on ice, shaking, for 30 minutes. Lysates were centrifuged at 13,000 xG for 20 minutes, supernatant was collected and stored at -80°C until the ELISA assay was carried out as per manufacturers instructions. Cell lysates were diluted 1:10 in the assay.

A two-way ANOVA with Dunnett's multiple comparisons test was used to compare the expression of inflammatory markers in cell lysates or secreted into the media. The results are summarised above in Table 3.11. Both IL-1α and TNFα significantly (****P<0.0001) upregulated secretion of VCAM-1 into the media after overnight incubation but LPS had no effect on secretion of any of these proteins into the media compared to the control. There was no significant increase of ICAM or E-Selectin secretion with any cytokine tested. IL-1α and TNFα, but not LPS, incubation resulted in a significant increase of VCAM, ICAM and E-Selectin detected in cell lysates (Table 3.11). This suggests that ECs are responding to inflammatory cytokines as expected. The effect of LPS on HUVECs, expected to illicit a response at 1µg/ml, may require a longer time point than IL-1α and TNFα to trigger the release of inflammatory markers.

Table 3.11 – Statistical analysis of inflammatory marker expression compared to the control

Media					Lysate				
VCAM	Mean concentration (ng/ml)	SD	N	P	VCAM	Mean concentration (ng/ml)	SD	N	P
Control	0.447	0.215	2		Control	2.084	2.659	3	
TNFα	20.084	7.987	2	**<0.0001**	IL-1α	45.568	6.375	2	**0.0260**
IL-1α	23.299	2.218	2	**<0.0001**	TNFα	47.347	8.283	3	**0.0101**
LPS	0.918	0.685	2	0.9952	LPS	2.083	0.717	2	>0.9999
ICAM					ICAM				
Control	0.046	0.0164	2		Control	8.230	8.998	2	
TNFα	3.144	1.294	2	0.4943	IL-1α	67.189	2.927	2	**0.0064**
IL-1α	4.199	2.157	2	0.2802	TNFα	71.892	10.438	2	**0.0036**
LPS	0.086	0.0160	2	>0.9999	LPS	22.297	21.456	2	0.7130
E-Selectin					E-Selectin				
Control	0.068	0.0261	2		Control	0.941	0.424	2	
TNFα	3.192	0.585	2	0.4880	IL-1α	134.301	29.372	2	**<0.0001**
IL-1α	3.523	0.764	2	0.4130	TNFα	125.882	42.556	2	**<0.0001**
LPS	0.069	0.022	2	>0.9999	LPS	4.955	5.425	2	0.9886
Mean concentrations are compared to the control mean concentration of each inflammaotry marker using two-way AONVA and Dunnett's multiple comparisons test									

In conclusion, HUVECs behaved as expected and increased expression of EC markers of activation in the presence of known EC activators, suggesting the cells are indeed endothelial and can be used in downstream experiments to study the roles of the collagen-binding integrins in the regulation of endothelial cell behaviour.

3.8 Adhesion of HUVECs to Short Peptides

The same adhesion assays described before, Chapter 3.4, for C2C12 cells were then carried out with HUVECs. Plates were coated with SPs, blocked with BSA, HUVECs were added at 15,000 cells/well and cells were left to adhere for one hour at room temperature. Plates were washed and remaining cells were lysed and quantified with the LDH cytotoxicity kit from Roche, as described above. Figure 3.10 shows the adhesion profile of HUVECs on SPs. Table 3.12 shows the statistical analysis of the adhesion data using two-way ANOVA and Dunnett's multiple comparisons test compared to the GPP10 negative control. The mean indicates the mean absorbance for each condition. Compared to GPP10, there was no significant binding to GHDGEK, GHDGDK, GPKHGER, GQKGEI, GVOGEA, GFOGDR and BSA. HUVECs appear to show a more active binding profile to collagen SPs than any of the C2C12 cells. Essentially, the

Figure 3.10. HUVEC adhesion to collagen toolkits and short peptides.

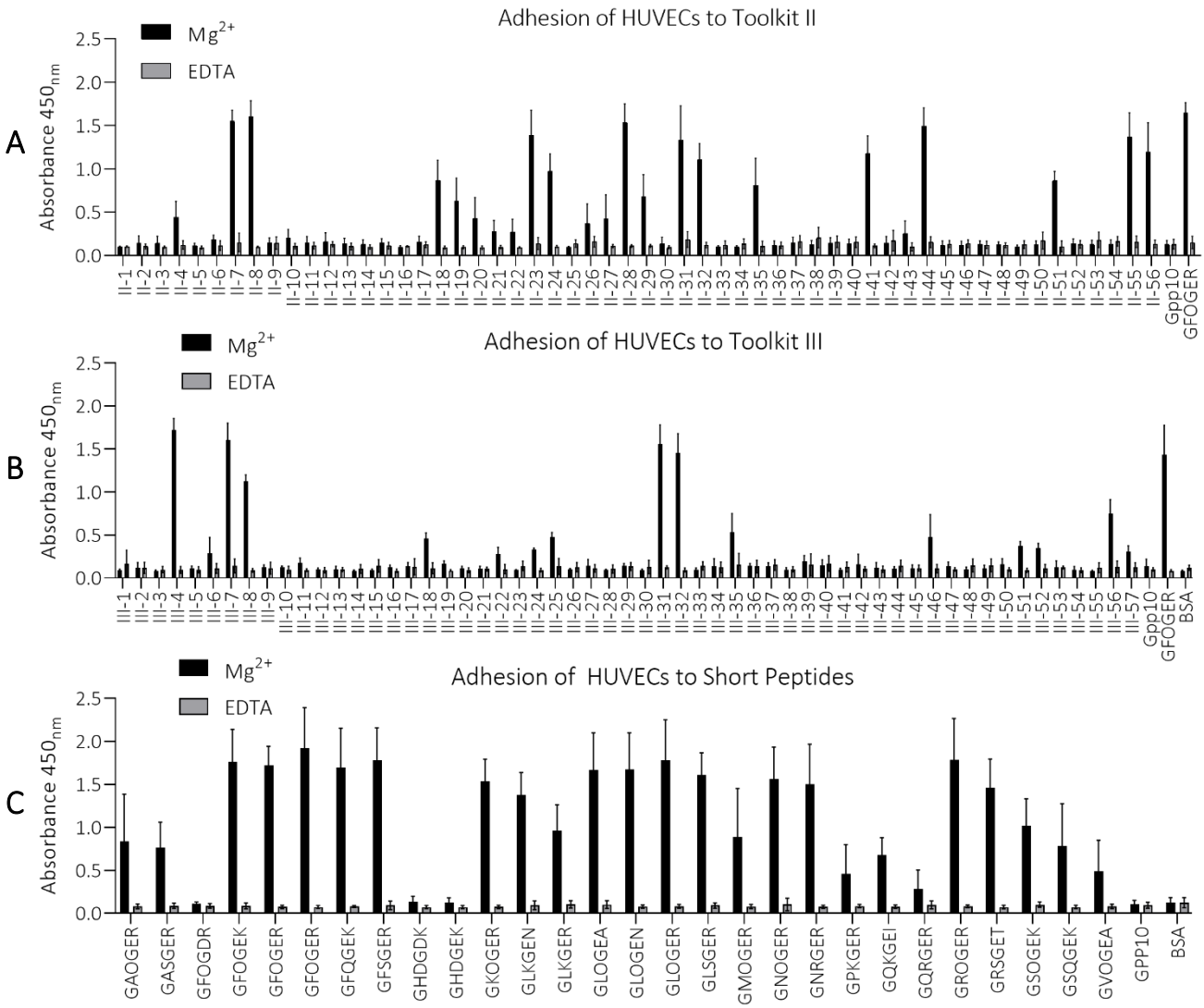

A) Adhesion of HUVECs to Toolkit II. B) adhesion of HUVECs to collagen Toolkit III. C) Adhesion of HUVECs to SPs. Each graph shows adhesion in the presence of Mg^{2+} or EDTA. Collagen-binding integrins are Mg^{2+} dependent, any adhesion seen in the presence of the metal ion chelator EDTA can be assumed to be nonspecific. No adhesion was seen in the presence of EDTA.

binding profile is the same as C2C12s transfected with ITGA2 but with enhanced binding to weaker motifs such as GMOGER and GAOGER. Binding to GSQGEK and GASGER was not observed in any transfected C2C12 cells but very weak binding is observed here for HUVECs. The rest of the motifs showed strong binding compared to GPP10 (****P<0.0001) or moderate in the case of GSOGEK (***P=0.0005). Differences in binding to SPs seen between transfected

C2C12 cells and HUVECs could be partially due to regulatory differences between the human and mouse β1-subunits. Perhaps the mouse β1-subunit supports a less active α-subunit conformation than the human β1. Alternatively, the integrins could be in a more active state in HUVECs as a result of association with a number of other focal adhesion proteins such as paxillin, talin or vinculin[251-254]. Integrins cluster together with these proteins to regulate cell spreading, adhesion and migration. Many proteins present in HUVECs but not in C2C12 cells and vice versa may influence integrin activity, explaining differences between HUVEC and C2C12 binding profiles.

Table 3.12 – Statistical analysis of HUVEC adhesion to SPs compared to GPP10

Peptide	Mean absorbance	SD	n	P	Peptide	Mean absorbance	SD	n	P
GAOGER	0.839	0.548	3	**0.0104**	GLOGER	1.781	0.467	3	**<0.0001**
GASGER	0.766	0.296	3	**0.0307**	GLSGER	1.605	0.260	3	**<0.0001**
GFOGDR	0.109	0.022	3	>0.9999	GMOGER	0.887	0.564	3	**0.0047**
GFOGEK	1.763	0.376	3	**<0.0001**	GNOGER	1.557	0.376	3	**<0.0001**
GFOGER	1.719	0.225	3	**<0.0001**	GNRGER	1.500	0.467	3	**<0.0001**
GFQGEK	1.922	0.467	3	**<0.0001**	GPKGER	0.459	0.338	3	0.6858
GFSGER	1.695	0.456	3	**<0.0001**	GQKGEI	0.678	0.202	3	0.0959
GHDGDK	1.782	0.374	3	0.9998	GQRGER	0.285	0.220	3	0.9950
GHDGEK	0.137	0.062	3	>0.9999	GROGER	1.784	0.482	3	**<0.0001**
GKOGER	0.123	0.055	3	**<0.0001**	GRSGET	1.462	0.332	3	**<0.0001**
GLKGEN	1.536	0.257	3	**<0.0001**	GSOGEK	1.020	0.311	3	**0.0005**
GLKGER	1.378	0.259	3	**0.0013**	GSQGEK	0.786	0.489	3	**0.0230**
GLOGEA	0.963	0.300	3	**<0.0001**	GVOGEA	0.486	0.365	3	0.5806
GLOGEN	1.667	0.432	3	**<0.0001**	BSA	0.105	0.043	3	0.9999

One-way ANOVA and Dunnett's multiple comparison test was used to analyse the mean absorbances for each peptide compared to the mean absorbance for GPP10.

In conclusion, the adhesion profile of HUVECs on SPs looks very similar to the α2β1 adhesion profile in transfected C2C12 cells, but with higher binding affinity seen for HUVECs, possibly due to other proteins present in focal adhesions or other adhesion complexes.

3.9 Adhesion of HUVECs to Collagen II and III Toolkits

Collagen Toolkits corresponding to collagens II and III have been designed and synthesised in Prof Farndale's group[233, 234, 243]. HUVEC adhesion to these toolkit libraries was tested here to probe integrin binding sites in these two collagen types. Immulon 2HB plates were coated with these Toolkit peptides and, after blocking with BSA, HUVECs were added at 15,000 cells per well, in the presence of Mg^{2+} to facilitate integrin binding, or EDTA to block

integrin binding by chelating metal ions. After one hour, plates were gently washed to remove unbound cells and the remaining cells were lysed and quantified using the colorimetric LDH cytotoxicity assay.

The Toolkit II and III sequences, in chapter 2.23, contain many integrin adhesion sites and some are expected to bind HUVECs. The adhesion data is shown in Figure 3.10 as the means for each condition with error bars depicting SD. Table 3.12 summarises the statistical analysis of the HUVEC adhesion to SPs using two-way ANOVA and Dunnett's multiple comparisons test to compare each mean absorbance value to the mean absorbance value for GPP10. The similarities and differences seen here between the adhesion of HUVEC and the integrin expressing C2C12 cells are summarised below:

- HUVECs adhered to GMOGER in II-31, III-31 and III-32 whereas GMOGER only bound very weakly to C2C12-ITGA2 cells
- Strong binding was seen for GLOGER in II-7 and II-8 which bound all transfected C2C12 cells except C2C12-ITGA1
- HUVECs bound strongly to GRSGET in II-55 and II-56, which binds C2C12-ITGA1 and C2C12-ITGA2 cells
- GLOGEN (or GLKGEN) in III-7 binds strongly to HUVECs, binds all integrins in C2C12 cells
- As expected, GFOGER in II-28 binds HUVECs strongly. This is well-characterised a motif for all collagen-binding integrins
- II-44 binds HUVECs strongly but does not contain an integrin binding motif. It contains GQRGER which is negative for integrin binding in C2C12 cells. However, this peptide is promiscuous, and binding has been reported for many other receptors
- III-35 contains GSOGER which could bind integrins, an analogue GSOGEK was a weak binder for α2β1 but the GER pattern could increase binding in this case
- GROGER in III-4 binds HUVECS, as well as C2C12-ITGA2 and C2C12-ITGA11
- RGD motifs could be responsible for binding in II-32, II-41 and II-51. Both avb3 and avb5 bind RGD and are present in ECs
- GNRGER in III-56 is an α2β1 specific peptide in C2C12 cells and is a strong binder for HUVECs as expected
- GLSGER binds strongly to HUVECs. In C2C12 cells, it binds all but α11β1, which is not expressed in HUVECs

In theory, the RGD motif is only active in its linear form, and so should not be active when part of the sequences of peptides adopting a triple helix conformation. Yet, although THPs predominantly adopt a triple helical structure, a small portion of peptide remains in an unfolded, monomeric conformation. This could explain the adhesion of HUVECs to RGD containing peptides. Interestingly, HUVECs bound strongly to II-23 which does not contain any immediately obvious integrin binding sequences (the II-23 amino acid sequence is GQOGVMGFOGPKGANGEOGKAGEKGLO). DDR1 and DDR2 are all reported to bind to GVMGFO, which is present in both II-22, II-23 and III-23. Yet, HUVECs only bound to II-23, so the presence of these receptors on the cell surface do not explain alone the binding to II-23. Additionally, some binding is also seen in II-24, suggesting that the last three triplets of the II-23 host sequence that are also present in II-24 (GKAGEKGLO) could be responsible for this binding. Alternatively, the motif that HUVECs recognise could be GVMGFO**GPK** in II-23. A different, lower affinity motif could then be responsible for binding in II-24 through a non-integrin receptor. To isolate the active binding sequence in each peptide, an alanine scan on II-23 and II-24 could be carried out. However, this is outside the scope of this project.

There are differences between the binding of SPs and Toolkit II and III peptides containing the same integrin motif. For example, GMOGER in the longer toolkit peptides is a strong binder for HUVECs and C2C12-ITGA2, whereas the GMOGER short motif alone is a weak binder. This could be due to conformational changes imposed by the longer peptide sequence or flanking sequences in the Toolkit peptides. The SPs are shorter and contain less amino acid residues likely to affect the triple helix stability and folding. This could influence the shape of the helix by making it tighter or looser compared to the longer Toolkit peptides, modifying the spatial arrangement of amino acid side chains and affecting integrin binding. Additionally, there are other motifs in the longer toolkit peptides that could bind other receptors on the surface of ECs. However, it is not in the scope of the project to investigate other collagen receptors in detail.

3.10 Conclusions

The adhesion profiles of purified, recombinant αI-domains and C2C12 cells differ substantially, possibly due to the regulatory effect of the β1 subunit, other co-receptors or

regulatory proteins present in the C2C12 cells. The results presented here highlight the importance of testing full-length receptors where possible as they behave differently to the αI-domains alone. For the ITGA1 αI-domain, the adhesion to THPs was more active in the isolated αI-domain than the C2C12 cells expressing the full-length α1β1. The opposite was observed for less active ITGA2 αI-domain compared to the C2C12s expressing the full-length α2β1.

The transfected C2C12 cells showed very similar adhesion profiles for the four integrins, making it impossible to use THPs alone to specifically target one type of integrin. Only α2β1 exhibited adhesion to specific THPs. The integrin adhesion motifs were varied and will tolerate deviations from the canonical GFOGER quite well.

HUVECs express the expected EC markers and exhibit the correct inflammatory response suggesting the HUVECs possess an endothelial phenotype. The ITGA2 subunit is the most abundant mRNA transcript, followed by ITGA10 and ITGA1, while ITGA11 is not detectable. DDR2 is expressed in similar levels to ITGA2 at the mRNA level and SPARC is abundant. Due to problems with antibody specificity it was not possible to study the relative amounts of each integrin present on the cell surface, at the protein level. This severely limits the conclusions that can be drawn about receptor expression levels. Differences in mRNA stability, translation efficiency, post-translational modifications and protein turnover will all affect the final amount of each receptor present on the cell surface. As a result, the relative expression of the mRNA transcript does not infer the true surface expression of each receptor.

Lastly, HUVECs show active adhesion profiles on SPs, Toolkit II and Toolkit III. HUVECs show a similar adhesion profile to C2C12-ITGA2 but with additional adhesion to GASGER, GHDGEK and GSQGEK. HUVECs also exhibited adhesion to all the integrin motifs in Toolkits II and III, as well as to other peptides where no evident binding motif has been characterised. The toolkit data shows there are varied and numerous adhesion sites for HUVECs in collagen II and III and active integrin binding profiles are present in HUVECs.

Chapter 4 – Characterisation of Integrin Inhibitors TC-I-15 and Obtustatin

Contents

4.1 Chapter Summary

This chapter focusses on characterising two integrin inhibitors, TC-I-15 and Obtustatin. TC-I-15 is a small-molecule commercially sold as a α2β1 inhibitor, and Obtustatin is a disintegrin that inhibits α1β1. These inhibitors are tested using recombinant αI-domains, integrin-expressing C2C12 cells and HUVECs on peptides, collagen and other extracellular matrix proteins to fully characterise their specificity and potency. All experiments are repeated a minimum of three times.

4.2 Introduction

In Chapter 3, Figure 3.4, the binding profiles of the four collagen-binding integrins to THPs proved to be too similar to use these peptides as a method for ligating or blocking specific integrins. Consequently, another method of modulating integrin expression or function needed to be established. Commercially available inhibitors were sought out and tested for their suitability in HUVECs. Obtustatin, depicted in figure 4.1, is a commercially available α1β1 inhibitor, also called a disintegrin, originating in the venom of *Vipera lebetina obtusa* [4, 165, 255-257]. Disintegrins are a family of integrin inhibitors first discovered as platelet aggregation antagonists in snake venoms. They are small cysteine-rich peptides containing an integrin-binding loop that interferes with integrin adhesion[258]. The integrin binding loop infers

selectivity; RGD binding integrins will be inhibited by a disintegrin containing an RGD motif in the integrin binding loop in a competitive manner. Other motifs found in disintegrins include KGD, WGD, VGD, RTS and KTS, using single amino acid code. Disintegrins show higher potency than their synthetic peptide counterparts, suggesting that the tertiary structure is important for inhibition. Amino acids adjacent to the RGD motif affect the potency of inhibition, since RGD**NP** is 10 times more potent than RGD**W** for α5β1[259] and viperistatin (WKTS**R**TSHYC) is 25 times more potent that Obtustatin (WKTS**L**TSHYC) for α1β1[258]. There are a huge number of disintegrins, and they can be split into four groups based on their size:

- Short disintegrins 41-51 residues and 4 S-S bonds (e.g. echistatin and Obtustatin)
- Medium length disintegrins approximately 70 residues and 6 S-S bonds (e.g. barbourin, flavoviridin, atrolysin)
- Long disintegrins 84 residues and 7 S-S bonds (e.g. bitistatin)
- Dimeric disintegrins, each subunit 67ish resides

Figure 4.1: Diagram of the Structure of Obtustatin.

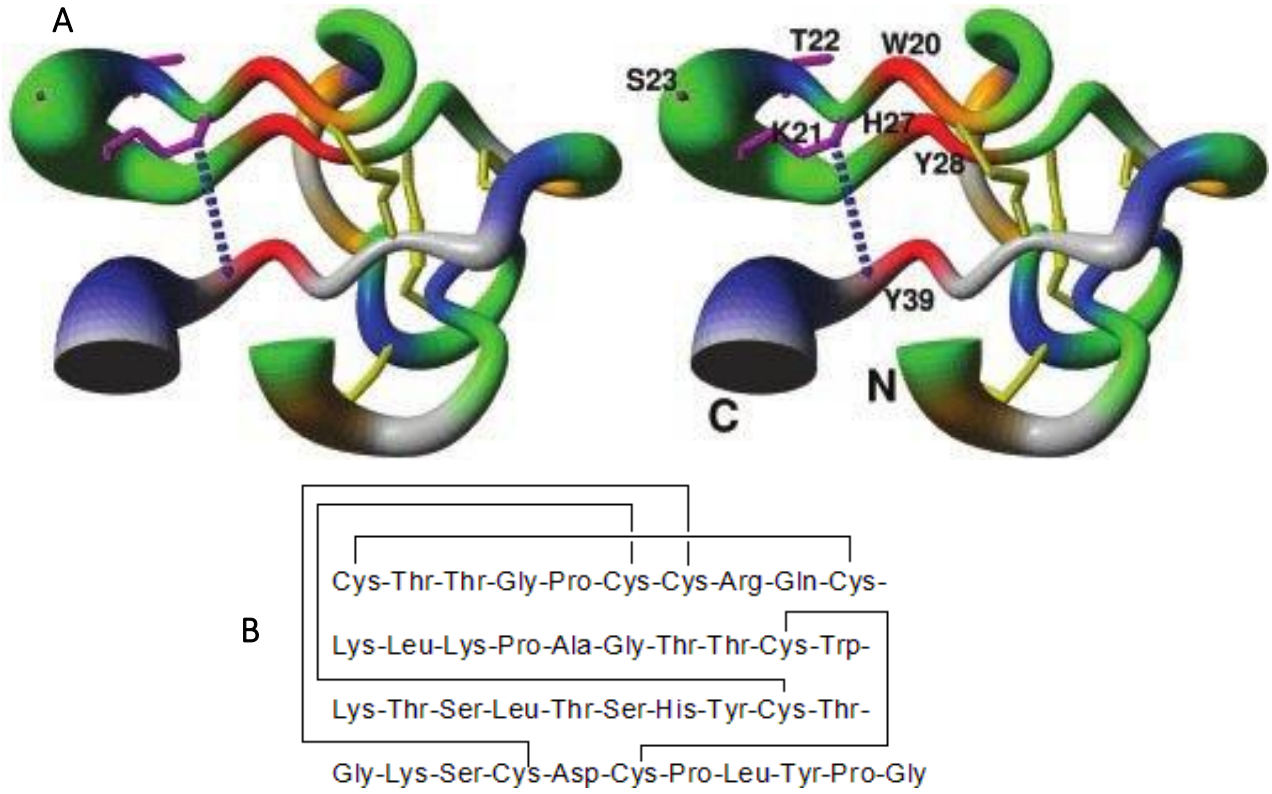

A) A structural diagram of obtustatin (PDB 1MPZ), adapted from '*Concerted motions of the integrin-binding loop and the c-terminal tail of the non-RGD integrin obtustatin' Monleon et al*[4]. S-S bonds are shown in yellow. B) A simplified diagram showing the individual residues, taken from the Tocris Biosciences website.

Obtustatin is a tiny disintegrin of just 41 residues and contains a W**KTS**LTSHY motif in the integrin binding loop, shown in Figure 4.1. This is interesting because the collagen recognition sequences for α1β1 described in Chapter 3 (Figure 3.4) do not contain any KTS motifs, and the KTS-loop is proposed to bind to the αI-domain to inhibit integrin binding. While the RGD-binding integrins are inhibited by RGD containing disintegrins, this is not the case for obtustatin and α1β1. Obtustatin inhibits cell-based α1β1 and the isolated full length α1β1 receptor but has no effect on isolated αI-domains[165]. This suggests that the method of inhibition could also employ the β1-subunit or the rest of the α1-subunit in addition to the αI-domain, differing from the RGD-disintegrins. Alternatively, the isolated αI-domain may just behave very differently to the full-length receptor, as seen in Chapter 3, Figures 3.3 and 3.4.

Obtustatin has been used to inhibit angiogenesis *in vitro* and *in vivo* in chick chorioallantoic membrane assays. It also reduced tumour development by 50% in the mouse Lewis lung carcinoma mouse model and blocked melanoma growth in mice[165, 204]. Another α1β1 specific KTS-containing disintegrin, jerdostatin, has been used to inhibit adhesion of α1β1 to collagen IV[260]. The same study also found that jerdostatin also inhibits migration and proliferation of rat aortic VSMCs and α1β1-dependent angiogenesis in HUVEC tube formation assays[260]. However, they also stated that VEGF-driven angiogenesis in HUVECs was only completely abolished when α2β1 was also inhibited by rhodocetin (another platelet aggregation inhibitor from snake venom), suggesting that there is some redundancy between the integrins in this role. Obtustatin has been found to reduce proliferation and stimulate apoptosis in human microvascular ECs (HMVECs)[204] but has not yet been well characterised in HUVECs.

Figure 4.2: Diagram of the Structure of TC-I-15.

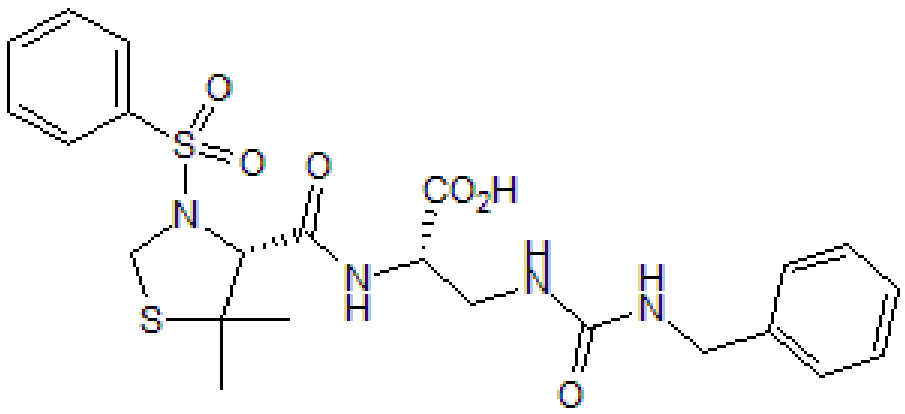

Adapted from the Tocris bioscience website

Figure 4.3: Proposed Method of Inhibition by TC-I-15.

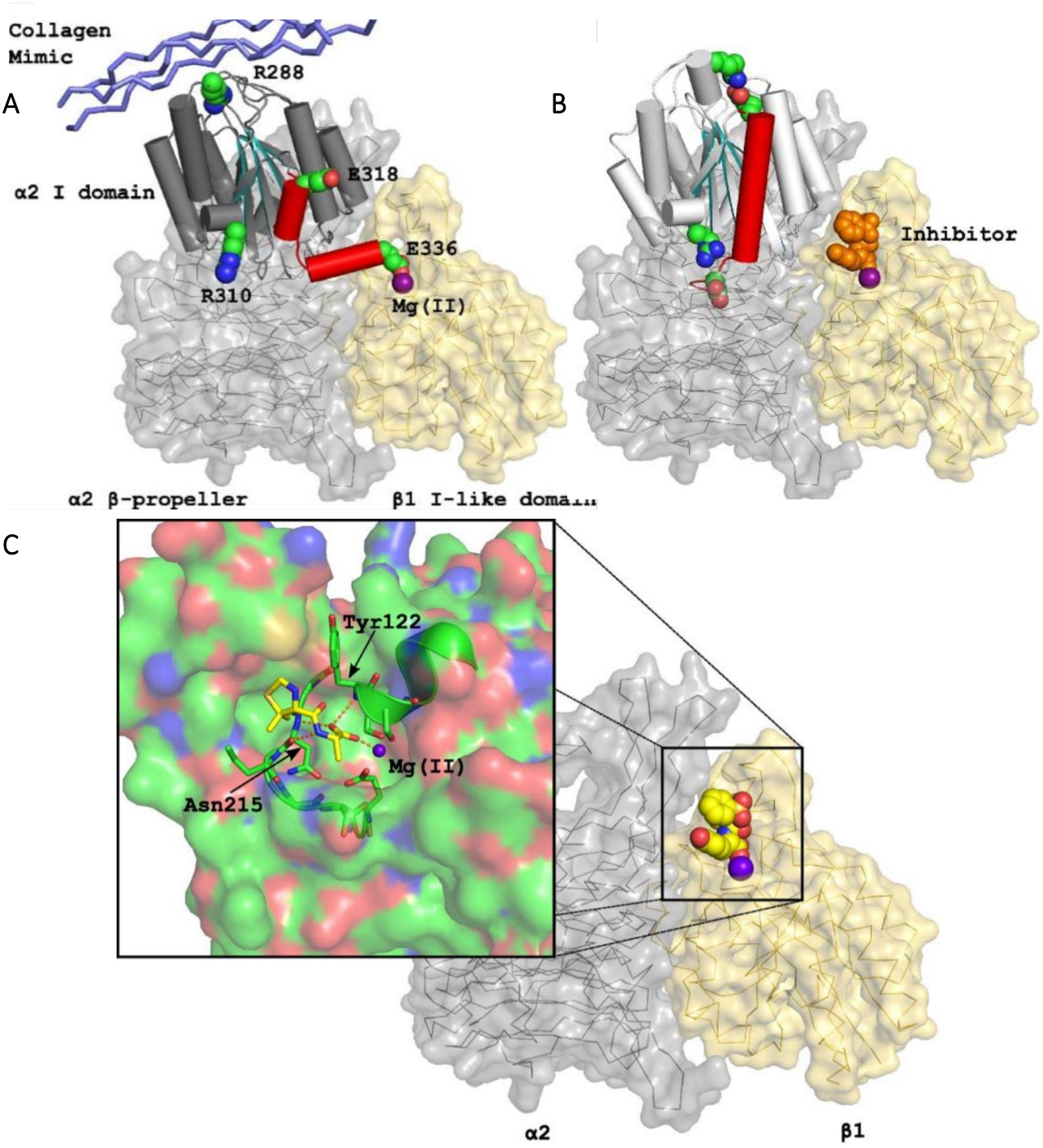

Adapted from '*Small-molecule inhibitors of integrin α2β1 that prevent pathological thrombus formation via an allosteric* mechanism' *Miller et al 2009*[2]. A) Structural representation of integrin α2β1 binding to collagen. B) and C) TC-I-15 binding to the βI-domain to stabilise the inactive conformation of α2β1. The β-propeller of ITGA2 is shown in grey with the αI-domain shown with solid blocks, and the β1 I-domain is shown in yellow. The C-helix is shown in red and collagen is shown in blue, TC-I-15 is shown in orange. When TC-I-15 is bound, the C-Helix moves to the closed conformation. C) Structural representation of TC-I-15 binding to the β1-Idomain via an interaction with an Mg^{2+}, Y122 and N215 in the βI-domain, locking the inhibitor in place and stabilising the closed confirmation of the αI-domain.

Disintegrins for α2β1 were not commercially available at the time of this project and so were too difficult to obtain. Instead, the small molecule α2β1 specific inhibitor, TC-I-15, was characterised and tested in detail here (Figure 4.2). TC-I-15 (compound 15 in[2]) inhibits α2β1 via an allosteric mechanism whereby it interacts with the βI-domain to stabilise the inactive conformation of the αI-domain (Figure 4.3). In platelets this results in potent inhibition of platelet adhesion to collagen and subsequent thrombosis in animal models[2]. In activated α2β1, the C-helix moves to coordinate an Mg^{2+} ion in the βI-domain to stabilise the active confirmation of the αI-domain (Figure 4.3). TC-I-15 interacts with this Mg^{2+} ion alongside Y122 and N215 in the βI-domain to stabilise the closed confirmation as the C-helix can no longer more to coordinate the Mg^{2+} ion. TC-I-15 reportedly has no effect on the constitutively active E318A mutation of α2β1[2], presumably because this integrin is already locked into the active state and so cannot be stabilised in the inactive confirmation by TC-I-15. TC-I-15 has reportedly been tested for cross-reactivity and no inhibition of αvβ3, α5β1, α6β1 and αIIbβ3 was observed according to the manufacturers' website.

An inhibitory antibody for α2β1, 6F1, was also used in this study as it has been validated and routinely used to target α2β1[261]. Obtustatin and 6F1 are soluble in PBS and so no vehicle controls were necessary, whereas TC-I-15 had to be warmed to 50°C in a 1.1M equal concentration of NaOH to solubilise. For this reason, the TC-I-15 vehicle control is a 1.1M equal concentration of NaOH where 200μM of TC-I-15 is used, 220μM NaOH is added for the vehicle control, called "TC-I-15 control" from this point forward.

4.3 Effects of Inhibitors on Recombinant αI-domain Adhesion to Peptides

TC-I-15 and Obtustatin were tested using the recombinant GST-tagged αI-domains expressed by Dr Samir Hamaia. Additionally, GST-tagged I-domains containing mutations (also expressed by Dr Samir Hamaia) were used, specifically $ITGA1^{R\text{-}G}$ and $ITGA2^{Y\text{-}G}$. The $ITGA1^{R\text{-}G}$ involves a mutation of R288 to G, which increases the affinity of α1β1 for collagen as this stabilises the active conformation of the αI-domain. The $ITGA2^{Y\text{-}G}$ involves a mutation from Y285 to a G, again stabilising the active conformation of the αI-domain. Adhesion to collagen peptides was tested in static adhesion assays, as described above, in the presence or absence of inhibitors or vehicle controls (Figure 4.4). GLOGEN-coated wells were used to test the binding of the ITGA1 and $ITGA1^{R\text{-}G}$ αI-domains, and GFOGER-coated wells were used for ITGA2 and $ITGA2^{Y\text{-}G}$ αI-domain, as these were the highest binders in previous assays. Wells coated

with BSA were included as negative controls. All αI-domains were added at 10µg/ml and left to adhere for one hour. One-way ANOVA and Sidak's multiple comparisons test were used to analyse the effects of the inhibitors on αI-domain binding. The statistical analysis is summarised in table 4.1 below.

No inhibition was observed for ITGA1 I-domain for any compound tested for the wildtype or the ITGA1^{R-G} mutant. In all conditions, both ITGA1 αI-domains bound strongly to GLOGEN compared to BSA. This suggests that either the rest of the α-subunit or the β1-subunit are necessary for the inhibition by Obtustatin. The KTS integrin-binding loop in Obtustatin may not interact with the I-domain of ITGA1 at all, and there could be secondary site on ITGA1 αI-domain that binds Obtustatin and facilitates inhibition.

There was no inhibition of either ITGA2 αI-domain by Obtustatin or TC-I-15, and both αI-domains bound strongly to GFOGER compared to BSA. 6F1 significantly inhibited adhesion of both ITGA2 αI-domains to GFOGER. This suggests that 6F1 inhibits the ITGA2 αI-domain directly and does not require the β1 subunit for inhibition, whereas TC-I-15 appears to work

Figure 4.4. Inhibition of αI-domains.

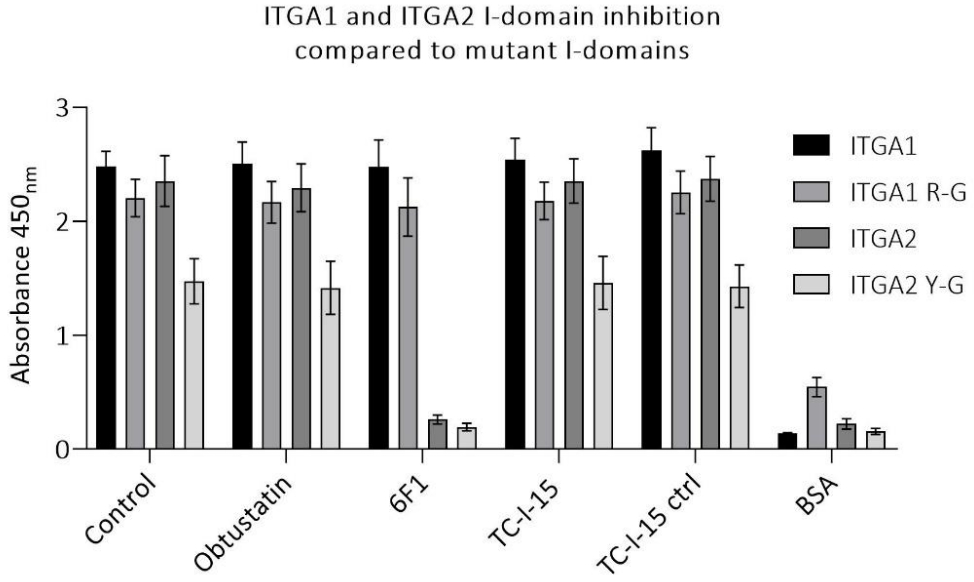

Static adhesion assay showing the binding of I-domain mutants to collagen peptides. Adhesion is shown as a function of absorbance. After strenuous washing, remaining I-domains were detected using anti-GST-HRP conjugated antibody and TMB substrate with H_2SO_4 to stop the reaction. GLOGEN was used for ITGA1 and ITGA1^{R-G}, and GFOGER was used for ITGA2 and ITGA2^{Y-G}. 200µM TC-I-15 and 20µM Obtustatin and 10µg/ml 6F1 were used in the presence of Mg^{2+}.

by encouraging the β1 subunit to stabilise the inactive conformation of the αI-domain (Figure 4.3)[2]. The ITGA2^{Y-G} mutant showed significantly lower adhesion than ITGA2 wildtype. This mutation seems to make the αI-domain less active overall which is the opposite of what the mutation should do. This could be an artefact of the experiment whereby the starting concentration of ITGA2^{Y-G} is not as accurate, as these are purified from bacterial lysates via a GST affinity column but could also contain other proteins which would affect the concentration determination. To correct this, High-performance liquid chromatography (HPLC) could have been used to purify these αI-domains further.

The data here agrees with the literature described earlier in that neither TC-I-15 nor Obtustatin will inhibit αI-domain adhesion to collagen, although the mode of inhibition by Obtustatin remains unclear.

Table 4.1 – Statistical Analysis of αI-domain inhibition

ITGA1 αI-domain					ITGA1^{R-G} αI-domain				
	Mean	SD	n	P		Mean	SD	n	P
Control	2.486	0.1293	2		Control	2.205	0.1640	2	
Obtustatin	2.509	0.1880	2	0.9999	Obtustatin	2.168	0.1817	2	0.9994
6F1	2.479	0.2352	2	>0.9999	6F1	2.127	0.2556	2	0.9894
BSA	0.1376	0.0093	2	**<0.0001**	BSA	0.5469	0.08307	2	**0.0004**
TC-I-15 Control	2.624	0.1980	2		TC-I-15 Control	2.255	0.1881	2	
TC-I-15	2.545	0.1842	2	0.9873	TC-I-15	2.181	0.1652	2	0.9911
ITGA2 αI-domain					ITGA2^{Y-G} αI-domain				
	Mean	SD	n	P		Mean	SD	n	
Control	2.355	0.2227	2		Control	1.475	0.1991	2	
Obtustatin	2.295	0.2104	2	0.9952	Obtustatin	1.417	0.2339	2	0.9963
6F1	0.2621	0.0393	2	**<0.0001**	6F1	0.1961	0.0331	2	**0.0014**
BSA	0.2223	0.0448	2	**<0.0001**	BSA	0.1582	0.0265	2	**0.0012**
TC-I-15 Control	2.373	0.1968	2		TC-I-15 Control	1.430	0.1873	2	
TC-I-15	2.354	0.1949	2	>0.9999	TC-I-15	1.461	0.2333	2	0.9997
Mean indicates mean absorbance at 450nm. One-way ANOVA and Sidak's multiple comparisons test were used to compare the mean absorbances to the control mean absorbance									

4.4 Inhibition of Integrin Expressing C2C12 Cells

To test these inhibitors in full length integrin heterodimers, C2C12 cells that have been stably transfected to express one of the four integrins were used, as described in Chapter 3, in static adhesion assays in the presence or absence of inhibitors or controls at varying concentrations. Plates were coated with GFOGER or GLOGEN, using GPP10 as the negative control. Cells were detached and inhibitors were added to the cells in a serial dilution for five

minutes before adding 15,000 cells/well on 96-well plates. After one hour, plates were gently washed, and cells were lysed with 2% TritonX100. The relative number of cells still adhered to the peptides was quantified using the Roche LDH cytotoxicity kit as described above. Cell adhesion is reported as a function of absorbance at 490nm in Figure 4.5. Non-linear curve fits were used to determine the IC_{50}s, summarised in Table 4.2

Obtustatin proved to be a potent, specific, inhibitor of α1β1 adhesion to both GFOGER and GLOGEN at concentrations of 10-20μM. No other integrin was affected by Obtustatin, suggesting that it can be used to inhibit α1β1 selectively (Figure 4.5). Here, TC-I-15 inhibited α2β1 as expected, albeit at rather high concentrations of approximately 200μM for GFOGER and much lower concentrations of <10μM for GLOGEN. GFOGER is a higher affinity ligand for α2β1 than GLOGEN. The difference in potency of TC-I-15 inhibition of adhesion to these two ligands suggests a competitive-like mode of inhibition whereby the higher affinity GFOGER requires a higher concentration of TC-I-15 to bind to the β-subunit for inhibition to take place. It is possible that, for GFOGER, the affinity of the αI-domain for the ligand overcomes some of the affinity of TC-I-15 for the inhibitory site on the βI-domain. In contrast, the lower affinity GLOGEN does not require such a high concentration of TC-I-15. Additionally, TC-I-15 inhibited α1β1 at concentrations of approximately 220μM, meaning that TC-I-15 is not specific for α2β1 and cannot be used to selectively inhibit α2β1. TC-I-15 inhibited α1β1 binding to both GFOGER and GLOGEN equally so there is no peptide-affinity effect seen here. TC-I-15 also shows weaker inhibition of α11β1 integrin at higher concentrations, in an affinity-dependent manner similar to α2β1. However, since HUVECs express tiny amounts of α11β1 (Figure 3.6) this is not of concern as the effects are assumed to be negligible. TC-I-15 had no effect on α10β1 adhesion to either peptide. Although TC-I-15 is proposed to bind to the β1 subunit, the α-subunit clearly plays a role in determining the specificity of TC-I-15 here. NaOH (the TC-I-15 vehicle control) had no effect on integrin binding, even at high concentrations. Therefore, all observed inhibition of integrin binding is due to the TC-I-15 and not the NaOH it is dissolved in.

In conclusion, Obtustatin can be used to selectively inhibit α1β1 on the surface of HUVECs, but TC-I-15 cannot be used as a selective inhibitor for α2β1. However, TC-I-15 can be used as a dual inhibitor for α1β1 and α2β1 together, and 6F1 can be used as a selective α2β1 inhibitor. In subsequent experiments, Obtustatin will be used at 20μM, while TC-I-15 will be used at 200μM as this was the concentration required to inhibit integrin binding in C2C12 cells.

Figure 4.5. Inhibition of C2C12 Cells Expressing integrins.

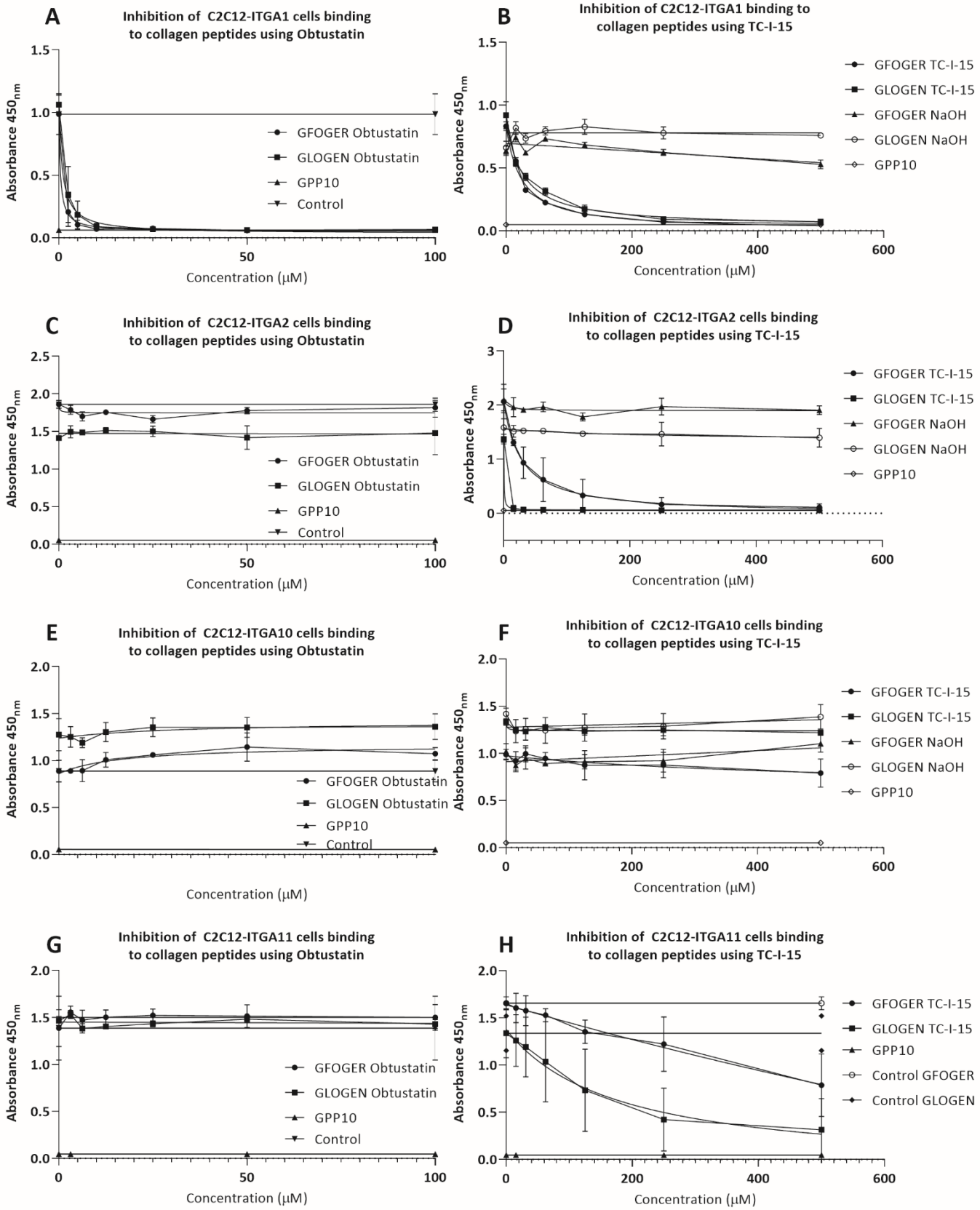

Dose curves showing the TC-I-15 and Obtustatin mediated inhibition of C2C12 cells expressing α1β1 (A and B), α2β1 (C and D), α10β1 (E and F) and α11β1 (G and H) adhesion to GFOGER, GLOGEN and GPP10. NaOH is used as the TC-I-15 vehicle control.

Table 4.2 – Comparison of IC_{50}s for C2C12 inhibition

	TC-I-15			Obtustatin		
ITGA1	IC 50	R^2	95% CI	IC_{50}	R^2	95% CI
GFOGER	23.55	0.9814	18.75 to 29.62	0.4457	0.8920	-infinity to 1.164
GLOGEN	24.43	0.9435	15.70 to 38.34	0.9634	0.2521	0.1940 to 2.191
ITGA2						
GFOGER	26.77	0.9066	15.32 to 47.67	N/A		
GLOGEN	0.3900	0.9943	-infinity to 1.089	N/A		
ITGA11						
GFOGER	3177	0.8025	151.1 to +infinity	N/A		
GLOGEN	177.2	0.7012	31.05 to +infinity	N/A		
Statistical test – non-linear regression curve fit – IC_{50}						

4.5 Inhibition of HT1080 Cell Adhesion to Collagen Peptides

To further investigate TC-I-15 inhibition of integrins, HT1080 cells were used in static adhesion binding assays with the addition of different concentrations of TC-I-15. HT1080 cells

Figure 4.6: Inhibition of HT1080 Adhesion to GFOGER.

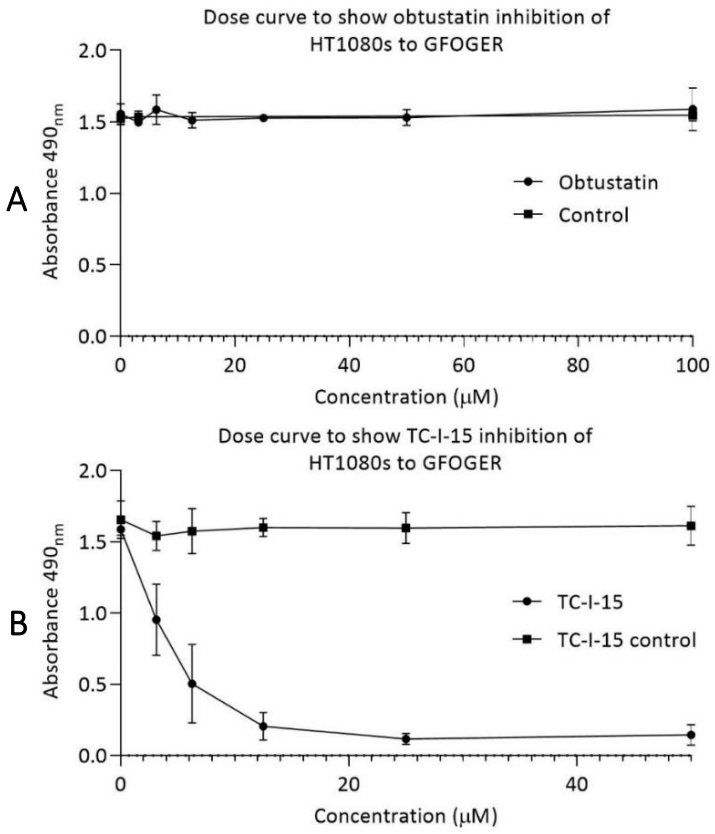

A) Obtustatin has no effect on HT1080 binding to GFOGER as HT1080s do not express α1β1. B) TC-I-15 abolishes binding to GFOGER at much lower concentrations than C2C12 cells, 20μM vs 200M respectively

are human fibrosarcoma tumorigenic cells commonly used to model tumour cell migration, that express α2β1 but none of the other collagen-binding integrins. Plates were coated with GFOGER and blocked with BSA before adding serial dilutions of inhibitors in HT1080s at 15,000 cells/well. GPP10, the negative control peptide, was taken as the baseline.

As expected, Obtustatin has no effect on HT1080 binding to collagen peptides as these cells do not express α1β1 and Obtustatin has been shown not to inhibit any other receptors tested here. TC-I-15 inhibits HT1080 binding to GFOGER at much lower concentrations than transfected C2C12-ITGA2 cells, around 15μM (Figure 4.6). The IC_{50} for TC-I-15 inhibition of HT1080 adhesion to GFOGER was 3.694μM (95% CI = 1.394μM to 8.961μM, R^2 = 0.8959), compared to 26.77μM (95% CI = 15.32μM to 47.67μM) for C2C12 cells expressing α2β1. This could be due to the C2C12 and HT1080 cells expressing different levels of α2β1. The C2C12s could express much higher levels of α2β1 and so will need more TC-I-15 molecules to bind to each βI-domain to stabilise the receptor in an inactive confirmation, whereas lower expression of α2β1 in HT1080s would require fewer TC-I-15 molecules to achieve the same inhibitory effect. Alternatively, the human β1 subunit in the HT1080s could behave differently to the C2C12 mouse β1 subunit, changing the affinity of TC-I-15 to the receptor and ultimately changing its efficacy. Lastly, the HT1080s may express other regulatory receptors or signalling molecules that affect integrin binding or integrin expression.

In conclusion, TC-I-15 inhibits α2β1 adhesion in both C2C12 cells, which express the mouse β1-subunit, and HT1080 cells which express the human β1-subunit.

4.6 Inhibition of HUVEC Adhesion to Collagen Peptides

Obtustatin and TC-I-15 have been characterised in C2C12 and HT1080 cells. Obtustatin is a potent inhibitor of α1β1 mediated adhesion at 20μM, and TC-I-15 inhibits α2β1 mediated adhesion at 200μM in C2C12s or 15μM in HT1080s. Next, these inhibitors were tested in HUVECs in the same static adhesion binding assays used above. 96-well Immulon 2HB plates were coated with peptides GFOGER, GLOGEN and GNRGER, an α2β1-specific peptide. A serial dilution of inhibitors was made in suspended HUVECs and added to the coated peptides at 15,000 cells/well. After one hour, plates were gently washed and remaining adherent cells were lysed in 2% TritonX100 before quantification using the LDH cytotoxicity colorimetric

assay. Figure 4.7 shows the quantification of TC-I-15 and obtustatin inhibition of HUVECs binding to GFOGER, GLOGEN and GNRGER.

Obtustatin had no effect on HUVEC adhesion to GFOGER, GLOGEN or GNRGER at any concentration tested. This is not surprising as HUVECs express α2β1 that will compensate for any loss of α1β1 binding to collagen peptides.

Secondly, TC-I-15 had varying effects depending on which peptide was used. HUVEC adhesion to the α2β1 specific peptide GNRGER was completely attenuated at 200μM. This can be explained by the fact that no integrin other than α2β1 will bind to GNRGER and all the α2β1 receptors are presumably locked into the closed conformation by TC-I-15 at this concentration.

Figure 4.7: Inhibition of HUVEC Adhesion to Peptides.

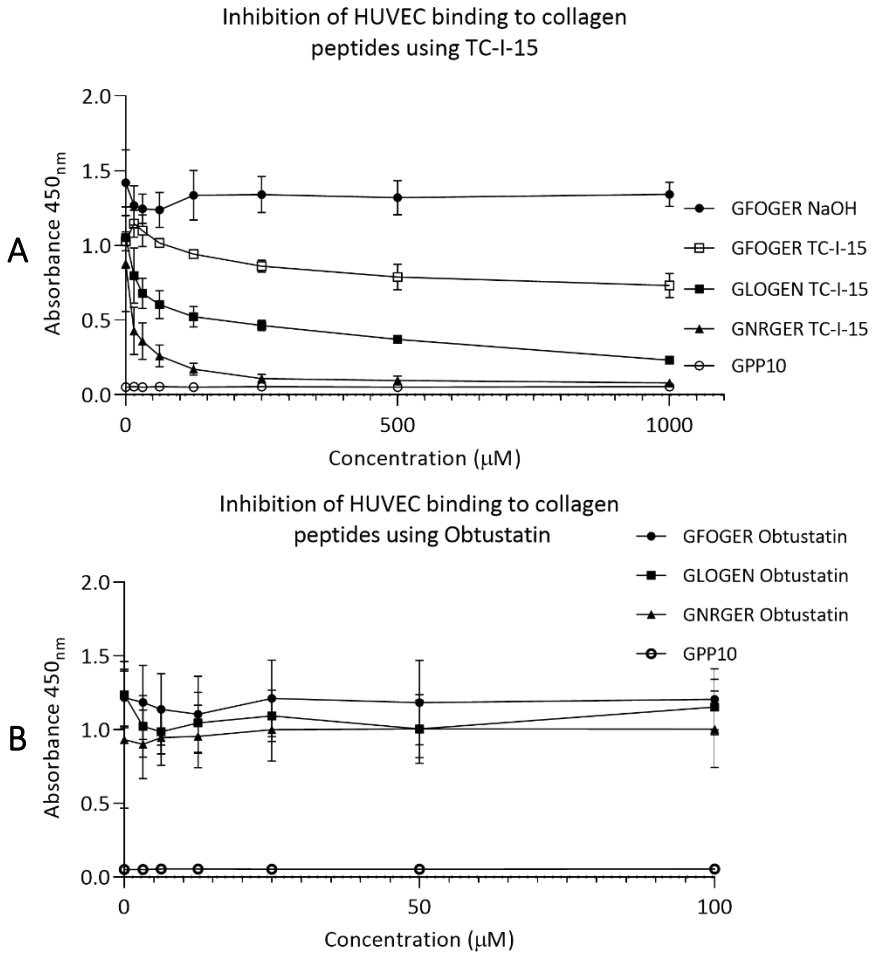

Inhibition of HUVEC adhesion to collagen peptides GFOGER, GLOGEN and GNRGER using TC-I-15 (A) and Obtustatin (B). Adhesion is shown as absorbance at 490nm which relates to the number of cells still bound after washing, using a colorimetric LDH assay.

HUVEC adhesion to GLOGEN and GFOGER was partially inhibited, but not fully. This could be due to compensatory adhesion of the α10β1 integrin, also binding to GFOGER and GLOGEN, which is present in HUVECs but, unlike α1β1, is not affected by TC-I-15. Additionally, the affinity of the GLOGEN and GFOGER peptides for α2β1 and α1β1 could be stronger than the affinity of TC-I-15 to the β1-subunit, compared to GNRGER, making the inhibitor less effective. GFOGER was inhibited to a lesser extent than GLOGEN, possibly because it is a higher affinity ligand for the more abundant α2β1 and so requires an excess of TC-I-15 to achieve further inhibition, as seen with C2C12 cells. Additionally, inhibition of C2C12-ITGA1 binding to both GFOGER and GLOGEN by TC-I-15 was very similar whereas the HUVEC inhibition profile seen here looks similar to that of C2C12-ITGA2. This is likely because α2β1 is expressed at higher levels in HUVECs. NaOH, the TC-I-15 vehicle control, has no effect on HUVEC binding and all integrin-binding inhibition can be assumed to be due to TC-I-15.

In conclusion, inhibiting α1β1 with Obtustatin has no effect on the adhesion of HUVECs to collagen peptides most likely because cell attachment through α2β1 will compensate for the loss of α1β1 functionality. Inhibition of α2β1 and α1β1 by TC-I-15 results in an inhibition profile very similar to that seen with C2C12-ITGA2, as this receptor is expressed in much higher levels.

4.7 Inhibition of HUVEC Adhesion to Extracellular Matrix Proteins

Obtustatin proved to be a very specific inhibitor for α1β1. However, TC-I-15 is more promiscuous and shows inhibition of α1β1, α2β1 and slightly to α11β1. Therefore, due to the observed promiscuity, TC-I-15 could also be affecting non-collagen-binding integrins as well. TC-I-15 associates in the interface between the α and β1 subunits (Figure 4.3), The β1 subunit can also form a heterodimer with α9, α4, α7, α6, α3 α8 α5 or αv, some of which may be present in HUVECs. According to the manufacturers' website, no cross reactivity with αvβ3, α5β1, α6β1 and αIIbβ3 is observed, but TC-I-15 could still interfere with α9, α4, α7, α3 α8 or αvβ1.

- α9β1 has been reported to bind Thrombospondin in Human Dermal Microvascular Endothelial Cells (HDMVECs) to regulate angiogenesis and proliferation[262] and it also binds VEGF-C and VEGF-D[263]
- α4β1 has been reported in proliferating ECs[264]. It binds fibronectin and VCAM
- α7β1 is a laminin receptor found in VSMCs but not ECs[265]

- α3β1 is a laminin receptor present in ECs that regulates angiogenesis in mice[266]

Figure 4.8: Diagram Depicting xCELLigence technology.

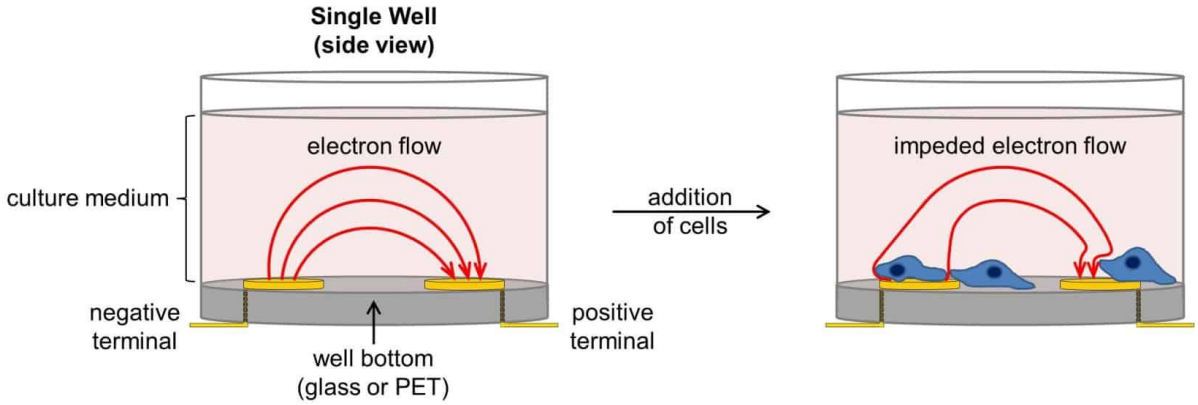

Adapted from the xCELLigence website: https://www.aceabio.com/products/rtca-sp/. Electrodes on the bottom of the wells pick up changes in current induced by the adhesion of cells to the bottom of the well. Adhesion and cell spreading can be quantified as a function of electrical impedance called Cell Index (CI). The gold electrodes cover 70-80% of the bottom surface of the well.

HUVEC adhesion to other matrix proteins was tested in real time adhesion studies using the xCELLigence electrical impedance system. In this system, matrix proteins or peptides are coated at 10µg/ml to xCELLigence E-plates, which contain electrodes capable of measuring tiny differences in electrical current imposed by cells binding to the bottom of the wells (Figure 4.8). This technique is very sensitive, and measurements are influenced by a range of environmental parameters such as temperature, media composition, well coatings, xCELLigence-plate batch and cell handling. As a result, the absolute values vary from one experiment to the next. Nevertheless, the overall trend is the same and the curves of the resulting graphs are identical and so only one out of three representative experimental repeats is shown here. Each experiment was performed in triplicate and the experimental repeat with the intermediate values was chosen here.

Figure 4.9 shows the effect of TC-I-15 on the adhesion of HUVECs to various matrix proteins and peptides. Both TC-I-15 and 6F1 inhibited HUVEC adhesion to collagen I and collagen IV, as expected, although there is some residual binding due to α10β1 or possibly

other collagen receptors present in HUVECs. HUVEC adhesion to fibronectin is unaffected, suggesting that α4β1, α5β1 and αvβ1 are not affected by TC-I-15.

HUVEC adhesion to laminin was completely attenuated by TC-I-15 and severely impeded by 6F1. Integrins α1β1 and α2β1 have been reported to bind to laminin, but HUVECs should also express other laminin receptors like α3β1, α6β4 and αvβ3 which should compensate for some of the loss of binding. TC-I-15 reportedly does not inhibit αvβ3 but has

Figure 4.9: Inhibition of HUVEC Adhesion to ECM Proteins

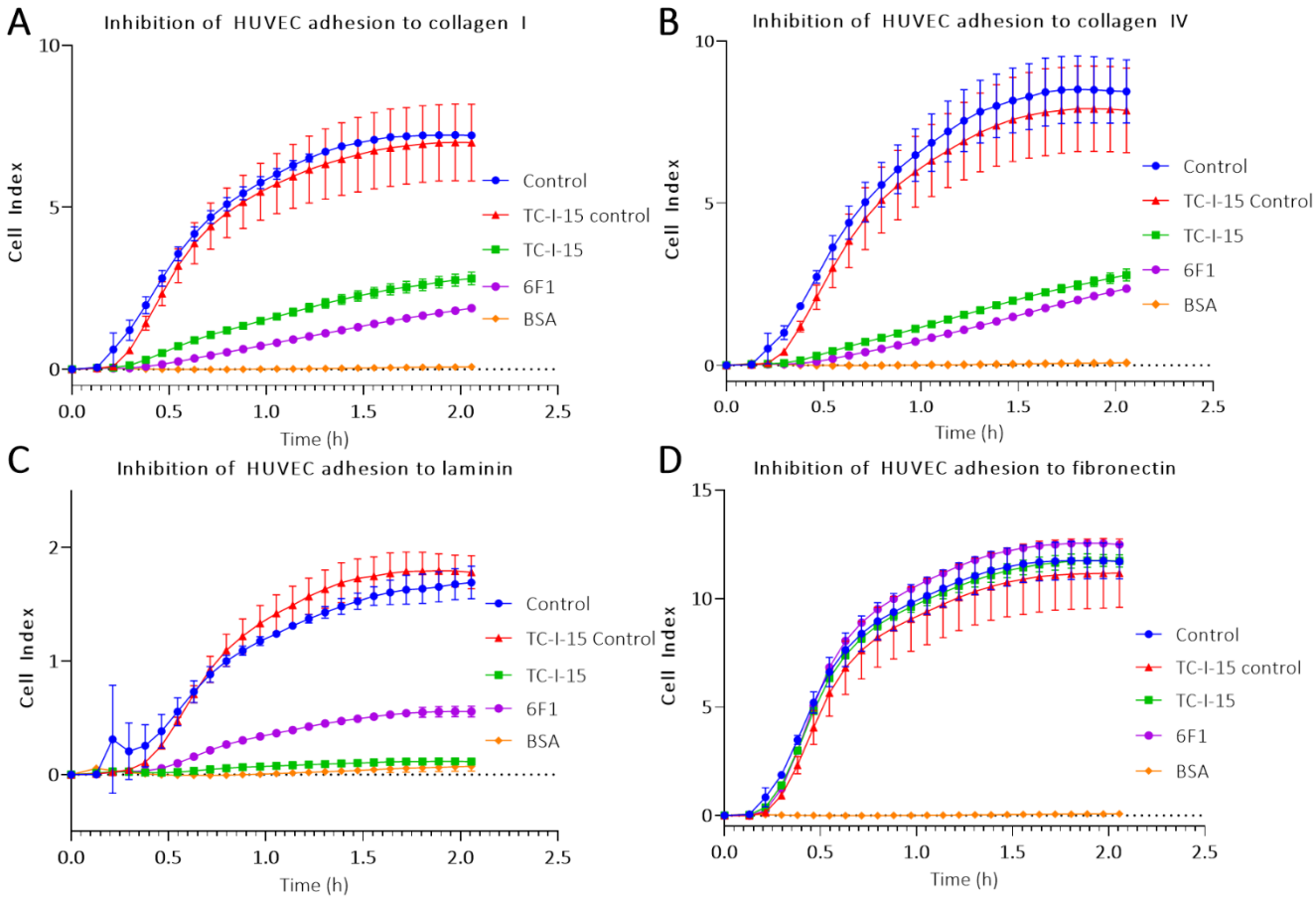

Real time adhesion studies showing the effects of TC-I-15 and 6F1 on the adhesion of HUVECs to collagen I (A), collagen IV (B), laminin (C) and fibronectin (D). xCELLigence E-plates were coated with matrix proteins or peptides and blocked before adding cells at 15,000 per well. Adhesion is quantified as Cell Index, which is measured as the electrical impedance induced by cell adhesion to the electrodes on the bottom of the wells. Three technical replicates were carried out for each experiment and three separate experiments were performed but only one experiment is shown here, as described above.

not been tested on α3β1 or α6β4. TC-I-15 may be inhibiting these other laminin receptors as well as resulting in a severe loss of adhesion. If so, α3β1 is most likely to be affected as it also contains the β1 subunit known to be targeted by TC-I-15. 6F1 is a specific α2β1 inhibitor and was sufficient to provoke severe inhibition of HUVEC adhesion to purified laminin. It is possible that in these conditions HUVECs mainly bind to laminin via α2β1 and α1β1, leading to a complete loss of binding on addition of TC-I-15. However, a detailed study of laminin binding by HUVECs or α3β1 falls outside of the scope of this project.

In conclusion, TC-I-15 is a more potent inhibitor when the ligand is of lower affinity for integrins. Also, TC-I-15 could possibly be affecting other laminin receptors in addition to α1β1 and α2β1, as the adhesion to laminin is completely abolished in the presence of TC-I-15 when HUVECs should express several laminin receptors.

4.8 Inhibition of α3β1 Adhesion to Laminin

In order to rule out TC-I-15 inhibition of α3β1 to laminin, a commercially available recombinant full-length α3β1 was purchased and used in static adhesion assays with collagen I, fibronectin and laminin in the presence of TC-I-15 or the vehicle control, NaOH. As before, Immulon 2HB plates were coated for one hour with extracellular matrix proteins in PBS for

Figure 4.10: Inhibition of α3β1 Adhesion to ECM Proteins.

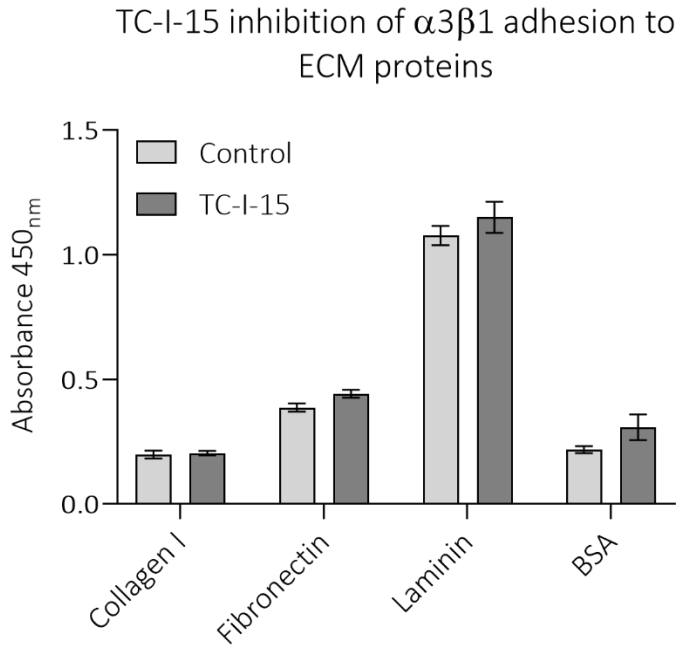

Initial static binding adhesion assay testing the effects of TC-I-15 inhibition on α3β1 adhesion to ECM proteins. TC-I-15 does not affect the adhesion of commercially purchase α3β1 to laminin. No adhesion is seen for fibronectin or collagen I.

laminin and fibronectin or in 0.01M AcOH for collagen I. Plates were blocked with 3% BSA in PBS before adding α3β1 at 10µg/ml for one hour, with or without TC-I-15. After washing with PBS, an anti-β1 antibody was used to detect the receptor and an anti-mouse HRP conjugate was used to detect the amount of α3β1 still bound to the plate with the TMB substrate as before (Figure 4.10). Two-way ANOVA with Sidak's multiple comparisons test was used to analyse the effects of TC-I-15 inhibition on the binding of α3β1 to matrix proteins. The statistical analysis is summarised in Table 4.2 below.

Table 4.3 – Statistical Analysis of α3β1 inhibition by TC-I-15 compared to the control

Control				TC-I-15			
	Mean absorbance	SD	n	Mean absorbance	SD	N	P
Collagen	0.198	0.016	3	0.204	0.009	3	0.9992
Fibronectin	0.387	0.017	3	0.442	0.016	3	0.2213
Laminin	1.077	0.039	3	1.150	0.063	3	0.0701
BSA	0.218	0.014	3	0.308	0.051	3	0.0193
Two-way ANOVA with Sidak's multiple comparisons test was used to compare mean absorbances between TC-I-15 and the control for each condition							

TC-I-15 had no effect on the adhesion of α3β1 to laminin, and no real adhesion was seen for α3β1 to collagen or fibronectin (Figure 4.9). This suggests that the TC-I-15 inhibitor is not affecting α3β1 on HUVECs, although the expression patterns of α3β1 in ECs should be tested in the future. Due to time constraints no further analysis of α3β1 was carried out to characterise this commercial recombinant protein. Further analysis should have been carried out to confirm the recombinant protein is the fully functional α3β1 heterodimer.

4.9 The effect of HUVEC activation or inhibition on integrin expression

HUVECs were cultured in EGM2 and stimulated overnight with cytokines alongside the inhibitors characterised here. Obtustatin, 6F1, TNFα, IL-1α, LPS, VEGF and TC-I-15 were added to HUVECs overnight and the effects of these compounds on the expression of collagen binding integrins was tested using qPCR. The results are shown in Figure 4.11 and the statistical analysis of the data is shown in table 4.4. The mean fold change, relative to HPRT1, values are plotted with error bars indicated SD. Addition of IL-1α increased expression of ITGA1 compared to the control (1.378-fold change relative to HPRT1 compared to 0.3337-fold change relative to HPRT1, *P=0.0218). None of the other conditions tested here increased mRNA expression of ITGA1. Additionally, no significant upregulation of either ITGA2 or ITGA10 was observed for

any condition tested. However, only one 24-hour time point was tested. It is possible that longer time points would reveal changes in integrin expression. Due to time constraints this was not repeated at other time points. VEGF has been shown to upregulate α2β1 and α1β1

Figure 4.11: Effects of HUVEC Activation and Integrin Inhibition on Integrin Expression

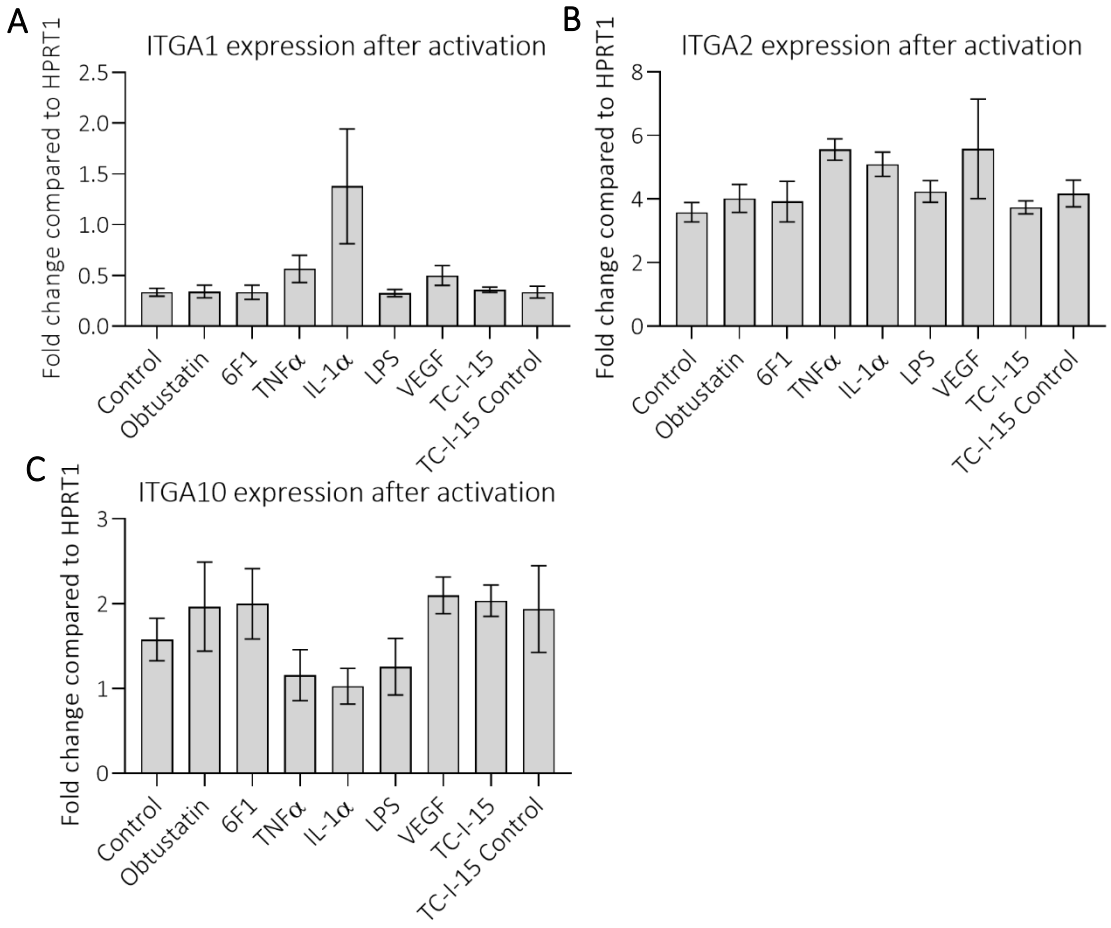

Graphs showing the differences in mean fold change, compared to HPRT1, for each integrin transcript after 24 hours activation or inhibition of integrins. A) shows the change in α1β1 expression, B) shows the change in α2β1 expression and C) shows the change in α10β1 expression Quantified by qPCR. Error bars show SD.

expression, so it was surprising not to see this effect here. In future, different concentrations and time points should be tested and analysed to investigate the effects of inflammatory cytokines and integrin inhibition on integrin expression in ECs.

Table 4.4 Statistical analysis of integrin expression after activation

	Mean fold change	SD	n	P	Mean fold change	SD	N	P
	ITGA1				ITGA2			
Control	0.3337	0.08527	5		3.59	0.6798	5	
Obtustatin	0.3406	0.1077	3	>0.9999	4.025	0.7633	3	0.9993
6F1	0.3347	0.1219	3	>0.9999	3.924	1.105	3	0.9999
TNFα	0.5642	0.2968	5	0.9897	5.56	0.7507	5	0.1389
IL-1α	1.378	1.265	5	0.0218	5.097	0.8539	5	0.4067
LPS	0.3258	0.07961	5	>0.9999	4.242	0.7582	5	0.9792
VEGF	0.4998	0.196	4	0.9991	5.581	3.135	4	0.1762
TC-I-15	0.3587	0.04712	3	>0.9999	3.742	0.3477	3	0.9997
TC-I-15 control	0.336	0.1009	3	>0.9999	4.175	0.7275	3	0.9993
One-way ANOVA with Sidak's multiple comparisons test was used to compare the mean fold change values of each condition with the appropriate control mean fold change.								

ITGA10	Mean fold change	SD	n	P
Control	1.578	0.5632	5	
Obtustatin	1.966	0.9098	3	0.9773
6F1	1.999	0.7199	3	0.9644
TNFα	1.157	0.6745	5	0.9262
IL-1α	1.027	0.4735	5	0.7670
LPS	1.257	0.7454	5	0.9821
VEGF	2.099	0.4311	4	0.8524
TC-I-15	2.036	0.3196	3	>0.9999
TC-I-15 control	1.937	0.8858	3	0.9773
One-way ANOVA with Sidak's multiple comparisons test was used to compare the mean fold change values of each condition with the appropriate control mean fold change.				

4.10 Conclusions

In conclusion, Obtustatin can be used to selectively inhibit α1β1 at 20μM. TC-I-15 can be used to inhibit both α1β1 and α2β1 simultaneously at 200μM. 6F1 can be used to selectively inhibit α2β1. However, no inhibitors exist for α10β1 so another method must be found to modulate the function of this integrin. CRISPR and siRNA are candidates for the modulation of integrin expression in the next chapter.

TC-I-15 is promiscuous and may also interact with other integrins on the surface of HUVECs. No inhibition was seen with TC-I-15 for recombinant α3β1 adhesion to laminin but no other integrins were tested due to time constraints. Additionally, TC-I-15 and 6F1 both severely

impede adhesion of HUVECs to laminin suggesting that α2β1 is the main laminin receptor in HUVECs in these conditions. This is in agreement with previous literature that states HUVECs use α2β1 to adhere to laminin[267].

Finally, integrin expression is not affected by overnight stimulation with inflammatory cytokines or overnight integrin inhibition.

Chapter 5 – CRISPR and siRNA as Techniques for Modulating Integrin Expression

Contents

5.1 Chapter Summary

This chapter focusses on using CRISPR to KO integrins first in BE cells to test the efficiency of the system and then in HUVECs using both lentiviral and liposomal methods of transfection. siRNA is also used to KD integrin in HUVECs and these KDs are characterised and validated using qPCR, western blots and adhesion assays.

5.2 Introduction

In this project, obtustatin has been further validated as a specific α1β1 inhibitor, but TC-I-15 has proved to be promiscuous and inhibits both α1β1 and α2β1. Consequently, TC-I-15 proved unsuitable for modulating the function of a single integrin but can be used to determine the effects of inhibition of α1β1 and α2β1 simultaneously. To assess the contribution of each single collagen-binding integrin on the regulation of EC function, CRISPR/Cas systems will be used to KO each receptor in turn.

CRISPR/Cas systems were discovered as a defence mechanism against viral phages in prokaryotes. 50% of bacterial and 85% of archaeal genes contain CRISPR/Cas systems[268-270]. CRISPRs are Clustered Regularly Interspaced Short Palindromic Repeats found in prokaryotic genomes, and Cas proteins are CRISPR-associated endonucleases. The CRISPR sequences were initially described by Dr Nakata's group years before their function was known[271]. CRISPR

repeats are separated by non-repeating DNA spacers which, when sequenced, were noticed to have homology to viral genomes and plasmids[272-274], the repeats were also always positioned near conserved genes, the Cas enzymes[275]. After a study discovered that the bacteria *Streptococcus thermophilus* integrated phage genomic sequences to these spacer sites following a viral challenge, it was clear the CRISPR repeats were involved in conferring a sort of bacterial immunity using the viral DNA[270, 276]. CRISPR systems are also transferable between different bacterial strains and so can be acquired[277]. Following phage or plasmid infection in bacteria, foreign double stranded viral DNA is cleaved by endonucleases and short stretches of the viral DNA are incorporated into the prokaryotic genome, between the CRISPR sites. These CRISPR sites plus the incorporated viral DNA are transcribed and processed into crRNA which associates with, and guides, Cas endonucleases to cleave incoming complementary viral DNA: the viral DNA is used against the virus[278]. The crRNA can be modified to target a gene of interest instead of viral DNA, guiding the Cas endonuclease to the target gene in the host genome. Complementary, specific sequences from a target gene can be inserted into the crRNA in the place of the viral genome fragments so that the Cas protein then cleaves the target gene, rendering it permanently inactive. Incorrect design of guide RNAs can introduce off-target effects and care must be taken to avoid this. Additionally, the target DNA must have a recognition sequence next to the crRNA binding site, called the protospacer-adjacent motif (PAM), for the CRISPR/Cas system to be functional[279-282]. The PAM sequence ensures that the CRISPR/Cas complex does not cleave its own genes as this is not present in the CRISPR array. In endogenous CRISPR/Cas systems, two short RNAs are required to form the active endonuclease Cas-RNA complex: the crRNA and the trans-activating crRNA (tacrRNA). By creating a single chimeric crRNA that contains crRNA and tacrRNA, called a single guide RNA (sgRNA), CRISPR/Cas9 systems can be reprogrammed to target any gene[279-282]. However, mismatches are tolerated in some CRISPR/Cas9 systems, more so at the end furthest from the PAM and off-target effects must be monitored closely[283, 284]. Figure 5.1 shows a representation of the CRISPR/Cas system and associated guide RNA targeting the host genome.

There are a number of different Cas proteins and Cas9 from *Streptococcus pyogenes* (spCas9) is most commonly used. The PAM sequence requirements for this spCas9 are simple (NGG) and spCas9 is a functional endonuclease. spCas9 creates blunt ends approximately 3 base pairs to the 5’ of the PAM sequence. Other Cas proteins include Cpf1 which creates a 5

Figure 5.1: Diagram of CRISPR/Cas9 Targeting DNA.

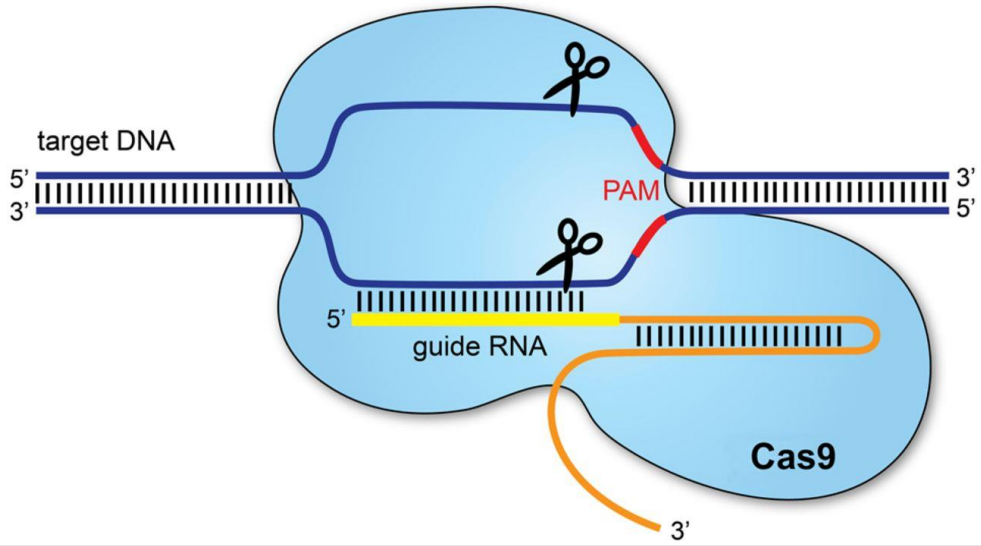

A graphical representation of the Cas9 endonuclease associated with the sgRNA targeting a complementary sequence in the host-DNA. The PAM sequence is shown on the left, and the scissors represent the DNA cleavage sites. The yellow represents the inserted sgRNA sequence while the orange represents the rest of the sgRNA structure. Figure taken from '*What is CRISPR/Ca9*' Redman et al, 2016[5].

base pairs overhang[285]. Cas proteins have a range of other functions: wildtype spCas9 causes blunt end double strand breaks (DSBs) which often results in insertion/deletions at the target site when the DNA is repaired via non-homologous end re-joining (NHEJ), but other Cas proteins are capable of converting specific bases at the target site, for example from C to T or A to G without introducing DSBs[286]. Additionally, an adenosine deaminase enzyme can be fused to a catalytically inactive Cas protein resulting in a C to G conversion at the target site [286]. It is possible to use CRISPR/Cas systems to introduce an early stop codon by fusing Cas9 to cytidine deaminases such as Apolipoprotein B mRNA editing enzyme, catalytic polypeptide 1 (APOBEC1), resulting in a site directed mutagenesis from C to a T in CGA, CAG and CCA codons, rendering the gene dysfunctional[287]. Similarly, a catalytically dead Cas9 that binds and remains attached to the target DNA has been engineered, disturbing transcription and transiently downregulating the target gene[288]. Fusing histone modifying enzymes like acetyltransferases to catalytically dead Cas9 leads to the modification of histones at target sites, resulting in gene activation or inactivation[289]. Finally, another CRISPR/Cas system fused the Cas protein with a tag displaying several binding sites for the synthetic transcription activator VP64 (4 copies of Herpes virus VP16), resulting in the recruitment of multiple

transcription activators to the Cas9 protein. The sgRNA then guides the catalytically dead Cas9 and multiple transcription activators to a target gene, resulting in as much as 50-fold increase in expression[282, 290].

Commercially available plasmid vectors containing the CRISPR sequences and associated Cas proteins are readily available for a variety of set-ups, with fluorescence reporter genes, antibiotic resistance genes, inducible expression systems and a range of endonuclease cloning sites. Addgene #57819 plasmid (pL-CRISPR.EFS.tRFP) was a kind gift from Dr Frank McCaughan (Biochemistry Department, Cambridge) and was used here to KO the gene coding for ITGA1. ITGA1 was selected as the first target as the aim was to knock each receptor out systematically.

Introducing DNA or RNA into primary cells like HUVECs can be troublesome, as they do not readily absorb DNA and they are particularly sensitive to toxicity. There are three main approaches when delivering the CRISPR/Cas system into mammalian cells, 1) introduction of a single plasmid containing both the Cas9 gene and the guide RNA, 2) delivery of mRNA encoding Cas9 alongside a separate guide RNA and 3) delivery of the Cas9/sgRNA ribonuclease protein complex. These can be delivered physically, by microinjection, or using vectors, either viral or non-viral[291]. Microinjection is the most efficient method, with efficiencies at almost 100% as vectors are injected directly into cells. There is no limit to the size of the vector for this method and concentrations of vectors or proteins can be carefully controlled. However, this method is not suitable for transfecting high numbers of cells and so would not be suitable for this application (it is more suited to injecting zygotes with CRISPR/Cas systems to create animal models[291]). Microinjection also requires specialised equipment such as 0.5-5µm needles and a microscope in a sterile environment that were not available for this project. Electroporation is another commonly used method of delivering CRISPR/Cas9 systems into cells: a high voltage pulse in the presence of DNA will transiently permeabilise the membrane allowing DNA to enter the cell. However, electroporation is somewhat toxic to sensitive primary cells and requires specialised equipment not available in this project. Additionally the transfection efficiencies are variable between cell types[291].

Liposome mediated transfection is a non-viral vector system. It works by encasing the negatively charged DNA into positively charged lipid nanoparticles that mimic the cell membrane phospholipid bilayer. The liposomes fuse with the membrane and the DNA or RNA

is released into the cell. Inside the cell, the vector is still encased within an endosome and so could be targeted for degradation before entering the nucleus, which in itself is another challenge[291]. This method is also potentially toxic, especially to primary cells, as the membrane structure is altered[291].

Viral methods include adeno-associated viruses (AAVs) and lentiviruses. AAV is a single stranded DNA virus that does not cause disease in humans and is capable of entering cells with little immune reaction[291, 292]. Lentiviruses are a subset of retroviruses and lentiviral systems have been exploited to find more efficient ways of transfecting CRISPR/Cas systems into primary mammalian cells. AAVs and lentiviral CRISPR/Cas systems use viral packaging proteins to form complexes that interact with host-cell endocytosis proteins, transporting the plasmid DNA into the cell, much like natural virus infection. AAVs have a limited capacity for large plasmids and only allow for 5kb of genomic material to be inserted, limiting the CRISPR/Cas system severely[291, 292]. In lentiviral systems, used here, the viral packaging protein gene sequences are contained on two plasmids. These are transfected into an easy-to-transfect cell line along with the CRISPR/Cas9 plasmid, where viral particles containing the CRISPR and associated Cas9 endonuclease are created. Lentiviral systems can accommodate much larger plasmid insertions. However, Cas9 from *Streptococcus pyogenes* is a large protein of 1366 amino acids, which poses problems when trying to package the CRISPR/Cas9 plasmid. Smaller Cas9 proteins were discovered in other strains, like *Staphylococcus aureus* which contains 1053 amino acids instead[293]. Since lentiviruses are retroviral, they can integrate into the host cell DNA and this could potentially increase off-target effects[291]. To make sure the viral system is safe, the gene components essential to creating viral particles are split between multiple plasmids; for 2nd generation lentiviral systems, three plasmids are used to ensure safety. One plasmid contains the packaging genes that are essential for making the viral capsid. A second plasmid contains the envelope protein genes, such as vesicular stomatitis virus G (VSV-G), and a third plasmid contains the viral genome, the CRISPR array and Cas9. Packaging plasmid psPAX2 and envelope plasmid pMD2.G were gifts from Dr Frank McCaughan and were used to create lentiviral particles to transport sgRNA/Cas9 complexes. psPAX2 contains genes sequences for *Gag, Pol, Rev* and *Tat*, and pMD2.G contains the VSV-G gene which is essential for the fusion of the viral and host-cell membranes; both have been used for successful viral transduction of mammalian cells[294].

Figure 5.2: Immunofluorescence Images of Transduced BE Cells.

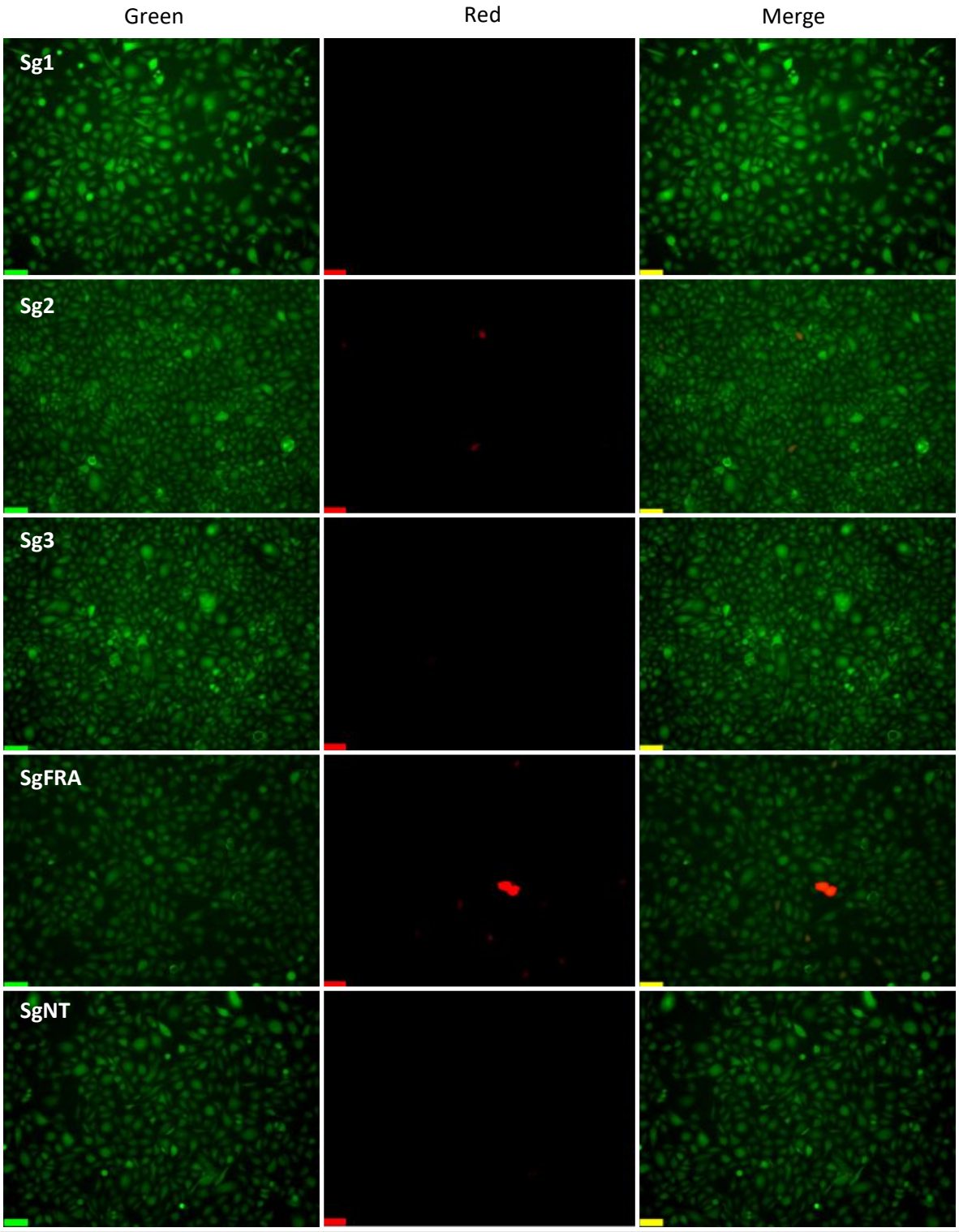

Left (green), middle (red) and right (merge) images are shown. Sg1, sg2 and sg3 are the three ITGA1 targeting sgRNA containing CRISPR plasmids, whereas sgNT denotes non-targeting sgRNA and sgFRA denotes a random targeting plasmid from Dr Frank McCaughan. BE cells express GFP and are green, the successfully transduced BE cells are red and green, merged. The scale bar represents 75µm.

5.3 Annealing of sgRNAs

First, three sets of complementary primers that anneal to form sgRNA sequences specific to one integrin (ITGA1 was chosen first to be systematic) were designed using the CRISPR design tools on the website http://crispr.mit.edu. Primers were annealed and cloned into CRISPR plasmid #57819. The resulting plasmids were electroporated into DH5α cells grown on ampicillin plates. After 24h, colonies were selected, plasmids were extracted and sequenced using PLKO U6 forward primer until 3 separate sgRNA CRISPR/Cas9 plasmids were obtained, called sg1, sg2 and sg3, as well as a non-targeting control (sgNT).

Cloning the sgRNAs into the CRISPR plasmid was surprisingly inefficient and the process had to be repeated a lot of times to obtain colonies expressing the CRISPR plasmid containing the sgRNA insert. For reasons unknown, the plasmid was prone to re-ligating without the sgRNA insert, even when the primers were treated with T4 polynucleotide Kinase (PNK), inferring ampicillin resistance to the DH5α without the insert. When the three sgRNAs were finally all cloned into the vector, these were transfected into HEK283T cells alongside psPAX2 and pMD2.G, using Lipofectamine 2000 reagent in 10cm tissue culture dishes to create viral particles. After 5 days the media was collected and filtered through a 0.45µm filter to obtain 3 sets of viral particles containing CRISPR/Cas9 plasmids with the sgRNA sequences. These viral particles were then transduced into BE cells (also from Dr Frank McCaughan). These plasmids included a red fluorescent protein (RFP) reporter gene, enabling the monitoring of successfully transfected cells after 3-5 days by detecting red fluorescence reporter on a Leica DM6000 microscope.

5.4 Transduction of lentiviral CRISPR/Cas9 into Immortalised Bronchial Epithelial Cells

Before testing the *ITGA1* gene targeting lentiviral CRISPR KO system in primary HUVECs, BE cells were tested, as they are immortalised, human and express α1β1. These BE cells express green fluorescent protein (GFP) and so can be easily monitored *in-situ* using green fluorescence. BE cells were cultured in tissue culture treated 6-well plates until 70% confluent, 100µl filtered viral particles were added to the wells along with 8µg/ml polybrene in serum-free, antibiotic free media. After 6 hours the media was changed to complete media and viral particles in cells were monitored every day for 5 days for red fluorescence. Figure 5.2 shows immunofluorescence images of live BE cells 5 days after transduction of viral particles. All BE

cells appear green and successfully transduced cells exhibit red fluorescence as well. The transduction efficiencies of these lentiviral CRISPR plasmids were very low, with very few RFP-positive cells. It was difficult to find any red cells at all: the images shown in Figure 5.2 capture non-representative fields of view where red cells were present to give an idea of what transfected cells would look like under the microscope and so this is an overrepresentation of successfully transfected cells. Higher transduction rates were expected for this lentiviral system. It is possible there were problems with the CRISPR/Cas plasmid as it was very difficult to clone the sgRNAs into the backbone when it should have been straightforward. Fresh bacteria, maxiprep kits, agar plates and antibiotics were purchased and tested, to no avail. On the other hand, the microscope may just not be sensitive enough to pick up other cells that may be RFP-positive but not bright enough. Next, a MoFlo® Astrios™ cell sorter was used to sort RFP-positive from RFP-negative cells, and HUVECs were used instead of BE cells.

5.5 Cell Sorting Analysis Confirms Transfection Efficiency is Low

Lentiviral transductions were repeated as described above with HUVECs and viral particles were added in serum-free EBM with polybrene, when cells were 70% confluent. After the 6-hour transduction, as before, cells were left for 3-5 days before detaching and running on the MoFlo Astrios cell sorter. Untreated cells were used as a baseline for red fluorescence to set up a sorting gate that only collects RFP-positive cells. However, there was some overlap between the RFP-positive and untreated populations and since it was necessary to collect only RFP-positive cells, the gating had to be very stringent (less than 0.1% untreated cells in the RFP-positive gate). Consequently, some of the RFP-positive cells were lost to ensure RFP-negative cells were not included. Figure 5.3 shows the cell sorting data from one experiment, with the top right graph showing the percentage of cells sorted as RFP-positive over three experiments. The transduction efficiencies were very variable between viral batches, from 0.1 to 15%.

After cell sorting, it was clear that the transfection efficiency is too low for this approach to be viable in HUVECs. HUVECs can only be passaged up to passage 5, as they begin to lose their endothelial phenotype and proliferative potential past this point. For immortalised cells and cell lines the RFP-positive cells can be separated and expanded many times to create a KO population, but this cannot be done when using primary cells. There are simply not enough RFP-positive cells to complete downstream experiments on cell function. The reason for the

very low transfection rate is unclear: the plasmids may have been damaged or degraded; there were difficulties extracting sterile, endotoxin-free plasmids using Qiagen Maxi-prep kits and the yields were often low. There were many points at which the transfection/transduction process could be losing efficacy. In the end liposomal transfection methods were tested instead of troubleshooting the lentiviral system due to time constraints.

Several transfection reagents were tested (Lipofectamine LTX with plus reagent, Promofectin and Transfex) in forward and reverse transfection set-ups but none yielded promising results (data not shown). It is also worth noting that RFP-positive cells are not necessarily KO cells: the CRISPR/Cas9 system could have silenced one copy of the targeted gene and not the others, or the transduction may have been successful, but the gene editing could have gone wrong. RFP-positive cells must then be analysed for ITGA1 gene expression

Figure 5.3: Flow Cytometry Analysis of HUVEC Transduction.

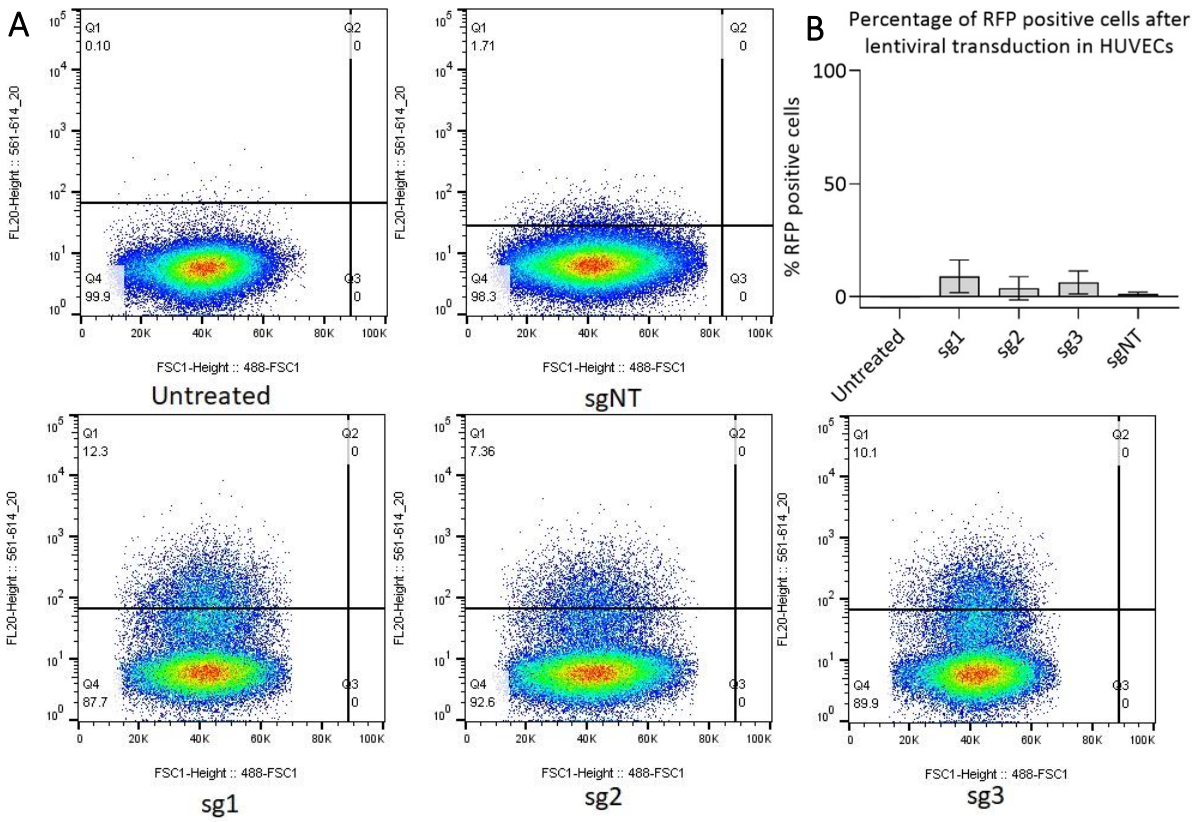

A) A series of graphs showing flow cytometry data from the gating used to sort RFP positive from RFP negative cells. The baseline was chosen so that the untreated cells displayed less than 0.1% positive cells, and this was copied to other populations. B) Graph showing collated data from 3 transductions in HUVECs. sgNT is the non-targeting CRISPR-Cas9 plasmid that contains a random guide RNA sequence.

by qPCR to confirm gene silencing. Since the transfection efficiency was too low to use in future experiments no further analysis was carried out for the RFP-positive cells.

In conclusion, neither lentiviral transduction systems nor conventional transfection reagents are suitable for use with CRISPR/Cas9 KO plasmids in HUVECs due to low transduction efficiency. Transient KD with siRNA may prove to be a more efficient and convenient tool for modulating integrin expression.

5.6 Optimisation of siRNA Knockdown using siGLO and GAPDH

Transient KD can be achieved with RNA interference (RNAi) using short interfering (si)RNA, which are short double stranded (ds)RNA molecules that induce gene silencing by targeting complementary mRNA for degradation[295]. Originally discovered as a method of gene regulation in *C. elegans*[296] and plants, RNAi is a gene silencing mechanism present in eukaryotes that can be manipulated to target an mRNA of interest. Long dsRNAs (like those in viruses) are cleaved and processed into 21 nucleotide siRNAs, with a 2-nucleotide overhang at the 3' end, by Dicer, a RNase-III-like enzyme. The siRNAs then associate with argonaute, a catalytic component of the RNA induced silencing complex (RISC), where the RNA strands are separated. The most stable strand is incorporated into the RISC. This single stranded RNA (ssRNA) guides the RISC complex to complementary mRNA and RISC cleaves the mRNA strand, marking it for degradation by RNases in the cell. Mammals and nematodes have a single Dicer enzyme that processes miRNAs and siRNAs, whereas *Drosophila melanogaster* expresses two and *Arabidopsis thaliana* has four[297]. Dicer proteins have two RNase III domains and each one cleaves one strand of the dsRNA to create the 2-nucleotide overhang. The length of the catalytic domains of Dicer effectively determine the length of the siRNA[298]. Endogenous siRNAs are degraded quickly by RNases and as a consequence commercial siRNAs are chemically modified to increase stability[299, 300].

As with CRISPR, it is tricky to transfect siRNAs into primary cells and liposomal mediated transfection is the most commonly used method. First, several transfection reagents were tested for suitability in HUVECs using commercially available fluorescent siRNA (siGLO) (Figure 5.4). Cells were reverse transfected with 50nM of siGLO and 1:50 dilution of transfection reagent (equal to 0.2µl in a 10µl transfection mix in a 96-well plate, described in materials and methods) for 8 hours in EGM2 without heparin, before changing the media to complete EGM2. After 24 hours, cells were detached and propidium iodide (PI) was added for 5 minutes to stain

dead cells before analysis on a C6 flow cytometer. Non-transfected cells that were incubated with siGLO in the absence of the transfection reagent were used as a negative control for transfected versus non transfected cells. Untreated cells without the addition of PI were used as a negative control for PI positive (dead) cells. Figure 5.4 (left) shows the comparison of transfection reagents. Table 5.1 summarises the statistical analysis of this data using one-way ANOVA and Tukey's multiple comparison test to compare the means of each condition to all the other means. DharmaFECT1 (D1), D2 and D4. D4 showed higher transfection efficiency than D1 (84.47% vs 44.38% and **P=0.0013) or D2 (57.83% and *P=0.0154) with no significant increase in cell death compared to D1 or D2 or the control. D4 was used as the transfection reagent in all further siRNA experiments. Control cells with siGLO in the absence of the transfection reagent were not positive for siGLO, confirming there is no passive up-take of siRNA.

Figure 5.4 (right) shows the optimisation of D4 concentration as subsequent percentage expression of both ITGA2 and GAPDH mRNA after siRNA KD. Table 5.2 summarises

Figure 5.4: Comparing siRNA Transfection Reagents.

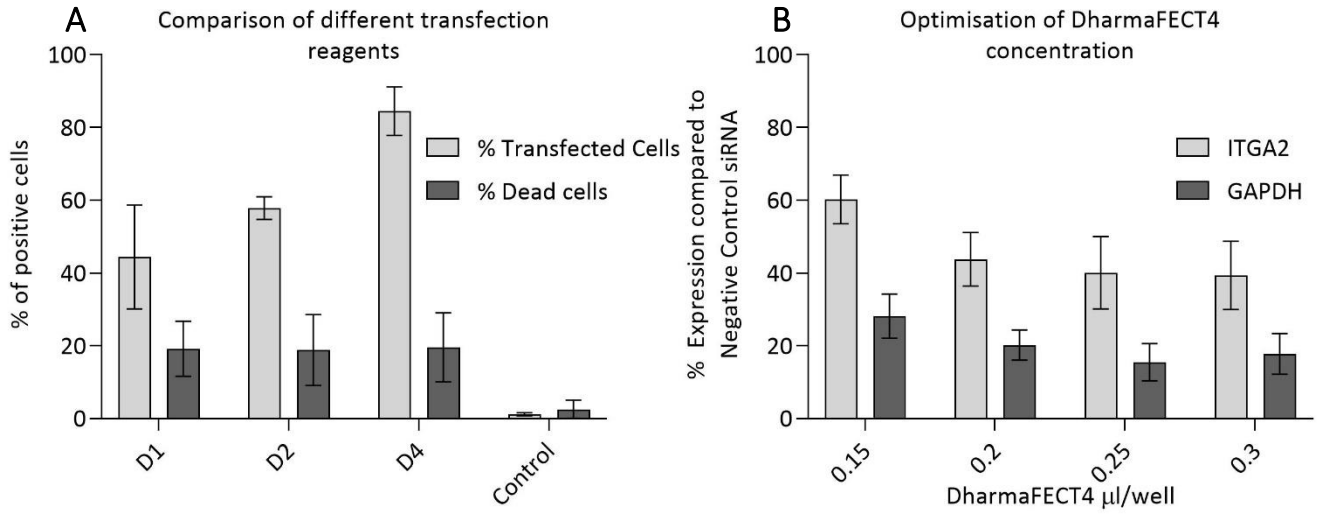

A) A comparison of 3 transfection reagents from DharmaFECT using flow cytometry and fluorescent siRNA, DharmaFECT4 (D4) shows the highest transfection efficiency for siGLO, without increasing the number of PI positive (dead) cells. The control bar shows the fluorescence of cells where siGLO was added but in the absence of transfection reagent, i.e. passive absorption of siGLO or background fluorescence. B) shows qPCR data after siRNA KD of ITGA2 and GAPDH using different concentrations of D4 (µl/well)

the statistical analysis of this data using two-way ANOVA and Tukey's multiple comparisons test to compare the mean percentage expression. For GAPDH siRNA there were no significant differences between the different concentrations used here. For ITGA2 KD, 0.15µl per well (60.23% expression) was significantly higher than 0.2µl per well (43.75% expression, **P=0.0065), 0.25µl per well (40.04% expression, ***P=0.0008) and 0.3µl per well (39.34% expression, ***P=0.0005). However, there were no significant differences between 0.2µl per well, 0.25µl per well and 0.3µl per well, suggesting that the optimal concentration would be 0.2µl per well for efficient KD while eliminating unnecessary costs and toxicity. From here on in, this dilution of D4 is used (1:50 or 0.2µl per well in a 96-well plate).

Table 5.1 Comparison of transfection reagent efficiency

	Percentage % of siGLO positive cells					
	Mean %	SD	n	P value vs D2	P value vs D4	P value vs control
D1	44.38	14.29	3	0.2481	**0.0013**	**0.0008**
D2	57.83	3.107	3		**0.0154**	**0.0001**
D4	84.47	6.691	3			**<0.0001**
Control	1.168	0.4417	3			
	Percentage of PI positive (dead) cells					
	Mean %	SD	n	P value vs D2	P value vs D4	P value vs control
D1	19.15	7.569	3	>0.9999	>0.9999	0.1188
D2	18.84	9.738	3		0.9995	0.1271
D4	19.54	9.493	3			0.1090
Control	2.474	2.602	3			
Two-way ANOVA and Tukey's multiple comparisons test to compare the mean percentage expression of each condition with all other conditions						

Table 5.2 – Optimisation of D4 concentration

	Percentage expression of ITGA2 after siRNA Knockdown					
ITGA2	Mean %	SD	n	P value vs 0.02	P value vs 0.25	P value vs 0.3
0.15	60.23	6.711	5	**0.0065**	**0.0008**	**0.0005**
0.2	43.75	7.383	5		0.8506	0.7731
0.25	40.04	9.930	5			0.9987
0.3	39.34	9.372	5			
	Percentage expression of GAPDH after siRNA Knockdown					
GAPDH	Mean %	SD	n	P value vs 0.02	P value vs 0.25	P value vs 0.3
0.15	28.12	6.067	4	0.4255	0.0881	0.2034
0.2	20.18	4.132	4		0.7948	0.9630
0.25	15.46	5.098	4			0.9710
0.3	17.72	5.573	4			
Two-way ANOVA and Tukey's multiple comparisons test to compare the mean percentage expression of each condition with all other conditions						

5.7 – Using siRNA to Modulate Integrin Expression

Silencer Select™ siRNAs were purchased from Thermo and two siRNAs for each target gene were pooled (detailed in materials and methods). The siRNAs were extensively tested and optimised for efficiency until a 90% KD was achieved using the D4 transfection reagent. Figure 5.5 shows the mean mRNA percentage expression 48 hours after siRNA transfection with error bars depicting SD. All means are normalised using the HPRT1 control and then shown as a percentage of the negative control siRNA condition. Table 5.3 shows the statistical analysis of integrin expression after siRNA KD. The mean percentage expression is compared to all other means using two-way ANOVA and Tukey's multiple comparisons test.

Table 5.3 – Statistical analysis of integrin expression after siRNA KD of each integrin

	Percentage expression of ITGA1 after siRNA Knockdown						
ITGA1	Mean %	SD	n	P value vs ITGA2 KD	P value vs ITGA10 KD	P value vs ALL KD	P value vs Control
ITGA1 KD	9.70	2.88	3	**<0.0001**	**<0.0001**	>0.9999	**<0.0001**
ITGA2 KD	98.89	6.83	3		0.9998	**<0.0001**	0.9999
ITGA10 KD	100.22	7.18	3			**<0.0001**	>0.9999
All KD	10.56	6.80	3				**<0.0001**
Control	100	0	3				
	Percentage expression of ITGA2 after siRNA Knockdown						
ITGA2	Mean %	SD	n	P value vs ITGA2 KD	P value vs ITGA10 KD	P value vs ALL KD	P value vs Control
ITGA1 KD	104.99	11.99	3	**<0.0001**	0.3098	**<0.0001**	0.9657
ITGA2 KD	12.61	1.44	3		**<0.0001**	0.9972	**<0.0001**
ITGA10 KD	120.08	27.88	3			**<0.0001**	0.0944
All KD	15.19	3.66	3				**<0.0001**
Control	100	0	3				
	Percentage expression of ITGA10 after siRNA Knockdown						
ITGA10	Mean %	SD	n	P value vs ITGA2 KD	P value vs ITGA10 KD	P value vs ALL KD	P value vs Control
ITGA1 KD	102.59	7.44	3	0.141	**<0.0001**	**<0.0001**	0.9971
ITGA2 KD	84.05	4.03	3		**<0.0001**	**<0.0001**	0.2587
ITGA10 KD	13.55	3.51	3			0.9975	**<0.0001**
All KD	16.04	12.73	3				**<0.0001**
Control	100	0	3				
two-way ANOVA and Sidak's multiple comparisons test to compare the mean percentage expression of each condition with all other conditions							

Overall this analysis shows that the siRNA KD was very efficient: 9-16% expression is seen for all targets compared to the negative control siRNA or compared to the siRNA KD of other integrins (for all of these comparisons: ****P<0.0001). The same is true for the triple KD condition where all three integrins are targeted with siRNA. There is no significant difference between the single integrin knockouts and the expression of the same integrin in the triple KD condition. There also does not seem to be any compensation by other integrins (Figure 5.5). For example, in the siRNA ITGA2-KD condition there is no upregulation of the ITGA1 or ITGA10 mRNA to compensate for the loss of ITGA2 after 48h. This is surprising as many studies have speculated that there is a functional redundancy between these integrins suggesting a compensatory mechanism may be present[168].

To ensure the KD was effective, quantitative protein expression western blots were carried out using HUVECs lysed directly in Laemmli's buffer 48h post siRNA. Cell lysates were boiled in Laemmli's buffer and run on SDS-PAGE gels before blotting onto PVDF membranes. The Licor Odyssey blocking buffer was used for blocking and antibody incubations, and Licor IR-dye secondary antibodies were used for detection of integrin bands. Various primary antibodies for ITGA1, ITGA2 and ITGA10 were all tested using cell lysates from the integrin-transfected C2C12 cells, but nearly all of them showed cross-reactivity to the other integrins and could not be used to target specifically one type of integrin. Only one antibody, targeting ITGA2, did not demonstrate any cross reactivity to the other integrins, so only western blots for ITGA2 KDs are shown here (Figure 5.5). All bands were normalised to a loading control (α-tubulin) and compared to the negative control siRNA to get a percentage value for protein expression. Data is shown as a percentage of fluorescence intensity, normalised to α-tubulin. Western blots showed a huge decrease in protein expression of ITGA2 in both the ITGA2 KD and KD of all three integrins, as expected. Timepoints from 48h to 120h post transfection were analysed and protein expression was found to be lowest at 48-72h post transfection. As a result, all downstream experiments were carried out at this time point. Figure 5.5 shows the western blot images obtained from the Licor from which fluorescence measurements were taken and analysed.

Figure 5.5. Quantification of siRNA Knockdown.

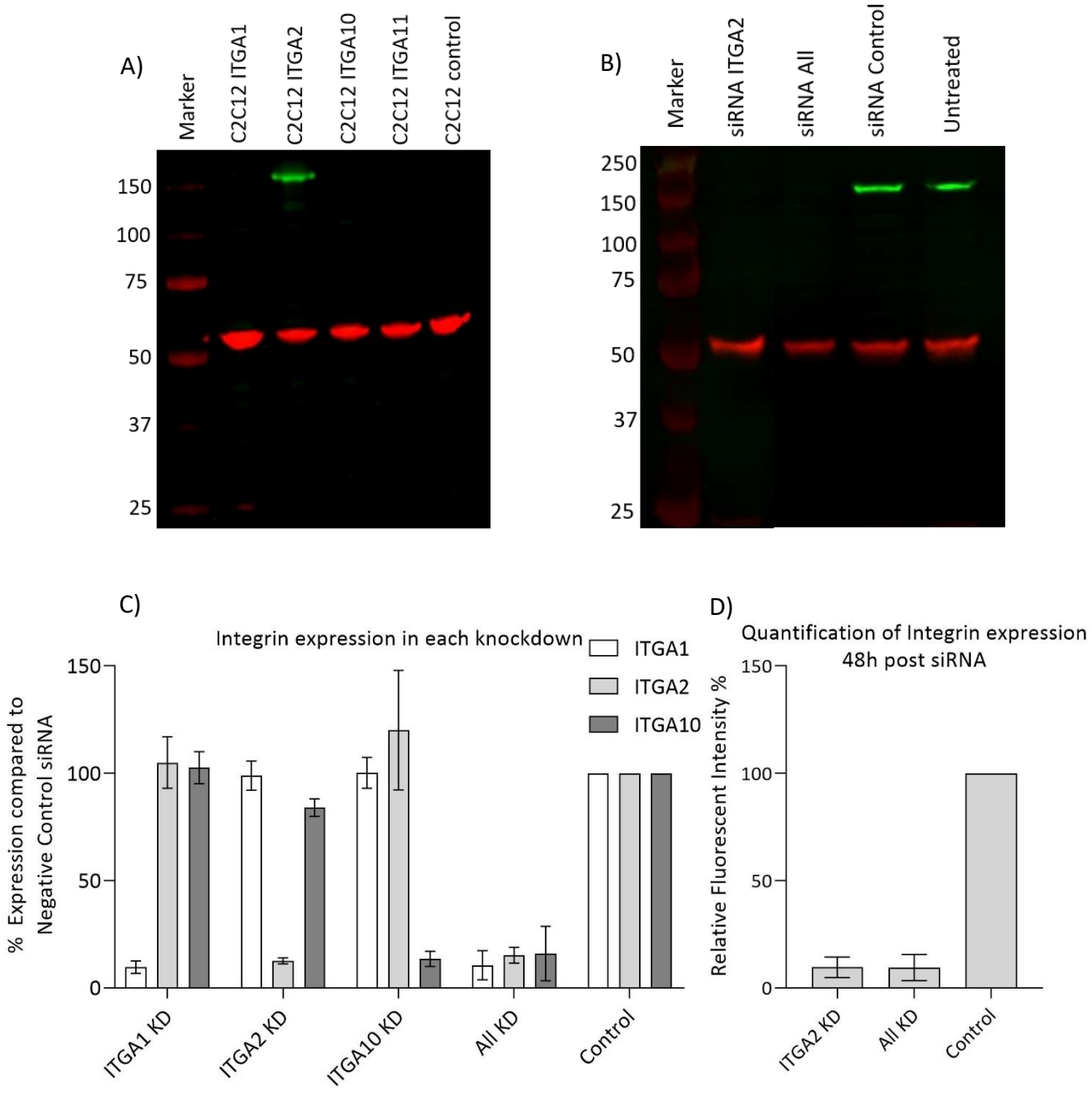

Quantification of siRNA knockdowns. A) shows the validation of ITGA2 antibody against cell lysates from C2C12 cell expressing each of the integrins, red = α-tubulin and green = ITGA2. B) Shows the detection of ITGA2 in HUVEC cell lysates 48 hours post siRNA using western blot. C) Shows qPCR quantification of integrin expression after each siRNA KD, normalised to the negative control siRNA, with a 90% KD for ITGA1 and ITGA2, and 80-85% KD for ITGA10. ITGA11 was included but not detected in any condition. KD of each integrin has no effect on the expression of other integrins at 48h time point. D) The quantification of western blot data from the Licor quantitative Western blot analysis, normalised to α-tubulin and then the negative control.

In conclusion, siRNA has proved to be an efficient way to KD integrin expression in HUVECs and will be used further to probe the effects of integrin KD on HUVEC cell function. Additionally, there does not seem to be any compensatory upregulation of integrin expression in each KD condition. This allowed us to selectively pinpoint the effect of individual integrins in cellular behaviour.

5.8 Functional Adhesion Tests Using HUVEC Knockdowns

Once the siRNA knockdown was established, functional assays were carried out to assess the effects of integrin KD on cell function. Since ECs adhere tightly to the ECM forming a barrier between the blood and surrounding tissues, HUVEC adhesion to collagen and peptides was first tested in each KD condition. Adhesion was studied in real-time xCELLIigence electrical impedance assays as described in Chapter 3. xCELLigence E-plates were coated with collagen and peptides before blocking and subsequently adding 15,000 cells/well. Adhesion was measured as a function of electrical impedance as cells adhered to the bottom of the wells and obstructed electrical currents between the E-plate electrodes.

Figure 5.6 shows the real-time effects of integrin KD on the binding of HUVECs to collagen I and the GFOGER THP. KD of ITGA1 and ITGA10 had no effect on HUVEC adhesion to either collagen I or GFOGER. This is dues to ITGA2 still being present on the cell surface to adhere to these ligands. In contrast, KD of the ITGA2 in both ITGA2-KD and All-KD severely depletes adhesion of HUVECs to collagen I and GFOGER. There is no difference between the ITGA2-KD and All-KD conditions, suggesting that the presence of ITGA1 and ITGA10 in the ITGA-KD condition does not contribute to the overall binding of HUVECs to collagen. ITGA2-KD is sufficient to deplete integrin binding to collagen and further KD of ITGA1 and ITGA10 does not inhibit HUVEC binding further. The ITGA1 or ITGA10 still present on the surface of HUVECs should bind to both collagen I and GFOGER, even in the absence of ITGA2, but there was no evidence of this happening here. It is possible that the expression of ITGA10 and ITGA1 are too low to begin with, or that they require interaction with ITGA2 to bind. In HUVECs, it appears the α2β1 integrin is the main adhesion receptor for collagen and the primary collagen-binding integrin, as our qPCR data suggested.

Figure 5.6: Functional Adhesion Assays After siRNA KD in HUVECs.

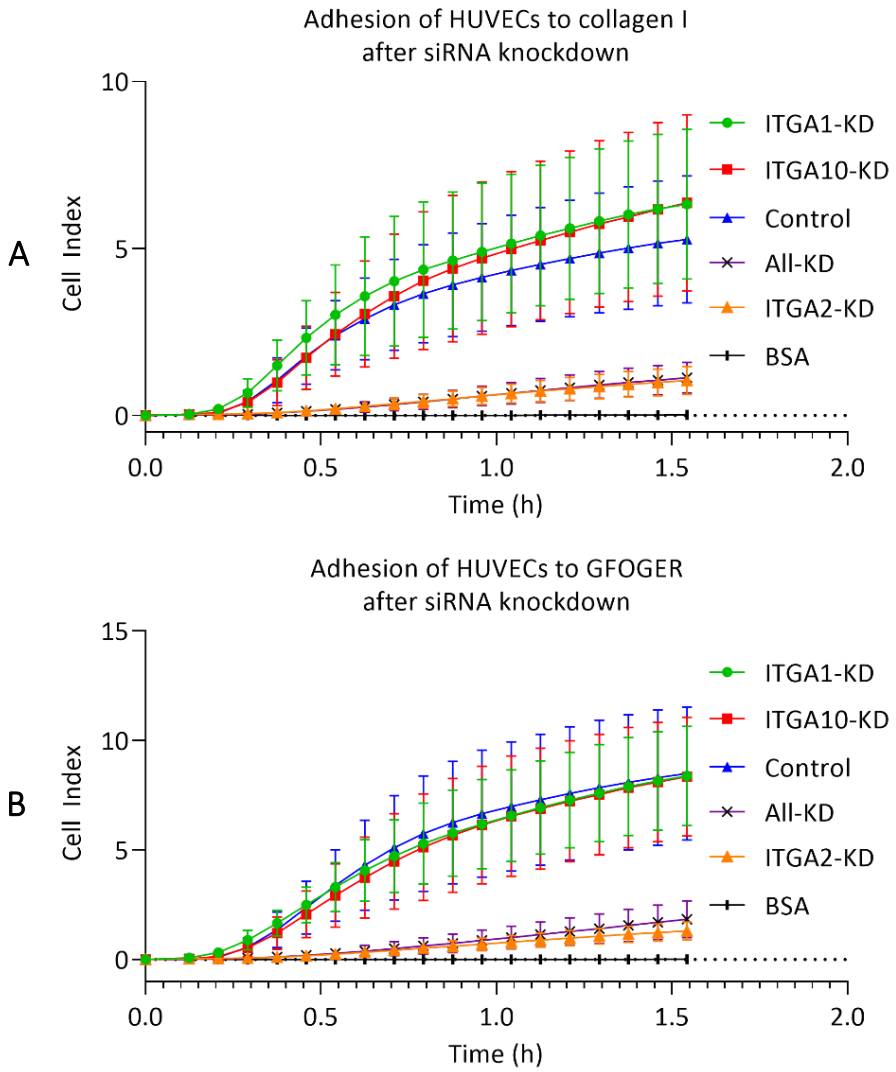

Real-time adhesion assays after siRNA KD of integrins. A) HUVECs 48 hours post-siRNA KD of each integrin adhering to soluble collagen I. B) HUVECs 48 hours post-siRNA KD of each integrin adhering to GFOGER. Knockdown of ITGA2 is enough to attenuate HUVEC binding to both collagen I and the integrin binding motif GFOGER.

5.9 Conclusions

In conclusion, CRISPR/Cas9 is not suitable for the KO of integrins in HUVECs as neither lentiviral transduction nor liposomal transfection could achieve high enough transfection efficiencies for downstream experiments in HUVECs. However, siRNA proved to be a reliable and effective method for the KD of integrins in HUVECs and will be used in all future experiments alongside inhibitors TC-I-15, obtustatin and 6F1 where possible. Adhesion to

collagen is impaired by both inhibition and KD of α2β1, but not α1β1 or α10β1. This is likely due to the fact that α2β1 is expressed in much high levels than α1β1 or α10β1. As a result, HUVEC attachment through α1β1 or α10β1 lost by KD of ITGA1 or ITGA10 genes may be compensated by binding through α2β1, but not vice versa. Very little α2β1-independent binding to collagen was detected, suggesting that the α1β1 and α10β1 integrins are not involved in HUVEC interaction with collagen in these conditions.

Chapter 6 – Effects of Integrin Inhibition or siRNA Knockdown on Proliferation and Cell Death

Contents

6.1 Chapter Summary

This chapter focusses on using the characterised integrin inhibitors and integrin siRNA KD to study the effects of integrin inhibition or KD on the proliferation of HUVECs. Proliferation was measured using cell number quantification assays and EdU incorporation assays on collagen coated surfaces. The effects of integrin inhibition and KD on HUVEC cell death were also explored. Fluorescently conjugated Annexin V was used to detect early stage apoptosis and cytotoxicity kits measuring LDH released into the media were used to measure necrosis.

6.2 Introduction

Cell proliferation describes the process by which cells divide and multiply. This process is essential in development to form an adult organism from an embryo. It is a tightly regulated process involving many cell cycle checkpoints[11]. The deregulation of cell proliferation has consequences in many disorders. For example, cancers occur when cell cycle checkpoints are deregulated in some cells. These cells undergo pathologically upregulated proliferation alongside pathologically upregulated cell survival and tumours can be formed from these incorrectly proliferating cells[11]. Psoriasis, a chronic inflammatory skin condition, is characterised by intensely itchy plaques of red or silver scales on the skin. These plaques are caused by unchecked, increased keratinocyte and dermal EC proliferation alongside an inflammatory response and they can cause severe discomfort in sufferers[301]. Carefully regulated proliferation is vital in sprouting angiogenesis as the stalk cells must proliferate to allow the tip cell to migrate away from the existing blood vessel. (see Chapter 8 for more details

on angiogenesis). This stalk-cell proliferation must then cease when the new vessel is formed[179].

Cell cycle progression (reviewed in[11]) involves several stages: first the cell enters a growth phase, then the DNA is replicated, the chromosome replicates are separated and the cell divides. Cyclins and their associated cyclin-dependent kinases (CDKs) play an important role in regulation of cell cycle progression[11]. CDKs are expressed stably throughout the cell cycle and their activity is regulated by modulating the expression of their activating cyclins. Figure 6.1 shows the general stages of cell cycle progression. G_0 denotes the resting cell state which applies to all non-proliferating cells, including the majority of ECs[87]. In response to growth factors or mitogens cells switch from the G_0 to G_1 phase, entering the growth phase of the cell cycle. This requires growth factor-stimulated upregulation of cyclin D which associate with CDK4 and 6. Cyclin E is upregulated to induce progression from G_1 into S phase, in which the process of DNA replication takes place. For post-replication transition into G_2 phase, Cyclin A binds to CDK2. Cyclin A and Cyclin B both associate with CDK1 to promote transition from G_2 into the M phase, where mitosis occurs. When CDKs are cyclin-activated, they phosphorylate target proteins that promote cell cycle progression. CDK4/6-Cyclin D phosphorylates the tumour suppressor pRb which results in the activation of transcription factors, which promote cell-cycle progression genes such as cyclin A. Cyclin expression promotes cell cycle progression and cyclins are broken down at the end of each phase via ubiquitin mediated degradation. Processes that regulate cyclin expression or CDK activation/inhibition will effectively influence cell cycle progression. CDK inhibitors (CDKIs) can either block cyclin binding or inactivate the cyclin-CDK complex resulting in cell-cycle arrest. Table 6.1 summarises some CDKIs and their targets. The CDKI p21 is transcriptionally upregulated by the tumour suppressor p53, while p15 and p27 are increased or activated in response to TGFβ, resulting in cell cycle arrest[11].

Table 6.1 – List of Cyclin Inhibitors

INK4 CDKI Family	Function	Cip/Kip CDKI Family	Function
p15, p16, p18, p19	Form stable complexes with CDK4 and CDK6 preventing binding to cyclin D	p21, p27, p57	Inhibit CDK4-Cyclin D and CDK6-Cyclin D complexes and CDK1-Cyclin B complexes

Figure 6.1. Cell Cycle Diagram.

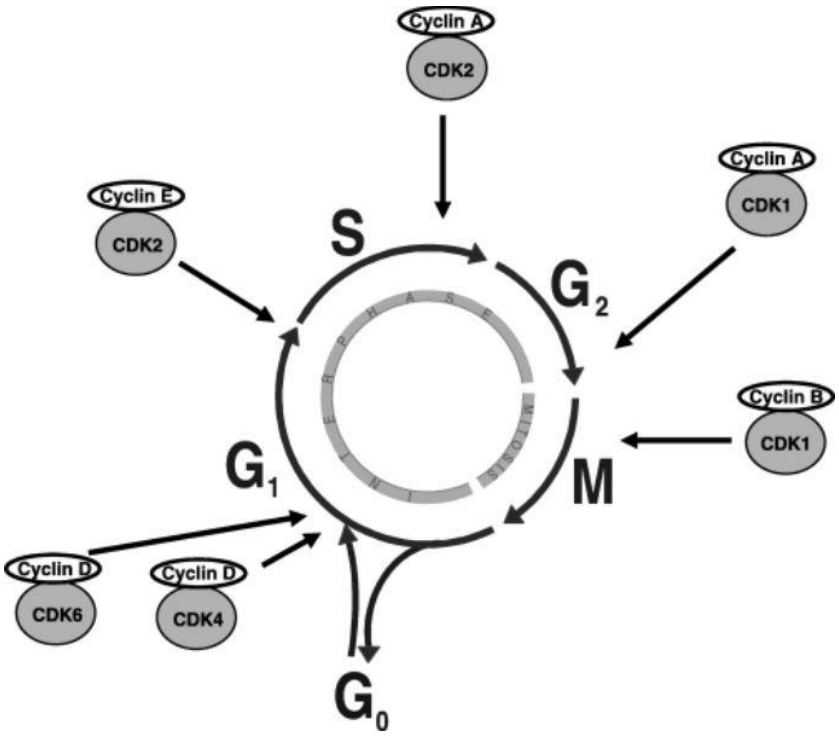

Figure 6.1. Cell Cycle Diagram.

A diagram adapted from '*The cell cycle: a review of regulation, deregulation and therapeutic targets in cancer*' Vermeulen et al 2003[11], showing the cell cycle progression and the CDK-Cyclin complexes associated with each stage.

For a cell to commit to cell cycle progression, many checkpoints must be overcome. For example, DNA damage checkpoints must be passed for the cell to progress from G_1 into S, and failure to pass this checkpoint will result in p53-mediated cell cycle arrest so that DNA repair can take place. Cancer cells generally contain mutations in genes that encode proteins that would normally contribute to cell cycle arrest or promote apoptosis. In conclusion, the regulation of cyclins, CDKs and CDKIs will control cell cycle progression and determine whether a cell proliferates, remains quiescent or dies (reviewed in[11]).

Adhesion to the ECM is required for proliferation and survival of adherent cells[302, 303]. Integrin signalling contributes to VEGF mediated extracellular signal-regulated kinases (ERK) activation[303] and ERK signalling is heavily implicated in the upregulation of EC proliferation[304]. Integrins also activate the MAPK c-Jun NH2-terminal kinase (JNK) which contributes to the regulation of cell cycle progression through G_1 phase. JNK phosphorylates c-Jun which binds c-Fos to create AP-1 transcription factor complex[303]. AP-1 in turn regulates many pathways involved in proliferation, including the expression of Cyclin D1. Additionally, integrins stimulate

p70 S6-kinase which is thought to promote cyclin D1 translation[167]. Generally, cell adhesion to the ECM downregulates the CDKIs p21 and p27, resulting in the activation of CDK2-Cyclin complexes[177]. Integrin α10β1 has been shown to regulate proliferation in Glioblastoma cells[169] and integrin α1β1 regulates collagen-dependent proliferation *in vivo* in mouse fibroblasts[305]. This suggests it is likely that integrin modulation in HUVECs could affect proliferation.

Apoptosis is a highly regulated process by which cells undergo organised cell death. Cells that fail to overcome cell cycle checkpoints will undergo apoptosis. Additionally, loss of cell adhesion to the ECM causes apoptosis, termed anoikis[303]. In EC dysfunction, sustained chronic inflammation in response to TNFα can result in apoptosis or detachment of ECs into the blood stream[88]. There are multiple integrin signalling pathways implicated in the regulation of cell survival. For example, integrin ligation to the ECM leads to focal adhesion kinase (FAK) activation which in turn activates PI3 Kinase, and protein kinase B. These signals promote cell survival by inactivating the pro-apoptotic proteins caspase-9 and Bad[303]. Additionally, antagonist blocking of αvβ3 induces apoptosis in proliferating ECs[306]. Clearly, EC attachment, proliferation and apoptosis are all linked to adhesion. Cell attachment through collagen-binding integrins could regulate these processes in HUVECs. To further study these interactions, proliferation and apoptosis studies were carried out in HUVECs after integrin inhibition and siRNA knockdown.

6.3 Effects of Integrin Inhibition or siRNA Knockdown on Proliferation

HUVECs were grown on collagen coated surfaces for all proliferation assays. First, 5-ethynyl-2-deoxyuridine (EdU) incorporation assays were carried out downstream of integrin inhibition or KD. EdU assays work in a similar way to (Bromodeoxyuridine) BrdU assays in that a Thymidine DNA base analogue, EdU, is added to live cells in culture for a limited duration. The cells then passively uptake the EdU and incorporate it into DNA during synthesis that occurs during the S phase. Copper-catalysed azide-alkyne (click) chemistry is then utilised to specifically label the DNA-incorporated EdU with a fluorescent tag, staining the nuclei of cells that have taken incorporated EdU into their DNA. EdU assays give a snapshot of the cells that are actively proliferating at the time of the experiment.

For assays involving inhibitors, HUVECs were seeded in EGM2 and left to attach overnight before adding inhibitors for 24 hours. For assays involving siRNA KD of integrins, the cells were seeded 48 hours post-siRNA transfection and incubated overnight in EGM2. After 24 hours, EdU was added to a final concentration of 10µM and the cells were incubated at 37°C for two hours to allow EdU incorporation into actively proliferating cells. Initially, this was quantified with flow cytometry using the Thermo Click-iT Alexa 488 EdU proliferation assay kit. However, the data obtained using this kit was extremely variable over several repeats and could not be used. The protocol for the flow cytometry EdU assay involves detaching cells, fixing them and then several staining, washing and spinning steps. It is possible that some cells were lost during these steps and this loss of cells managed to skew the data. Additionally, a nuclear stain was not used for this approach and as such the total number of cells may not have been entirely accurate. On top of that, the Accuri C6 Flow Cytometer was problematic and broke down many times during the course of this project and as such the data obtained may have been affected by faults within the cytometer. Either way, the kits did not return reliable data in this set-up. Instead, the cells were fixed directly in the wells of the tissue culture plate, stained with Hoechst and the EdU Click-iT Alexa 488 dye and a Leica DM6000 microscope was used to take 10 randomly selected fields of view per well. From these images, cell counts were performed using ImageJ and the percentage of green EdU-positive cells was calculated using the Hoechst staining to calculate the total cell number. Figure 6.2 shows one

Figure 6.2: EdU staining in HUVECs.

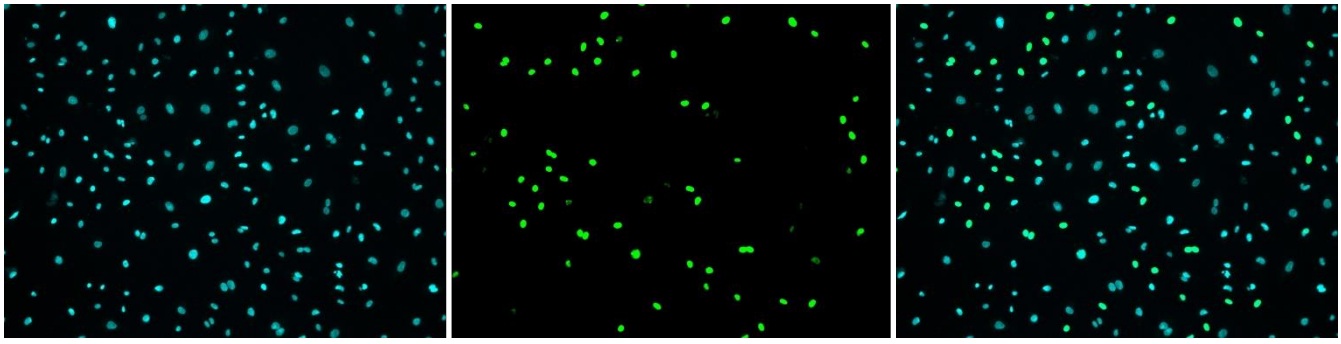

A representation of the EdU staining seen with the Thermo Click-iT EdU Proliferation kit on the Leica microscope.. Left panel: Hoechst staining (blue); middle panel: EdU staining (green); right panel: merge. A field of view from the negative control siRNA condition is seen here, but all the images were very similar. Approximately 200 cells were analysed per field of view, 10 fields of view were taken for each well and three wells were analysed per condition.

representative field of view from the Control siRNA condition as an example of the Images obtained with this approach. The staining was clear and crisp with virtually zero background staining and the cell nuclei were sparse enough for accurate automatic cell counting using ImageJ.

In addition to EdU incorporation analysis, a cell number quantification assay was carried out using the Roche LDH cytotoxicity kit to determine cell number over 3 days. HUVECs were seeded on collagen I coated surfaces in 96 well plates at a low density, 2,000 cells per well, in EGM2. The cells were then left for 6, 24, 48 or 72 hours. At each time point the media was carefully aspirated and 50µl of 2% Triton X100 in H2O was added to each well to lyse the cells, releasing the LDH. A cell number standard curve was created in the same lysis buffer and 50µl of the LDH detection reagent was added to quantify the amount of LDH released by cell lysis. The cell number was then quantified using the standard curve. This proliferation assay was only carried out downstream of siRNA KD and was not carried out using integrin inhibitors, as the stability of the inhibitors over the three-day duration of this experiment is unknown. Additionally, re-adding inhibitors each day would involve changing the media continuously which would involve replenishing the growth factors bFGF, VEGF, EGF and IGF every 24 hours. This could have undesirable effects on the proliferation of HUVECs and so inhibitors were avoided entirely for this assay. One-way ANOVA and Sidak's multiple comparison test was used to analyse the effect of integrin inhibition on the percentage of EdU positive cells. One-way ANOVA with Dunnett's multiple comparisons test was used to analyse the effect of siRNA KD on the percentage of EdU positive cells. Table 6.2 summarises the statistical analysis from these tests. The mean percentage of EdU positive cells is compared to the appropriate control condition mean percentage.

Table 6.2 – Statistical analysis of EdU incorporation assays

	Mean %	SD	n	P		Mean %	SD	n	P
Control	29.98	4.176	6		ITGA1	28.04	1.458	6	0.9932
Obtustatin	30	4.946	6	>0.9999	ITGA2	30.51	3.372	6	0.8766
6F1	29.84	4.523	6	>0.9999	ITGA10	26.48	4.401	6	0.6545
TC-I-15 Control	30.17	5.333	6		All	30.07	4.041	6	0.9601
TC-I-15	29.98	4.176	6	0.6951	Control	28.85	2.559	6	
					Untreated	29.67	4.213	6	0.9944
One-way ANOVA and Sidak's multiple comparison test (inhibitors) or Dunnett's multiple comparison Test (siRNA) was used to compare the mean percentages of EdU positive cells for each condition to the mean percentage of EdU positive cells for the appropriate control condition									

Figure 6.3 (top) shows the effects of integrin inhibition or siRNA knockdown on EdU incorporation in HUVECs after 24 hour of integrin inhibition or 48-hours post siRNA integrin KD. There was no significant difference between the percentage of EdU positive cells in any condition tested, with inhibitors or siRNA. The percentage of EdU positive cells remains constant, at around 30%, for all conditions tested. This suggests that inhibition of α2β1 or α1β1

Figure 6.3: Quantification of Proliferation in HUVECs.

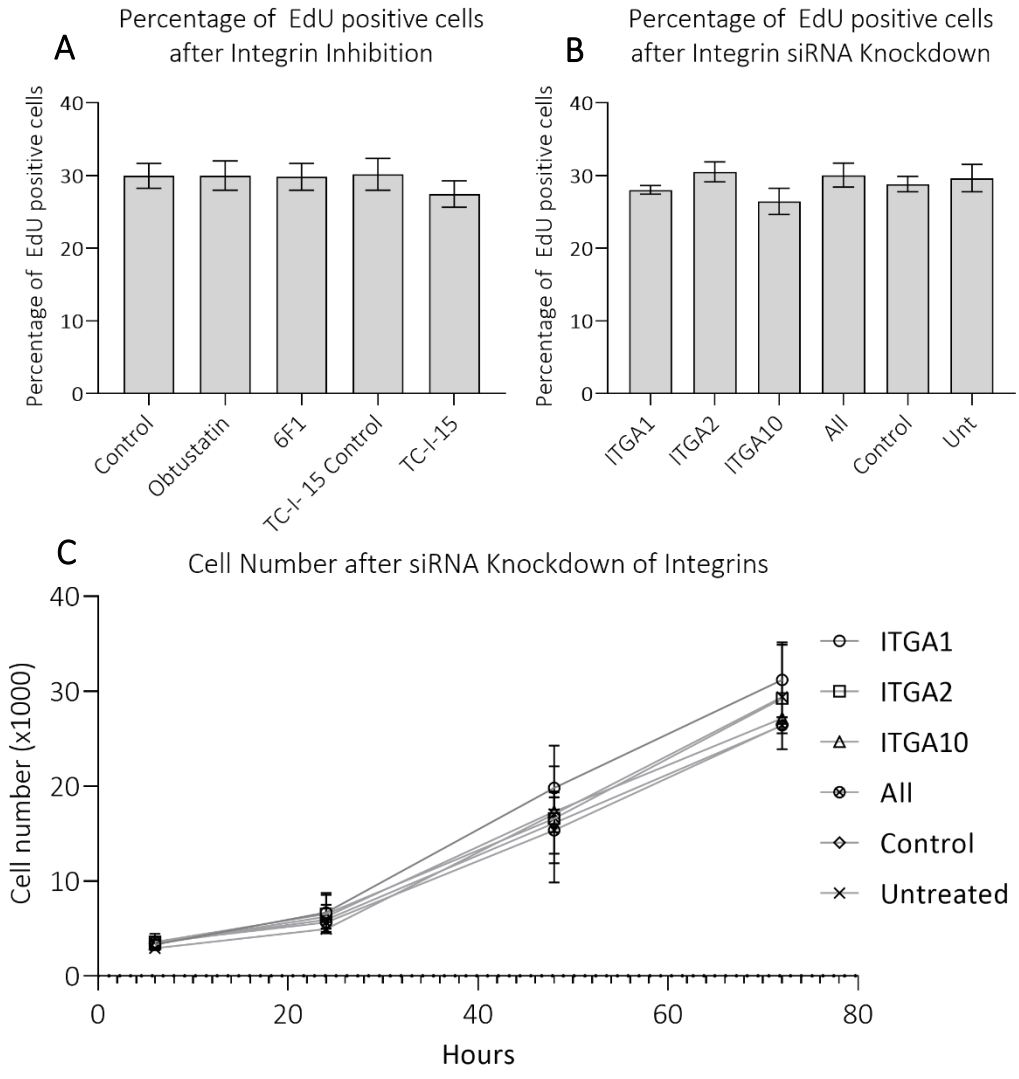

The quantification of proliferation as the percentage of EdU positive cells in HUVECs after A) integrin inhibition for 24 hours or B) KD using siRNA. There is no significant difference between any of the conditions tested. C) quantification of cell number over three days, after siRNA KD of each integrin. Again, integrin KD had no effect on the cell number after three days.

or siRNA KD of ITGA1, ITGA2 or ITGA10 effectively does not influence the number of actively proliferating cells at a given time point. Figure 6.3 (lower) shows the quantification of cell number over three days, 24-72 hours post siRNA transfection. Again, siRNA KD of each integrin had no effect on the proliferation rates of HUVECs over three days in the conditions tested.

The EdU analysis essentially gives a snapshot of the percentage of actively proliferating cells in a two-hour time window. This experiment is based on the assumption that this percentage is constant and will accurately reflect the proliferation rate of all the cells. To test this, a comparison was made between the EdU proliferation assay and a simpler cell-count assay. Additionally, culturing HUVECs in media without growth factors or FBS considerably slows their proliferation rate. To compare the two quantification methods, HUVECs were cultured in EGM2 or EBM and the EdU proliferation assay was carried out in these two conditions. The percentage of EdU positive cells was calculated as before, alongside the average number of cells per field of view and the two were compared (Figure 6.4). The two

Figure 6.4. Comparison of Proliferation Assay Methods

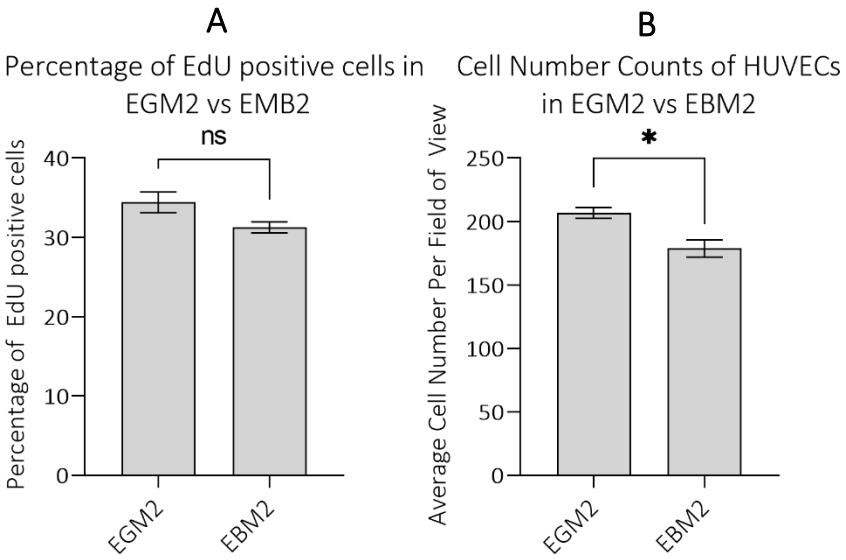

A comparison of the EdU proliferation assay quantification vs a simple cell count using the Hoechst stained cells from the same experiment. A) EdU quantification of actively proliferating cells. B) Differences in cell number in the same conditions. The same images were used for both quantifications of cell proliferation. An unpaired T-test found no significant difference between EGM2 (34.41, SD=2.6) and EBM2 (31.27, SD=1.4) P=0.0775 using the EdU analysis. The same test found a significant decrease in cell number in EBM2 (178.8, SD=13.48) compared to EGM2 (206.7, SD=8.394) P=0.0126. N=3 for each of these experiments.

methods of quantitation both used the same images. When using the EdU proliferation assay analysis there is no significant difference in proliferation between HUVECs cultured in EGM2 compared to EBM2 using an unpaired t-test (34.41% for EGM2 vs 31.27% for EBM, the difference was 3.141 ± 1.477, P=0.07775,). However, when using the simpler system of counting the cells in each field of view, there is a statistical difference between the two conditions using the same t-test (*P=0.0126, 206.7 cells for EGM2 vs 178.8 cells for EBM2, the difference is 27.93 ± 7.938). The differences could be seen by eye in the tissue culture dish, so it is interesting that they do not show up on the EdU analysis. EdU appears to be a less sensitive method for determining differences in cell proliferation and so in future should be used in conjunction with a second proliferation assay. Due to time constraints and the fact that differences in proliferation were negligible when using integrin inhibitors or integrin KD, this was not pursued further.

In conclusion, the data here suggests that inhibition of α1β1 and α2β1 has no effect on HUVEC proliferation over a 24-hour time point as measured by EdU incorporation. Inhibition of α1β1 was not expected to decrease proliferation as the α2β1 integrin will compensate for any loss of adhesion incurred by α1β1 Inhibition. Inhibition of α2β1 and α1β1 together with TC-I-15 was shown in chapter 4 to impede HUVEC adhesion but this deficit in adhesion is not translated to a change in cell proliferation. This is possibly due to other adhesion receptors anchoring the cell to the ECM to stabilise the cell and allow proliferation such as αvβ3. Cells that do not adhere at all will not undergo apoptosis but clearly these cells overcome α1β1 and α2β1 inhibition and do attach to the collagen coated plates through other means. Perhaps over the 24-hour time period the HUVECs that attach weakly to the collagen coated surface will secrete their own extracellular matrix. This would allow the cells to adhere more strongly. Additionally, the HUVECs may overcome the TC-I-15-induced inhibition by another means, for example breaking down the TC-I-15 inhibitor over time.

6.4 Effects of Integrin Inhibition or siRNA Knockdown on Apoptosis

To study the effects of integrin signalling on cell death, HUVECs were cultured in the presence of TNFα to simulate chronic inflammation associated with EC dysfunction. Additionally, HUVECs were cultured in low serum conditions (0.2%) to create cell stress in response to a pro-apoptotic environment. Assays were either carried out in the presence of inhibitors or 48 hours post siRNA KD of integrins. Zeocin was used as a positive control to

induce apoptosis in HUVECs. Annexin V was used to detect phosphatidylserine (PS) exposure on the membranes of early-stage apoptotic cells using both flow cytometry and microscopy. The Helix NIR far-red nuclear stain, or propidium iodide (PI) was used also to detect dead cells in flow cytometry, but not in microscopy because the Leica microscope available in the laboratory did not contain the correct filter for far red detection.

Figure 6.5 shows the quantification of cell death in HUVECs 24 hours after inhibition of integrins in the presence of TNFα in serum starved conditions. None of the inhibitors significantly increased the Annexin V binding to the surface of HUVECs. Only Zeocin upregulated Annexin V detection of PS on the cell membranes compared to the control (10.9%, 30.79%, *P=0.0125). As described earlier, adherent cells will undergo apoptosis if adhesion is prevented. While TC-I-15 and 6F1 impede adhesion assays over one-hour time frames, they do not block all adhesion over longer time periods. As with the migration assays, the cells do adhere to the collagen surface over time and so would not undergo apoptosis due to anoikis. However, it is surprising that the inhibition of α2β1 adhesion does not affect cell survival at all. It is possible the cells overcome the inhibition either by receptor turnover or by destabilising the inhibitor. Once the cells have overcome the inhibition they would adhere to collagen and

Figure 6.5. Quantification of Apoptosis after Integrin Inhibition

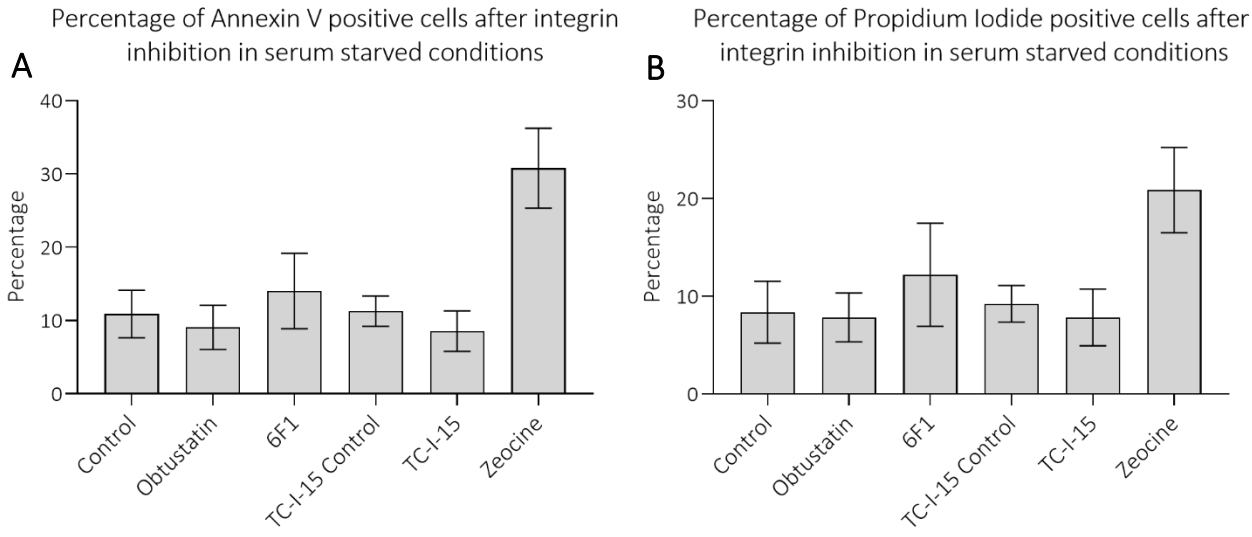

Graphs quantifying the percentage of annexin V positive cells after A) integrin inhibition and B) the percentage of PI positive cells after integrin inhibition. The mean percentage of three experiments is plotted with error bars indicating SD.

start to secrete their own ECM proteins and remodel their environment, facilitating adhesion and cell survival. It is important to note that the Zeocin positive control also did not significantly upregulate the percentage of PI positive cells and so this indicates that the experimental set-up was not optimised. Unfortunately, due to time constraints this could not be addressed further. Additionally, the flow cytometry experiments used here involved first detaching cells from the ECM before staining with Annexin V and PI and its possible that apoptotic and dead cells are being missed in this step. If cells have already undergone apoptosis or necrosis, they would not be picked up by the flow cytometer. Similarly, late stage apoptotic cells may be more fragile than live, healthy cells and may not survive the detachment and subsequent centrifugation steps required for the assay.

Table 6.3. Statistical analysis of apoptosis in HUVECs after integrin inhibition

	Percentage of Annexin V positive cells				Percentage of PI positive cells			
	Mean %	SD	N	P	Mean %	SD	N	P
Control	10.9	5.622	3		8.37	5.48	3	
Obtustatin	9.077	5.218	3	0.9955	7.83	4.325	3	>0.9999
6F1	14.04	8.907	3	0.9665	12.21	9.139	3	0.9132
TC-I-15 Control	11.28	3.572	3		9.247	3.252	3	
TC-I-15	8.56	4.796	3	0.9801	7.847	5.022	3	0.9978
Zeocin	30.79	9.427	3	**0.0125**	20.88	7.562	3	0.1069

One-way ANOVA and Sidak's multiple comparison test was used to compare the percentage means of each condition with the percentage mean of the appropriate control. Significant P values are shown in bold

Next, the effects of integrin KD on HUVEC cell survival were tested. Flow cytometry and fluorescent Annexin V was used to detect exposed PS on the membranes of apoptotic cells and Helix NIR was used to stain dead cells instead of PI in these experiments. Additionally, annexin V was also used to detect exposed PI on the membranes of apoptotic cells in fluorescence microscopy experiments and this was quantified using ImageJ as fluorescence intensity. A colorimetric LDH assay was also carried out to detect LDH secreted into the media by apoptotic or necrotic cells 24 hours after the addition of TNFα in EBM media. Figure 6.6 shows the quantification of cell death after siRNA KD of each integrin in the presence of 20ng/ml TNFα and 0.2% FBS. One-way ANOVA and Dunnett's multiple comparison tests were used to analyse all the data presented in Figure 6.6, showing the effects of siRNA KD of each integrin on cell death in each condition. The statistical analysis is summarised in Table 6.4 and compares the

mean percentage of Annexin V/NIR positive cells of each condition compared to the control mean.

Figure 6.6. Quantification of Cell Death After siRNA Knockdown of Integrins

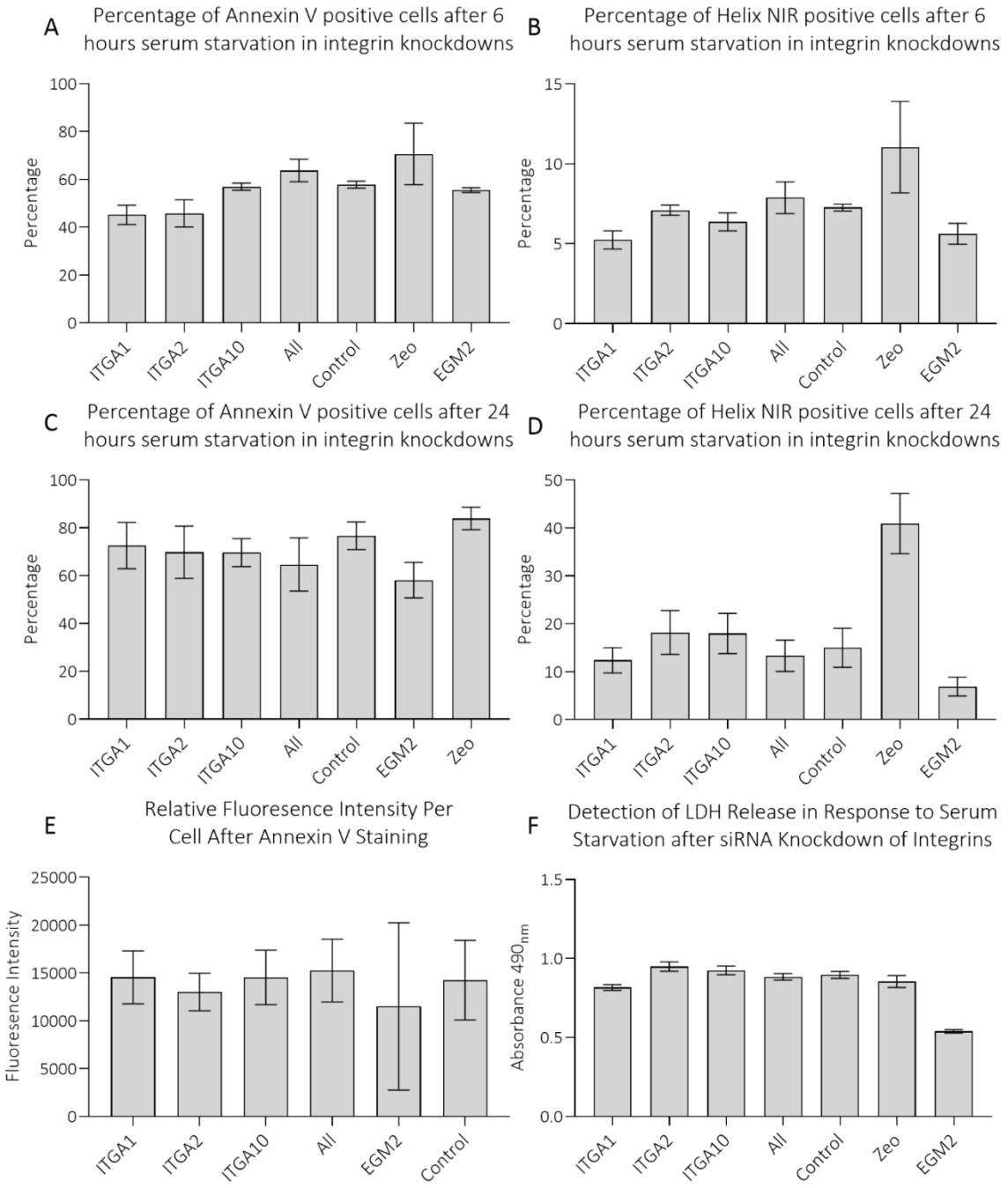

A) to D) Annexin V binding to PS exposed on the membranes of HUVECs undergoing apoptosis was quantified using flow cytometry at 6 and 24 hours. E) microscopic analysis of annexin V using ImageJ relative fluorescence intensity at 24 hours. F) LDH release in the media of HUVECs was quantified using a colorimetric LDH cytotoxicity kit.

Table 6.4 – Statistical Analysis of Annexin V and NIR staining after siRNA

	Percentage of Annexin V positive cells %				Percentage of NIR positive cells %			
	6 hour				6 hour			
	Mean %	SD	N	P	Mean %	SD	N	P
ITGA1	45.19	7.021	3	0.4841	5.243	1.136	4	0.7083
ITGA2	45.82	9.878	3	0.5315	7.098	0.6417	4	0.9999
ITGA10	56.93	2.598	3	0.9999	6.368	1.121	4	0.9888
All	63.74	8.1	3	0.9488	7.875	1.979	4	0.9980
Control	57.84	2.477	3		7.263	0.4424	4	
Zeo	70.64	22.33	3	0.4729	11.05	5.726	4	0.1610
EGM2	55.54	1.68	3	0.9996	5.62	1.304	4	0.8456
	24 hour				24 hour			
ITGA1	72.53	19.39	4	0.9980	12.38	5.311	4	0.9944
ITGA2	69.77	21.81	4	0.9788	18.19	9.134	4	0.9841
ITGA10	69.63	11.72	4	0.9767	17.99	8.421	4	0.9886
All	64.67	22.17	4	0.8039	13.33	6.552	4	0.9996
Control	76.67	11.51	4		14.98	8.202	4	
Zeo	83.91	9.368	4	0.9733	40.94	12.61	4	**0.0011**
EGM2	58.13	14.8	4	0.4351	6.883	3.931	4	0.5513
	Relative Fluorescence Intensity				Detection of LDH – Absorbance 490nm			
	24 hour				24 hour			
ITGA1	14547	4775	3	>0.9999	0.8165	0.03106	3	0.1596
ITGA2	13009	3391	3	0.9997	0.9489	0.05045	3	0.4978
ITGA10	14533	4936	3	>0.9999	0.9245	0.04724	3	0.9147
All	15252	5690	3	0.9998	0.8835	0.03562	3	0.9979
Control	14254	7197	3	>0.9999	0.8961	0.03807	3	
Zeo					0.8546	0.06502	3	0.7059
EGM2	11500	15142	3	0.9899	0.5391	0.01867	3	**<0.0001**
One-way ANOVA and Dunnett's multiple comparison tests were used to compare each siRNA condition to the control for percentage of annexin V and NIR positive cells, for mean fluorescence intensity calculated in ImageJ, and for the mean absorbance in LDH detection assays								

For the six-hour time point none of the siRNA conditions tested had any effect on the percentage of Annexin V positive cells or NIR positive cells as quantified by flow cytometry. At 24 hours only the Zeocin significantly increased the percentage of NIR positive cells, but not the percentage of Annexin V positive cells. When annexin V was quantified by microscopy a similar situation was seen, none of the siRNA conditions resulted in an increase in Annexin V detection.

Figure 6.6 also shows the quantification of LDH released into the media after siRNA KD and treatment with TNFα in serum starved media (EBM). The statistical analysis for this is also shown in table 6.4. None of the siRNA conditions resulted in an increase or decrease of LDH detected in the media of HUVECs. However, when the cells were left in EGM2, instead of EBM

and TNFα there was a significant decrease in the amount of LDH detected in the media. This indicates a decrease in cell death. This is expected as the cells in this condition are not subjected to TNFα or serum starved conditions and have not undergone siRNA transfection.

In hindsight, the transfection method used to transport siRNA inside the cells could have a pro-apoptotic affect. When HUVECs were left overnight in the transfection media there was a huge amount of cell death. Therefore, the transfection time was limited to eight hours only. These experiments are carried out 48-72 hours after siRNA transfection, but this may still not be enough time for cells to fully recover from the transfection process. The positive control for these apoptosis assays, Zeocine, used untreated cells that had not undergone siRNA transfection and so may not be appropriate as a positive control in these conditions. These results show no difference in cell death between the siRNA KD conditions and Zeocine but in reality, these two measures are not comparable. With more time, these apoptosis assays would have been further optimised to give a more relevant comparison. However, there is still no increase of cell death when comparing the integrin KD siRNA to the negative control siRNA and so it can be concluded that the KD of integrin receptors does not increase cell death as measured by Annexin V staining or NIR staining after TNFα stimulation and serum starving HUVECs.

6.5 Conclusions

Integrin inhibition or KD has no effect on HUVEC proliferation as quantified by cell number quantification or EdU incorporation analysis. This is likely due to the fact that the cells are still adhered for the duration of this experiment and so the process by which non-adhered cells stop proliferating does not occur here. Obtustatin was not expected to impede HUVEC proliferation severely due to the low expression levels of α1β1 compared to α2β1, in this condition the α2β1 integrin would adhere to the collagen. It is possible that the inhibition of α2β1 and α1β1 by TC-I-15 or the inhibition of α2β1 by 6F1 is cleared over time. This would facilitate the return of integrin mediated adhesion and subsequent proliferation. Further studies to elucidate the exact mechanism and stability of integrin inhibition would be needed to clarify this.

Similarly, knockdown or inhibition of integrins has no effect on the apoptosis or necrosis of HUVECs in response to TNFα stimulation and serum starvation. However, the

positive control, Zeocine, also did not always increase the apoptosis of these cells and so this study may have not been optimised fully to measure cell death in this set-up. The results were also variable, suggesting that the experimental protocol was not sufficiently optimised. Additionally, the siRNA transfection protocol may have increased apoptosis in HUVECs, clouding the results. Due to time constraints, further experiments could not be carried out to further investigate this.

Chapter 7 – Effects of integrin inhibition or siRNA knockdown on migration

Contents

7.1 Chapter Summary

This chapter focusses on quantifying the effects of integrin inhibition or siRNA KD of integrins on HUVEC cell spreading and migration on collagen I coated surfaces. Migration is quantified as random migration over a substrate, in time lapse assays. This project aims to study the roles of collagen-binding integrins and their inhibition in the regulation of HUVEC migration on collagen surfaces with a focus on α10β1 as this integrin is the second most abundant in HUVECs but has not been characterised in these cells.

7.2 Introduction

Cell migration is an essential function in embryonic development, wound healing, immune response and angiogenesis[194] but can also be pathological when deregulated, for example when cancer cells become highly motile and metastasise[196]. Pathological migration is also seen in chronic inflammatory diseases, vascular diseases, multiple sclerosis, osteoporosis and mental retardation[194]. Cell migration relies on the careful regulation of detachment, actin cytoskeleton reorganisation and cell adhesion in response to external stimuli like chemotactic gradients[194]. Different areas of the cell need to be coordinated so that the leading edge moves forward and the rear detaches and moves with it. This is achieved by cell polarisation[194]. The generation of polarity involves vesicle trafficking and cytoskeletal organisation, thought to be regulated partly by Cell Division Control Protein 42 (Cdc42). Cdc42 localises to the leading edge; inhibition or global activation of Cdc42 will disrupt directional

migration[307]. Phosphatidylinositol (PI)P_3 and PIP_2 are signalling molecules that help to polarise cells exposed to a chemoattractant. PI3 kinase phosphorylates PIP_2 to PIP_3, which binds to proteins with a pleckstrin homology (PH) domain. Phosphatase and Tensin homolog protein (PTEN) dephosphorylates PIP3 back to PIP2, negatively regulating the pathway. PI3 Kinase accumulates at the leading edge while PTEN is found in abundance at the trailing edge, and this contributes to the polarity seen in migrating cells[308].

Cell migration is a complicated process involving many steps. In response to chemotactic, haptotactic or other migratory stimuli, the cell polarises and the membrane at the leading edge protrudes outwards, fuelled by actin filament polymerisation from a cellular pool of profilin-bound ATP-actin monomers[309-312]. Actin filaments are polarised double helical structures wherein the actin monomers are arranged head-to-tail. They have a barbed end, oriented at the leading edge onto which ATP-bound actin monomers are added, and a pointed end at the trailing side of the filament[312]. The filaments are disassembled over time and recycled to form new filaments at the leading edge; hydrolysis of ATP, to ADP, held in the actin filament signals that filament for disassembly[312]. Actin polymerisation is regulated by a large number of proteins, including the Rho family of GTPases[251]. The life cycle of actin filaments is as follows (reviewed in[194, 312]):

1) Extracellular stimuli activate Rho GTPases, such as Rac, Cdc42, RhoA and RhoG which activate the WASP/Scar pathway
2) WASP/Scar activates the Arp2/3 complex which initiates actin polymerisation into filaments from ATP-actin monomers, branching from an existing filament
3) Barbed ends of actin filaments elongate as actin is polymerised in lamellipodia to push membrane forwards, until capping proteins bind the barbed ends to block polymerisation
4) ATP hydrolysis in the filament occurs as the filament ages, signalling the filament for depolymerisation. The ATP hydrolysis is fairly quick, but the phosphate takes much longer to disassociate, and the phosphate disassociation step signals the filament for degradation
5) ADF/Cofilin depolymerises the actin at the pointed end, creating monomers of ADP-actin

6) Profilin exchanges the ADP for ATP and actin monomers are recycled. They move to the barbed ends again, until profilin is inhibited by LIM-kinase/PAK pathway

Proteins that modify any one of these steps will affect the rate of actin filament polymerisation, altering the rate of protrusion and cell migration. The rate of actin polymerisation depends partly on the concentration of Actin-ATP and so a constant pool must be available. This is maintained by constant depolymerisation of actin filaments into actin monomers and capping of barbed ends in cells[312]. Capping ensures filaments are shorter and stiffer while ensuring growth of filaments only occurs in necessary areas, i.e. in protrusions[309, 311]. There are two main types of cell protrusions: filopodia and lamellipodia. Filopodia are thin cylinders that contain a tight bundle of orientated actin filaments held together by crosslinking proteins such as fascin, fimbrin, α-actinin and filamin[310]. Lamellipodia are wide sheets of membrane and cytoplasm that protrude out from the leading edge consisting of webs of actin filaments created by activated Arp2/3[312]. Arp2/3 is a complex of Actin-Related Protein (Arp) 2 and Arp3 that binds actin filaments to initiate the branching of a new filament from the existing one. *In vitro,* the branching angle of Arp2/3 is 70°, but *in vivo* data have suggested a wider range of angles are seen from 15-90°[312, 313]. Cortactin, filamin A and α-actinin all stabilise actin networks by crosslinking branches[194]. The actin filaments themselves flow away from the leading edge in the opposite direction of cell movement at a variable rate, termed the retrograde flow rate[252, 314]. The rate of protrusion is the difference between the rate of actin polymerisation and the retrograde flow rate; if the retrograde flow rate is inhibited, the protrusions will form faster and the velocity of the subsequent cell migration is faster[252, 315]. Actin polymerisation is regulated by proteins that affect the available pool of actin-ATP monomers, the rate of polymerisation, the stability of the filaments, the rate of retrograde flow or the depolymerisation of filaments into monomers[309, 311].

Membrane protrusions that are formed must then adhere to the ECM. Strong adhesions and contractile forces will create traction and strong adhesions in the leading edge will inhibit retrograde flow by helping to stabilise the protrusions and anchor the actin cytoskeleton to the ECM[197]. Conversely, retrograde flow can be stimulated to decrease protrusion rate and migration[252]. The influence of adhesion proteins on migration vary: vinculin and talin have been shown to allow slippage[316] relative to the ECM whereas integrins are thought to adhere strongly and do not move with the actin filament retrograde flow[252]. Finally, the rear tail of

the cell must detach and retract from the ECM to allow the cell to move forward[194, 317]. Strongly adherent cells, like cultured fibroblasts, may exhibit reduced tail de-adhesion and instead leave a trail of membrane and cytoplasmic fragments in their wake[311]. Similarly, neuronal growth cones lack tail retraction completely, as they produce axons as they migrate[318]. Tail de-adhesion involves the severing of integrin-ECM adhesion or integrin-cytoskeletal association and may involve the endocytosis and turnover of integrin receptors[194, 197]. Rho/ROCK signalling is involved in adhesion disassembly and tail retraction; inhibition of Rho kinase results in impaired tail detachment in monocytes and accumulation of β2 in the still-attached tails[317].

Myosins are a family of motor proteins that have functions in cell movement, intracellular transport and adhesion[319]. Myosin molecules, fuelled by ATP, move along actin filaments. Depending on their function, this movement can result in transport of molecules along actin filaments, contractile tension in actin filaments or the pushing and sliding of filaments relative to myosin[320]. They contain N-terminal ATPase domains that are activated on actin-binding and C-terminal helical domains which either bind cellular cargo or associate into filaments with other myosin monomers[320]. Myosin dimers can then attach to actin filaments to form large myosin-crosslinked contractile bundles. Myosin II is a bipolar protein that associates with actin to form contractile bundles. It is found as myosin IIA and myosin IIB[319]. Myosin II can affect the rate of retrograde flow and can also affect tail-retraction and adhesion stability[319]. Myosin IIA and IIB deficient cells show increased, continuous protrusion with immature adhesions whereas wildtype cells exhibit pauses in protrusion that allow adhesion complexes to mature[319, 321]. In ECs, myosin II is responsible for maintaining stress fibres. The myosin II inhibitor blebbistatin promotes stress fibre disassembly and ablates EC tension without inhibiting actin polymerisation[322]. In bovine aortic ECs, myosin IIA localises at the leading edge while myosin IIB is found in the retracting tail[319, 323]. The localisation of myosin IIB is regulated by Rho and inhibition of Rho leads to impeded tail retraction while leaving protrusion unaffected, resulting in elongated cells[323].

Adhesion proteins, such as integrins, regulate adhesion between the ECM and the cytoskeleton and so are implicated in the regulation of cell migration. Integrins at the leading edge will be adherent whereas integrins at the rear must detach to allow the cell to move forward[194, 197]. Upon ligand binding, activated integrins cluster to form complexes that link the

ECM to the cytoskeleton, termed focal adhesions for the large adhesions and nascent adhesions or focal complexes if they are newer and smaller[194]. Nascent adhesions form initially and they either form and disassemble with rapid turnover or they mature into focal complexes and much later, focal adhesions[324]. Early nascent adhesions rely on Rac1 signalling and suppression of RhoA but as the adhesions mature into large focal adhesions Rac1 becomes supressed and RhoA is stimulated, possibly mediated by ROCK-induced myosin activity that encourages stress fibre formation[324]. Focal adhesions contain over 150 associated molecules and are complex signalling hubs[197]. Nascent adhesions and focal complexes are both smaller, dynamic adhesion structures located at the leading edge to promote actin polymerisation[314], they are generally present in very motile cells and form less organised adhesions. Larger, highly organised adhesions like focal adhesions correlate with slower migration and vice versa as they are very adhesive and will not allow much cell movement[197]. Nascent adhesions, focal complexes and focal adhesions vary in size and complexity but contain many of the same proteins such as clustered integrins, signalling molecules and structural proteins such as vinculin, talin, filamin and α-actinin[325] that link integrins to the cytoskeleton where actin filaments converge. They have been characterised in ECs[326], skeletal muscle[253] and neuronal growth cones[254]. Vinculin can transiently recruit Arp2/3 to the adhesions to locally stimulate actin polymerisation. Ablation of vinculin-Arp2/3 binding results in diminished lamellipodial protrusion[327]. Signalling proteins found in adhesions include Src, FAK, PAK, paxillin and ILK (integrin linked kinase) and the Rho family of GTPases which regulate actin polymerisation, adhesion formation and facilitate crosstalk between integrins[197, 328]. The affinity of integrins for the ECM proteins can be regulated by integrin activation: activation of αvβ3 is seen in lamellipodia at the leading edge of ECs[197, 329]. Talin and kindlins are examples of regulators of integrin activation[330, 331], talin binds the cytoplasmic tails of several β-subunits including β1, β2 and β3[332]. There is a wealth of evidence linking integrin adhesion to the regulation of cell migration, summarised in bullet points below for simplicity:

- The integrin expression profile can change the migrative potential of a cell, for example αvβ3 expression in melanomas correlates with increased tumour invasion[333]
- α2β1 integrin upregulation in rhabdomyosarcoma is associated with higher levels of metastasis, but not an increased growth rate[334]

- Localised activation of Protein Kinase A (PKA) and Focal Adhesion Kinase (FAK) induced by integrin ligation happens early in the migration process[335]
- Integrins are thought to help regulate actin polymerisation and therefore localise protrusion[336]
- Endothelial β1 integrin is essential for migration, adhesion and angiogenesis, β1-null ECs showed deficient adhesion and migration on collagen and laminin, while cell adhesion to fibronectin was unaffected[35].
- In HMVECs both α1β1 and α2β1 regulate haptotactic migration towards collagen I and VEGF dependent chemotaxis through a collagen matrix. Inhibition of both integrins results in reduced tumour growth and angiogenesis of human squamous cell carcinoma xenografts[160].
- In HUVECs, α2β1 has been shown to regulate EC attachment, spreading and migration on collagen while αvβ3 mediates attachment spreading and migration on vitronectin[337]
- In platelets, α2β1 activation is dependent on cdc42 and actin polymerisation[338]
- DDR1 activation supresses cell spreading by inhibiting α2β1-dependent Cdc42 activation in MDCK cells[339].
- The α1β1 inhibitor lebestatin decreases HMEC-1 adhesion and migration, and reduces angiogenesis in chick chorioallantoic membrane model[340]
- Decorin, expressed preferentially in sprouting ECs, activates IGF-IR and Rac in ECs and this promotes α2β1 dependent cell adhesion and migration on collagen I[341]
- Integrin α10β1 regulates migration, proliferation and cell survival in glioblastoma. α10β1 KD results in decreased migration and increased cell death. α10B1 is upregulated in glioblastoma[169].
- Integrin α10β1 is also upregulated in malignant melanoma and reduced α10β1 indicates reduced migratory potential[170]

Invasive cancer cells can form invadopodia, which are integrin-mediated actin-rich adhesions that can degrade matrix proteins. They contain rapid actin-polymerisation machinery to promote localised membrane protrusion and migration. They contain β1, β2, and β3 integrins and actin regulatory proteins like cortactin, gelsolin, WASP, Rho GTPases, and the actin nucleating Arp 2/3 complex[196]. Contact inhibition, the cessation of cell migration and membrane protrusion on contact with other cells, is also lost in cancer cells[342].

7.3 Effects of Integrin Inhibition or siRNA Knockdown on HUVEC Cell Spreading

KD of ITGA2 had a profound effect on HUVEC adhesion to collagen in Chapter 5, Figure 5.6, but KD of ITGA1 and ITGA10 did not. However, adhesion is just one measure of cell function, HUVECs form a tight monolayer by adhering and then spreading out on collagen to form contacts with neighbouring cells. Integrins are adhesion receptors that help the cells anchor, spread and migrate on the ECM so next, the effects of integrin inhibition or KD on cell spreading was tested. The cells were placed on collagen or THP coated plates and left for 45 minutes to spread, either 48-72 hours after siRNA or in the presence of inhibitors. Cells were fixed with 4% PFA and stained with Hoechst, to stain the nuclei and determine cell number, and rhodamine phalloidin to stain the actin filaments. Fluorescent images were taken on a Leica DM6000 microscope at 10x magnification and ImageJ was used to quantify the area of the cells to measure cell spreading. Figure 7.1 shows the quantification of cell spreading as the average area per cell, in pixels. One-way ANOVA and Sidak's multiple comparison test was used to analyse the effects of integrin inhibition on cell spreading. Obtustatin and 6F1 are compared

Figure 7.1: Quantification of HUVEC Cell Spreading on Collagen I

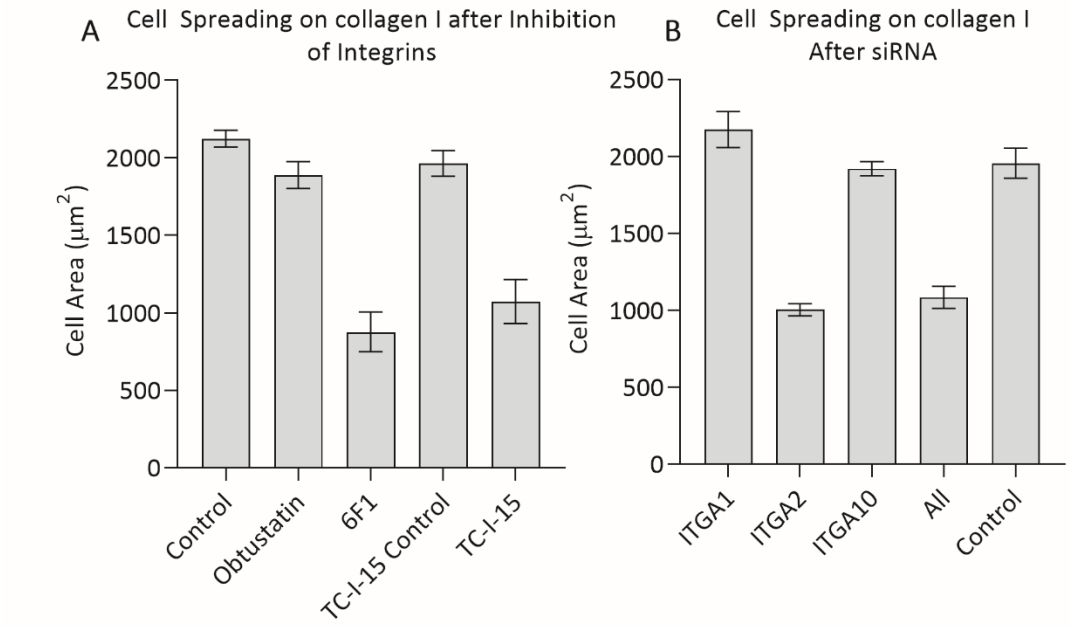

Quantification of cell spreading after A) inhibition of integrins or B) siRNA KD of integrins (right). Cells were seeded on collagen I and left to spread for 45 minutes before fixing and staining with Hoechst and rhodamine phalloidin. ImageJ was used to quantify the cell area in pixels and count the cell number. Data is shown as average area per cell. Experiments were performed in triplicate and repeated three times

to the control and TC-I-15 is compared to the TC-I-15 control. One-way ANOVA and Dunnett's multiple comparisons test was used to analyse the effects of siRNA KD of each integrin on cell spreading, with condition compared to the control. Table 7.1 summarises the statistical analysis of each of these tests. The P values shown in the table are comparisons between the inhibitor or siRNA KD and the appropriate control mean. The P value for TC-I-15 control is compared to the control. Figure 7.2 shows representative images of inhibition of HUVEC cell spreading on collagen I. These images were used to quantify cell spreading as the area (in pixels) per cell.

Table 7.1 – Statistical analysis of cell spreading on collagen I

	Mean area (pixels/cell)	SD	N	P		Mean area (pixels/cell)	SD	N	P
Control	2124	92.54	3		ITGA1	2175	202	3	0.2269
Obtustatin	1888	149.9	3	0.4501	ITGA2	1004	69.99	3	**<0.0001**
6F1	876.7	221.5	3	**<0.0001**	ITGA10	1920	80.01	3	0.9921
TC-I-15 Control	1964	142.4	3	0.7598	All	1085	124.1	3	**<0.0001**
TC-I-15	1073	246.6	3	**0.0005**	Control	1956	169.3	3	

HUVEC spreading on collagen I was significantly impeded by TC-I-15 (1073 μm^2) compared with the TC-I-15 control (1964 μm^2) ***P0.0005, and by 6F1 (876 μm^2) compared to the control with no inhibitor or antibody (2124 μm^2) ****P<0.0001. There was no further inhibition of cell spreading using TC-I-15 than using 6F1, suggesting that the inhibition of α2β1 is enough to impede cell spreading, and that the additional inhibition of α1β1 and possibly other receptors does not affect cell spreading further. Obtustatin had no significant effect on cell spreading compared to the control (1888 μm^2 compared to 2124 μm^2, P=0.4501), demonstrating that α1β1 is not required in HUVECs for cell spreading, possibly because these cells express α2β1 in high levels to facilitate cell spreading. Additionally, inhibition of α2β1 via 6F1 or α2β1 and α1β1 via TC-I-15 resulted in a change in cell morphology to irregularly shaped cells with many small membrane protrusions compared to obtustatin and control cells which were rounded and flat (Figure 7.2). Inhibition of α2β1 could be impeding the adhesion of membrane protrusions. The weaker adhesions may be unable to stabilise lamellipodia in these conditions, leading to an irregular shape where filopodia continue to extend but cannot properly adhere.

Figure 7.2: Effect of Integrin Inhibition on HUVEC Cell Spreading.

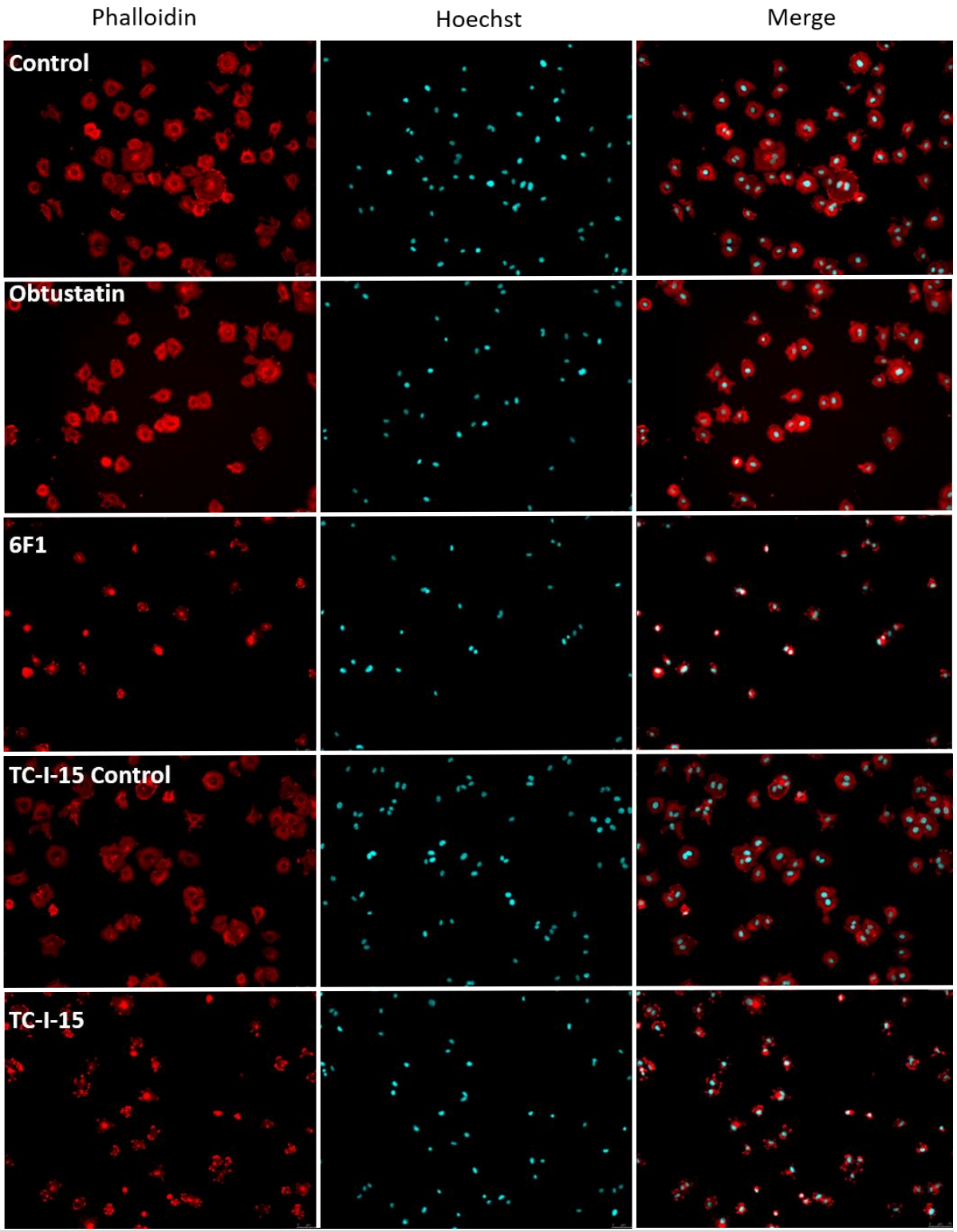

Fluorescence Images used to quantify cell spreading after integrin inhibition. The left column shows rhodamine phalloidin (red) staining on fixed cells after one hour of attachment and spreading on collagen I. The middle column shows Hoechst nuclear staining (blue) of the same cells and the right column shows a merge of the two channels.

Figure 7.3: Effect of Integrin siRNA Knockdown on HUVEC Cell Spreading

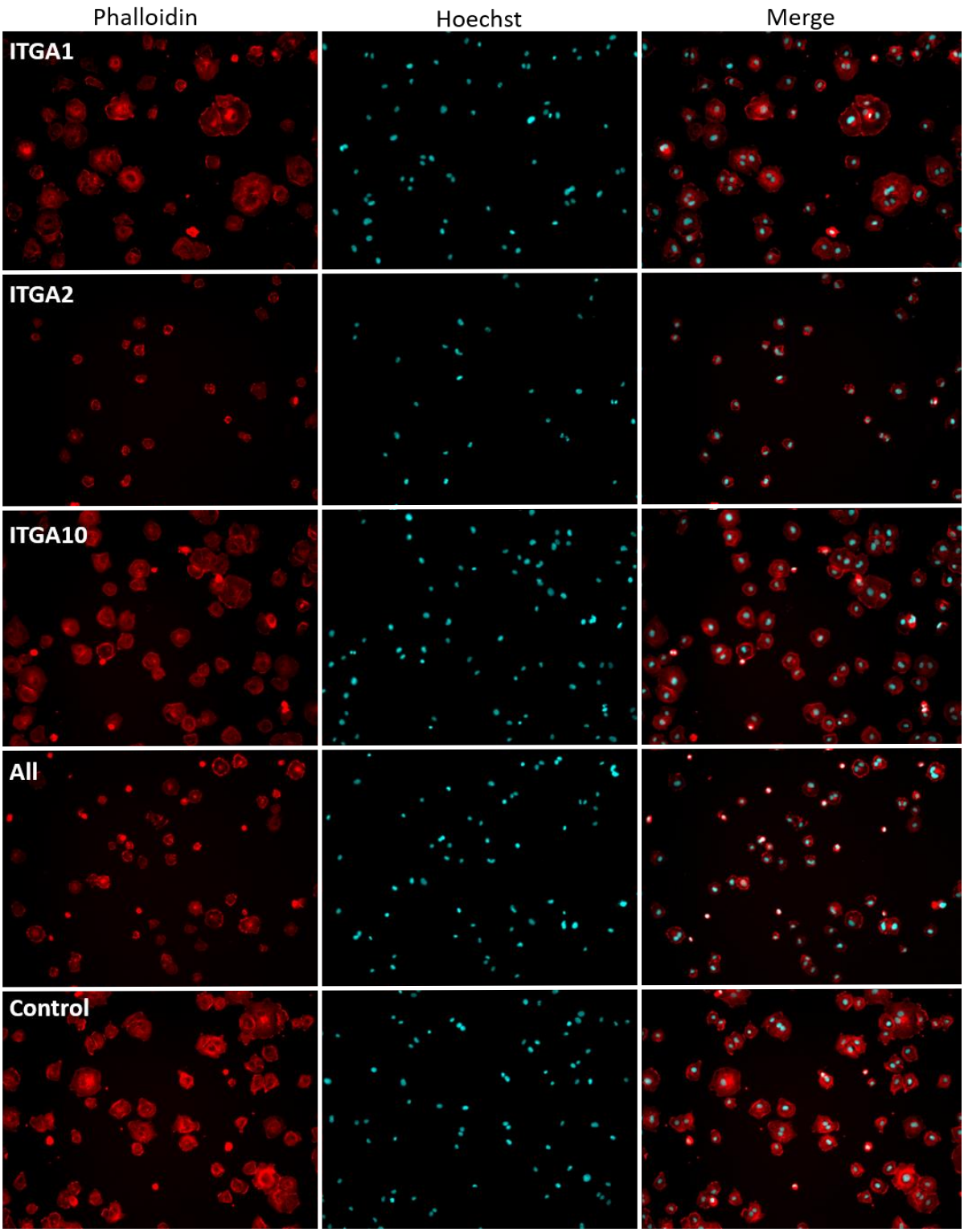

Fluorescence Images used to quantify cell spreading after siRNA KD of integrins. The left column shows rhodamine phalloidin (red) staining on fixed cells after one hour of attachment and spreading on collagen I. The middle column shows Hoechst nuclear staining (blue) of the same cells and the right column shows a merge of the two channels.

Similarly, siRNA KD of ITGA1 or ITGA10 had no effect on cell spreading compared to the negative control siRNA (2175 μm^2 vs 1956 μm^2, P=0.2269 and 1920 μm^2 and 1956 μm^2, 0.9921 respectively), as α2β1 can compensate for any loss of these integrins. However, siRNA KD of ITGA2 or of all the collagen-binding integrins at once, severely impedes cell spreading on collagen I (1004 μm^2 for ITGA2 and 1085 μm^2 for All, vs 1956 μm^2, ****P<0.0001 for both conditions), suggesting α2β1 is the main integrin used for adhesion and spreading of these cells on collagen. Again, KD of α2β1 is enough to impede cell spreading and further KD of α1β1 and α10β1 achieves no further inhibition of cell spreading. The same change in cell morphology was seen in ITGA2 KD and KD of all integrins, these cells were irregular in shape while the control and ITGA1 or ITGA10 KD cells were spread into more rounded, regular shapes. The irregular shape could be a result of the filopodia protruding from the cell but not then adhering to the collagen surface enough to stabilise the adhesion and inhibit actin retrograde flow. The protrusions may be constantly forming and then flowing back to the cell after failing to adhere to the substrate due to a lack of α2β1 adhesion.

7.4 Effects of Integrin Inhibition on Migration

Figure 7.4: Representation of TrackMate analysis

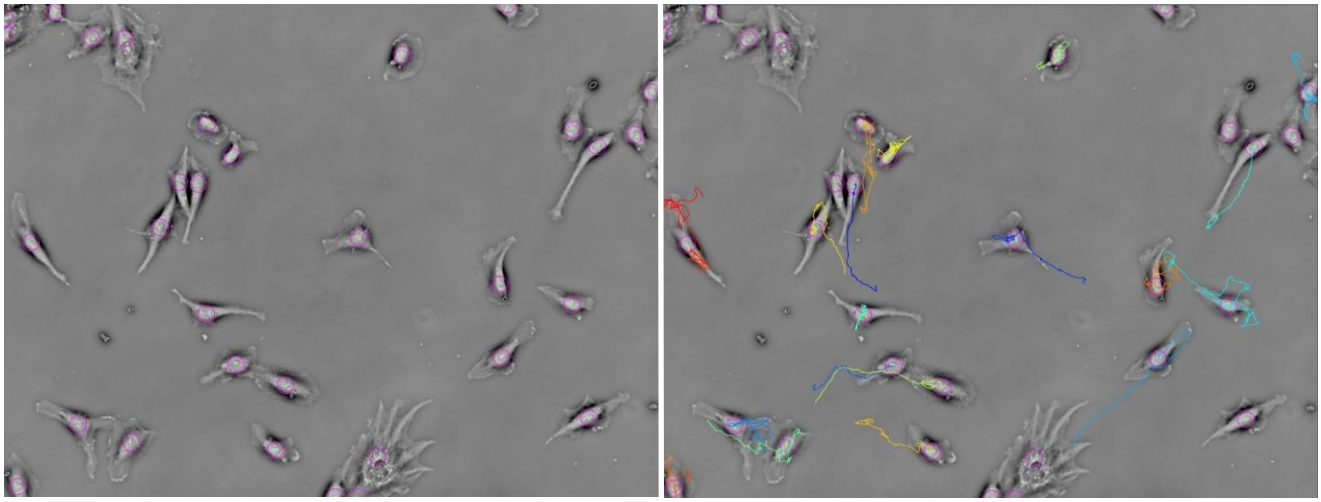

Showing the TrackMate analysis of migration images. A time lapse video is uploaded into the TrackMate ImageJ plug-in and the image on the left shows the TrackMate plug-in identifying "blobs" or cells. These cells are then linked from frame-to-frame and a track is displayed showing the distance moved by each cell. This image shows untreated cells migrating over collagen I coated surfaces.

The involvement of integrins α1β1 and α2β1 in regulating EC migration has been characterised well. However, the role of α10β1, which is the second most abundant integrin in HUVECS, has not been characterised in ECs. The integrin inhibitor TC-I-15 has also not been characterised in HUVECs and so migration experiments were carried out to investigate the effect of this inhibitor. Ibidi 4-well µ-slides Ph+ were coated with collagen I or peptides overnight and blocked with BSA, before seeding a low density (17,000 cells/ml) of HUVECs, either 48h post-siRNA or in the presence of inhibitors. Cells were left to attach for 4 hours before taking time-lapse images over a 9-hour period to track cell movement. The TrackMate ImageJ plugin was used to quantify cell migration over this time period, quantified as Track Displacement. This is the average distance (in µm) from the starting position and the finish position of each cell. Figure 7.4 shows a representative image of the TrackMate program tracking untreated HUVECs migrating over collagen I coated surfaces. At the time, it was not possible to calculate total track length using TrackMate and so track displacement was used as a measure of cell migration. Mean, minimum and maximum velocity were also calculated by TrackMate and are shown here. Figure 7.5 shows the quantification of cell migration after the addition of obtustatin or TC-I-15. One-way ANOVA and Sidak's multiple comparison test was used to analyse the effects of integrin inhibition on cell migration. Obtustatin was compared to the control and TC-I-15 was compared to the TC-I-15 control. Table 7.2 summarises the statistical analysis for these tests.

Table 7.2 – Statistical Analysis of HUVEC migration after integrin inhibition

	Average Distance Migrated (µm)				Mean velocity (µm/5min)			
	Mean	SD	N	P	Mean	SD	N	P
Control	89.62	8.371	3		3.814	0.2854	3	
Obtustatin	87.68	1.939	3	0.8790	3.714	0.2838	3	0.8997
TC-I-15 Control	90.83	5.156	3		3.696	0.3465	3	
TC-I-15	61.34	1.47	3	0.0002	3.131	0.2221	3	0.0843
	Maximum velocity (µm/5min)				Minimum velocity (µm/5min)			
Control	19.04	0.9312	3		0.2283	0.02542	3	
Obtustatin	18.09	1.562	3	0.6852	0.2231	0.0152	3	0.9235
TC-I-15 Control	18.55	1.951	3		0.2247	0.008779	3	
TC-I-15	17.39	0.9768	3	0.5736	0.1756	0.01587	3	0.0169
One-way ANOVA and Sidak's multiple comparison test was used to compare the means to the control mean								

Figure 7.5: Quantification of HUVEC Migration After Integrin Inhibition

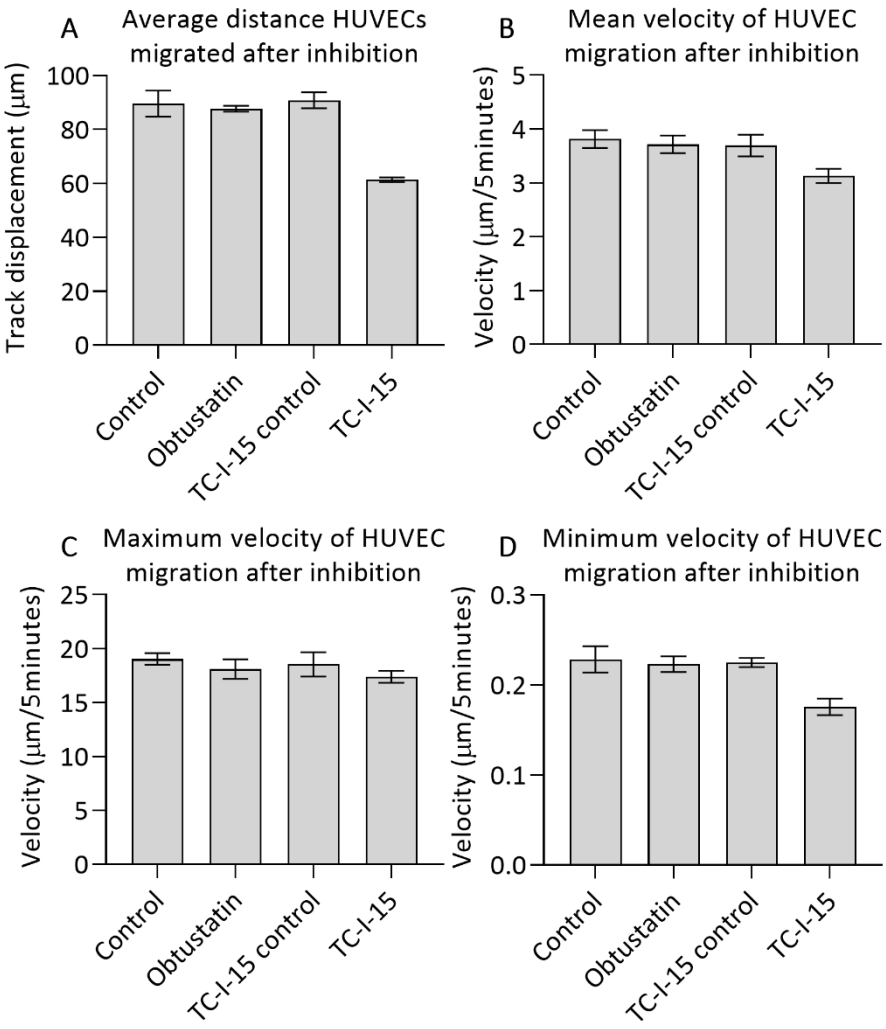

Quantification of the effects of integrin inhibition on HUVEC migration as measured by A) distance migrated, B) mean velocity, C) maximum velocity and D) minimum velocity. Migration is quantified below as distance migrated (track displacement) mean, maximum and minimum velocity of HUVEC migration. Means are shown with error bars depicting SD.

Inhibition of α2β1 and α1β1 by TC-I-15 resulted in a significant decrease in track displacement compared to the TC-I-15 vehicle control (61.34µm vs 90.83 µm, ***P=0.0002). Conversely, inhibition of α1β1 by obtustatin had no effect on track displacement compared to the control (87.68 µm vs 89.62 µm, P=0.8790), as the more abundant α2β1 is present to facilitate cell adhesion and migration. TC-I-15 is likely to the disrupt adhesion complexes at the leading edge. α2β1 stabilises protrusions, effectively decreasing the retrograde flow of actin filaments away from the leading edge. In the presence of TC-I-15 α2β1 and α1β1 can no longer adhere to the collagen or anchor the cytoskeleton to the ECM, resulting in decreased adhesion

and increased retrograde flow. This would impede protrusion formation and subsequent migration

The maximum velocity and mean velocity were unaffected by TC-I-15 or obtustatin (Table 7.2). However, the minimum velocity was reduced in the presence of TC-I-15 compared to the TC-I-15 control (0.01587µm/5min vs 0.008779µm/5min *P=0.0169). The maximum velocity takes the fastest speed reached by any cell at any point in the 9-hour period and can be dramatically affected on a single fast-migrating cell. This suggests that some cells were able to overcome the α2β1 inhibition to migrate normally across the collagen I. The minimum speed is lowered, suggesting that at least some cells were unable to move as quickly as normal, which fits with the notion that α2β1 inhibition impedes the ability of the adhesion complexes to stabilise actin filaments and protrusions at the leading edge. The TC-I-15 vehicle control, added to the media as NaOH, had no effect on cell migration and so it can be assumed that TC-I-15 is responsible for the decrease in migration distance seen here.

The signalling pathways downstream of integrin activation and clustering involve GTPase exchange factors (GEFs) and GTPase activating proteins (GAPs), the regulators of GTPase activity[197]. Integrins do not harbour any intrinsic catalytic activity, but their cytoplasmic tails provide a scaffold for the localisation of other proteins such as FAK and Src[197]. After integrin adhesion and clustering in nascent adhesions, FAK associates with the β-subunit cytoplasmic tail, leading to the autophosphorylation of FAK on Y397 which in turn binds Src to form an activated FAK/Src complex[197]. This FAK/Src complex phosphorylates the adhesion protein paxillin, among other signalling molecules, and results in the downstream recruitment of the GEF β-Pix at the nascent adhesion and subsequent activation of Rac, which in turn regulates actin polymerisation via WASP/Scar/Arp2/3[343]. Paxillin is essential for the formation of focal adhesions and reorganisation of the actin cytoskeleton[344, 345]. ILK (integrin linked kinase) is also an integrin-mediated signalling protein, it associates with the β1 and β3 cytoplasmic tails to form signalling complexes with other adaptor proteins like PINCH and α- and β-parvin that also result in the activation of the GEFs α- and β-Pix, again resulting in the regulation of the actin cytoskeleton[324]. The inhibitor TC-I-15 stabilises the β1-subunit in the inactive conformation in α2β1, and presumably α1β1, inhibiting the adhesion of these integrins to collagen[2]. This presumably results in reduced integrin clustering which diminishes the density of cytoplasmic β-subunit tails that are available to facilitate the cytoplasmic co-localisation of signalling molecules described earlier. As a result, the Rac pathway is not

activated downstream of integrin activation and the associated upregulation of the actin polymerisation cannot happen, resulting in impaired EC migration. However, the cells still express a number of other collagen binding adhesion receptors such as DDR1 and DDR2, and so while migration is impeded, it is not completely abolished in HUVECs. Other cells, like leukocytes, can exhibit integrin-independent migration[346]. In one study, pan-integrin KO or talin KO did not result in migratory deficiency in dendritic cells on 2D surfaces, but did abolish migration through 3D matrices[346], so it is also possible that HUVECs are employing an integrin-independent migration mechanism.

7.5 Knockdown of ITGA2 inhibits HUVEC Migration

The same experiments were repeated with HUVECs that had undergone siRNA silencing of integrins 48 hours previously. Ibidi 4-well µ-slides Ph+ were coated with collagen I overnight and blocked with BSA, before seeding a low density (17,000 cells/ml) of post-siRNA HUVECs. Phase images were taken every 5 minutes over a 9-hour period and analysed with TrackMate as before. One-way ANOVA and Dunnett's multiple comparisons test was used to analyse the effects of siRNA KD of each integrin on cell migration. Table 7.3 summarises the statistical analysis of these tests, the means of each condition were compared to the means from the control condition.

Figure 7.6 shows the quantification of the effects of siRNA KD of integrins on the migration of HUVECs over collagen I coated surfaces. of ITGA2 using siRNA significantly reduced the track displacement (57µm vs 92.81µm, *P=0.0095 for ITGA2 and 57.61µm vs 92.81µm *P=0.0106 for All), which represents the average distance moved by each cell, compared to the negative control. Neither ITGA1 or ITGA10 knockdown had any effect on the migration distance of HUVECs, and knockdown of all three integrins had no cumulative effects on integrin-mediated migration. There was no significant difference in the track displacement of ITGA2 KD compared to KD of all three integrins. There were also no significant differences in migration velocity in any condition. This suggests HUVECs use α2β1 as the main integrin adhesion receptor in the regulation of migration, and the expression of ITGA1 or ITGA10 does not contribute further to the regulation of HUVEC migration as a function of random walk across collagen I coated surfaces. Again, this can be explained as α2β1 is the most abundant integrin on the surface of HUVECs. In the event of ITGA1 or ITGA10 KD, the α2β1 integrin will adhere to collagen, become activated, cluster in nascent adhesions and facilitate the co-

localisation and activation of FAK and Src. This leads to the downstream activation of Rac and the promotion of actin polymerisation at the leading edge, ultimately leading to increased migration. Conversely, in the event of an ITGA2 KD, there is not enough ITGA1 or ITGA10 to compensate and overcome the loss of integrin-mediated adhesion and nascent adhesions are not formed as efficiently, resulting in impaired FAK and Src activation and decreased Rac activation, ultimately resulting in reduced migration.

Table 7.3 – Statistical analysis of HUVEC migration after siRNA

Figure 7.6: Quantification of HUVEC Migration After Integrin siRNA Knockdown

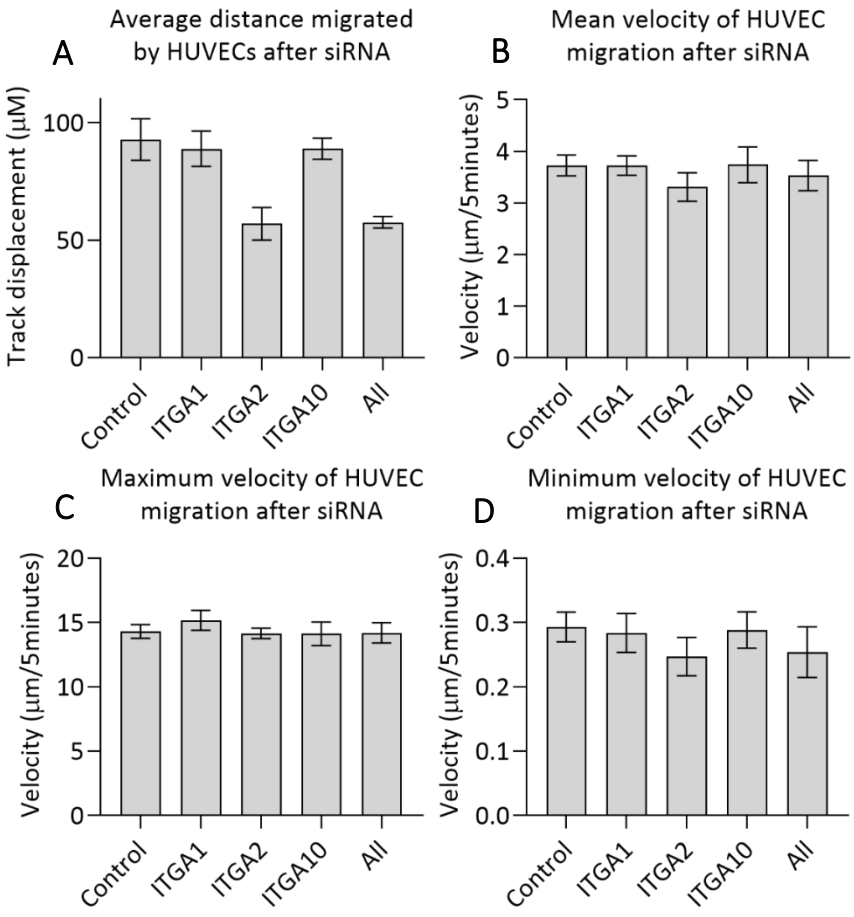

Effects of siRNA knockdown of each integrin on HUVEC migration as measured by A) distance migrated, B) mean velocity, C) maximum velocity and D) minimum velocity. Migration is quantified below as distance migrated (track displacement) mean, maximum and minimum velocity of HUVEC migration. Means are shown with error bars depicting SD.

	Average Distance Migrated (µm)				Mean velocity (µm/5min)			
	Mean	SD	N	P	Mean	SD	N	P
Control	92.81	15.39	3		3.724	0.3488	3	
ITGA1	88.88	13.02	3	0.9772	3.725	0.3263	3	>0.9999
ITGA2	57	11.95	3	**0.0095**	3.307	0.4762	3	0.6508
ITGA10	88.94	7.752	3	0.9784	3.74	0.5985	3	>0.9999
All	57.61	4.265	3	**0.0106**	3.528	0.5043	3	0.9563
	Maximum velocity (µm/5min)				Minimum velocity (µm/5min)			
Control	14.31	0.9111	3		0.2934	0.04001	3	
ITGA1	15.17	1.347	3	0.8055	0.2839	0.05266	3	0.9981
ITGA2	14.16	0.6987	3	0.9993	0.2469	0.05181	3	0.6742
ITGA10	14.13	1.581	3	0.9990	0.2886	0.04914	3	0.9998
All	14.2	1.348	3	0.9998	0.2539	0.06846	3	0.7762
One-way ANOVA and Dunnett's multiple comparisons test was used to compare the mean values to the control mean								

7.6 Effect of Peptide Affinity on HUVEC Migration

In VSMCs maximal velocity is seen when cell attachment is intermediate, where adhesion and detachment can both happen efficiently[347]. Similarly, a study using Chinese Hamster Ovary (CHO) cells expressing α5β1 and $\alpha_{IIb}\beta3$ found that the velocity of migration is dependent on integrin expression levels, ligand concentration and integrin-ligand affinity; the optimal ligand concentration for maximal velocity decreases with increased integrin expression levels and increased integrin-ligand affinity[348], suggesting that an equilibrium is formed between attachment and detachment to facilitate cell migration. We therefore tested HUVEC migration as random movement on a range of different affinity peptides to test the function of collagen-binding integrins in affinity-related migration.

To test the effect of substrate affinity on the ability of HUVECs to migrate across 2D coated surfaces, different peptides were coated onto 4-well µ-slides Ph+ overnight. After blocking with BSA, HUVECS were seeded at 17,000 cells/ml. Adhesion studies were undertaken (Chapter 3) to determine the adhesion affinities of different peptides. GFOGER and GLOGEN were used as high affinity peptides, GMOGER was used as a low affinity peptide, VWF III is a low affinity peptide that binds to DDR1 and DDR2, and GPP10 was used as a negative control

peptide. BSA was used as a control for the BSA blocking procedure. One-way ANOVA and Dunnett's multiple comparisons tests were used to compare the migration of HUVECs across each peptide surface. Table 7.4 summarises the statistical analysis. Figure 7.7 shows the quantification of HUVEC migration over different peptides.

There were no significant differences in the migration of HUVECs across the integrin-binding peptides over the course of the experiment. However, both GFOGER and GNRGER supported a small but significant increase in migration distances compared to BSA. In addition,

Figure 7.7: Quantification of HUVEC migration of different peptides

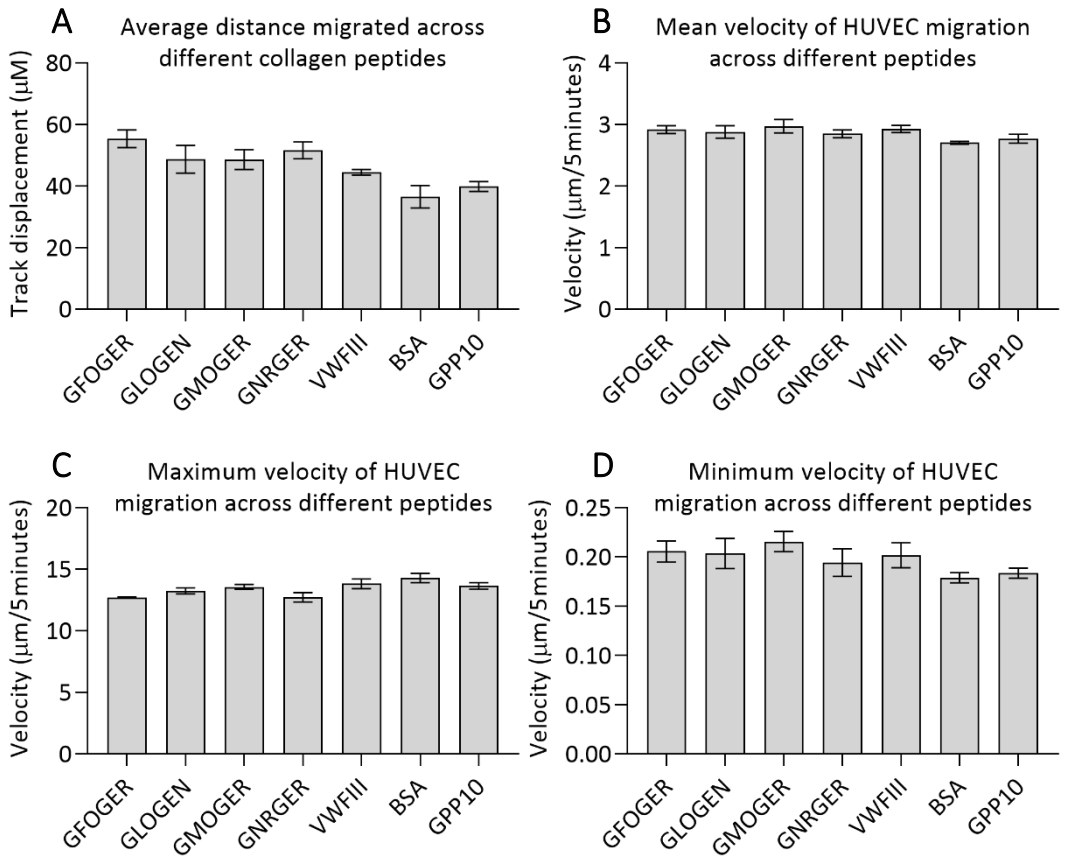

Quantification of the effects of peptide affinity of each integrin on HUVEC migration as measured by A) distance migrated, B) mean velocity, C) maximum velocity and D) minimum velocity. Migration is quantified below as distance migrated (track displacement) mean, maximum and minimum velocity of HUVEC migration. Means are shown with error bars depicting SD.

GFOGER supported significantly longer migration distances than GPP10, again the difference was small. This suggests that integrin ligation could have a modest effect on the ability of HUVECs to migrate over peptide surfaces. However, the affinity of the peptides did not influence HUVEC migration. This could be due to the intrinsic ability of HUVECs to secrete their own matrix over time, although the experiment was performed over a relatively short time frame (four hours to adhere and nine hours to migrate). The differences in affinities between the integrin-binding peptides may not be sufficiently important to induce differential migration across these surfaces. With the exception of VWF III, these peptides all ligate α2β1. Perhaps even low affinity peptides are sufficient to cause the formation of nascent adhesion complexes and the associated integrin clustering that leads to FAK/Src activation and eventual Rac signalling that mediates actin filament elongation and migration. BSA does not support HUVEC adhesion in static adhesion binding assays but here it supports adhesion and subsequent migration here. This is likely due to the differences in timeframe for adhesion assays (one hour) compared to these migration assays (13-15 hours). In one hour, BSA cannot support cell adhesion, but over the longer time frames the BSA coating may not completely obscure the tissue culture surface underneath and the cells maybe be able to degrade the BSA to attach to this surface. Additionally, HUVECs secrete their own ECM and so could, over time, adhere to the BSA non-specifically and then secrete their own ECM proteins onto this.

Interestingly, the track displacement (distance migrated) is decreased when the surface is coated with peptides compared to collagen I coated surfaces. The control conditions for both the inhibitors and siRNA experiments were around 90µm whereas the peptide coatings all result in a migration distance of around 50µm. Additionally, the mean velocity is slower in these peptide migration assays than with surfaces coated with collagen I, (3.7 vs 2.9). Both the peptides and the collagen are coated at 10µg/ml, meaning that the peptides will exhibit a far higher concentration of integrin binding sites than the collagen I due to a huge difference in size between the two molecules. This indicates a concentration dependent effect where an increase of integrin binding sites slows down the migration of HUVECs across the substrate. Due to time constraints this was not explored further.

Table 7.4 – Statistical analysis of migration across different THPs

	Average Distance Migrated (µm)			Mean velocity (µm/5mins)			Maximum velocity (µm/5mins)			Minimum velocity (µm/5mins)		
	Mean	SD	N	Mean	SD	N	Mean	SD	N	Mean	SD	N
GFOGER	55.38	4.934	3	2.917	0.1101	3	12.71	0.1101	3	0.2055	0.01844	3
GLOGEN	48.75	7.87	3	2.879	0.1783	3	13.23	0.4278	3	0.2035	0.02644	3
GMOGER	48.6	5.516	3	2.973	0.1924	3	13.56	0.3347	3	0.2155	0.01761	3
GNRGER	51.61	4.722	3	2.85	0.1083	3	12.71	0.6607	3	0.1943	0.02423	3
VWFIII	44.51	1.5	3	2.927	0.09836	3	13.82	0.6888	3	0.2017	0.02209	3
GPP10	39.87	2.759	3	2.769	0.1271	3	13.65	0.457	3	0.1836	0.00895	3
BSA	36.5	6.412	3	2.704	0.0421	3	14.29	0.6639	3	0.1788	0.00896	3

P values obtained using Dunnett's multiple comparison test comparing the means above

	P value for Average Distance Migrated	P value for Mean velocity	P value for Maximum velocity	P value for Minimum velocity
GFOGER vs. GLOGEN	0.7087	0.9998	0.8639	>0.9999
GFOGER vs. GMOGER	0.6882	0.998	0.449	0.9943
GFOGER vs. GNRGER	0.9691	0.9948	>0.9999	0.989
GFOGER vs. VWFIII	0.2119	>0.9999	0.19	>0.9999
GFOGER vs. GPP10	**0.033**	0.8015	0.3368	0.7954
GFOGER vs. BSA	**0.0078**	0.4618	**0.0278**	0.6248
GLOGEN vs. GMOGER	>0.9999	0.9708	0.985	0.9853
GLOGEN vs. GNRGER	0.9922	>0.9999	0.8695	0.9961
GLOGEN vs. VWFIII	0.9464	0.9992	0.8042	>0.9999
GLOGEN vs. GPP10	0.4082	0.9373	0.9485	0.8552
GLOGEN vs. BSA	0.1259	0.6632	0.2327	0.6987
GMOGER vs. GNRGER	0.9898	0.9026	0.4563	0.8168
GMOGER vs. VWFIII	0.9546	0.9994	0.9952	0.9704
GMOGER vs. GPP10	0.4269	0.5062	>0.9999	0.4396
GMOGER vs. BSA	0.1336	0.2263	0.6094	0.2929
GNRGER vs. VWFIII	0.6444	0.989	0.194	0.9988
GNRGER vs. GPP10	0.153	0.9852	0.343	0.9919
GNRGER vs. BSA	**0.039**	0.8104	**0.0285**	0.9495
VWFIII vs. GPP10	0.9205	0.7513	0.9996	0.9007
VWFIII vs. BSA	0.5204	0.4104	0.913	0.7627
GPP10 vs. BSA	0.9821	0.9956	0.7379	>0.9999

Conclusions

Cell spreading is impeded by inhibition of α2β1 using TC-I-15 or 6F1. This inhibition results in irregularly shaped cells, possibly due to the lack of integrin adhesion in the membrane protrusions at the leading edge. Adhesions formed at the leading may be weaker in the absence of α2β1 leading to less stable cytoskeletal-ECM linkages. These weaker adhesions may be less capable of inhibiting actin retrograde flow, leading to decreased membrane protrusion in filopodia or lamellipodia and decreased cell spreading.

Inhibition or siRNA KD of integrin α2β1 inhibits HUVEC migration over a collagen I substrate as measured by track displacement. Inhibition or KD of α2β1 is sufficient to impede HUVEC migration and further KD of α1β1 or α10β1 does not decrease migration further. This is likely due to the increased prevalence of α2β1 compared to α1β1 and α10β1. Again, the inhibition or siRNA KD of integrin α2β1 may result in weaker adhesions that lead to increased actin retrograde flow and decreased membrane protrusions. If the protrusions cannot adhere to the ECM, they cannot create traction and pull the cell forward.

HUVEC migration over collagen peptides is not dependent on the affinity of HUVECs for the peptide, but there could be a concentration dependent effect where peptide coating supports slower migration than collagen I coated surfaces. The concentration of integrin binding sites is much higher with peptide coated surfaces than with collagen coated surfaces as the peptides consist of integrin binding sequence plus some GPP repeats whereas collagen I one has a far lower density of integrin binding sites per μg. Peptides were coated here at 10μg/ml and the integrin binding sites could have reached saturation at this concentration. A range of concentrations, with 10μg/ml as the maximum, should have been tested to more closely resemble physiological settings. Future experiments using different concentrations of peptide could be carried out to investigate this.

Chapter 8 – Effects of Integrin Inhibition and Knockdown on Tube Formation

Contents

8.1 Chapter Summary

This chapter focusses on using integrin inhibitors and siRNA to modulate integrin function before quantifying the effects on angiogenesis in tube formation assays using Geltrex as a substrate. Tube formation is quantified using the Angiogenesis Analyzer plug-in for ImageJ.

8.2 Introduction

Angiogenesis is the growth of new blood vessels from existing vasculature and is an important process in tissue repair, embryonic development and tumour progression[18, 179, 200]. Whereas vasculogenesis describes the formation of the first blood vessels from the mesoderm in the embryo and is an important process in embryonic development, described in chapter 1. Embryos cannot develop without a healthy, functioning vasculature to transport essential metabolites, nutrients, growth factors and hormones to and from tissues[31, 32]. Insufficient blood-supply results in ischaemia and tissue necrosis due to a lack of oxygen and nutrients and a build-up of toxic metabolic end-products. Most blood vessels form via angiogenesis from existing vasculature; in response to certain stimuli a new vessel will 'sprout' from an existing one. Angiogenesis is a tightly regulated process involving many signalling pathways that control EC proliferation, apoptosis, migration and adhesion. It is driven through angiogenic signalling molecules such as VEGF, bFGF or TNFα[31, 32, 195, 349, 350]. The regulation of cellular responses to VEGF is tightly regulated depending on the cell type and location. Different cells will express different VEGF receptors, VEGFR1, VEGFR2 being the most common[195]. Some VEGF molecules will also bind neuropilins (NRPs) which are receptors originally found in neurons that help regulate neuronal migration[351].

The VEGF family (VEGFA, VEGFB, VEGFC, VEGFD, viral VEGFE and placental growth factor (PLGF))[349] all have conserved cysteine-knot structures that share homology with platelet derived growth factors (PDGFs)[195, 352]. VEGFA is the most critical and is highly conserved between species, showing high homology between fish and mammals. Tiger pufferfish (*Fugu rubripes*) VEGFA shares 68% homology with human $VEGF_{189}$[353]. VEGF homologs are even observed in non-vertebrates without vasculature such as nematode worms and jellyfish, where they regulate neurogenesis and cell migration[195]. VEGFA has 8 exons, while the rest of the family have 7. VEGFA has several isoforms arising from alternative splicing of the VEGFA gene, each isoform has a different function, summarised in Table 8.1. VEGF generally exists as a head-to-tail homodimer with VEGFR binding sites at each pole and each monomer contains the cysteine-knot structure held together by disulphide bonds[354]. VEGFA binds to NRP-1 through exon 6, the heparin binding domain, plus exons 7 and 8. Heparin binding domains help to localise VEGF molecules and sequester VEGF in the ECM, and this contributes to the formation of the VEGF gradients that drive cell migration. The VEGF isoforms that bind to the ECM and are not diffusible will concentrate close to where they are secreted, whereas the smaller, soluble $VEGF_{120}$ will diffuse through tissues resulting in action over a longer distance but a shallower VEGF gradient[355]. Additionally, VEGF isoforms that are sequestered in the ECM via their heparin binding domains can be released by proteolytic degradation of the ECM.

Table 8.1 – Summary of different VEGFA isoforms.

Isoform	Exons	Characteristics
$VEGF_{121}$	1-5 and 8	Soluble and diffusible Secreted as covalently linked homodimer Does not bind heparin
$VEGF_{145}$	1-6 and 8	Binds NRP2 but not NRP1
$VEGF_{165}$	1-5, 7 and 8	Most abundant and biologically active Soluble and diffusible, binds NRP1 and NRP2 Contains a heparin binding domain Glycosylated on N74
$VEGF_{165b}$	1-5, 7 and alternate 8	Inhibitory form of $VEGF_{165}$
$VEGF_{183}$	1-5, short exon 6, 7 and 8	Sequestered in ECM
$VEGF_{189}$	1-8	Cell surface or bound to ECM, not readily diffusible
$VEGF_{206}$	1-8 plus extra exon 6 sequence	Cell surface or bound to ECM Not readily diffusible
Adapted from Holmes, D. I, Zachary, I, 2005. *The vascular endothelial growth factor (VEGF) family: angiogenic factors in health and disease*[195]		

Tumours without their own surrounding vasculature are growth-limited to less than 2-3mm[356, 357] presumably by a nutrient deficit as metabolites must diffuse and transport through surrounding tissues before reaching the tumour cells. Whereas tumours that have acquired a vasculature can transport metabolites and waste products directly to and from the blood stream and can grow much more quickly as a result[358-360]. Additionally, tumours require vasculature or the lymph system for efficient metastasis. Therefore, eliminating or preventing tumour angiogenesis is a useful tool for fighting cancer progression[361]. Tumours can recruit vasculature by encouraging angiogenesis of nearby blood vessels or by the capture of rare circulating EC progenitors[362]. Generally, the vasculature is quiescent: it maintains tissue homeostasis and helps regulates platelet aggregation until signals downstream of EC damage, hypoxia, infection or inflammation signal a change in EC state to a more proliferative or angiogenic phenotype[87]. Tumours must promote a change in the EC state from quiescent to pro-proliferative and pro-angiogenic before they can recruit their own vasculature. This is termed the angiogenic switch[360]. The turnover of non-tumour ECs has been estimated to be 47-23000 days compared to 2.4-13 days for tumour endothelium, so there is clearly an upregulation of EC proliferation in tumour vasculature[363]. Both VEGF and bFGF have been found elevated in cancers as well as in the urine and serum of cancer patients; 47% of patients with metastatic cancer showed elevated bFGF[357, 364].

Angiogenesis can occur by two methods. Sprouting angiogenesis is the branching of ECs in the existing vessel wall into tubes that invade the surrounding tissue and then mature into new vessels[179]. Intussusceptive angiogenesis involves the splitting of a single vessel into two and involves reorganisation of existing vasculature[365]. The basic process of sprouting angiogenesis first involves an increase in VEGFA signalling in the surrounding tissue; ECs that receive the VEGFA signal at high enough amounts become tip cells that degrade the basement membrane and start to migrate into the tissue towards the VEGFA source[350]. ECs adjacent to this tip cell then proliferate to facilitate the growth of a stalk behind the migrating tip cell. This then becomes a tube which grows until it fuses with a second tip cell branching from an opposite vessel towards the same VEGFA gradient (Figure 8.1). Once the sprouting tubes have converged and fused, oxygenated blood can be perfused through the new lumen and the new vessel is stabilised with pericytes. Hypoxia will drive some cells to secrete VEGFA, which will encourage the formation of tip cells and attract them to chemotactically migrate towards the

hypoxic environment. Once a network of vessels has formed the unwanted, immature vessels are 'pruned' and degraded leaving an efficient, mature vascular tree behind. Immature vessels depend on VEGF for survival and so pruning is mediated by the withdrawal of VEGF, often induced by hyperoxia[366, 367].

Figure 8.1: Diagram of Sprouting Angiogenesis.

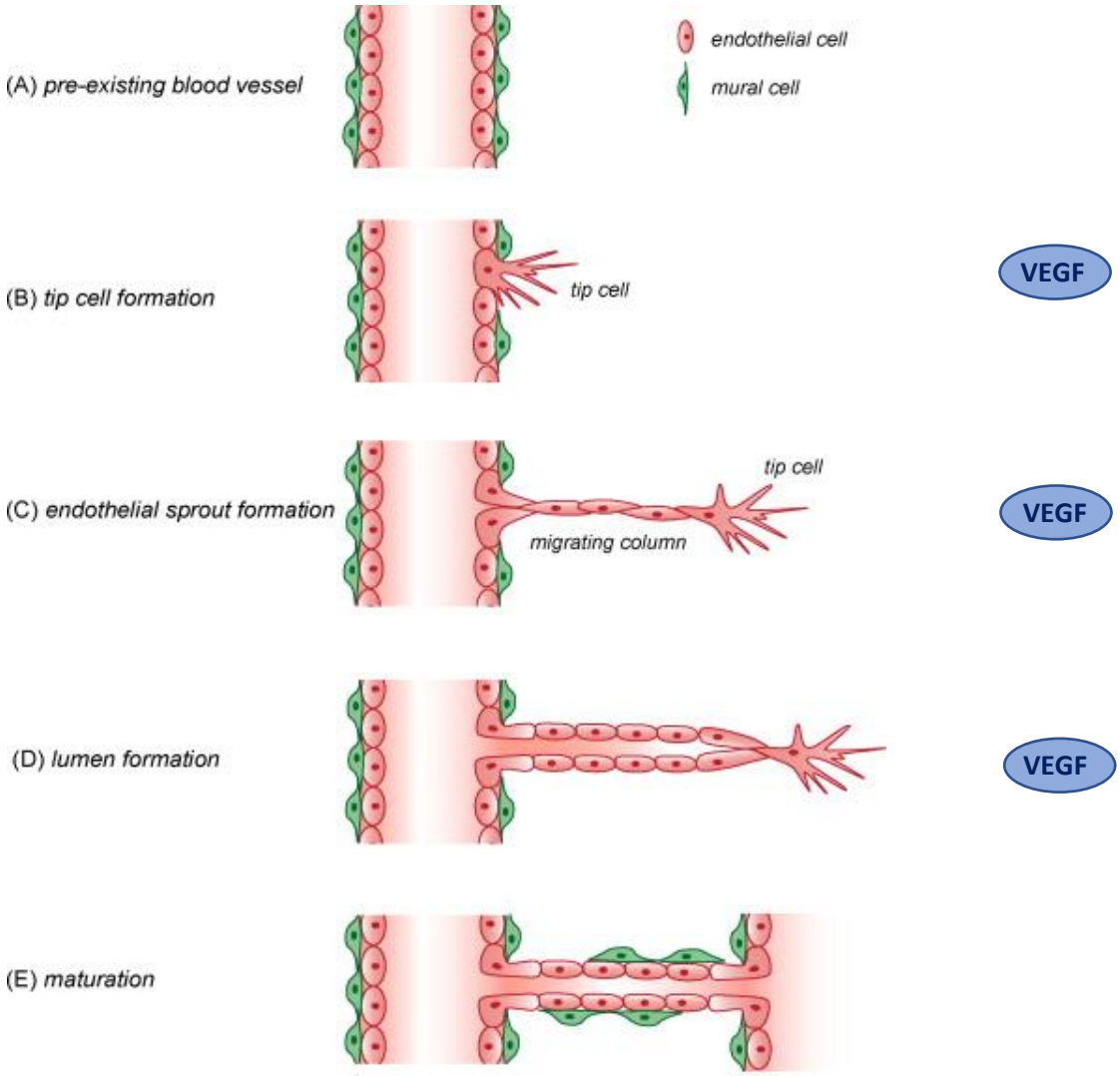

A diagram showing the progression of tip cells in sprouting angiogenesis. A) shows the quiescent vessel with ECs and surrounding pericytes. B) shows the formation of multiple filopodia on the tip cell. C) Shows the migration of the tip cell outwards and the following stalk cells. D) describes the column of cells forming a lumen through which blood will perfuse and E) shows the mature new blood vessel after connecting with an opposite vessel. Once a new blood vessel is formed the tip cell phenotype is lost and the ECs become quiescent again. Adapted from https://thoracickey.com/arteriogenesis-and-angiogenesis/

Tip cells are specialised, highly polarised ECs containing protease-secreting filopodia that degrade the ECM and pave the way for the sprouting cell to migrate[350]. These filopodia are induced by VEGFA and contain increased levels of VEGFR2 to 'sense' increasing VEGFA concentrations by chemotaxis[350]. Tip cells also express higher levels of PDGF-B than their neighbouring ECs[350]. As the tip cell migrates into the ECM the 'stalk' ECs behind it proliferate and move with the tip cell creating a sprout. Tip cells essentially guide the sprouting stalk of ECs towards VEGFA. As many sprouts are likely to be converging on the source of the VEGFA, the tip cells of two sprouts will meet and fuse together to create a continuous lumen through which blood is then perfused. It is important that the migration of tip cells ceases when two converge and fuse together. The shear stress created by blood flow through the newly formed lumen will contribute to vessel maturation, as will the recruitment of pericytes and the deposition of ECM components[179]. Tip cell formation is highly regulated as tip cells are essential for angiogenesis. However, if all the surrounding ECs turn into tip cells there would be no stalk to form the new vessel. Notch signalling is thought to help supress VEGFR2 expression in stalk cells to supress the tip cell phenotype. Tip cells express delta-like-4 (DL4) in response to VEGFA. This DL4 then interacts with and activates Notch on neighbouring cells[368, 369]. The activated Notch supresses VEGFR2 expression and the tip cell phenotype. Inhibition or knockdown of DL4 results in increased numbers of tip cells[369]. VEGFA expression is tightly controlled and deletion of one VEGFA allele is embryonic lethal since the vasculature is unable to form correctly[32, 370]. Excess VEGFA seen in tumour angiogenesis results in overproduction of tip cells and disorganised vasculature[371]. Different VEGF isoforms will induce different cellular reactions. For example $VEGF_{188}$ induces many long filopodia and a highly branched, thin vessel network in mouse hindbrains whereas filopodia are much shorter in the presence of $VEGF_{120}$ resulting in a poorly branched network with larger vessels[355]. Mice expressing only $VEGF_{165}$, which is soluble and diffuses through tissues freely, displayed no vessel abnormalities. Heparin binding VEGF tends to build up steep gradients whereas $VEGF_{120}$, which is diffusible, travels over large distances to stimulate EC proliferation[355]. As well as regulating the tip cell specialisation and migration, VEGF also upregulates the stalk cell proliferation[350].

Intussusceptive angiogenesis (Figure 8.2) is much faster than sprouting angiogenesis, mainly because it does not rely on the proliferation of ECs and instead only requires vessel wall reorganisation as the vessel wall extends into the lumen and splits the vessel[372].

Intussusceptive angiogenesis is important in the bifurcation of veins and arteries and the pruning of larger microvessels[372]. Firstly, ECs opposite each other in the capillary wall develop membrane folds that protrude across the lumen of a capillary to contact the opposite side creating tissue pillars. These pillars eventually split the vessel in two creating two capillaries[372].

After blood vessels are formed, they are stabilised by pericytes that proliferate and migrate along the vessels in a VEGF dependent manner[373, 374]. The association of newly formed capillaries with pericytes protects the vessel from hyperoxia-induced degradation in the pruning process of vascular remodelling. Pericyte coverage of vessels happens days after the formation of blood vessels in the mouse retina, allowing time for the remodelling process to occur before vessel stabilisation[373]. Pericytes express α-smooth muscle actin and are thought to be related to VSMCs. Both VSMCs and pericytes interact with ECs and GJ exist between ECs and pericytes[374].

There is significant crosstalk between neurons and ECs. Sprouting vessels in the retinas of new-born mice are guided by a network of astrocytes which forms days before the blood vessels sprout. The filopodia of tip cells then migrates exclusively along the existing astrocyte network and disruption of the astrocyte network impedes angiogenesis[375]. The astrocytes also

Figure 8.2 – Diagram of Intussusceptive Angiogenesis.

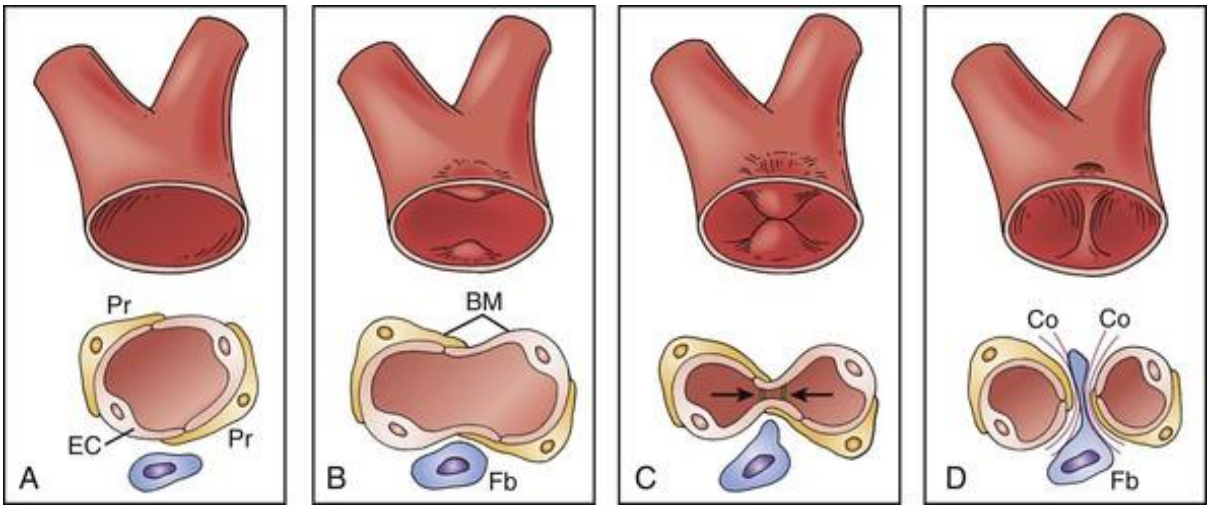

Diagram showing the stages of intussusceptive angiogenesis. Pr = pericytes, BM = basement membrane, Fb = fibroblast, EC = endothelial cell, Co = collagen. A shows the vessel before intussusceptive angiogenesis starts. B shows the vessel wall starting to protrude into the lumen. C describes protrusions coming together and cell-cell junctions forming at the point of contact. D shows the final vessel splitting and a fibroblast moving into the space created by the vessel splitting in two. Image taken from: https://thoracickey.com/arteriogenesis-and-angiogenesis/

respond to EC tip cells and mature on contact with tip cells[375]. Astrocytes produce VEGF in response to hypoxia and culturing primary astrocytes in an oxygen rich environment abolishes VEGF production[376]. Blood vessels and axons often align, and they share some of the same regulatory pathways. For example, Unc5b and netrin1 are both involved in axon guidance and EC migration[377, 378]. Unc5b is expressed in the EC tip cells; loss of Unc5b leads to excessive branching of vessels in mice. EphrinB, a neural cell migration regulator, is also involved in both axon guidance and angiogenesis and mice lacking ephrinB2 die in utero at embryonic day 11.5 due to vascular remodelling defects[379]. Also, $VEGF_{165}$ binds to NRP1 which is a receptor that guides axons in neurons but is also expressed in ECs and is also thought to enhance the interaction between $VEGF_{165}$ and VEGFR2[351]. The same study found that Inhibition of NRP1-$VEGF_{165}$ interaction decreases $VEGF_{165}$ binding to VEGFR2 and subsequent HUVEC proliferation. Additionally, mice overexpressing NRP1 die at embryonic day 17.5 due to vascular defects and abnormal capillaries[380], suggesting a role for the neuronal guidance receptor NRP in the regulation of EC behaviour.

Angiogenin is an upregulator of angiogenesis expressed in some tumour cells. It is associated with poor prognosis as it increases cell survival, proliferation and tumour angiogenesis which in turn facilitates metastasis[199]. Angiogenin is a member of the RNase A superfamily that stimulates MMP-2 expression through ERK1/2 phosphorylation[199]. Endogenous regulators of angiogenesis also include fragments of basement membrane proteins that are released by proteolysis. The main component of the endothelial ECM is collagen IV, which exists as 6 α-chain isoforms, α1-α6. The α1 and α2 isoforms are ubiquitously expressed whereas the other chains are distributed in a tissue specific manner. The non-collagenous domains of some collagens, and other ECM proteins, exhibit angiogenic properties summarised as bullet points below:

- Arresten is a 26kDA fragment of the non-collagenous domain of collagen IV α1 chain that inhibits squamous cell carcinoma invasion and angiogenesis via α1β1 inhibition and induction of EC apoptosis[185, 381, 382]
- Tumstatin is produced by MMP-9 proteolysis of the α3 chain of type IV collagen and inhibits angiogenesis and proliferation on vitronectin, fibronectin and collagen I via αvβ3[383-385]. Overexpression of tumstatin in tumour cells inhibits their growth in B16F1 melanoma cells[386]

- Canstantin is a fragment of the non-collagenous domain of the α2 chain of collagen IV. It induces apoptosis though mitochondrial damage induced via αvβ3 and αvβ5 and inhibits angiogenesis and migration in ECs[387-389]
- Endostatin is a fragment of collagen XVIII. It potently inhibits angiogenesis and tumour growth through interaction with α5 and αv integrins on ECs[390]
- The α6 chain of type IV collagen inhibits angiogenesis and tumour growth[391]
- Angiostatin, a proteolytic fragment of plasminogen, inhibits tumour metastasis by blocking angiogenesis[392]

Angiogenesis involves many cell processes including migration, adhesion, apoptosis and proliferation and so many receptors, including integrins, are involved[18, 160, 179, 180, 200]. The αvβ3 and αvβ5 integrins are known to regulate angiogenesis and many collagen fragments described above exert their angiogenic properties through these integrins. Additionally, fibronectin ligation of α5β1 induces angiogenesis in chick embryos in a VEGF-independent manner and α5β1 is upregulated in human tumour biopsies, suggesting that this integrin is important in angiogenesis[393]. Peptide, antibody and small molecule inhibition of α5β1 blocked bFGF, TNFα and IL-8 driven angiogenesis but not VEGF-mediated angiogenesis. In contrast, fibronectin blocking inhibited both bFGF and VEGF induced angiogenesis, suggesting other fibronectin receptors could play a role in regulating angiogenesis[393]. Fibronectin itself is upregulated in blood vessels during wound healing[394] and has been shown to regulate proliferation in CHOα5 cells[395]. Fibronectin KO in mice is embryonic lethal due to defects in vascular development as well as mesoderm and neural tube development[396]. KO of the αv subunit, eliminating αβv1, αvβ3, αvβ5, αvβ6 and αvβ8, in mice results in 80% embryonic lethality with 20% surviving until birth but displaying intestinal and intracerebral haemorrhages and cleft palates[397].

A number of studies have found roles for α1β1 and α2β1 in angiogenesis. For example, α2β1 has been implicated in the regulation of lumen formation in HUVECs[398] and the α1β1 inhibitor, arresten, inhibits VEGF driven angiogenesis[185]. VEGF has been shown to exert angiogenic properties partially through upregulation of α1β1, α2β1[157] and αvβ3 surface expression. An *in vivo* study has also shown that antibodies blocking α1β1 and α2β1 inhibit VEGF mediated angiogenesis[157]. The same study found that VEGF-driven α1β1 and α2β1 upregulation correlated with an increase in cell spreading in Human Dermal Microvascular

Endothelial Cells[157]. HUVECs are cultured in EMG2 which contains low levels of VEGF165 but only very weak α1β1 expression was observed. The effects of VEGF on integrin expression in HUVECs was tested here, in Chapter 3, and no upregulation of α2β1 or α1β1 was observed after addition of increased VEGF. The expression of integrins is expected to vary with the cell-type: for instance, HUVECs are large vein ECs and will show a different expression profile to microvascular ECs. It is also worth noting that with *in vivo* experiments involving antibody inhibition of α1β1 and α2β1, these receptors would be inhibited in all cell types. Therefore, the decrease in angiogenesis seen after α1β1 or α2β1 inhibition could conceivably be due to α1β1 or α2β1 inhibition on other cell types, for example VSMCs or pericytes, rather than on ECs specifically.

The effects of TC-I-15 induced α2β1 and α1β1 inhibition on HUVEC migration have been described in Chapter 7. Since angiogenesis involves migration of the tip cells and the stalk cells to create a new vessel, TC-I-15 is expected to exert some effects on angiogenesis as well. In this Chapter, the effects of TC-I-15 mediated inhibition of α2β1 and α1β1 on angiogenic capability are presented, using tube formation assays using HUVECs on Geltrex. The effects of siRNA KD on tube formation are also tested.

8.3 The Effects of Integrin Inhibition on Tube Formation

Geltrex was plated into Ibidi Angiogenesis μ-slides and incubated at 37°C for one hour to induce gelation. Once a gel had formed, 4500 HUVECs were added per well in EGM2 in the presence or absence of Obtustatin or TC-I-15 inhibitors, as well as the 6F1 antibody, and incubated at 37°C for 24 hours. Phase contrast images, ten fields of view per well, were taken on a DM6000 Leica microscope at 10x magnification at 6 hours and 24 hours and three repeat experiments were quantified using the Angiogenesis Analyser plugin for ImageJ created by Giles Carpentier. This program quantifies angiogenesis by analysing many parameters and the most relevant were chosen here. Nodes and junctions are both points at which branches of the vascular network converge and so are taken as a measure of vascular complexity. Junctions are quantified as groups of nodes. A mesh describes an area completely closed by branches of the network and so measures the connectedness of the network. Isolated segments are cells or branches that have not connected to the rest of the network and so indicate unconnected cells and disorganised networks.

Figure 8.3 shows representative phase images taken at the six-hour time point after integrin inhibition and the corresponding ImageJ Angiogenesis Analyzer program analysis. From these images there is clearly a difference in the number of connections in the networks between the controls and 6F1 or TC-I-15. The networks formed in the presence of TC-I-15 and 6F1 seem less complete, with some cells not connected to the network at all. Figure 8.4 shows the quantification of the analysis and Table 8.2 shows the statistical analysis of the data using one-way ANOVA and Sidak's multiple comparisons test to compare each condition to the appropriate control. P values in bold signify statistical significance.

Figure 8.3. Tube Formation After Integrin Inhibition

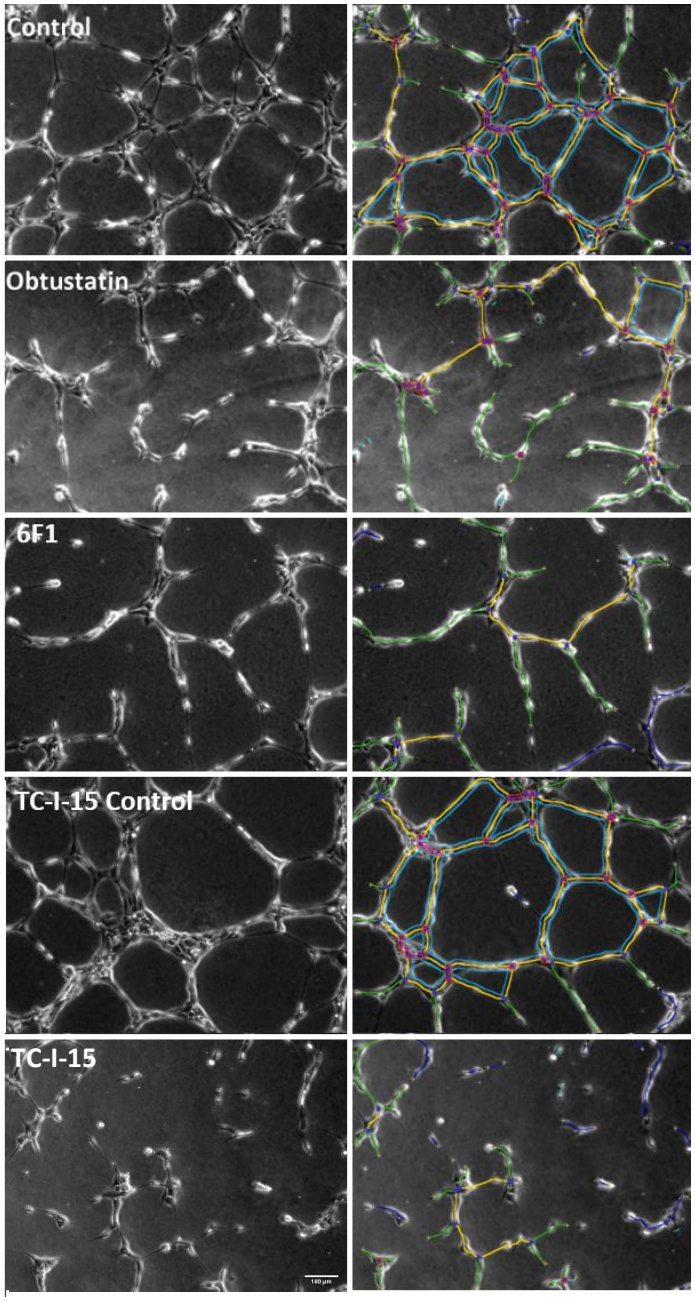

Figure 8.3. Phase contrast images of tube formation assays after 6 hours of integrin inhibition

Representative phase images of angiogenesis experiments alongside the Angiogenesis Analyzer Plug-in quantification of parameters. Yellow and green denote branches, purple denotes junctions, which are made up of nodes. Light blue shows the meshes and dark blue shows twigs (branches that are a dead-end). Images were taken on a 10x objective using a Leica microscope. The scale bar indicates 100µm (bottom left panel)

Figure 8.4: Quantification of Tube Formation After Integrin Inhibition.

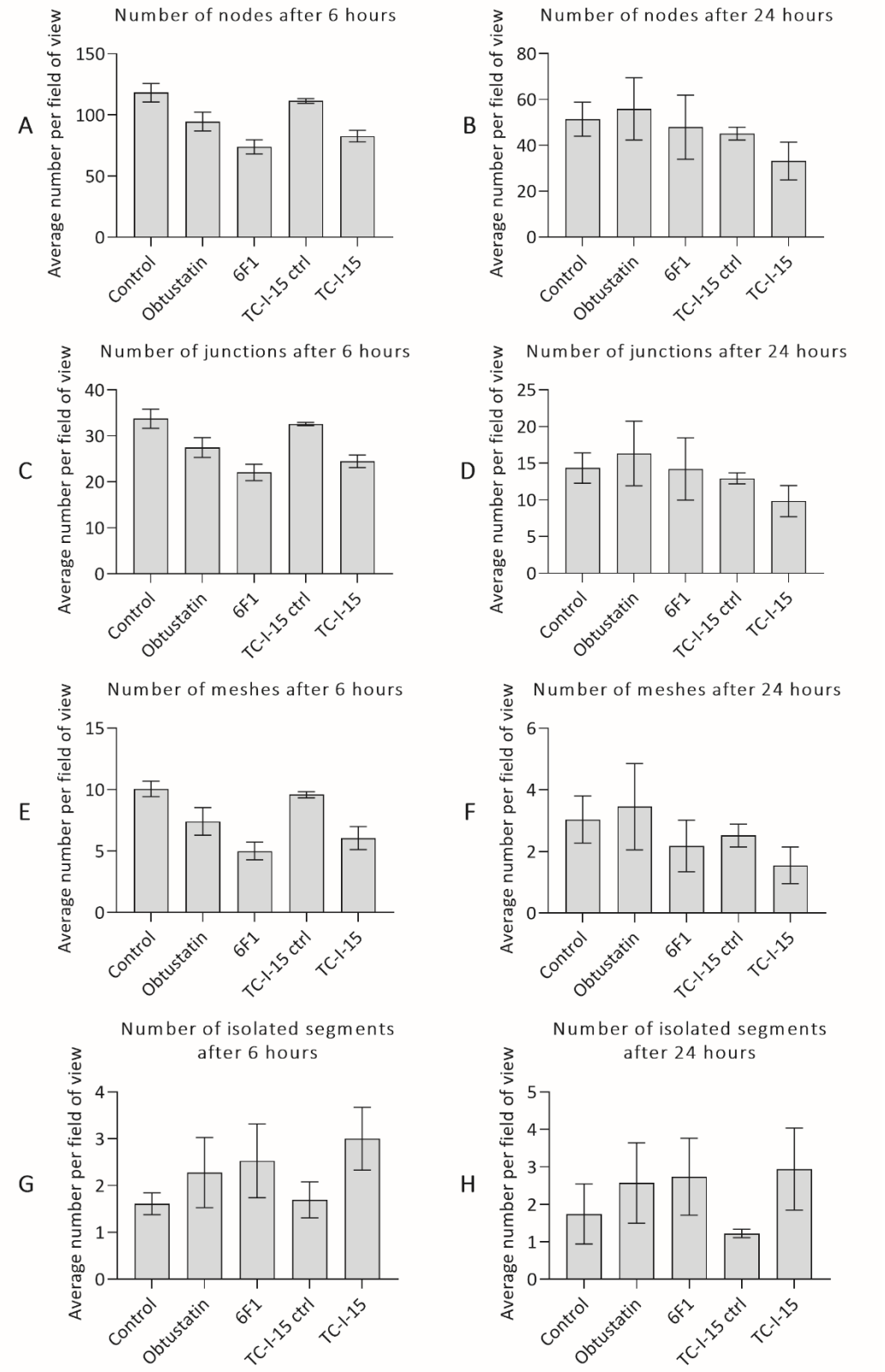

Quantitation of the effects of integrin inhibition on angiogenesis as measured by the number of nodes (A, B), junctions (C, D), Meshes (E, F) and isolated segments (G, H). Means are plotted with error bars indicating SD. The left column shows the quantification of images taken at six hours and the right column indicates the 24-hour time point.

Table 8.2 – Statistical analysis of tube formation after integrin inhibition

	6 hours				24 hours			
	Number of Nodes per field of view							
	Mean	SD	N	P	Mean	SD	N	P
Control	118.3	15.11	4		51.44	12.83	4	
Obtustatin	94.5	15.38	4	**0.0371**	55.94	23.6	4	0.9861
6F1	73.89	11.6	4	**0.0003**	47.93	24.2	4	0.9932
TC-I-15 Control	111.5	3.735	4		45.15	4.875	4	
TC-I-15	82.68	9.48	4	**0.0110**	33.16	14.28	4	0.8066
	Number of Junctions per field of view							
Control	33.75	4.138	4		14.33	3.571	4	
Obtustatin	27.47	4.31	4	0.0542	16.33	7.625	4	0.9587
6F1	22.06	3.543	4	**0.0005**	14.2	7.34	4	>0.9999
TC-I-15 Control	32.58	0.7335	4		12.93	1.326	4	
TC-I-15	24.48	2.749	4	**0.0115**	9.831	3.703	4	0.8677
	Number of Meshes per field of view							
Control	10.06	1.259	4		3.037	1.326	4	
Obtustatin	7.417	2.245	4	0.0930	3.454	2.427	4	0.9825
6F1	5	1.443	4	**0.0012**	2.176	1.452	4	0.8732
TC-I-15 Control	9.583	0.5	4		2.519	0.6415	4	
TC-I-15	6.063	1.873	4	**0.0195**	1.55	1.027	4	0.8309
	Number of Isolated Segments per field of view							
Control	1.611	0.467	4		1.741	1.389	4	
Obtustatin	2.278	1.503	4	0.8330	2.569	1.856	4	0.8364
6F1	2.528	1.578	4	0.6604	2.736	1.782	4	0.9710
TC-I-15 Control	1.694	0.7665	4		1.222	0.1925	4	
TC-I-15	3	1.346	4	0.3836	2.942	1.899	4	0.9888
one-way ANOVA and Sidak's multiple comparisons test were used to compare the means of each condition to the appropriate control mean. P values in bold signify statistical significance								

After quantification and statistical analysis, Obtustatin (94 compared to 118.3 nodes per field of view, *P=0.0371), 6F1 (73.89 compared to 118.3 nodes per field of view ***P=0.0003) and TC-I-15 (82.68 compared to 111.5 nodes per field of view*P=0.0110) all significantly decreased the number of nodes per field of view at 6 hours compared to the appropriate control, but no significant differences were seen for the number of nodes at 24 hours for any condition tested. However, only 6F1 (22.06 compared to33.75 junctions per field

of view, ***P=0.0005) and TC-I-15 (24.48 compared to 32.58 junctions per field of view, *P=0.02) significantly decreased the number of junctions at 6 hours, with no significant differences seen with obtustatin (P=0.0542). Similarly, these differences were not seen at 24 hours. In terms of meshes, both 6F1 (**P=0.0012) and TC-I-15 (*P=0.0195) impeded mesh formation at 6 hours but that difference was not significant at 24 hours. Lastly, there were no significant differences in the number of isolated segments, due to the high variability of this parameter in the acquired images. The tubes formed quickly, and networks were becoming visible after only 2 hours in the control conditions. By 6 hours the networks were well defined in control conditions but not so well defined in the presence of 6F1 and TC-I-15. However, by 24 hours the tubes were beginning to disintegrate in all conditions. .

Overall, this suggests that inhibition of α2β1 using 6F1 or TC-I-15 impedes the formation of a vascular network in tube formation assays at early time points. These results also raise the possibility that obtustatin could also affect tube formation despite the α1β1 integrin being expressed in extremely low mRNA levels in HUVECs. The inhibition of tube formation seen with TC-I-15 and 6F1 is likely due, in part, to the effects of α2β1 inhibition on cell migration seen in Chapter 7. The cells will migrate more slowly in the presence of α2β1 inhibitors and this would impede the formation of the network. However, there is likely another process by which α2β1 inhibition impedes tube formation as these cells did not simply form the same networks more slowly, but instead never reached the complexity of the control networks seen at 6 hours. The fact that there are no significant differences seen at 24 hours is more indicative of the tubes in all conditions disintegrating than the 6F1 and TC-I-15 conditions catching up to the controls. The case for α1β1 is more complicated as differences are seen when comparing the number of nodes in the presence of obtustatin compared to the control, but not the number of junctions, despite both of these functions evaluating very similar characteristics. This is likely explained by slight differences in the sensitivities of these two measurements in that the effect of Obtustatin is very small and is minimally picked up when quantifying the number of nodes but is just missed when quantifying the number of junctions. It is highly likely that repeating this experiment with ECs that express higher levels of α1β1 would see greater differences in tube formation inhibition in the presence of Obtustatin[165]. As seen before, there is a similar inhibition of angiogenesis seen when inhibiting α2β1 with 6F1

and inhibition of both α1β1 and α2β1 simultaneously with TC-I-15, suggesting that inhibition of α2β1 is the main avenue by which TC-I-15 inhibits angiogenesis in HUVECs.

8.4 Effects of Integrin siRNA Knockdown on Tube Formation

A role has clearly been established for α2β1 and α1β1 in the regulation of angiogenesis in ECs, both in this chapter and in the literature described earlier[160, 165]. However, no role has been established for α10β1. To study the effects of integrin KD on HUVEC tube formation, HUVECs were cultured in EGM2 and subjected to siRNA KD of each integrin, and all three together. 48-72 hours following the transfection, tube formation assays were repeated as before on Geltrex substrates. 4500 cells were added to each well and left to form tubes for 24 hours. Phase contrast images, five fields of view per well, were taken at 6 hours and 24 hours and three experimental repeats were quantified using the Angiogenesis analyser as before. One-way ANOVA and Dunnett's multiple comparison test was used to analyse the data obtained from the Angiogenesis Analyzer plug-in. Table 8.3 summarises the statistical analysis. Figure 8.5 shows the quantification of tube formation after siRNA KD of each integrin.

The tube formation was variable, as a consequence the SDs for each condition are larger here than with the integrin inhibitors. Due to time constraints, only three repeats of this experiment were carried out. It's possible this was not enough to properly investigate the effects of siRNA KD of integrins on HUVEC tube formation. The only parameter that returned a statistically significant difference was the KD of ITGA10 on the quantification of isolated segments. KD of ITGA10 resulted in significantly (0.5481 per field of view vs 1.07 per field of view *P=0.0057) less isolated segments compared to the control at the six-hour time point. This decrease in isolated segments was not seen when all integrins were knocked down with siRNA simultaneously. There were no significant differences in any of the other parameters tested (nodes, junctions, meshes or isolated segments), even with siRNA knockdown of all collagen-binding integrins expressed in HUVECs. This was surprising as the role of α2β1 in EC migration and angiogenesis has been established in this study and is well documented in the literature described earlier. As such, KD of all integrins was expected to impede tube formation. Previously, siRNA KD of ITGA2 significantly decreased cell migration over collagen substrates in a manner similar to the inhibition of α2β1 by 6F1 and TC-I-15. KD of ITGA2 was thus expected to impede angiogenesis in a similar way to 6F1 and TC-I-15 but this was not the case. Instead,

the inhibitors were more potent at impeding angiogenesis than the siRNA. There are several possible explanations for this.

Figure 8.5: Tube Formation After siRNA Knockdown of Integrins

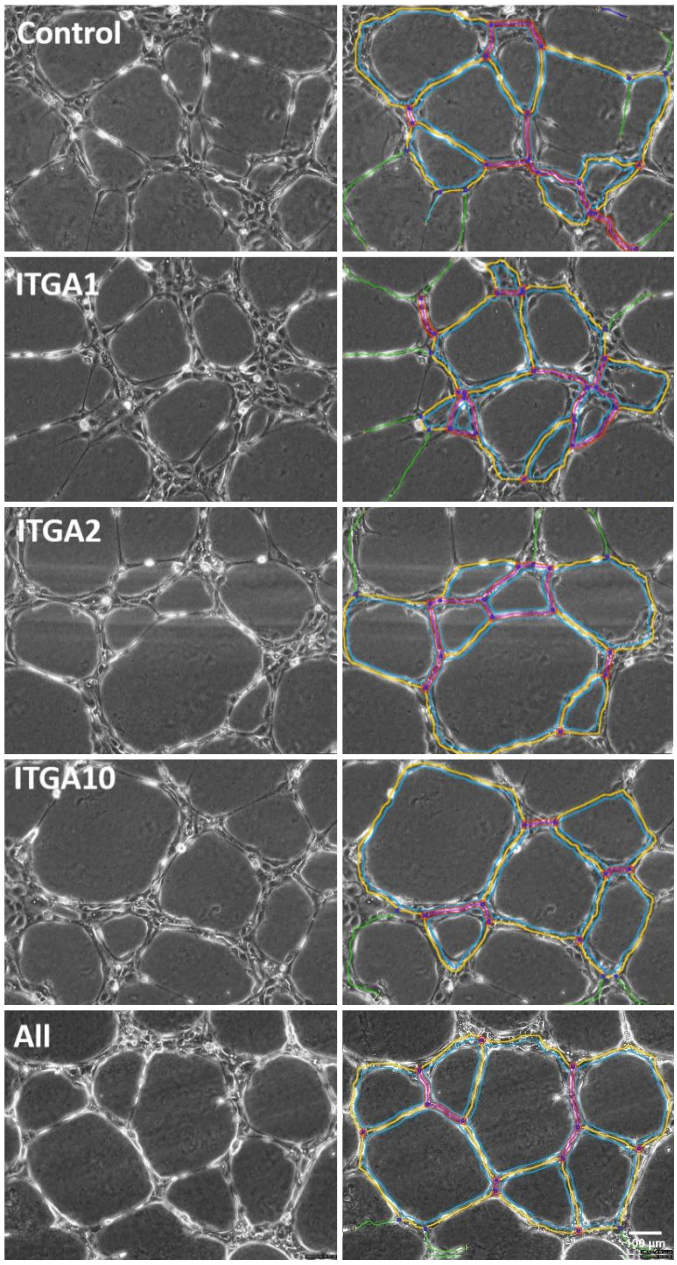

Representative phase contrast images taken six-hours after seeding siRNA treated HUVECs. Experiments were carried out 48 hours post-siRNA treatment. The left hand column shows the phase images obtained at the six-hour time point and the right-hand column shows the Angiogenesis Analyser analysis of the images. Images were taken on a 10x objective using the Leica microscope as before. Yellow and green denote branches, purple denotes junctions, which are made up of nodes. Light blue shows the meshes and dark blue shows twigs (branches that are a dead-end).

The scale bar on the bottom right panel represents 100µm.

Figure 8.6: Quantification of Tube Formation After siRNA Knockdown of Integrins

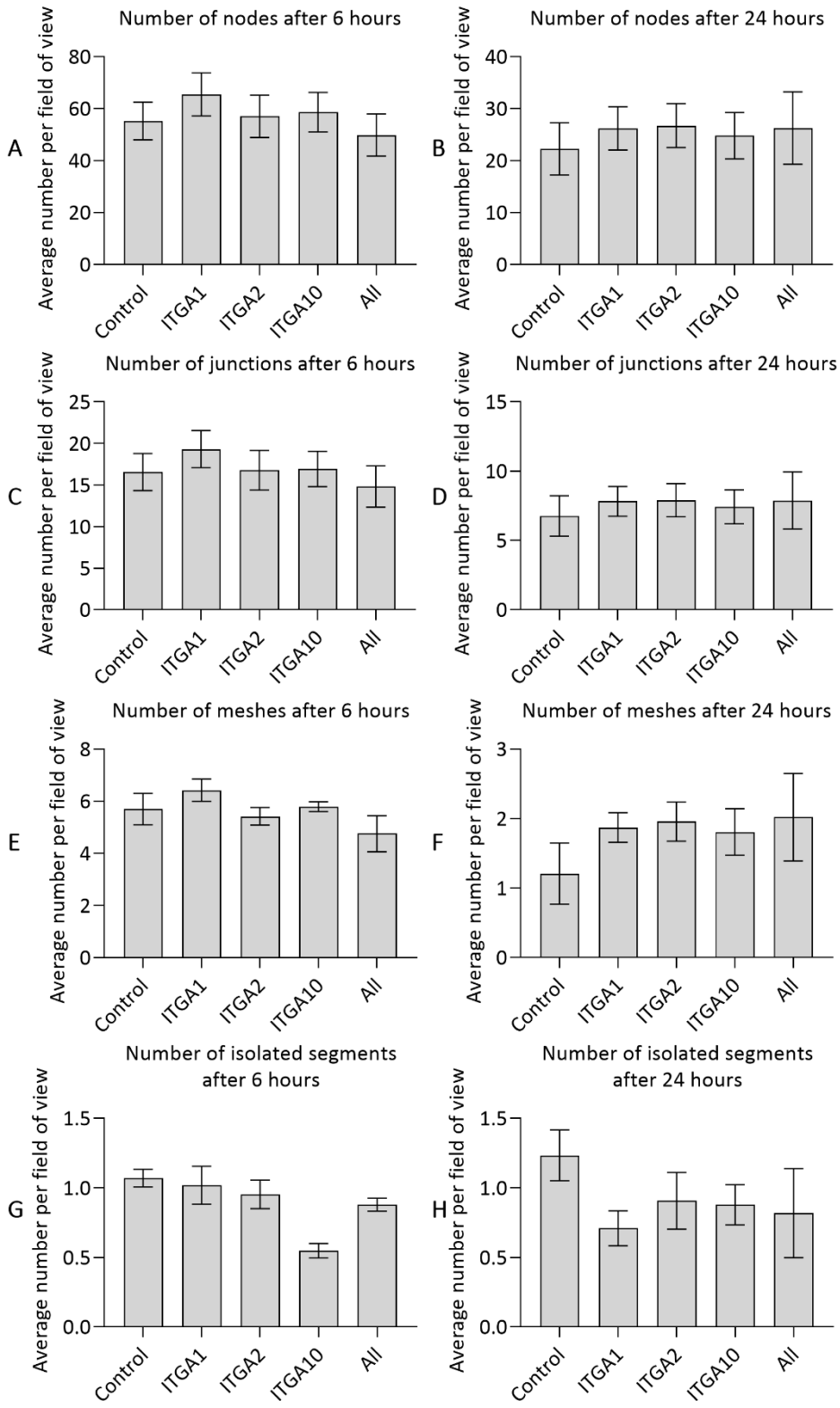

Quantitation of the effects of integrin inhibition on angiogenesis as measured by the number of nodes (A, B), junctions (C, D), Meshes (E, F) and isolated segments (G, H). Means are plotted with error bars indicating SD. The left column shows the quantification of images taken at six hours and the right column indicates the 24-hour time point.

Table 8.3 – Statistical Analysis of Tube Formation After siRNA

	6 hours				24 hours			
	Mean	SD	N	P	Mean	SD	N	P
	Number of Nodes per field of view							
Control	55.25	12.61	3		22.25	8.685	3	
ITGA1	65.48	14.43	3	0.7719	26.21	7.165	3	0.9464
ITGA2	57.04	14.21	3	0.9993	26.73	7.304	3	0.9205
ITGA10	58.67	13.15	3	0.9934	24.79	7.752	3	0.9886
All	49.81	14.02	3	0.9650	26.26	12.06	3	0.9442
	Number of Junctions per field of view							
Control	16.56	3.852	3		6.759	2.531	3	
ITGA1	19.33	3.878	3	0.8079	7.82	1.862	3	0.9566
ITGA2	16.78	4.131	3	>0.9999	7.893	2.08	3	0.9462
ITGA10	16.94	3.677	3	0.9998	7.426	2.132	3	0.9916
All	14.83	4.302	3	0.9528	7.878	3.568	3	0.9485
	Number of Meshes per field of view							
Control	5.696	1.042	3		1.207	0.7626	3	
ITGA1	6.422	0.7374	3	0.6788	1.87	0.3699	3	0.6208
ITGA2	5.423	0.5771	3	0.9822	1.956	0.4904	3	0.5281
ITGA10	5.794	0.3256	3	0.9997	1.807	0.577	3	0.6909
All	4.757	1.196	3	0.4840	2.019	1.089	3	0.4636
	Number of Isolated Segments per field of view							
Control	1.07	0.1091	3		1.233	0.3168	3	
ITGA1	1.019	0.2364	3	0.9795	0.709	0.2174	3	0.2789
ITGA2	0.9529	0.1778	3	0.7479	0.9074	0.3528	3	0.6461
ITGA10	0.5481	0.08981	3	**0.0057**	0.8778	0.2502	3	0.5816
All	0.8794	0.07973	3	0.3885	0.8185	0.5545	3	0.4600
One-way ANOVA and Dunnett's multiple comparisons tests were used to compare the means of each condition to the control mean. P values indicating a significant difference and shown in bold								

Firstly, the inhibitors TC-I-15 and 6F1 act with immediate effect and impede integrin binding just before adding cells to the Geltrex substrate without allowing for the cells to compensate in any way. In contrast, siRNA is a much slower process involving gene regulation over two to three days, giving the HUVECs time to upregulate other compensatory receptors and thus allowing the cells to form tubes adequately in the absence of ITGA2. No upregulation of other collagen binding integrins was seen here with ITGA2 KD (Chapter 5.6), but there are

many other integrins, as well as non-integrin receptors, that could be upregulated to facilitate adhesion, migration and angiogenesis in the absence of α2β1. For example, the αvβ3, αvβ5 and α5β1 described above would all contribute to angiogenesis and could be upregulated to compensate for the loss of ITGA2-mediated adhesion.

Secondly, the differences in cell migration in the presence and absence of inhibitors and in siRNA KD were witnessed over collagen I substrates. In this setting, collagen-binding receptors such as α2β1 and α1β1 play crucial roles in cell behaviours, whereas Geltrex is made up of a vast array of basal lamina proteins including laminin, collagen IV, entactin, fibronectin, fibrinogen, dynein, desmin, myosin, transferrin and heparin sulphates proteoglycans, as well as some low levels of growth factors like bFGF, TGFβ, PDGF, IGF and EGF[192, 193]. The complexity of Geltrex will affect the behaviour of ECs. There are many other protein-protein interactions taking place in the angiogenesis experiments presented here, that would not be occurring in an EC-collagen I interface. For example, laminin receptor like α3β1, α6β1, αvβ3 could all bind laminin in Geltrex and facilitate adhesion, promoting angiogenesis[399, 400]. Fibronectin receptors like α5β1 have also been implicated in the regulation of angiogenesis[401]. These receptors would all be highly active on a Geltrex substrate but not on collagen I, and so can compensate for the loss of collagen-binding integrins after siRNA knockdown. Additionally, even the low levels of growth factors seen in the growth-factor-reduced Geltrex could be affecting numerous signalling pathways to ablate the effects of siRNA KD on HUVEC behaviour.

Lastly, there is a difference between inhibition of an existing receptor and the complete absence of this receptor. The presence of an non-ligated integrin receptor could signal downstream processes that register the cell as 'not adhered' whereas the absence of these receptors cannot signal their non-ligated state, forcing the cell to instead rely on signals from other receptors which are unaffected by siRNA KD. In this case, where there is redundancy in function, for example adhesion, the cell may be not sensitive to the lack of α2β1, α1β1 or α10β1 at all if there are other signals that mark the cell as adherent and functioning. TC-I-15 stabilises the inactive conformation of α2β1, and presumably α1β1, and so would result in non-ligated signals being transduced into the cell. The inactive, non-ligated integrin may actively inhibit cell migration and angiogenesis whereas an absent receptor would not.

8.5 Conclusions

TC-I-15 and 6F1 inhibition of α2β1 in HUVECs inhibits tube formation on a Geltrex substrate at six-hour time points. This could be partially due to the TC-I-15 and 6F1 mediated inhibition of adhesion and migration seen previously in Chapter 7 whereby the HUVECs migrated more slowly over collagen substrates. The TC-I-15 treated cells are less capable of migrating into the tube formation network and this could explain why the networks were not as complex.

Conversely, siRNA KD of integrins in HUVECs had no effect on the HUVECs ability to form tubes on a Geltrex substrate. This could partially be due to a lack of non-ligated signal downstream of the absent receptor. Additionally, the HUVECs could be upregulating other receptors involved in adhesion, migration and angiogenesis to compensate for the loss of α2β1. While no upregulation of collagen binding integrins was seen with siRNA KD of each integrin, other non-integrin or other integrin receptors were not studied in detail downstream of integrin siRNA KD.

Chapter 9 – General Discussion

Contents

9.1 Chapter Summary

In this chapter I aim to summarise my findings with an emphasis on the physiological relevance of each finding.

9.2 Discussion

The work described here set out to study and characterise the roles of the four collagen-binding integrins (α1β1, α2β1, α10β1 and α11β1) in the regulation of EC behaviour. In the literature described in the introduction, α1β1 and α2β1 have both been shown to contribute to the regulation of EC proliferation, migration and angiogenesis. This work aims to build on this knowledge with the intention of additionally characterising the roles of α10β1 and α11β1.

This project began by studying the binding preferences of the four collagen-binding integrins in Chapter 3. The αI-domains of α1β1 and α2β1 were expressed in bacteria as GST-tagged constructs, by Dr Samir Hamaia, and purified using GST-affinity columns. These recombinant αI-domains were tested in static adhesion assays with THPs containing integrin-binding motifs from the triple helical domains of different collagens. The expression of the recombinant α10β1 and α11β1 αI-domains was problematic and no functional proteins were recovered. For the αI-domains of α1β1 and α2β1, all adhesion was Mg^{2+}-dependent and no non-specific binding was seen in the presence of the metal ion chelator EDTA, implying that the observed adhesion was integrin-specific and occurred through the αI-domains functioning as in the full-length α-β heterodimer. The αI-domain of α1β1 showed a far more active binding profile than that of α2β1 on the collagen peptides tested. The α2β1 αI-domain bound relatively few THPs while the αI-domain for α1β1 bound to the majority of THPs. This was unexpected,

as the αI-domains of these integrins are proposed to behave similarly due to their high homology. Integrins exist in varying states of activation. It is possible that the expression of the recombinant αI-domains results in varying states of activation: the recombinant α1β1 αI-domain may be inadvertently expressed in a more active state whereas the α2β1 αI-domain is expressed in a less active state in comparison. There are conformational changes that take place in the αI-domain and β1-subunit upon adhesion to collagen and it is possible that the αI-domains of each integrin, when expressed in this manner, exist in different conformations. This would result in varying affinities for these two αI-domains to collagen. Additionally, the β1-subunit that would be present in the full-length receptor is absent here. The β1-subunit interacts with the α-subunit and this interaction could be important for adhesion. It is also important to note that these αI-domains are expressed as GST-tagged constructs and GST will dimerise[402], resulting in an increased signal. A significant limitation of the work presented here is the absence of a GST-only control. This should have been included to rule out binding of the GST construct to the peptides. Therefore, the αI-domain adhesion assays are not the best method for studying integrin adhesion and it is important to validate findings in full-length heterodimers.

To study the integrin binding preferences in a more physiologically relevant setting, C2C12 cells that express the α-subunit from one of the four integrins were used to test the full-length receptor adhesion to THPs. C2C12 cells are a mouse myofibroblast cell line and were chosen because they do not express any native collagen-binding receptors. Any subsequent adhesion to collagen in the transfected cells can be attributed to the transfected integrin α-subunit . The C2C12 cells have been transfected with one of the integrin α-subunits and these associate with the native mouse β1-subunit to form the functional full integrin heterodimer. The adhesion profiles of all four integrin receptors on THPs proved to be very similar. Similarities were expected, but the extent of homology was surprising. There were three peptide motifs that were specific for α2β1 (GNRGER, GNOGER and GKOGER). There were also other THPs that were selective for some integrins over others, for example GFQGEK, found in collagen IV, bound only to α1β1 and α2β1. GROGER, (found in collagens I, III, VII and X) did not bind to α10β1, as described in a publication I co-authored[243]. The homology seen in the binding profiles of the four integrins meant that THPs could not be used to ligate each integrin. The differences between the adhesion profiles of the I-domains and the full-length receptors

for α1β1 and α2β1 can be partially attributed to the absence of the β1-subunit and any regulatory function it might serve. Similarly, the rest of the α-subunit is also absent and could potentially modulate the function of the αI-domain.

The C2C12 adhesion profiles revealed integrin binding motifs are widely distributed across the collagens (Table 3.2). The motifs GFOGEK, GFOGER and GLOGEK bound to all integrins, these motifs are found in abundance in collagen IV, the main collagen component of the EC basal lamina. Collagen IV also contains some α2β1 specific motifs, GAOGER, and GSOGEK alongside the selective motifs GFQGEK (α1β1 and α2β1 only), GLKGER (α10β1 and α2β1 only) and GLOGEA (not α11β1). Many of the collagen types contain several integrin-binding motifs. For example, collagen I contains GFOGER and GLOGER (binds all four integrins), GKOGER and GMOGER (α2β1 only) and GROGER (binds all but α10β1). Other collagens did not contain any of the integrin binding motifs that were tested. The motifs found in collagens VIII, XV, XIX, XX, XXIII, XXV and XXVIII did not return any positive binding peptides. However, this does not mean that these collagens would not bind integrins through other motifs not identified here. This highlights the complexity of the collagen-integrin interactions and the abundance of integrin-binding sites found across the collagen family.

Next, the mRNA expression profiles of the four collagen-binding integrins were explored using qPCR. At the mRNA transcript level, α2β1 was the most abundant transcript by far, followed by α10β1, and then α1β1. α11β1 was barely detectable. The low expression of α1β1 was surprising as this integrin has been studied in ECs in the literature[157, 160]. Both α1β1 and α2β1 have been shown to be upregulated by VEGF[156], which is present in EGM2 in low levels. Addition of further VEGF did not increase the expression of α1β1 mRNA. Four different pools of HUVECs were tested and the results were consistent, confirming that mRNA corresponding to α1β1 is expressed in low levels in HUVECs. However, low levels of mRNA do not necessarily translate to a non-existent receptor at the protein level and vice versa. It was not possible during this project to detect or quantify the presence of these integrins at the protein level due to problems with antibody specificity. Therefore, the assumption was made that α1β1 and α10β1 are present and functional on the HUVECs' cell surface and could regulate EC behaviour. The endothelial phenotype of HUVECs was characterised using several EC-specific markers and each pool of HUVECs was found to be positive for VWF, PECAM, CD146 and VE-Cadherin, confirming that HUVECs used throughout this project are indeed endothelial

cells. HUVECs also displayed typical endothelial behaviour. For example, when HUVECs were stimulated with TNFα or IL-1α overnight, they increased expression of inflammatory markers VCAM, ICAM and E-Selectin. Surprisingly, the addition of LPS at 1μg/ml did not affect the expression of inflammatory markers. It is possible that LPS may take longer to induce an inflammatory phenotype, or higher concentrations may have been required.

The adhesion profile of HUVECs on the collagen THPs is very similar to C2C12 cells expressing α2β1. This was expected because α2β1 is the most abundant collagen-binding receptor in HUVECs and displays the most active binding profile to THPs. The prevalence of α2β1 in HUVECs indicates that this integrin is the main collagen receptor HUVECs, and α2β1-mediated binding is likely to mask the adhesion of the other integrins. HUVECs showed a slightly more active adhesion profile than the C2C12 cells expressing α2β1. In addition to the C2C12-α2β1 positive motifs, HUVECs also adhered to GASGER, GHDGEK and GSQGEK. Additional attachment to these THPs could be due to a more active conformation of α2β1 in HUVECs than in C2C12 cells expressing the α2β1 receptor. HUVECs will also express the human β1-subunit whereas C2C12 express a mouse β1-subunit, which could affect the specificity of the αI-domain. Lastly, HUVECs could express a number of other receptors or signalling molecules that could co-localise with integrins and modulate integrin activity. These might not be present in C2C12 cells.

Due to the lack of integrin specific motifs in THPs, these could not be used to modulate integrin function. Instead, inhibitors for the integrins were sought out and tested. TC-I-15, a commercially available α2β1 inhibitor and obtustatin, an α1β1 inhibitor, were characterised using I-domains, C2C12 cells, HT1080s and HUVECs. TC-I-15 was promiscuous and inhibited adhesion of both α1β1 and α2β1, but not recombinant α3β1 adhesion to collagen, laminin or THPs. Meanwhile, obtustatin was found to be specific for α1β1. Neither TC-I-15 nor obtustatin had any effect on the adhesion of αI-domains to THPs, suggesting that the mode of inhibition also involves the rest of the receptor. This finding agrees with the literature proposing that TC-I-15 adheres to the β1-subunit to stabilise the inactive conformation of the αI-domain[2]. Obtustatin is proposed to bind to the αI-domain via a KTS motif located within an integrin-binding motif[4, 255]. However, the isolated αI-domain from α1β1 was unaffected by Obtustatin. This suggests that the mode of Obtustatin inhibition might also employ the β1-subunit, or the rest of the α-subunit. TC-I-15 also had varying potencies depending on the THP motif used. The

THPs may have different affinities for the integrin receptors which could affect the efficacy of the receptor. In C2C12 cells expressing ITGA2, TC-I-15 attenuated adhesion on GLOGEN at very low concentrations, the IC_{50} was 0.39μM compared to 26.77μM for GFOGER. This was not seen for C2C12 cells expressing ITGA1 where the inhibition of adhesion to GFOGER and GLOGEN was similar with IC_{50}s at 23.55μM and 24.43μM respectively. The reason for these differences is unclear. α2β1 has a lower affinity for GLOGEN than GFOGER and it is possible that a lower concentration is necessary to attenuate adhesion, whereas the affinity for α1β1 to GFOGER and GLOGEN is similar, leading to an equally similar mode of inhibition. However, in static adhesion assays the C2C12-ITGA1 adhesion to GLOGEN has a lower mean absorbance than for GFOGER (1.342 +/- 0.085 compared to 2.116 +/- 0.090) suggesting that there could be a difference in affinity here that does not translate to a difference in inhibition by TC-I-15. Further studies would be necessary to determine the cause for these differences of TC-I-15 IC_{50}s in C2C12 cells. Nevertheless, these newly characterised inhibitors were used throughout the project to investigate the functions of these integrins in the regulation of EC behaviour as measured by changes in proliferation, apoptosis, migration and tube formation.

There were no commercially available inhibitors for α10β1 and so a lentiviral CRISPR system was created to KO each integrin in HUVECs. However, the transduction efficiencies of the lentiviral delivery system were disappointing. Liposomal transfection methods were also tested but to no avail. Primary cells cannot be cultured indefinitely, as they lose their phenotype and de-differentiate. HUVECs were not used beyond passage 5 in this project. Therefore, it would not have been possible to isolate the few successfully transfected cells and expand them for use in downstream assays. CRISPR was abandoned due to the low transduction and transfection efficiency and siRNA was optimised instead. Using Silencer Select siRNAs, 85-90% KDs were achieved for ITGA1, ITGA2 and ITGA10. These KDs were reproducible and efficient. The ITGA2 KD was stable over 5 days at the protein level in quantitative western blots. Due to problems with antibody cross-reactivity, only ITGA2 could be detected in western blots and it was assumed that the ITGA1 and ITGA10 KDs would occur similarly. Downstream experiments were all carried out 24-72 hours post siRNA KD.

In adhesion assays, both the inhibition of α2β1 and siRNA KD of the ITGA2 transcript severely impeded HUVEC attachment to collagen, THPs and laminin, with no effect on the adhesion of HUVECs to fibronectin. Inhibition or siRNA KD of α1β1 or α10β1 had no effect on

HUVEC adhesion to any substrate tested. This suggests that HUVECs use α2β1 as their main collagen and laminin adhesion receptor. Laminin is a major constituent of the endothelial basal lamina. Therefore, other endothelial laminin receptors were expected to compensate for the loss of α2β1 adhesion, but this was not the case. Although it is outside the scope of this project to further investigate laminin receptors, it would be interesting to characterise the expression levels of other laminin-binding integrins, such as α3β1 α6β1 α7β1 and α6β4. Additionally, TC-I-15 inhibition of these receptors could also have been tested. Interestingly, the interaction between laminin and α2β1 has been implicated in the progression of endothelial quiescence[403].

In proliferation assays, none of the inhibitors tested had any effect on the ability of HUVECs to proliferate as measured in EdU incorporation assays. This was surprising as there are several studies outlining the effects of integrin signalling on cell proliferation[7, 197, 302, 303, 404]. Similarly, no effect on proliferation was seen after integrin siRNA KD. Cell number quantification assays also detected no change in proliferation over 72 hours for each integrin siRNA KD condition compared to the negative control siRNA. Although a positive control for cell-cycle arrest should have been included. Lastly, Integrin inhibition or siRNA KD also had no effect on apoptosis, as measured by Annexin V detection of PS exposed on the membranes of apoptotic cells and PI or NIR nuclear labelling of membrane compromised dead cells.

Adherent cells, such as HUVECs, must attach to the ECM for proliferation to occur. A complete loss of attachment will initiate apoptosis. Over the 24-hour experiment, HUVECs did adhere to collagen despite integrin inhibition, which could account for the lack of effect on proliferation or apoptosis. Perhaps other adhesion pathways compensate for the loss of α1β1 and α2β1 adhesion seen after inhibition with obtustatin, TC-I-15 or 6F1. Similarly, HUVECs may be able to overcome α1β1 and α2β1 inhibition over the 24-hour period to facilitate adhesion and subsequent proliferation or cell survival. It is also possible that the HUVECs attach weakly to the collagen coated surface and secrete their own ECM proteins, thus allowing them to adhere through non-collagen receptors. HUVECs also adhered to BSA coated wells overnight. It is possible that the surface coatings are eroded over the 24-hour time period of the experiment and that HUVECs are then able to attach to the tissue culture treated surface underneath independent of collagen-binding integrins. The collagen structure is also less stable at 37°C and the triple helical structure may dissociate over 24 hours at this temperature leading

to exposure of other adhesion motifs, like the RGD motif seen in the collagen II and III toolkits. These exposed, non-helical sequences may facilitate adhesion of other integrins such as αvβ3, which can facilitate EC proliferation.

Both integrin inhibition and siRNA KD of α2β1 decreased HUVEC cell spreading and migration across collagen I coated surfaces. This was expected as integrin-mediated adhesion stabilises the actin cytoskeletal-ECM interaction at membrane protrusions leading to decreased actin retrograde flow and increased protrusion in filopodia and lamellipodia[197]. When integrins adhere to the ECM they cluster with each other and with other adhesion receptors to form adhesion complexes, such as nascent adhesions that eventually mature into focal adhesions[194, 252]. These adhesion receptor clusters associate with the actin cytoskeleton and contribute to the regulation of actin polymerisation[197]. Integrin-mediated adhesion at the leading edge will also facilitate traction between the cell and the ECM which pulls the rest of the cell forward, thus promoting cell migration. α2β1 inhibition or KD translated into a destabilisation of adhesion in membrane protrusions which ultimately resulted in decreased cell spreading and migration. Inhibition or siRNA KD of α1β1 and α10β1, however, did not affect adhesion, and subsequent cell spreading or migration, because α2β1 could compensate for the loss of the less abundant α1β1 and α10β1 adhesion. Simultaneous KD of all three integrins expressed in HUVECs did not add any cumulative inhibition, suggesting that ECs do not rely on α1β1 or α10β1 to migrate.

Inhibition of α2β1 using TC-I-15 or 6F1 reduced the complexity of networks formed in tube formation assays, possibly due to the inhibition of α2β1-mediated adhesion and subsequent cell migration. Inhibition of α1β1 using Obtustatin led to a significant decrease in the number of nodes per field of view. In all other parameters tested, Obtustatin had a small but not significant effect. Once again, α2β1-mediated adhesion and migration still present in this condition was speculated to be the driving force for tube formation. Obtustatin should also be tested in ECs that express higher levels of the α1β1 integrin to study the effects on α1β1 in ECs. Conversely, siRNA KD of α2β1 had no effect on tube formation. This could be due to upregulation of compensatory receptors in response to integrin absence. The KD of integrins using siRNA takes place over several days, which would allow the HUVECs to upregulate any compensatory receptors. In contrast, the inhibition of receptors is instantaneous, and this does now allow time for the cells to compensate. Additionally, in the presence of inhibitors, the cell

could be receiving an active non-ligated signal which conveys the non-adhered state of the cell. In the absence of the receptor altogether after siRNA KD, this non-ligated signal would not be created. This could affect the downstream processes involved in tube formation, in that HUVECs could just rely on other receptors to facilitate adhesion, migration and tube formation.

Overall, modulation of collagen binding integrins did not affect their ability to proliferate or survive in response to TNFα and serum starvation. Inhibition or siRNA KD of α2β1 resulted in decreased adhesion, migration and cell spreading. Inhibition, but not siRNA KD, of α2β1 decreased angiogenesis as measured by tube formation. Inhibition of α1β1 only impaired tube formation, while α1β1 KD had no effect on cellular response. The lesser influence of α1β1 compared to α2β1 can be explained by the lower levels of α1β1 mRNA expression compared to α2β1. α10β1 did not seem to play an active role in the regulation of EC behaviour in these experiments. However, due to the lack of a specific inhibitor for α10β1, we could not thoroughly investigate the impact of α10β1 inhibition on HUVEC behaviour.

Lastly, the data presented here highlights a role for TC-I-15 in the inhibition of endothelial α2β1 to decrease EC migration and angiogenesis. TC-I-15 could have therapeutic value in limiting tumour angiogenesis. Further studies should be carried out to characterise the effects of TC-I-15 in co-culture experiments or in vivo. Similarly, TC-I-15 could be used to inhibit α2β1 on other cell types where this integrin plays a major role in adhesion. For example, TC-I-15 could be tested on platelets to investigate whether inhibition of platelet α2β1 could have therapeutic value in preventing inappropriate platelet adhesion such as that seen in stroke or atherosclerosis. With respect to cardiovascular research in general, the work presented here contributes to the fundamental understanding of the interactions between ECs and their surrounding ECM and highlights the importance of integrin α2β1, but not α1β1 or α10β1, in the regulation of EC behaviour. TC-I-15 is shown to be an effective inhibitor of EC migration and angiogenesis and α10β1 is shown to be present but ineffective in ECs. The work presented here helps to characterise the roles that these collagen-binding integrins play in regulating EC behaviour and rules out integrin α10β1 as a potential target for anti-angiogenic therapeutics.

9.3 Limitations of the Current Work

The techniques used in this work were limited due to the difficulty in obtaining specific antibodies for targeting the four collagen-binding integrins. Several antibodies were purchased and tested but proved to be non-specific, probably due to the high homology seen between

these four receptors. C2C12 cells were used to test integrin antibodies for flow cytometry and western blots but nearly all the antibodies tested displayed cross-reactivity for the other integrin receptors and so could not be used. This highlights the importance of rigorous antibody testing before use in downstream experiments.

The collagen used here is soluble, meaning it has been digested with pepsin to remove the non-helical telopeptides and so exists as single triple helices. In contrast, collagen found in the basal lamina would be fibrillar, containing the telopeptide sequences. The tertiary structure of fibrillar collagen could behave differently to that of soluble collagen as integrin binding motifs could be hidden or revealed in the fibres. Therefore, these experiments do not entirely reflect the physiological EC-ECM interaction.

With respect to presentation, most of the data shown here is displayed in bar charts that show the mean with error bars representing standard deviation. In hindsight, dot plots would have been a more informative way of showing this data as they also convey the spread of the data by showing each data point. This is especially important when the data obtained doesn't follow a normal distribution.

ECs display heterogeneity dependant on the age and gender of the donor and cardiovascular diseases are far less prevalent in premenopausal women than in men of the same age[405]. For example, reproductive-age women display higher numbers of CEPCs than men[406]. A lower number of CEPCs has been linked to a higher prevalence of cardiovascular disease because the CEPCs will help regenerate existing vasculature by replacing damaged and dysfunctional ECs[99, 407]. Additionally, female CEPCs show better functionality than those found in males, due to the EC protecting function of oestrogen[406]. Oestrogen receptors are present in ECs and oestrogen encourages increased production and secretion of NO, which contributes to a more relaxed vascular tone and decreased atherogenesis[408]. Oestrogen has also been shown to promote EC proliferation, migration and angiogenesis (reviewed in[408]). In this work, pools of HUVECs obtained from a mixture of male and female donors were chosen to attempt to mitigate the effects of gender on EC function. This also means no gender specific effects would be picked up here.

The HUVECs used for the duration of this project were isolated from new-born umbilical cords and so no age-dependant characteristics could be studied. Age is a major contributor to EC dysfunction and cardiovascular disease, so it is important to also study EC

dysfunction in ECs obtained from older patients. ECs undergo constant damage and stress, accelerated by unhealthy lifestyle choices, that contribute to EC dysfunction and damage[409]. This damage accumulates over time leading to an increase in EC dysfunction and associated cardiovascular disease. ECs are also more likely to undergo senescence as time goes on[409]. Many factors contribute to the accumulation of damage to the endothelium including oxidative stress, decreased NO bioavailability, increased glucose and lipid blood concentrations, decreased prostacyclin expression, increased genomic instability and sustained chronic inflammation (reviewed in[409]). Oxidative stress can change NO to ONOO-·, which in turn irreversibly converts tyrosine to nitrotyrosine, which can be used as a marker for oxidative stress; nitrotyrosine is associated with aged arteries[410]. None of these age-related changes would be present in HUVECs obtained from new-borns and this must be taken into consideration when interpreting data. Understandably, ECs are not as readily available from older patients as they are from umbilical cords and HUVECs were chosen in part due to their wide-spread use and easy availability. Additionally, it is likely that ECs obtained from adult patients could display varying degrees of EC damage and dysfunction related to the lifestyle of the donor, resulting in less reproducible data. In conclusion, neither gender nor age-specific conditions could be studied in the scope of this project.

Migration was quantified as track displacement, which is an oversimplification of migration distance. This is the linear distance, in μm, between the starting point of the cell in the first frame of a time lapse video and the end point of the same cell in the last frame of the video. HUVEC migration did not occur in a linear straight line and the cells tended to move around randomly, back and forth, in these experiments. Track displacement does not measure this back-and-forth movement and therefore may not be an accurate measurement of cell migration. Track displacement may underestimate the migration of many cells and it's possible that bigger differences would be seen in these experiments if total track length was quantified instead. Additionally, ECs exist in monolayers surrounding the blood vessels and are generally quiescent and non-migratory unless stimulated by chemoattractants such as VEGF, therefore it would have been more physiologically relevant to track the migration of EC monolayers in response to a VEGF gradient in chemotaxis assays. The optimisation of these chemotaxis assays was started but, due to time constraints, was not completed.

The tube formation assays performed here are used as a measure of angiogenesis but bear little resemblance to physiological angiogenesis which occurs in a 3D matrix alongside other cell types. Tube formation is a simplification of this process and as such, the tubes may not form a lumen. There is no blood flow and no shear stress, which has been shown to regulate EC differentiation. Additionally, fibroblasts have been reported to form networks on Matrigel. The tube formation assays carried out for this project are therefore an indicator of HUVECs' angiogenic potential, but do not provide a complete measure of angiogenesis. To truly measure angiogenesis, in vivo assays must be carried out and these were outside the scope of this project.

Finally, ECs exist in a monolayer that lines blood vessels. None of the experiments here were carried out using EC monolayers and so care must be taken when extrapolating this data to physiological settings. The cell-cell interactions seen in monolayers are important in maintaining the barrier function of ECs. This barrier function varies depending on the type and location of the ECs in question. For example, blood-brain barrier ECs will have a much more stringent barrier function than ECs found in the liver or kidney as solutes that pass into the brain must be restricted. However, using a monolayer of HUVECs would require ECs to reach confluency before experiments. In standard cell culture conditions this is generally not recommended as cell-cell contacts induce quiescence. Comparisons between confluent and non-confluent ECs could be tested to investigate this.

9.4 Future Work

If more time was available, other EC characteristics could have been explored. For example, the barrier function of ECs is integral to their function. Studies exploring the effects of integrin inhibition or siRNA KD on the permeability of EC monolayers could also be carried out. ECs grown to confluence on collagen coated semi-permeable membranes would be probed for any increases in permeability using fluorescently tagged high molecular weight dextran molecules. A range of different collagens could be used in future experiments. For example, fibrillar collagens or 3D collagen scaffolds could be used as a better approximation of physiological settings.

Chemotaxis experiments using VEGF, bFGF and other chemoattractants could also be carried out. All future migration experiments should quantify total cell migration rather than the track displacement, as this is a more accurate measure of cell movement across a

substrate. Additionally, co-cultures of ECs with VSMCs or pericytes imbedded in collagen scaffolds or gels would include the interactions between different cell types in a 3D setting, creating a more physiologically relevant environment.

Lastly, the compensation that may be taking place to facilitate the tube formation seen with integrin KD would be investigated. The effects of integrin KD on the expression of other ECM adhesion receptors will be tested using qPCR, RNA sequencing and quantitative western blots to determine which, if any, receptors are up or downregulated in response to a loss of integrin signalling.

References

1. Augustin, H.G. and G.Y. Koh, *Organotypic vasculature: From descriptive heterogeneity to functional pathophysiology.* Science, 2017. **357**(6353).
2. Miller, M.W., et al., *Small-molecule inhibitors of integrin alpha2beta1 that prevent pathological thrombus formation via an allosteric mechanism.* Proc Natl Acad Sci U S A, 2009. **106**(3): p. 719-24.
3. Sokeland, G. and U. Schumacher, *The functional role of integrins during intra- and extravasation within the metastatic cascade.* Mol Cancer, 2019. **18**(1): p. 12.
4. Monleon, D., et al., *Concerted motions of the integrin-binding loop and the C-terminal tail of the non-RGD disintegrin obtustatin.* J Biol Chem, 2003. **278**(46): p. 45570-6.
5. Redman, M., et al., *What is CRISPR/Cas9?* Arch Dis Child Educ Pract Ed, 2016. **101**(4): p. 213-5.
6. Bella, J., *Collagen structure: new tricks from a very old dog.* Biochem J, 2016. **473**(8): p. 1001-25.
7. Barczyk, M., S. Carracedo, and D. Gullberg, *Integrins.* Cell Tissue Res, 2010. **339**(1): p. 269-80.
8. Emsley, J., et al., *Crystal structure of the I domain from integrin alpha2beta1.* J Biol Chem, 1997. **272**(45): p. 28512-7.
9. Pober, J.S. and W.C. Sessa, *Evolving functions of endothelial cells in inflammation.* Nat Rev Immunol, 2007. **7**(10): p. 803-15.
10. Ricard-Blum, S., *The collagen family.* Cold Spring Harb Perspect Biol, 2011. **3**(1): p. a004978.
11. Vermeulen, K., D.R. Van Bockstaele, and Z.N. Berneman, *The cell cycle: a review of regulation, deregulation and therapeutic targets in cancer.* Cell Prolif, 2003. **36**(3): p. 131-49.
12. Rajendran, P., et al., *The vascular endothelium and human diseases.* Int J Biol Sci, 2013. **9**(10): p. 1057-69.
13. Roberts, A.C. and K.E. Porter, *Cellular and molecular mechanisms of endothelial dysfunction in diabetes.* Diab Vasc Dis Res, 2013. **10**(6): p. 472-82.
14. Cines, D.B., et al., *Endothelial cells in physiology and in the pathophysiology of vascular disorders.* Blood, 1998. **91**(10): p. 3527-61.
15. Pozzi, A. and R. Zent, *Regulation of endothelial cell functions by basement membrane- and arachidonic acid-derived products.* Wiley Interdiscip Rev Syst Biol Med, 2009. **1**(2): p. 254-72.
16. Tousoulis, D., et al., *The role of nitric oxide on endothelial function.* Curr Vasc Pharmacol, 2012. **10**(1): p. 4-18.
17. Sitia, S., et al., *From endothelial dysfunction to atherosclerosis.* Autoimmun Rev, 2010. **9**(12): p. 830-4.
18. Patel-Hett, S. and P.A. D'Amore, *Signal transduction in vasculogenesis and developmental angiogenesis.* Int J Dev Biol, 2011. **55**(4-5): p. 353-63.
19. Vokes, S.A. and P.A. Krieg, *Endoderm is required for vascular endothelial tube formation, but not for angioblast specification.* Development, 2002. **129**(3): p. 775-85.
20. Pearson, S., et al., *The stepwise specification of embryonic stem cells to hematopoietic fate is driven by sequential exposure to Bmp4, activin A, bFGF and VEGF.* Development, 2008. **135**(8): p. 1525-35.
21. Marcelo, K.L., L.C. Goldie, and K.K. Hirschi, *Regulation of endothelial cell differentiation and specification.* Circ Res, 2013. **112**(9): p. 1272-87.
22. Hirashima, M., *Regulation of endothelial cell differentiation and arterial specification by VEGF and Notch signaling.* Anat Sci Int, 2009. **84**(3): p. 95-101.
23. Cox, C.M. and T.J. Poole, *Angioblast differentiation is influenced by the local environment: FGF-2 induces angioblasts and patterns vessel formation in the quail embryo.* Dev Dyn, 2000. **218**(2): p. 371-82.
24. Adamo, L., et al., *Biomechanical forces promote embryonic haematopoiesis.* Nature, 2009. **459**(7250): p. 1131-5.

25. Lucitti, J.L., et al., *Vascular remodeling of the mouse yolk sac requires hemodynamic force.* Development, 2007. **134**(18): p. 3317-26.
26. Kelly, M.A. and K.K. Hirschi, *Signaling hierarchy regulating human endothelial cell development.* Arterioscler Thromb Vasc Biol, 2009. **29**(5): p. 718-24.
27. Dyer, M.A., et al., *Indian hedgehog activates hematopoiesis and vasculogenesis and can respecify prospective neurectodermal cell fate in the mouse embryo.* Development, 2001. **128**(10): p. 1717-30.
28. Vokes, S.A., et al., *Hedgehog signaling is essential for endothelial tube formation during vasculogenesis.* Development, 2004. **131**(17): p. 4371-80.
29. Ugwuagbo, K.C., et al., *Prostaglandin E2 promotes embryonic vascular development and maturation in zebrafish.* Biol Open, 2019. **8**(4).
30. Hofmann, J.J. and M.L. Iruela-Arispe, *Notch signaling in blood vessels: who is talking to whom about what?* Circ Res, 2007. **100**(11): p. 1556-68.
31. Coultas, L., K. Chawengsaksophak, and J. Rossant, *Endothelial cells and VEGF in vascular development.* Nature, 2005. **438**(7070): p. 937-45.
32. Carmeliet, P., et al., *Abnormal blood vessel development and lethality in embryos lacking a single VEGF allele.* Nature, 1996. **380**(6573): p. 435-9.
33. Shalaby, F., et al., *Failure of blood-island formation and vasculogenesis in Flk-1-deficient mice.* Nature, 1995. **376**(6535): p. 62-6.
34. Thurston, G., *Role of Angiopoietins and Tie receptor tyrosine kinases in angiogenesis and lymphangiogenesis.* Cell Tissue Res, 2003. **314**(1): p. 61-8.
35. Carlson, T.R., et al., *Cell-autonomous requirement for beta1 integrin in endothelial cell adhesion, migration and survival during angiogenesis in mice.* Development, 2008. **135**(12): p. 2193-202.
36. Goncharov, N.V., et al., *Markers and Biomarkers of Endothelium: When Something Is Rotten in the State.* Oxid Med Cell Longev, 2017. **2017**: p. 9759735.
37. Tzima, E., et al., *A mechanosensory complex that mediates the endothelial cell response to fluid shear stress.* Nature, 2005. **437**(7057): p. 426-31.
38. Vestweber, D., *VE-cadherin: the major endothelial adhesion molecule controlling cellular junctions and blood vessel formation.* Arterioscler Thromb Vasc Biol, 2008. **28**(2): p. 223-32.
39. Rondaij, M.G., et al., *Dynamics and plasticity of Weibel-Palade bodies in endothelial cells.* Arterioscler Thromb Vasc Biol, 2006. **26**(5): p. 1002-7.
40. Utgaard, J.O., et al., *Rapid secretion of prestored interleukin 8 from Weibel-Palade bodies of microvascular endothelial cells.* J Exp Med, 1998. **188**(9): p. 1751-6.
41. Wolff, B., et al., *Endothelial cell "memory" of inflammatory stimulation: human venular endothelial cells store interleukin 8 in Weibel-Palade bodies.* J Exp Med, 1998. **188**(9): p. 1757-62.
42. Ozaka, T., et al., *Weibel-Palade bodies as a storage site of calcitonin gene-related peptide and endothelin-1 in blood vessels of the rat carotid body.* Anat Rec, 1997. **247**(3): p. 388-94.
43. Vischer, U.M. and D.D. Wagner, *CD63 is a component of Weibel-Palade bodies of human endothelial cells.* Blood, 1993. **82**(4): p. 1184-91.
44. Fiedler, U., et al., *The Tie-2 ligand angiopoietin-2 is stored in and rapidly released upon stimulation from endothelial cell Weibel-Palade bodies.* Blood, 2004. **103**(11): p. 4150-6.
45. Huber, D., et al., *Tissue-type plasminogen activator (t-PA) is stored in Weibel-Palade bodies in human endothelial cells both in vitro and in vivo.* Blood, 2002. **99**(10): p. 3637-45.
46. Flaherty, J.T., et al., *Endothelial nuclear patterns in the canine arterial tree with particular reference to hemodynamic events.* Circ Res, 1972. **30**(1): p. 23-33.
47. Alberts, B., *Molecular biology of the cell*. 4th ed. 2002, New York: Garland Science. xxxiv, 1548 p.
48. Bazzoni, G. and E. Dejana, *Endothelial cell-to-cell junctions: molecular organization and role in vascular homeostasis.* Physiol Rev, 2004. **84**(3): p. 869-901.

49. Dvorak, A.M., et al., *The vesiculo-vacuolar organelle (VVO): a distinct endothelial cell structure that provides a transcellular pathway for macromolecular extravasation.* J Leukoc Biol, 1996. **59**(1): p. 100-15.
50. Balda, M.S. and K. Matter, *Tight junctions at a glance.* J Cell Sci, 2008. **121**(Pt 22): p. 3677-82.
51. Krause, G., et al., *Structure and function of claudins.* Biochim Biophys Acta, 2008. **1778**(3): p. 631-45.
52. Cereijido, M., et al., *Tight junction and polarity interaction in the transporting epithelial phenotype.* Biochim Biophys Acta, 2008. **1778**(3): p. 770-93.
53. Bradfield, P.F., et al., *JAM family and related proteins in leukocyte migration (Vestweber series).* Arterioscler Thromb Vasc Biol, 2007. **27**(10): p. 2104-12.
54. Ebnet, K., et al., *Junctional adhesion molecules (JAMs): more molecules with dual functions?* J Cell Sci, 2004. **117**(Pt 1): p. 19-29.
55. Gonzalez-Mariscal, L., S. Lechuga, and E. Garay, *Role of tight junctions in cell proliferation and cancer.* Prog Histochem Cytochem, 2007. **42**(1): p. 1-57.
56. Wang, Z., et al., *The second loop of occludin is required for suppression of Raf1-induced tumor growth.* Oncogene, 2005. **24**(27): p. 4412-20.
57. Vestweber, D., et al., *Cell adhesion dynamics at endothelial junctions: VE-cadherin as a major player.* Trends Cell Biol, 2009. **19**(1): p. 8-15.
58. Weiss, E.E., et al., *Vinculin is part of the cadherin-catenin junctional complex: complex formation between alpha-catenin and vinculin.* J Cell Biol, 1998. **141**(3): p. 755-64.
59. Vestweber, D., A. Broermann, and D. Schulte, *Control of endothelial barrier function by regulating vascular endothelial-cadherin.* Curr Opin Hematol, 2010. **17**(3): p. 230-6.
60. Orsenigo, F., et al., *Phosphorylation of VE-cadherin is modulated by haemodynamic forces and contributes to the regulation of vascular permeability in vivo.* Nat Commun, 2012. **3**: p. 1208.
61. Gavard, J., V. Patel, and J.S. Gutkind, *Angiopoietin-1 prevents VEGF-induced endothelial permeability by sequestering Src through mDia.* Dev Cell, 2008. **14**(1): p. 25-36.
62. Hatanaka, K., et al., *Fibroblast growth factor signaling potentiates VE-cadherin stability at adherens junctions by regulating SHP2.* PLoS One, 2012. **7**(5): p. e37600.
63. Busse, R.M., Alexander; Fleming, Ingrid; Hecker, Markus, *Mechanisms of Nitric Oxide Release From the Vascular Endothelium.[Miscellaneous Article].* Circulation, 1993. **Volume 87(5S)**(Volume 87(5S) Supplement 2, May 1993, pp V18-V25).
64. Furchgott, R.F. and J.V. Zawadzki, *The obligatory role of endothelial cells in the relaxation of arterial smooth muscle by acetylcholine.* Nature, 1980. **288**(5789): p. 373-6.
65. Rubanyi, G.M., J.C. Romero, and P.M. Vanhoutte, *Flow-induced release of endothelium-derived relaxing factor.* Am J Physiol, 1986. **250**(6 Pt 2): p. H1145-9.
66. Forstermann, U. and W.C. Sessa, *Nitric oxide synthases: regulation and function.* Eur Heart J, 2012. **33**(7): p. 829-37, 837a-837d.
67. Rapoport, R.M., M.B. Draznin, and F. Murad, *Endothelium-dependent relaxation in rat aorta may be mediated through cyclic GMP-dependent protein phosphorylation.* Nature, 1983. **306**(5939): p. 174-6.
68. Durand, M.J. and D.D. Gutterman, *Diversity in mechanisms of endothelium-dependent vasodilation in health and disease.* Microcirculation, 2013. **20**(3): p. 239-47.
69. Radomski, M.W., R.M. Palmer, and S. Moncada, *The anti-aggregating properties of vascular endothelium: interactions between prostacyclin and nitric oxide.* Br J Pharmacol, 1987. **92**(3): p. 639-46.
70. Kubes, P., M. Suzuki, and D.N. Granger, *Nitric oxide: an endogenous modulator of leukocyte adhesion.* Proc Natl Acad Sci U S A, 1991. **88**(11): p. 4651-5.
71. Moncada, S., E.A. Higgs, and J.R. Vane, *Human arterial and venous tissues generate prostacyclin (prostaglandin x), a potent inhibitor of platelet aggregation.* Lancet, 1977. **1**(8001): p. 18-20.

72. Sans, M., et al., *VCAM-1 and ICAM-1 mediate leukocyte-endothelial cell adhesion in rat experimental colitis.* Gastroenterology, 1999. **116**(4): p. 874-83.
73. Hassan, M.I., A. Saxena, and F. Ahmad, *Structure and function of von Willebrand factor.* Blood Coagul Fibrinolysis, 2012. **23**(1): p. 11-22.
74. Andrews, R.K. and M.C. Berndt, *Platelet physiology and thrombosis.* Thromb Res, 2004. **114**(5-6): p. 447-53.
75. Yun, S.H., et al., *Platelet Activation: The Mechanisms and Potential Biomarkers.* Biomed Res Int, 2016. **2016**: p. 9060143.
76. Starke, R.D., et al., *Endothelial von Willebrand factor regulates angiogenesis.* Blood, 2011. **117**(3): p. 1071-80.
77. Smith, S.A., R.J. Travers, and J.H. Morrissey, *How it all starts: Initiation of the clotting cascade.* Crit Rev Biochem Mol Biol, 2015. **50**(4): p. 326-36.
78. Palta, S., R. Saroa, and A. Palta, *Overview of the coagulation system.* Indian J Anaesth, 2014. **58**(5): p. 515-23.
79. Drake, T.A., J.H. Morrissey, and T.S. Edgington, *Selective cellular expression of tissue factor in human tissues. Implications for disorders of hemostasis and thrombosis.* Am J Pathol, 1989. **134**(5): p. 1087-97.
80. Maroney, S.A., et al., *Comparison of the inhibitory activities of human tissue factor pathway inhibitor (TFPI)alpha and TFPIbeta.* J Thromb Haemost, 2013. **11**(5): p. 911-8.
81. Girard, T.J., et al., *Functional significance of the Kunitz-type inhibitory domains of lipoprotein-associated coagulation inhibitor.* Nature, 1989. **338**(6215): p. 518-20.
82. Baugh, R.J., G.J. Broze, Jr., and S. Krishnaswamy, *Regulation of extrinsic pathway factor Xa formation by tissue factor pathway inhibitor.* J Biol Chem, 1998. **273**(8): p. 4378-86.
83. Wood, J.P., et al., *Biology of tissue factor pathway inhibitor.* Blood, 2014. **123**(19): p. 2934-43.
84. Barnes, M.J. and R.W. Farndale, *Collagens and atherosclerosis.* Exp Gerontol, 1999. **34**(4): p. 513-25.
85. Montecucco, F. and F. Mach, *Common inflammatory mediators orchestrate pathophysiological processes in rheumatoid arthritis and atherosclerosis.* Rheumatology (Oxford), 2009. **48**(1): p. 11-22.
86. Tanner, F.C., et al., *Nitric oxide modulates expression of cell cycle regulatory proteins: a cytostatic strategy for inhibition of human vascular smooth muscle cell proliferation.* Circulation, 2000. **101**(16): p. 1982-9.
87. Schwartz, B.G., et al., *The endothelial cell in health and disease: its function, dysfunction, measurement and therapy.* Int J Impot Res, 2010. **22**(2): p. 77-90.
88. Rastogi, S., et al., *TNF-alpha response of vascular endothelial and vascular smooth muscle cells involve differential utilization of ASK1 kinase and p73.* Cell Death Differ, 2012. **19**(2): p. 274-83.
89. Woywodt, A., et al., *Circulating endothelial cells: life, death, detachment and repair of the endothelial cell layer.* Nephrol Dial Transplant, 2002. **17**(10): p. 1728-30.
90. Damani, S., et al., *Characterization of circulating endothelial cells in acute myocardial infarction.* Sci Transl Med, 2012. **4**(126): p. 126ra33.
91. Boos, C.J., G.Y. Lip, and A.D. Blann, *Circulating endothelial cells in cardiovascular disease.* J Am Coll Cardiol, 2006. **48**(8): p. 1538-47.
92. Farinacci, M., et al., *Circulating endothelial cells as biomarker for cardiovascular diseases.* Res Pract Thromb Haemost, 2019. **3**(1): p. 49-58.
93. Del Papa, N., et al., *Circulating endothelial cells as a marker of ongoing vascular disease in systemic sclerosis.* Arthritis Rheum, 2004. **50**(4): p. 1296-304.
94. George, F., et al., *Cytofluorometric detection of human endothelial cells in whole blood using S-Endo 1 monoclonal antibody.* J Immunol Methods, 1991. **139**(1): p. 65-75.
95. Leeuwenberg, J.F., et al., *E-selectin and intercellular adhesion molecule-1 are released by activated human endothelial cells in vitro.* Immunology, 1992. **77**(4): p. 543-9.

96. Videm, V. and M. Albrigtsen, *Soluble ICAM-1 and VCAM-1 as markers of endothelial activation.* Scand J Immunol, 2008. **67**(5): p. 523-31.
97. Chen, H., et al., *Cytokine-induced cell surface expression of adhesion molecules in vascular endothelial cells in vitro.* J Tongji Med Univ, 2001. **21**(1): p. 68-71.
98. Gill, M., et al., *Vascular trauma induces rapid but transient mobilization of VEGFR2(+)AC133(+) endothelial precursor cells.* Circ Res, 2001. **88**(2): p. 167-74.
99. Bompais, H., et al., *Human endothelial cells derived from circulating progenitors display specific functional properties compared with mature vessel wall endothelial cells.* Blood, 2004. **103**(7): p. 2577-84.
100. Peichev, M., et al., *Expression of VEGFR-2 and AC133 by circulating human CD34(+) cells identifies a population of functional endothelial precursors.* Blood, 2000. **95**(3): p. 952-8.
101. Asahara, T., et al., *Isolation of putative progenitor endothelial cells for angiogenesis.* Science, 1997. **275**(5302): p. 964-7.
102. Yin, A.H., et al., *AC133, a novel marker for human hematopoietic stem and progenitor cells.* Blood, 1997. **90**(12): p. 5002-12.
103. Beerepoot, L.V., et al., *Increased levels of viable circulating endothelial cells are an indicator of progressive disease in cancer patients.* Ann Oncol, 2004. **15**(1): p. 139-45.
104. Beerepoot, L.V., et al., *Circulating endothelial cells in cancer patients do not express tissue factor.* Cancer Lett, 2004. **213**(2): p. 241-8.
105. Kim, H.K., et al., *Circulating numbers of endothelial progenitor cells in patients with gastric and breast cancer.* Cancer Lett, 2003. **198**(1): p. 83-8.
106. Mancuso, P., et al., *Resting and activated endothelial cells are increased in the peripheral blood of cancer patients.* Blood, 2001. **97**(11): p. 3658-61.
107. Zhang, H., et al., *Circulating endothelial progenitor cells in multiple myeloma: implications and significance.* Blood, 2005. **105**(8): p. 3286-94.
108. Schieber, M. and N.S. Chandel, *ROS function in redox signaling and oxidative stress.* Curr Biol, 2014. **24**(10): p. R453-62.
109. Fleury, C., B. Mignotte, and J.L. Vayssiere, *Mitochondrial reactive oxygen species in cell death signaling.* Biochimie, 2002. **84**(2-3): p. 131-41.
110. Seeger, W., et al., *Hydrogen peroxide-induced increase in lung endothelial and epithelial permeability--effect of adenylate cyclase stimulation and phosphodiesterase inhibition.* Microvasc Res, 1995. **50**(1): p. 1-17.
111. Barnard, M.L. and S. Matalon, *Mechanisms of extracellular reactive oxygen species injury to the pulmonary microvasculature.* J Appl Physiol (1985), 1992. **72**(5): p. 1724-9.
112. Hotter, G., et al., *Free radical enhancement promotes leucocyte recruitment through a PAF and LTB4 dependent mechanism.* Free Radic Biol Med, 1997. **22**(6): p. 947-54.
113. Scalia, R. and A.M. Lefer, *In vivo regulation of PECAM-1 activity during acute endothelial dysfunction in the rat mesenteric microvasculature.* J Leukoc Biol, 1998. **64**(2): p. 163-9.
114. Peterson, T.E., et al., *Opposing effects of reactive oxygen species and cholesterol on endothelial nitric oxide synthase and endothelial cell caveolae.* Circ Res, 1999. **85**(1): p. 29-37.
115. Lubos, E., D.E. Handy, and J. Loscalzo, *Role of oxidative stress and nitric oxide in atherothrombosis.* Front Biosci, 2008. **13**: p. 5323-44.
116. Li, H., S. Horke, and U. Forstermann, *Vascular oxidative stress, nitric oxide and atherosclerosis.* Atherosclerosis, 2014. **237**(1): p. 208-19.
117. Stocker, R. and J.F. Keaney, Jr., *Role of oxidative modifications in atherosclerosis.* Physiol Rev, 2004. **84**(4): p. 1381-478.
118. Hadi, H.A., C.S. Carr, and J. Al Suwaidi, *Endothelial dysfunction: cardiovascular risk factors, therapy, and outcome.* Vasc Health Risk Manag, 2005. **1**(3): p. 183-98.
119. Attwell, D., et al., *What is a pericyte?* J Cereb Blood Flow Metab, 2016. **36**(2): p. 451-5.
120. Coon, B.G., et al., *Intramembrane binding of VE-cadherin to VEGFR2 and VEGFR3 assembles the endothelial mechanosensory complex.* J Cell Biol, 2015. **208**(7): p. 975-86.

121. Deng, D.X., et al., *Differences in vascular bed disease susceptibility reflect differences in gene expression response to atherogenic stimuli.* Circ Res, 2006. **98**(2): p. 200-8.
122. Swerlick, R.A., et al., *Human dermal microvascular endothelial but not human umbilical vein endothelial cells express CD36 in vivo and in vitro.* J Immunol, 1992. **148**(1): p. 78-83.
123. Girard, J.P. and T.A. Springer, *High endothelial venules (HEVs): specialized endothelium for lymphocyte migration.* Immunol Today, 1995. **16**(9): p. 449-57.
124. Sowa, G., *Caveolae, caveolins, cavins, and endothelial cell function: new insights.* Front Physiol, 2012. **2**: p. 120.
125. Simionescu, M., A. Gafencu, and F. Antohe, *Transcytosis of plasma macromolecules in endothelial cells: a cell biological survey.* Microsc Res Tech, 2002. **57**(5): p. 269-88.
126. Bendayan, M., *Morphological and cytochemical aspects of capillary permeability.* Microsc Res Tech, 2002. **57**(5): p. 327-49.
127. Aird, W.C., *Phenotypic heterogeneity of the endothelium: I. Structure, function, and mechanisms.* Circ Res, 2007. **100**(2): p. 158-73.
128. Jackson, C.J. and M. Nguyen, *Human microvascular endothelial cells differ from macrovascular endothelial cells in their expression of matrix metalloproteinases.* Int J Biochem Cell Biol, 1997. **29**(10): p. 1167-77.
129. Dvorak, A.M. and D. Feng, *The vesiculo-vacuolar organelle (VVO). A new endothelial cell permeability organelle.* J Histochem Cytochem, 2001. **49**(4): p. 419-32.
130. Dvorak, H.F., et al., *Vascular permeability factor/vascular endothelial growth factor, microvascular hyperpermeability, and angiogenesis.* Am J Pathol, 1995. **146**(5): p. 1029-39.
131. Siow, R.C., *Culture of human endothelial cells from umbilical veins.* Methods Mol Biol, 2012. **806**: p. 265-74.
132. Bouis, D., et al., *Endothelium in vitro: a review of human vascular endothelial cell lines for blood vessel-related research.* Angiogenesis, 2001. **4**(2): p. 91-102.
133. Durr, E., et al., *Direct proteomic mapping of the lung microvascular endothelial cell surface in vivo and in cell culture.* Nat Biotechnol, 2004. **22**(8): p. 985-92.
134. Lacorre, D.A., et al., *Plasticity of endothelial cells: rapid dedifferentiation of freshly isolated high endothelial venule endothelial cells outside the lymphoid tissue microenvironment.* Blood, 2004. **103**(11): p. 4164-72.
135. Gahmberg, C.G., et al., *Regulation of integrin activity and signalling.* Biochim Biophys Acta, 2009. **1790**(6): p. 431-44.
136. Takada, Y., X. Ye, and S. Simon, *The integrins.* Genome Biol, 2007. **8**(5): p. 215.
137. Arnaout, M.A., B. Mahalingam, and J.P. Xiong, *Integrin structure, allostery, and bidirectional signaling.* Annu Rev Cell Dev Biol, 2005. **21**: p. 381-410.
138. Alique, M., et al., *Integrin-linked kinase plays a key role in the regulation of angiotensin II-induced renal inflammation.* Clin Sci (Lond), 2014. **127**(1): p. 19-31.
139. Emsley, J., et al., *Structural basis of collagen recognition by integrin alpha2beta1.* Cell, 2000. **101**(1): p. 47-56.
140. Santala, P. and J. Heino, *Regulation of integrin-type cell adhesion receptors by cytokines.* J Biol Chem, 1991. **266**(34): p. 23505-9.
141. Bennett, J.S., *Structure and function of the platelet integrin alphaIIbbeta3.* J Clin Invest, 2005. **115**(12): p. 3363-9.
142. Hynes, R.O., *Integrins: bidirectional, allosteric signaling machines.* Cell, 2002. **110**(6): p. 673-87.
143. Arnaout, M.A., *Biology and structure of leukocyte beta 2 integrins and their role in inflammation.* F1000Res, 2016. **5**.
144. Hall, D.E., et al., *The alpha 1/beta 1 and alpha 6/beta 1 integrin heterodimers mediate cell attachment to distinct sites on laminin.* J Cell Biol, 1990. **110**(6): p. 2175-84.
145. Elices, M.J. and M.E. Hemler, *The human integrin VLA-2 is a collagen receptor on some cells and a collagen/laminin receptor on others.* Proc Natl Acad Sci U S A, 1989. **86**(24): p. 9906-10.

146. Fassler, R. and M. Meyer, *Consequences of lack of beta 1 integrin gene expression in mice.* Genes Dev, 1995. **9**(15): p. 1896-908.
147. Lei, L., et al., *Endothelial expression of beta1 integrin is required for embryonic vascular patterning and postnatal vascular remodeling.* Mol Cell Biol, 2008. **28**(2): p. 794-802.
148. Gardner, H., et al., *Deletion of integrin alpha 1 by homologous recombination permits normal murine development but gives rise to a specific deficit in cell adhesion.* Dev Biol, 1996. **175**(2): p. 301-13.
149. Pozzi, A., et al., *Elevated matrix metalloprotease and angiostatin levels in integrin alpha 1 knockout mice cause reduced tumor vascularization.* Proc Natl Acad Sci U S A, 2000. **97**(5): p. 2202-7.
150. Blumbach, K., et al., *Dwarfism in mice lacking collagen-binding integrins alpha2beta1 and alpha11beta1 is caused by severely diminished IGF-1 levels.* J Biol Chem, 2012. **287**(9): p. 6431-40.
151. Schwartz, M.A. and R.K. Assoian, *Integrins and cell proliferation: regulation of cyclin-dependent kinases via cytoplasmic signaling pathways.* J Cell Sci, 2001. **114**(Pt 14): p. 2553-60.
152. Assoian, R.K., *Anchorage-dependent cell cycle progression.* J Cell Biol, 1997. **136**(1): p. 1-4.
153. Bengtsson, T., et al., *Loss of alpha10beta1 integrin expression leads to moderate dysfunction of growth plate chondrocytes.* J Cell Sci, 2005. **118**(Pt 5): p. 929-36.
154. Schulz, J.N., et al., *Reduced granulation tissue and wound strength in the absence of alpha11beta1 integrin.* J Invest Dermatol, 2015. **135**(5): p. 1435-1444.
155. Popova, S.N., et al., *Alpha11 beta1 integrin-dependent regulation of periodontal ligament function in the erupting mouse incisor.* Mol Cell Biol, 2007. **27**(12): p. 4306-16.
156. Garmy-Susini, B. and J.A. Varner, *Roles of integrins in tumor angiogenesis and lymphangiogenesis.* Lymphat Res Biol, 2008. **6**(3-4): p. 155-63.
157. Senger, D.R., et al., *Angiogenesis promoted by vascular endothelial growth factor: regulation through alpha1beta1 and alpha2beta1 integrins.* Proc Natl Acad Sci U S A, 1997. **94**(25): p. 13612-7.
158. San Antonio, J.D., et al., *A key role for the integrin alpha2beta1 in experimental and developmental angiogenesis.* Am J Pathol, 2009. **175**(3): p. 1338-47.
159. Niland, S. and J.A. Eble, *Integrin-mediated cell-matrix interaction in physiological and pathological blood vessel formation.* J Oncol, 2012. **2012**: p. 125278.
160. Senger, D.R., et al., *The alpha(1)beta(1) and alpha(2)beta(1) integrins provide critical support for vascular endothelial growth factor signaling, endothelial cell migration, and tumor angiogenesis.* Am J Pathol, 2002. **160**(1): p. 195-204.
161. Byzova, T.V., et al., *A mechanism for modulation of cellular responses to VEGF: activation of the integrins.* Mol Cell, 2000. **6**(4): p. 851-60.
162. Gardner, H., et al., *Absence of integrin alpha1beta1 in the mouse causes loss of feedback regulation of collagen synthesis in normal and wounded dermis.* J Cell Sci, 1999. **112 (Pt 3)**: p. 263-72.
163. Boudjadi, S., J.C. Carrier, and J.F. Beaulieu, *Integrin alpha1 subunit is up-regulated in colorectal cancer.* Biomark Res, 2013. **1**(1): p. 16.
164. Boudjadi, S., et al., *Involvement of the Integrin alpha1beta1 in the Progression of Colorectal Cancer.* Cancers (Basel), 2017. **9**(8).
165. Marcinkiewicz, C., et al., *Obtustatin: a potent selective inhibitor of alpha1beta1 integrin in vitro and angiogenesis in vivo.* Cancer Res, 2003. **63**(9): p. 2020-3.
166. Ibaragi, S., et al., *Induction of MMP-13 expression in bone-metastasizing cancer cells by type I collagen through integrin alpha1beta1 and alpha2beta1-p38 MAPK signaling.* Anticancer Res, 2011. **31**(4): p. 1307-13.
167. Sottnik, J.L., et al., *Integrin alpha2beta 1 (alpha2beta1) promotes prostate cancer skeletal metastasis.* Clin Exp Metastasis, 2013. **30**(5): p. 569-78.

168. Zeltz, C. and D. Gullberg, *The integrin-collagen connection--a glue for tissue repair?* J Cell Sci, 2016. **129**(4): p. 653-64.
169. Munksgaard Thoren, M., et al., *Integrin alpha10, a Novel Therapeutic Target in Glioblastoma, Regulates Cell Migration, Proliferation, and Survival.* Cancers (Basel), 2019. **11**(4).
170. Wenke, A.K., et al., *Expression of integrin alpha10 is induced in malignant melanoma.* Cell Oncol, 2007. **29**(5): p. 373-86.
171. Okada, T. and S. Singer, *Integrin-alpha10 drives tumorigenesis in sarcoma.* Oncoscience, 2017. **4**(3-4): p. 31-32.
172. Shen, B., et al., *Integrin alpha11 is an Osteolectin receptor and is required for the maintenance of adult skeletal bone mass.* Elife, 2019. **8**.
173. Honda, E., K. Yoshida, and H. Munakata, *Transforming growth factor-beta upregulates the expression of integrin and related proteins in MRC-5 human myofibroblasts.* Tohoku J Exp Med, 2010. **220**(4): p. 319-27.
174. Carracedo, S., et al., *The fibroblast integrin alpha11beta1 is induced in a mechanosensitive manner involving activin A and regulates myofibroblast differentiation.* J Biol Chem, 2010. **285**(14): p. 10434-45.
175. Talior-Volodarsky, I., et al., *alpha11 integrin stimulates myofibroblast differentiation in diabetic cardiomyopathy.* Cardiovasc Res, 2012. **96**(2): p. 265-75.
176. Bansal, R., et al., *Integrin alpha 11 in the regulation of the myofibroblast phenotype: implications for fibrotic diseases.* Exp Mol Med, 2017. **49**(11): p. e396.
177. Popov, C., et al., *Integrins alpha2beta1 and alpha11beta1 regulate the survival of mesenchymal stem cells on collagen I.* Cell Death Dis, 2011. **2**: p. e186.
178. Huang, N.F., et al., *The modulation of endothelial cell morphology, function, and survival using anisotropic nanofibrillar collagen scaffolds.* Biomaterials, 2013. **34**(16): p. 4038-47.
179. Senger, D.R. and G.E. Davis, *Angiogenesis.* Cold Spring Harb Perspect Biol, 2011. **3**(8): p. a005090.
180. Neve, A., et al., *Extracellular matrix modulates angiogenesis in physiological and pathological conditions.* Biomed Res Int, 2014. **2014**: p. 756078.
181. Riikonen, T., et al., *Integrin alpha 2 beta 1 is a positive regulator of collagenase (MMP-1) and collagen alpha 1(I) gene expression.* J Biol Chem, 1995. **270**(22): p. 13548-52.
182. Ronziere, M.C., et al., *Integrin alpha1beta1 mediates collagen induction of MMP-13 expression in MC615 chondrocytes.* Biochim Biophys Acta, 2005. **1746**(1): p. 55-64.
183. Furumatsu, T., et al., *Endostatin inhibits adhesion of endothelial cells to collagen I via alpha(2)beta(1) integrin, a possible cause of prevention of chondrosarcoma growth.* J Biochem, 2002. **131**(4): p. 619-26.
184. Boosani, C.S., et al., *Inhibitory effects of arresten on bFGF-induced proliferation, migration, and matrix metalloproteinase-2 activation in mouse retinal endothelial cells.* Curr Eye Res, 2010. **35**(1): p. 45-55.
185. Nyberg, P., et al., *Characterization of the anti-angiogenic properties of arresten, an alpha1beta1 integrin-dependent collagen-derived tumor suppressor.* Exp Cell Res, 2008. **314**(18): p. 3292-305.
186. Brodsky, B. and J.A.M. Ramshaw, *The collagen triple-helix structure.* Matrix Biology, 1997. **15**(8): p. 545-554.
187. Gordon, M.K. and R.A. Hahn, *Collagens.* Cell Tissue Res, 2010. **339**(1): p. 247-57.
188. Heikkinen, A., H. Tu, and T. Pihlajaniemi, *Collagen XIII: a type II transmembrane protein with relevance to musculoskeletal tissues, microvessels and inflammation.* Int J Biochem Cell Biol, 2012. **44**(5): p. 714-7.
189. Franzke, C.W., et al., *Collagenous transmembrane proteins: collagen XVII as a prototype.* Matrix Biol, 2003. **22**(4): p. 299-309.

190. Dennis, J., et al., *Collagen XIII induced in vascular endothelium mediates alpha1beta1 integrin-dependent transmigration of monocytes in renal fibrosis.* Am J Pathol, 2010. **177**(5): p. 2527-40.
191. Gialeli, C., A.D. Theocharis, and N.K. Karamanos, *Roles of matrix metalloproteinases in cancer progression and their pharmacological targeting.* FEBS J, 2011. **278**(1): p. 16-27.
192. Hughes, C.S., L.M. Postovit, and G.A. Lajoie, *Matrigel: a complex protein mixture required for optimal growth of cell culture.* Proteomics, 2010. **10**(9): p. 1886-90.
193. Vukicevic, S., et al., *Identification of multiple active growth factors in basement membrane Matrigel suggests caution in interpretation of cellular activity related to extracellular matrix components.* Exp Cell Res, 1992. **202**(1): p. 1-8.
194. Ridley, A.J., et al., *Cell migration: integrating signals from front to back.* Science, 2003. **302**(5651): p. 1704-9.
195. Holmes, D.I. and I. Zachary, *The vascular endothelial growth factor (VEGF) family: angiogenic factors in health and disease.* Genome Biol, 2005. **6**(2): p. 209.
196. Yamaguchi, H. and J. Condeelis, *Regulation of the actin cytoskeleton in cancer cell migration and invasion.* Biochim Biophys Acta, 2007. **1773**(5): p. 642-52.
197. Huttenlocher, A. and A.R. Horwitz, *Integrins in cell migration.* Cold Spring Harb Perspect Biol, 2011. **3**(9): p. a005074.
198. Haralabopoulos, G.C., et al., *Inhibitors of basement membrane collagen synthesis prevent endothelial cell alignment in matrigel in vitro and angiogenesis in vivo.* Lab Invest, 1994. **71**(4): p. 575-82.
199. Miyake, M., et al., *Angiogenin promotes tumoral growth and angiogenesis by regulating matrix metallopeptidase-2 expression via the ERK1/2 pathway.* Oncogene, 2015. **34**(7): p. 890-901.
200. Campbell, N.E., et al., *Extracellular matrix proteins and tumor angiogenesis.* J Oncol, 2010. **2010**: p. 586905.
201. Wong, B.W., et al., *Endothelial cell metabolism in health and disease: impact of hypoxia.* EMBO J, 2017. **36**(15): p. 2187-2203.
202. Forsythe, J.A., et al., *Activation of vascular endothelial growth factor gene transcription by hypoxia-inducible factor 1.* Mol Cell Biol, 1996. **16**(9): p. 4604-13.
203. St Croix, B., et al., *Genes expressed in human tumor endothelium.* Science, 2000. **289**(5482): p. 1197-202.
204. Brown, M.C., et al., *Angiostatic activity of obtustatin as alpha1beta1 integrin inhibitor in experimental melanoma growth.* Int J Cancer, 2008. **123**(9): p. 2195-203.
205. Framson, P.E. and E.H. Sage, *SPARC and tumor growth: where the seed meets the soil?* J Cell Biochem, 2004. **92**(4): p. 679-90.
206. Bradshaw, A.D. and E.H. Sage, *SPARC, a matricellular protein that functions in cellular differentiation and tissue response to injury.* J Clin Invest, 2001. **107**(9): p. 1049-54.
207. Murphy-Ullrich, J.E., et al., *SPARC mediates focal adhesion disassembly in endothelial cells through a follistatin-like region and the Ca(2+)-binding EF-hand.* J Cell Biochem, 1995. **57**(2): p. 341-50.
208. Brekken, R.A., et al., *Enhanced growth of tumors in SPARC null mice is associated with changes in the ECM.* J Clin Invest, 2003. **111**(4): p. 487-95.
209. Kamihagi, K., et al., *Osteonectin/SPARC regulates cellular secretion rates of fibronectin and laminin extracellular matrix proteins.* Biochem Biophys Res Commun, 1994. **200**(1): p. 423-8.
210. Alkabie, S., et al., *SPARC expression by cerebral microvascular endothelial cells in vitro and its influence on blood-brain barrier properties.* J Neuroinflammation, 2016. **13**(1): p. 225.
211. Kato, Y., et al., *Induction of SPARC by VEGF in human vascular endothelial cells.* Biochem Biophys Res Commun, 2001. **287**(2): p. 422-6.
212. Goldblum, S.E., et al., *SPARC (secreted protein acidic and rich in cysteine) regulates endothelial cell shape and barrier function.* Proc Natl Acad Sci U S A, 1994. **91**(8): p. 3448-52.

213. Mendis, D.B., G.O. Ivy, and I.R. Brown, *SPARC/osteonectin mRNA is induced in blood vessels following injury to the adult rat cerebral cortex.* Neurochem Res, 1998. **23**(8): p. 1117-23.
214. Vogel, W., et al., *The discoidin domain receptor tyrosine kinases are activated by collagen.* Mol Cell, 1997. **1**(1): p. 13-23.
215. Itoh, Y., *Discoidin domain receptors: Microenvironment sensors that promote cellular migration and invasion.* Cell Adh Migr, 2018. **12**(4): p. 378-385.
216. Xu, H., et al., *Collagen binding specificity of the discoidin domain receptors: binding sites on collagens II and III and molecular determinants for collagen IV recognition by DDR1.* Matrix Biol, 2011. **30**(1): p. 16-26.
217. Shitomi, Y., et al., *ADAM10 controls collagen signaling and cell migration on collagen by shedding the ectodomain of discoidin domain receptor 1 (DDR1).* Mol Biol Cell, 2015. **26**(4): p. 659-73.
218. Olaso, E., et al., *Discoidin domain receptor 2 regulates fibroblast proliferation and migration through the extracellular matrix in association with transcriptional activation of matrix metalloproteinase-2.* J Biol Chem, 2002. **277**(5): p. 3606-13.
219. Chen, S.C., et al., *Hypoxia induces discoidin domain receptor-2 expression via the p38 pathway in vascular smooth muscle cells to increase their migration.* Biochem Biophys Res Commun, 2008. **374**(4): p. 662-7.
220. Xu, H., et al., *Discoidin domain receptors promote alpha1beta1- and alpha2beta1-integrin mediated cell adhesion to collagen by enhancing integrin activation.* PLoS One, 2012. **7**(12): p. e52209.
221. Nemeth, K., et al., *The role of osteoclast-associated receptor in osteoimmunology.* J Immunol, 2011. **186**(1): p. 13-8.
222. Barrow, A.D., et al., *OSCAR is a collagen receptor that costimulates osteoclastogenesis in DAP12-deficient humans and mice.* J Clin Invest, 2011. **121**(9): p. 3505-16.
223. Merck, E., et al., *OSCAR is an FcRgamma-associated receptor that is expressed by myeloid cells and is involved in antigen presentation and activation of human dendritic cells.* Blood, 2004. **104**(5): p. 1386-95.
224. Goettsch, C., et al., *The osteoclast-associated receptor (OSCAR) is a novel receptor regulated by oxidized low-density lipoprotein in human endothelial cells.* Endocrinology, 2011. **152**(12): p. 4915-26.
225. Tang, X., et al., *Leukocyte-associated Ig-like receptor-1-deficient mice have an altered immune cell phenotype.* J Immunol, 2012. **188**(2): p. 548-58.
226. Meyaard, L., *The inhibitory collagen receptor LAIR-1 (CD305).* J Leukoc Biol, 2008. **83**(4): p. 799-803.
227. Meyaard, L., et al., *LAIR-1, a novel inhibitory receptor expressed on human mononuclear leukocytes.* Immunity, 1997. **7**(2): p. 283-90.
228. Jandrot-Perrus, M., et al., *Cloning, characterization, and functional studies of human and mouse glycoprotein VI: a platelet-specific collagen receptor from the immunoglobulin superfamily.* Blood, 2000. **96**(5): p. 1798-807.
229. Kuijpers, M.J., et al., *Complementary roles of glycoprotein VI and alpha2beta1 integrin in collagen-induced thrombus formation in flowing whole blood ex vivo.* FASEB J, 2003. **17**(6): p. 685-7.
230. Rohlenova, K., et al., *Endothelial Cell Metabolism in Health and Disease.* Trends Cell Biol, 2018. **28**(3): p. 224-236.
231. Shoulders, M.D. and R.T. Raines, *Collagen structure and stability.* Annual review of biochemistry, 2009. **78**: p. 929-958.
232. Farndale, R.W., et al., *Cell-collagen interactions: the use of peptide Toolkits to investigate collagen-receptor interactions.* Biochem Soc Trans, 2008. **36**(Pt 2): p. 241-50.
233. Lisman, T., et al., *A single high-affinity binding site for von Willebrand factor in collagen III, identified using synthetic triple-helical peptides.* Blood, 2006. **108**(12): p. 3753-6.

234. Farndale, R.W., *Collagen-binding proteins: insights from the Collagen Toolkits.* Essays Biochem, 2019.
235. Knight, C.G., et al., *The collagen-binding A-domains of integrins alpha(1)beta(1) and alpha(2)beta(1) recognize the same specific amino acid sequence, GFOGER, in native (triple-helical) collagens.* J Biol Chem, 2000. **275**(1): p. 35-40.
236. Tiger, C.F., et al., *alpha11beta1 integrin is a receptor for interstitial collagens involved in cell migration and collagen reorganization on mesenchymal nonmuscle cells.* Dev Biol, 2001. **237**(1): p. 116-29.
237. Naci, D. and F. Aoudjit, *Alpha2beta1 integrin promotes T cell survival and migration through the concomitant activation of ERK/Mcl-1 and p38 MAPK pathways.* Cell Signal, 2014. **26**(9): p. 2008-15.
238. Humphries, J.D., A. Byron, and M.J. Humphries, *Integrin ligands at a glance.* J Cell Sci, 2006. **119**(Pt 19): p. 3901-3.
239. Rich, R.L., et al., *Trench-shaped binding sites promote multiple classes of interactions between collagen and the adherence receptors, alpha(1)beta(1) integrin and Staphylococcus aureus cna MSCRAMM.* J Biol Chem, 1999. **274**(35): p. 24906-13.
240. Lahti, M., et al., *Structure of collagen receptor integrin alpha(1)I domain carrying the activating mutation E317A.* J Biol Chem, 2011. **286**(50): p. 43343-51.
241. Zhang, W.M., et al., *alpha 11beta 1 integrin recognizes the GFOGER sequence in interstitial collagens.* J Biol Chem, 2003. **278**(9): p. 7270-7.
242. Davidenko, N., et al., *Evaluation of cell binding to collagen and gelatin: a study of the effect of 2D and 3D architecture and surface chemistry.* J Mater Sci Mater Med, 2016. **27**(10): p. 148.
243. Hamaia, S.W., et al., *Unique charge-dependent constraint on collagen recognition by integrin alpha10beta1.* Matrix Biol, 2017. **59**: p. 80-94.
244. Goldsmith, E.C., et al., *The collagen receptor DDR2 is expressed during early cardiac development.* Anat Rec (Hoboken), 2010. **293**(5): p. 762-9.
245. Zhang, S., et al., *A host deficiency of discoidin domain receptor 2 (DDR2) inhibits both tumour angiogenesis and metastasis.* J Pathol, 2014. **232**(4): p. 436-48.
246. Roig, B., et al., *Expression of the tyrosine kinase discoidin domain receptor 1 (DDR1) in human central nervous system myelin.* Brain Res, 2010. **1336**: p. 22-9.
247. Bellis, S.L., *Variant glycosylation: an underappreciated regulatory mechanism for beta1 integrins.* Biochim Biophys Acta, 2004. **1663**(1-2): p. 52-60.
248. Gu, J., et al., *Potential roles of N-glycosylation in cell adhesion.* Glycoconj J, 2012. **29**(8-9): p. 599-607.
249. Staudinger, L.A., et al., *Interactions between the discoidin domain receptor 1 and beta1 integrin regulate attachment to collagen.* Biol Open, 2013. **2**(11): p. 1148-59.
250. Tichet, M., et al., *Tumour-derived SPARC drives vascular permeability and extravasation through endothelial VCAM1 signalling to promote metastasis.* Nat Commun, 2015. **6**: p. 6993.
251. Nobes, C.D. and A. Hall, *Rho, rac, and cdc42 GTPases regulate the assembly of multimolecular focal complexes associated with actin stress fibers, lamellipodia, and filopodia.* Cell, 1995. **81**(1): p. 53-62.
252. Guo, W.H. and Y.L. Wang, *Retrograde fluxes of focal adhesion proteins in response to cell migration and mechanical signals.* Mol Biol Cell, 2007. **18**(11): p. 4519-27.
253. Turner, C.E., et al., *Localization of paxillin, a focal adhesion protein, to smooth muscle dense plaques, and the myotendinous and neuromuscular junctions of skeletal muscle.* Exp Cell Res, 1991. **192**(2): p. 651-5.
254. Cypher, C. and P.C. Letourneau, *Identification of cytoskeletal, focal adhesion, and cell adhesion proteins in growth cone particles isolated from developing chick brain.* J Neurosci Res, 1991. **30**(1): p. 259-65.
255. Daidone, I., et al., *Structural and dynamical properties of KTS-disintegrins: A comparison between Obtustatin and Lebestatin.* Biopolymers, 2013. **99**(1): p. 47-54.

256. Paz Moreno-Murciano, M., et al., *NMR solution structure of the non-RGD disintegrin obtustatin.* J Mol Biol, 2003. **329**(1): p. 135-45.
257. Moreno-Murciano, M.P., et al., *Amino acid sequence and homology modeling of obtustatin, a novel non-RGD-containing short disintegrin isolated from the venom of Vipera lebetina obtusa.* Protein Sci, 2003. **12**(2): p. 366-71.
258. Kisiel, D.G., et al., *Structural determinants of the selectivity of KTS-disintegrins for the alpha1beta1 integrin.* FEBS Lett, 2004. **577**(3): p. 478-82.
259. Scarborough, R.M., et al., *Characterization of the integrin specificities of disintegrins isolated from American pit viper venoms.* J Biol Chem, 1993. **268**(2): p. 1058-65.
260. Bolas, G., et al., *Inhibitory effects of recombinant RTS-jerdostatin on integrin alpha1beta1 function during adhesion, migration and proliferation of rat aortic smooth muscle cells and angiogenesis.* Toxicon, 2014. **79**: p. 45-54.
261. Coller, B.S., et al., *Collagen-platelet interactions: evidence for a direct interaction of collagen with platelet GPIa/IIa and an indirect interaction with platelet GPIIb/IIIa mediated by adhesive proteins.* Blood, 1989. **74**(1): p. 182-92.
262. Staniszewska, I., et al., *Interaction of alpha9beta1 integrin with thrombospondin-1 promotes angiogenesis.* Circ Res, 2007. **100**(9): p. 1308-16.
263. Vlahakis, N.E., et al., *The lymphangiogenic vascular endothelial growth factors VEGF-C and -D are ligands for the integrin alpha9beta1.* J Biol Chem, 2005. **280**(6): p. 4544-52.
264. Garmy-Susini, B., et al., *Integrin alpha4beta1-VCAM-1-mediated adhesion between endothelial and mural cells is required for blood vessel maturation.* J Clin Invest, 2005. **115**(6): p. 1542-51.
265. Yousif, L.F., J. Di Russo, and L. Sorokin, *Laminin isoforms in endothelial and perivascular basement membranes.* Cell Adh Migr, 2013. **7**(1): p. 101-10.
266. da Silva, R.G., et al., *Endothelial alpha3beta1-integrin represses pathological angiogenesis and sustains endothelial-VEGF.* Am J Pathol, 2010. **177**(3): p. 1534-48.
267. Languino, L.R., et al., *Endothelial cells use alpha 2 beta 1 integrin as a laminin receptor.* J Cell Biol, 1989. **109**(5): p. 2455-62.
268. Grissa, I., G. Vergnaud, and C. Pourcel, *The CRISPRdb database and tools to display CRISPRs and to generate dictionaries of spacers and repeats.* BMC Bioinformatics, 2007. **8**: p. 172.
269. Richter, C., J.T. Chang, and P.C. Fineran, *Function and regulation of clustered regularly interspaced short palindromic repeats (CRISPR) / CRISPR associated (Cas) systems.* Viruses, 2012. **4**(10): p. 2291-311.
270. Barrangou, R., et al., *CRISPR provides acquired resistance against viruses in prokaryotes.* Science, 2007. **315**(5819): p. 1709-12.
271. Ishino, Y., et al., *Nucleotide sequence of the iap gene, responsible for alkaline phosphatase isozyme conversion in Escherichia coli, and identification of the gene product.* J Bacteriol, 1987. **169**(12): p. 5429-33.
272. Mojica, F.J., et al., *Intervening sequences of regularly spaced prokaryotic repeats derive from foreign genetic elements.* J Mol Evol, 2005. **60**(2): p. 174-82.
273. Pourcel, C., G. Salvignol, and G. Vergnaud, *CRISPR elements in Yersinia pestis acquire new repeats by preferential uptake of bacteriophage DNA, and provide additional tools for evolutionary studies.* Microbiology, 2005. **151**(Pt 3): p. 653-63.
274. Bolotin, A., et al., *Clustered regularly interspaced short palindrome repeats (CRISPRs) have spacers of extrachromosomal origin.* Microbiology, 2005. **151**(Pt 8): p. 2551-61.
275. Jansen, R., et al., *Identification of genes that are associated with DNA repeats in prokaryotes.* Mol Microbiol, 2002. **43**(6): p. 1565-75.
276. Makarova, K.S., et al., *A putative RNA-interference-based immune system in prokaryotes: computational analysis of the predicted enzymatic machinery, functional analogies with eukaryotic RNAi, and hypothetical mechanisms of action.* Biol Direct, 2006. **1**: p. 7.

277. Sapranauskas, R., et al., *The Streptococcus thermophilus CRISPR/Cas system provides immunity in Escherichia coli.* Nucleic Acids Res, 2011. **39**(21): p. 9275-82.
278. Brouns, S.J., et al., *Small CRISPR RNAs guide antiviral defense in prokaryotes.* Science, 2008. **321**(5891): p. 960-4.
279. Jinek, M., et al., *A programmable dual-RNA-guided DNA endonuclease in adaptive bacterial immunity.* Science, 2012. **337**(6096): p. 816-21.
280. Jinek, M., et al., *RNA-programmed genome editing in human cells.* Elife, 2013. **2**: p. e00471.
281. Mali, P., et al., *RNA-guided human genome engineering via Cas9.* Science, 2013. **339**(6121): p. 823-6.
282. Adli, M., *The CRISPR tool kit for genome editing and beyond.* Nat Commun, 2018. **9**(1): p. 1911.
283. Fu, Y., et al., *High-frequency off-target mutagenesis induced by CRISPR-Cas nucleases in human cells.* Nat Biotechnol, 2013. **31**(9): p. 822-6.
284. Hsu, P.D., et al., *DNA targeting specificity of RNA-guided Cas9 nucleases.* Nat Biotechnol, 2013. **31**(9): p. 827-32.
285. Fonfara, I., et al., *The CRISPR-associated DNA-cleaving enzyme Cpf1 also processes precursor CRISPR RNA.* Nature, 2016. **532**(7600): p. 517-21.
286. Gaudelli, N.M., et al., *Programmable base editing of A*T to G*C in genomic DNA without DNA cleavage.* Nature, 2017. **551**(7681): p. 464-471.
287. Billon, P., et al., *CRISPR-Mediated Base Editing Enables Efficient Disruption of Eukaryotic Genes through Induction of STOP Codons.* Mol Cell, 2017. **67**(6): p. 1068-1079 e4.
288. Qi, L.S., et al., *Repurposing CRISPR as an RNA-guided platform for sequence-specific control of gene expression.* Cell, 2013. **152**(5): p. 1173-83.
289. Hilton, I.B., et al., *Epigenome editing by a CRISPR-Cas9-based acetyltransferase activates genes from promoters and enhancers.* Nat Biotechnol, 2015. **33**(5): p. 510-7.
290. Tanenbaum, M.E., et al., *A protein-tagging system for signal amplification in gene expression and fluorescence imaging.* Cell, 2014. **159**(3): p. 635-46.
291. Lino, C.A., et al., *Delivering CRISPR: a review of the challenges and approaches.* Drug Deliv, 2018. **25**(1): p. 1234-1257.
292. Daya, S. and K.I. Berns, *Gene therapy using adeno-associated virus vectors.* Clin Microbiol Rev, 2008. **21**(4): p. 583-93.
293. Ran, F.A., et al., *In vivo genome editing using Staphylococcus aureus Cas9.* Nature, 2015. **520**(7546): p. 186-91.
294. Nasri, M., A. Karimi, and M. Allahbakhshian Farsani, *Production, purification and titration of a lentivirus-based vector for gene delivery purposes.* Cytotechnology, 2014. **66**(6): p. 1031-8.
295. Dana, H., et al., *Molecular Mechanisms and Biological Functions of siRNA.* Int J Biomed Sci, 2017. **13**(2): p. 48-57.
296. Fire, A., et al., *Potent and specific genetic interference by double-stranded RNA in Caenorhabditis elegans.* Nature, 1998. **391**(6669): p. 806-11.
297. Carthew, R.W. and E.J. Sontheimer, *Origins and Mechanisms of miRNAs and siRNAs.* Cell, 2009. **136**(4): p. 642-55.
298. Macrae, I.J., et al., *Structural basis for double-stranded RNA processing by Dicer.* Science, 2006. **311**(5758): p. 195-8.
299. Hoerter, J.A., et al., *siRNA-like double-stranded RNAs are specifically protected against degradation in human cell extract.* PLoS One, 2011. **6**(5): p. e20359.
300. Braasch, D.A., et al., *RNA interference in mammalian cells by chemically-modified RNA.* Biochemistry, 2003. **42**(26): p. 7967-75.
301. Ayala-Fontanez, N., D.C. Soler, and T.S. McCormick, *Current knowledge on psoriasis and autoimmune diseases.* Psoriasis (Auckl), 2016. **6**: p. 7-32.
302. Meredith, J.E., Jr. and M.A. Schwartz, *Integrins, adhesion and apoptosis.* Trends Cell Biol, 1997. **7**(4): p. 146-50.
303. Giancotti, F.G. and E. Ruoslahti, *Integrin signaling.* Science, 1999. **285**(5430): p. 1028-32.

304. Srinivasan, R., et al., *Erk1 and Erk2 regulate endothelial cell proliferation and migration during mouse embryonic angiogenesis.* PLoS One, 2009. **4**(12): p. e8283.
305. Pozzi, A., et al., *Integrin alpha1beta1 mediates a unique collagen-dependent proliferation pathway in vivo.* J Cell Biol, 1998. **142**(2): p. 587-94.
306. Brooks, P.C., et al., *Integrin alpha v beta 3 antagonists promote tumor regression by inducing apoptosis of angiogenic blood vessels.* Cell, 1994. **79**(7): p. 1157-64.
307. Itoh, R.E., et al., *Activation of rac and cdc42 video imaged by fluorescent resonance energy transfer-based single-molecule probes in the membrane of living cells.* Mol Cell Biol, 2002. **22**(18): p. 6582-91.
308. Merlot, S. and R.A. Firtel, *Leading the way: Directional sensing through phosphatidylinositol 3-kinase and other signaling pathways.* J Cell Sci, 2003. **116**(Pt 17): p. 3471-8.
309. Cooper, J.A. and D.A. Schafer, *Control of actin assembly and disassembly at filament ends.* Curr Opin Cell Biol, 2000. **12**(1): p. 97-103.
310. Matsudaira, P., *Actin crosslinking proteins at the leading edge.* Semin Cell Biol, 1994. **5**(3): p. 165-74.
311. Mitchison, T.J. and L.P. Cramer, *Actin-based cell motility and cell locomotion.* Cell, 1996. **84**(3): p. 371-9.
312. Pollard, T.D. and G.G. Borisy, *Cellular motility driven by assembly and disassembly of actin filaments.* Cell, 2003. **112**(4): p. 453-65.
313. Koestler, S.A., et al., *Differentially oriented populations of actin filaments generated in lamellipodia collaborate in pushing and pausing at the cell front.* Nat Cell Biol, 2008. **10**(3): p. 306-13.
314. Alexandrova, A.Y., et al., *Comparative dynamics of retrograde actin flow and focal adhesions: formation of nascent adhesions triggers transition from fast to slow flow.* PLoS One, 2008. **3**(9): p. e3234.
315. Ananthakrishnan, R. and A. Ehrlicher, *The forces behind cell movement.* Int J Biol Sci, 2007. **3**(5): p. 303-17.
316. Hu, K., et al., *Differential transmission of actin motion within focal adhesions.* Science, 2007. **315**(5808): p. 111-5.
317. Worthylake, R.A., et al., *RhoA is required for monocyte tail retraction during transendothelial migration.* J Cell Biol, 2001. **154**(1): p. 147-60.
318. Bray, D., *Mechanical tension produced by nerve cells in tissue culture.* J Cell Sci, 1979. **37**: p. 391-410.
319. Vicente-Manzanares, M., et al., *Regulation of protrusion, adhesion dynamics, and polarity by myosins IIA and IIB in migrating cells.* J Cell Biol, 2007. **176**(5): p. 573-80.
320. Vicente-Manzanares, M., et al., *Non-muscle myosin II takes centre stage in cell adhesion and migration.* Nat Rev Mol Cell Biol, 2009. **10**(11): p. 778-90.
321. Giannone, G., et al., *Periodic lamellipodial contractions correlate with rearward actin waves.* Cell, 2004. **116**(3): p. 431-43.
322. Goeckeler, Z.M., P.C. Bridgman, and R.B. Wysolmerski, *Nonmuscle myosin II is responsible for maintaining endothelial cell basal tone and stress fiber integrity.* Am J Physiol Cell Physiol, 2008. **295**(4): p. C994-1006.
323. Kolega, J., *Asymmetric distribution of myosin IIB in migrating endothelial cells is regulated by a rho-dependent kinase and contributes to tail retraction.* Mol Biol Cell, 2003. **14**(12): p. 4745-57.
324. Lawson, C.D. and K. Burridge, *The on-off relationship of Rho and Rac during integrin-mediated adhesion and cell migration.* Small GTPases, 2014. **5**: p. e27958.
325. Calderwood, D.A., S.J. Shattil, and M.H. Ginsberg, *Integrins and actin filaments: reciprocal regulation of cell adhesion and signaling.* J Biol Chem, 2000. **275**(30): p. 22607-10.
326. Kano, Y., et al., *Macromolecular composition of stress fiber-plasma membrane attachment sites in endothelial cells in situ.* Circ Res, 1996. **79**(5): p. 1000-6.

327. DeMali, K.A., C.A. Barlow, and K. Burridge, *Recruitment of the Arp2/3 complex to vinculin: coupling membrane protrusion to matrix adhesion.* J Cell Biol, 2002. **159**(5): p. 881-91.
328. Huveneers, S. and E.H. Danen, *Adhesion signaling - crosstalk between integrins, Src and Rho.* J Cell Sci, 2009. **122**(Pt 8): p. 1059-69.
329. Kiosses, W.B., et al., *Rac recruits high-affinity integrin alphavbeta3 to lamellipodia in endothelial cell migration.* Nat Cell Biol, 2001. **3**(3): p. 316-20.
330. Moser, M., et al., *Kindlin-3 is essential for integrin activation and platelet aggregation.* Nat Med, 2008. **14**(3): p. 325-30.
331. Tadokoro, S., et al., *Talin binding to integrin beta tails: a final common step in integrin activation.* Science, 2003. **302**(5642): p. 103-6.
332. Calderwood, D.A., et al., *The Talin head domain binds to integrin beta subunit cytoplasmic tails and regulates integrin activation.* J Biol Chem, 1999. **274**(40): p. 28071-4.
333. Seftor, R.E., et al., *Role of the alpha v beta 3 integrin in human melanoma cell invasion.* Proc Natl Acad Sci U S A, 1992. **89**(5): p. 1557-61.
334. Chan, B.M., et al., *In vitro and in vivo consequences of VLA-2 expression on rhabdomyosarcoma cells.* Science, 1991. **251**(5001): p. 1600-2.
335. Lim, C.J., et al., *Integrin-mediated protein kinase A activation at the leading edge of migrating cells.* Mol Biol Cell, 2008. **19**(11): p. 4930-41.
336. Galbraith, C.G., K.M. Yamada, and J.A. Galbraith, *Polymerizing actin fibers position integrins primed to probe for adhesion sites.* Science, 2007. **315**(5814): p. 992-5.
337. Leavesley, D.I., et al., *Integrin beta 1- and beta 3-mediated endothelial cell migration is triggered through distinct signaling mechanisms.* J Cell Biol, 1993. **121**(1): p. 163-70.
338. Pula, G. and A.W. Poole, *Critical roles for the actin cytoskeleton and cdc42 in regulating platelet integrin alpha2beta1.* Platelets, 2008. **19**(3): p. 199-210.
339. Yeh, Y.C., C.Z. Wang, and M.J. Tang, *Discoidin domain receptor 1 activation suppresses alpha2beta1 integrin-dependent cell spreading through inhibition of Cdc42 activity.* J Cell Physiol, 2009. **218**(1): p. 146-56.
340. Olfa, K.Z., et al., *Lebestatin, a disintegrin from Macrovipera venom, inhibits integrin-mediated cell adhesion, migration and angiogenesis.* Lab Invest, 2005. **85**(12): p. 1507-16.
341. Fiedler, L.R., et al., *Decorin regulates endothelial cell motility on collagen I through activation of insulin-like growth factor I receptor and modulation of alpha2beta1 integrin activity.* J Biol Chem, 2008. **283**(25): p. 17406-15.
342. Mayor, R. and C. Carmona-Fontaine, *Keeping in touch with contact inhibition of locomotion.* Trends Cell Biol, 2010. **20**(6): p. 319-28.
343. Lamorte, L., et al., *Crk associates with a multimolecular Paxillin/GIT2/beta-PIX complex and promotes Rac-dependent relocalization of Paxillin to focal contacts.* Mol Biol Cell, 2003. **14**(7): p. 2818-31.
344. Nakamura, K., et al., *Tyrosine phosphorylation of paxillin alpha is involved in temporospatial regulation of paxillin-containing focal adhesion formation and F-actin organization in motile cells.* J Biol Chem, 2000. **275**(35): p. 27155-64.
345. Burridge, K., C.E. Turner, and L.H. Romer, *Tyrosine phosphorylation of paxillin and pp125FAK accompanies cell adhesion to extracellular matrix: a role in cytoskeletal assembly.* J Cell Biol, 1992. **119**(4): p. 893-903.
346. Lammermann, T., et al., *Rapid leukocyte migration by integrin-independent flowing and squeezing.* Nature, 2008. **453**(7191): p. 51-5.
347. DiMilla, P.A., et al., *Maximal migration of human smooth muscle cells on fibronectin and type IV collagen occurs at an intermediate attachment strength.* J Cell Biol, 1993. **122**(3): p. 729-37.
348. Palecek, S.P., et al., *Integrin-ligand binding properties govern cell migration speed through cell-substratum adhesiveness.* Nature, 1997. **385**(6616): p. 537-40.
349. Li, X. and U. Eriksson, *Novel VEGF family members: VEGF-B, VEGF-C and VEGF-D.* Int J Biochem Cell Biol, 2001. **33**(4): p. 421-6.

350. Gerhardt, H., et al., *VEGF guides angiogenic sprouting utilizing endothelial tip cell filopodia.* J Cell Biol, 2003. **161**(6): p. 1163-77.
351. Soker, S., et al., *Neuropilin-1 is expressed by endothelial and tumor cells as an isoform-specific receptor for vascular endothelial growth factor.* Cell, 1998. **92**(6): p. 735-45.
352. Keck, P.J., et al., *Vascular permeability factor, an endothelial cell mitogen related to PDGF.* Science, 1989. **246**(4935): p. 1309-12.
353. Gong, B., et al., *Characterization of the zebrafish vascular endothelial growth factor A gene: comparison with vegf-A genes in mammals and Fugu.* Biochim Biophys Acta, 2004. **1676**(1): p. 33-40.
354. Muller, Y.A., et al., *Vascular endothelial growth factor: crystal structure and functional mapping of the kinase domain receptor binding site.* Proc Natl Acad Sci U S A, 1997. **94**(14): p. 7192-7.
355. Ruhrberg, C., et al., *Spatially restricted patterning cues provided by heparin-binding VEGF-A control blood vessel branching morphogenesis.* Genes Dev, 2002. **16**(20): p. 2684-98.
356. Gimbrone, M.A., Jr., et al., *Tumor dormancy in vivo by prevention of neovascularization.* J Exp Med, 1972. **136**(2): p. 261-76.
357. Folkman, J., *Seminars in Medicine of the Beth Israel Hospital, Boston. Clinical applications of research on angiogenesis.* N Engl J Med, 1995. **333**(26): p. 1757-63.
358. Nyberg, P., L. Xie, and R. Kalluri, *Endogenous inhibitors of angiogenesis.* Cancer Res, 2005. **65**(10): p. 3967-79.
359. Folkman, J., *Tumor angiogenesis: therapeutic implications.* N Engl J Med, 1971. **285**(21): p. 1182-6.
360. Hanahan, D. and J. Folkman, *Patterns and emerging mechanisms of the angiogenic switch during tumorigenesis.* Cell, 1996. **86**(3): p. 353-64.
361. Ferrara, N. and R.S. Kerbel, *Angiogenesis as a therapeutic target.* Nature, 2005. **438**(7070): p. 967-74.
362. Lyden, D., et al., *Impaired recruitment of bone-marrow-derived endothelial and hematopoietic precursor cells blocks tumor angiogenesis and growth.* Nat Med, 2001. **7**(11): p. 1194-201.
363. Hobson, B. and J. Denekamp, *Endothelial proliferation in tumours and normal tissues: continuous labelling studies.* Br J Cancer, 1984. **49**(4): p. 405-13.
364. Nguyen, M., et al., *Elevated levels of an angiogenic peptide, basic fibroblast growth factor, in the urine of patients with a wide spectrum of cancers.* J Natl Cancer Inst, 1994. **86**(5): p. 356-61.
365. Burri, P.H. and M.R. Tarek, *A novel mechanism of capillary growth in the rat pulmonary microcirculation.* Anat Rec, 1990. **228**(1): p. 35-45.
366. Alon, T., et al., *Vascular endothelial growth factor acts as a survival factor for newly formed retinal vessels and has implications for retinopathy of prematurity.* Nat Med, 1995. **1**(10): p. 1024-8.
367. Benjamin, L.E., et al., *Selective ablation of immature blood vessels in established human tumors follows vascular endothelial growth factor withdrawal.* J Clin Invest, 1999. **103**(2): p. 159-65.
368. Shutter, J.R., et al., *Dll4, a novel Notch ligand expressed in arterial endothelium.* Genes Dev, 2000. **14**(11): p. 1313-8.
369. Hellstrom, M., et al., *Dll4 signalling through Notch1 regulates formation of tip cells during angiogenesis.* Nature, 2007. **445**(7129): p. 776-80.
370. Ferrara, N., et al., *Heterozygous embryonic lethality induced by targeted inactivation of the VEGF gene.* Nature, 1996. **380**(6573): p. 439-42.
371. Adair, T.H. and J.P. Montani, in *Angiogenesis*. 2010: San Rafael (CA).
372. Burri, P.H., R. Hlushchuk, and V. Djonov, *Intussusceptive angiogenesis: its emergence, its characteristics, and its significance.* Dev Dyn, 2004. **231**(3): p. 474-88.

373. Benjamin, L.E., I. Hemo, and E. Keshet, *A plasticity window for blood vessel remodelling is defined by pericyte coverage of the preformed endothelial network and is regulated by PDGF-B and VEGF.* Development, 1998. **125**(9): p. 1591-8.
374. Bergers, G. and S. Song, *The role of pericytes in blood-vessel formation and maintenance.* Neuro Oncol, 2005. **7**(4): p. 452-64.
375. Dorrell, M.I., E. Aguilar, and M. Friedlander, *Retinal vascular development is mediated by endothelial filopodia, a preexisting astrocytic template and specific R-cadherin adhesion.* Invest Ophthalmol Vis Sci, 2002. **43**(11): p. 3500-10.
376. Stone, J., et al., *Development of retinal vasculature is mediated by hypoxia-induced vascular endothelial growth factor (VEGF) expression by neuroglia.* J Neurosci, 1995. **15**(7 Pt 1): p. 4738-47.
377. Lu, X., et al., *The netrin receptor UNC5B mediates guidance events controlling morphogenesis of the vascular system.* Nature, 2004. **432**(7014): p. 179-86.
378. Carmeliet, P. and M. Tessier-Lavigne, *Common mechanisms of nerve and blood vessel wiring.* Nature, 2005. **436**(7048): p. 193-200.
379. Adams, R.H., et al., *Roles of ephrinB ligands and EphB receptors in cardiovascular development: demarcation of arterial/venous domains, vascular morphogenesis, and sprouting angiogenesis.* Genes Dev, 1999. **13**(3): p. 295-306.
380. Kitsukawa, T., et al., *Overexpression of a membrane protein, neuropilin, in chimeric mice causes anomalies in the cardiovascular system, nervous system and limbs.* Development, 1995. **121**(12): p. 4309-18.
381. Aikio, M., et al., *Arresten, a collagen-derived angiogenesis inhibitor, suppresses invasion of squamous cell carcinoma.* PLoS One, 2012. **7**(12): p. e51044.
382. Colorado, P.C., et al., *Anti-angiogenic cues from vascular basement membrane collagen.* Cancer Res, 2000. **60**(9): p. 2520-6.
383. Hamano, Y., et al., *Physiological levels of tumstatin, a fragment of collagen IV alpha3 chain, are generated by MMP-9 proteolysis and suppress angiogenesis via alphaV beta3 integrin.* Cancer Cell, 2003. **3**(6): p. 589-601.
384. Pedchenko, V., R. Zent, and B.G. Hudson, *Alpha(v)beta3 and alpha(v)beta5 integrins bind both the proximal RGD site and non-RGD motifs within noncollagenous (NC1) domain of the alpha3 chain of type IV collagen: implication for the mechanism of endothelia cell adhesion.* J Biol Chem, 2004. **279**(4): p. 2772-80.
385. Maeshima, Y., et al., *Extracellular matrix-derived peptide binds to alpha(v)beta(3) integrin and inhibits angiogenesis.* J Biol Chem, 2001. **276**(34): p. 31959-68.
386. Pasco, S., et al., *In vivo overexpression of tumstatin domains by tumor cells inhibits their invasive properties in a mouse melanoma model.* Exp Cell Res, 2004. **301**(2): p. 251-65.
387. Panka, D.J. and J.W. Mier, *Canstatin inhibits Akt activation and induces Fas-dependent apoptosis in endothelial cells.* J Biol Chem, 2003. **278**(39): p. 37632-6.
388. Magnon, C., et al., *Canstatin acts on endothelial and tumor cells via mitochondrial damage initiated through interaction with alphavbeta3 and alphavbeta5 integrins.* Cancer Res, 2005. **65**(10): p. 4353-61.
389. Kamphaus, G.D., et al., *Canstatin, a novel matrix-derived inhibitor of angiogenesis and tumor growth.* J Biol Chem, 2000. **275**(2): p. 1209-15.
390. Rehn, M., et al., *Interaction of endostatin with integrins implicated in angiogenesis.* Proc Natl Acad Sci U S A, 2001. **98**(3): p. 1024-9.
391. Mundel, T.M., et al., *Type IV collagen alpha6 chain-derived noncollagenous domain 1 (alpha6(IV)NC1) inhibits angiogenesis and tumor growth.* Int J Cancer, 2008. **122**(8): p. 1738-44.
392. O'Reilly, M.S., et al., *Angiostatin: a novel angiogenesis inhibitor that mediates the suppression of metastases by a Lewis lung carcinoma.* Cell, 1994. **79**(2): p. 315-28.

393. Kim, S., et al., *Regulation of angiogenesis in vivo by ligation of integrin alpha5beta1 with the central cell-binding domain of fibronectin.* Am J Pathol, 2000. **156**(4): p. 1345-62.
394. Clark, R.A., et al., *Blood vessel fibronectin increases in conjunction with endothelial cell proliferation and capillary ingrowth during wound healing.* J Invest Dermatol, 1982. **79**(5): p. 269-76.
395. Sechler, J.L. and J.E. Schwarzbauer, *Control of cell cycle progression by fibronectin matrix architecture.* J Biol Chem, 1998. **273**(40): p. 25533-6.
396. George, E.L., et al., *Defects in mesoderm, neural tube and vascular development in mouse embryos lacking fibronectin.* Development, 1993. **119**(4): p. 1079-91.
397. McCarty, J.H., et al., *Defective associations between blood vessels and brain parenchyma lead to cerebral hemorrhage in mice lacking alphav integrins.* Mol Cell Biol, 2002. **22**(21): p. 7667-77.
398. Davis, G.E. and C.W. Camarillo, *An alpha 2 beta 1 integrin-dependent pinocytic mechanism involving intracellular vacuole formation and coalescence regulates capillary lumen and tube formation in three-dimensional collagen matrix.* Exp Cell Res, 1996. **224**(1): p. 39-51.
399. Brooks, P.C., R.A. Clark, and D.A. Cheresh, *Requirement of vascular integrin alpha v beta 3 for angiogenesis.* Science, 1994. **264**(5158): p. 569-71.
400. Bouvard, C., et al., *Tie2-dependent knockout of alpha6 integrin subunit in mice reduces post-ischaemic angiogenesis.* Cardiovasc Res, 2012. **95**(1): p. 39-47.
401. van der Flier, A., et al., *Endothelial alpha5 and alphav integrins cooperate in remodeling of the vasculature during development.* Development, 2010. **137**(14): p. 2439-49.
402. Parker, M.W., M. Lo Bello, and G. Federici, *Crystallization of glutathione S-transferase from human placenta.* J Mol Biol, 1990. **213**(2): p. 221-2.
403. Cailleteau, L., et al., *alpha2beta1 integrin controls association of Rac with the membrane and triggers quiescence of endothelial cells.* J Cell Sci, 2010. **123**(Pt 14): p. 2491-501.
404. Short, S.M., G.A. Talbott, and R.L. Juliano, *Integrin-mediated signaling events in human endothelial cells.* Mol Biol Cell, 1998. **9**(8): p. 1969-80.
405. Mendelsohn, M.E. and R.H. Karas, *The protective effects of estrogen on the cardiovascular system.* N Engl J Med, 1999. **340**(23): p. 1801-11.
406. Fadini, G.P., et al., *Gender differences in endothelial progenitor cells and cardiovascular risk profile: the role of female estrogens.* Arterioscler Thromb Vasc Biol, 2008. **28**(5): p. 997-1004.
407. Rosenzweig, A., *Circulating endothelial progenitors--cells as biomarkers.* N Engl J Med, 2005. **353**(10): p. 1055-7.
408. Cid, M.C., H.W. Schnaper, and H.K. Kleinman, *Estrogens and the vascular endothelium.* Ann N Y Acad Sci, 2002. **966**: p. 143-57.
409. Donato, A.J., et al., *Cellular and molecular biology of aging endothelial cells.* J Mol Cell Cardiol, 2015. **89**(Pt B): p. 122-35.
410. Myatt, L., et al., *Nitrotyrosine residues in placenta. Evidence of peroxynitrite formation and action.* Hypertension, 1996. **28**(3): p. 488-93.